A

THE EFFECT OF
ON THE DIST
FROM A SERIE

Robert

Hoover, a 31 KT nuclea

crater at the Nevada Test Si

ater. The 108 m depth of

ed unwelded, weakly welde

ne two dry, densely welde

The apparent crater ha

a volume of 1.7×10^6 m^3.

diverse blocks from the

the weakly welded tuff.

of the ejecta, cons

symmetrically outward fr

Six rays are separated

continuous ejecta field

the uppermost in situ uni

ejecta. Rays are over

are partially eroding

ejecta field also exhibits

maximum range of 2150 m.

concentrated radially o

The logical sequenc

stratigraphic ordering of

ABSTRACT

THE EFFECT OF THE GEOLOGIC SETTING ON THE DISTRIBUTION OF EJECTA FROM A BURIED NUCLEAR DETONATION

By

Robert Warren Henny

Schooner, a 31 KT nuclear excavation experiment, was detonated at the Nevada Test Site in a horizontally layered tuff sequence. The 108 m depth of burst was slightly below a 65 m thick, nearly saturated, weakly welded tuff layer which was sandwiched between two dry, densely welded tuff layers.

The apparent crater has a radius of 130 m, a depth of 63 m, and a volume of 1.7×10^6 m^3. Ejecta are strongly bimodal with boulder-size blocks from the densely welded tuff and sand-size fines from the weakly welded tuff. The continuous ejecta field contains over 90% of the ejecta, concentrated in eleven rays distributed nonsymmetrically outward from the crater to an average distance of 510 m. Rays are separated by valleys which contain little ejecta. The continuous ejecta field exhibits an inverted stratigraphic order with lowermost in situ units concentrated towards ray axes and the crater rim. Rays are overlain by mixed fines which flowed, smoothing over and partially eroding underlying deposits. The discontinuous ejecta field also exhibits an inverted stratigraphic order to its maximum range of 2150 m. Unlike in the continuous, ejecta tend to be concentrated radially outward from valleys.

The logical sequence of observed events and the detailed stratigraphic ordering of the ejecta field suggests that formational

were ordered. Such p

setting. Water co

acceleration phase

dispersed ejecta fie

were: major joint t

ring and foliation cha

physical propertie

and structure of the

enlargement of the c

plication of the

First, as an ana

craters through dire

as a basis from which

for other geologic

processes were ordered. Such processes were strongly affected by the geologic setting. Water content was most important, fueling a massive gas acceleration phase which produced the large crater and the widely dispersed ejecta field. Other controlling geologic parameters were: major joint trends (orientation of major rays), joint spacing and foliation characteristics (ejecta block size and shape), bulk physical properties (bimodal ejecta characteristics and morphology and structure of the ejecta field), and surface gradient (downhill enlargement of the crater and discontinuous ejecta field).

The application of the Schooner results to cratering analyses is twofold. First, as an analog to aid in the interpretation of existing craters through direct comparison of similar features. And second, as a basis from which to hypothesize crater and ejecta processes for other geologic and source environments.

THE EFFECT OF

ON THE DIST

FROM A SERIE

Rober

Michig

in partial ful

f

Doc

Dep

THE EFFECT OF THE GEOLOGIC SETTING ON THE DISTRIBUTION OF EJECTA FROM A BURIED NUCLEAR DETONATION

By

Robert Warren Henny

A DISSERTATION

Submitted to
Michigan State University
in partial fulfillment of the requirements
for the degree of

DOCTOR OF PHILOSOPHY

Department of Geology

1977

ACKN

[illegible] to Dr. Willi

[illegible] presently at Purd

[illegible] science, and technic

[illegible]ty. I appreciate th

[illegible]partment, Michigan S

[illegible] particularly thank

[illegible] other committee

[illegible] James Trow, for

[illegible] Dave Roddy (USGS/F

[illegible] have both spent

[illegible] discussing various as

[illegible]ch in correspondenc

[illegible] for their meaning

I am obliged to seve

[illegible] residency at Mi

[illegible] from a NASA Re

[illegible] in conducting th

[illegible] the Schooner detona

[illegible] of the United Sta

[illegible]ation, the former

[illegible] necessary in proc

[illegible], the Civil Engi

ACKNOWLEDGMENTS

I am indebted to Dr. William Hinze, formally of Michigan State University and presently at Purdue University, for his continued interest, patience, and technical guidance throughout the long course of this study. I appreciate the every assistance given by the Geology Department, Michigan State University, during the past several years. I particularly thank my committee chairman, Dr. William Cambray, and other committee members, Drs. Hugh Bennett, Russell Harmon, and James Trow, for their considered guidance.

Dr. Dave Roddy (USGS/Flagstaff) and Dr. Henry Moore (USGS/Menlo Park) have both spent much time with me over the past several years discussing various aspects of the Schooner crater and ejecta field, both in correspondence and at the Schooner site. I am grateful for their meaningful and valued comments.

I am obliged to several organizations for financial support. During my residency at Michigan State University I received financial assistance from a NASA Research Fellowship. The considerable expense involved in conducting the necessary field work, both before and after the Schooner detonation was borne by the Defense Nuclear Agency and the United States Air Force, Space and Missile Organization. In addition, the former provided much of the drafting and photographic support necessary in producing this document. Most of all, my employer, the Civil Engineering Research Division, Air Force Weapons

...Albuquerque, New Mex...
...cial and clerical supp...
...complete this study.
...ally, I thank my wife,
...r their never ending ...
...these "hard" years.

Laboratory, Albuquerque, New Mexico, has been a continued source of both financial and clerical support without which I would have been unable to complete this study.

Finally, I thank my wife, Marilyn, and children, Kirsten and Robert, for their never ending understanding and encouragement during those "hard" years.

TABL

INTRODUCTION

A. Statement of the

B. Previous Research

1. Terrestrial
2. Laboratory C
3. High-Explosiv

C. The Schooner Eve

D. Approach to the

GEOLOGIC SETTING

A. Physiography

B. Stratigraphy

C. Structure

D. Physical Prope

TRANSIENT CRATERIN

A. Major Processe

1. Mounding
2. Ejection
3. Deposition
4. Base Surg
5. Cloud For

B. Ejecta Impact

1. Mapping
2. Distribu
3. Time Seq

TABLE OF CONTENTS

TABLE OF

ENSIONAL CHARACTER
AND EJECTA FIELD

A. Definition of Ma

1. Crater
2. Lip

B. Dimensional Relat

1. Apparent Cra
2. Apparent Lip

a. Crests
b. Troughs
c. Rays
d. Valleys

C. Areal Relations

1. Apparent Cr
2. Apparent L

D. Volumetric Rel

1. Apparent L
2. Ray-Valley
3. Ray 1 Var
4. Cumulativ

GEOMORPHIC CHARAC
CONTINUOUS EJE

A. General

B. Apparent Cra

1. Surface

a. Over
b. Soil
c. Wall
d. Fall
e. Floo

TABLE OF CONTENTS (cont'd)

TABLE OF

TABLE OF CONTENTS (cont'd)

TABLE OF

TABLE OF CONTENTS (cont'd)

TABLE OF

TABLE OF CONTENTS (cont'd)

TABLE OF C

TABLE OF CONTENTS (cont'd)

LI

LIST OF FIGURES

LIST OF

LIST OF FIGURES (cont'd)

LIST OF

LIST OF FIGURES (cont'd)

LIST OF FIGURES (cont'd)

LIST O

LIST OF FIGURES (cont'd)

LIST OF

LIST OF FIGURES (cont'd)

LIST OF TABLES

(Maps are lo

. ...mpbic Crater and E

. ...mpbic Crater and E

. ...mpbic Crater and E

. ...logic Map of the Cra

...logic Map of the Tre

...logic Map of the Cr

LIST OF MAPS

(Maps are located in the map pocket)

1. Geomorphic Crater and Ejecta Map - Surface Features
2. Geomorphic Crater and Ejecta Map - Block Size
3. Geomorphic Crater and Ejecta Map - Block Areal Density
4. Geologic Map of the Crater Lip
5. Geologic Map of the Trench
6. Geologic Map of the Crater and Continuous Ejecta Field

KEY TO SYM

Unless otherwise specif

All elevations are re

Figures 10 and 11 and Tab

R_1 Crest 1 (also

h_1 Maximum depth

h'_1 Maximum depth (see text)

h_2 Maximum depth

X_3 Depth of burs

E Youngs Modulu

f Shape factor

h_{el} Apparent lip

h_{el} Ejecta thick

h_{tl} True lip cre

E_c Yield of ex Joules)

D_{cl} Crater lip s

W_a Mass of appa

W_c Mass of cont

W_d Mass of disc

W_e Mass of tot

W_f Mass of fal

W_k Mass of clo

KEY TO SYMBOLS AND ABBREVIATIONS

Unless otherwise specified, all distances are referenced to SGZ and all elevations are referenced to preshot ground surface. See Figures 23 and D1 and Table 2 for added information on terms.

C-1	Crest 1 (also C-2, 3, ..., 11)
D_a	Maximum depth of apparent crater
D_a'	Maximum depth of "corrected" apparent crater (see text)
D_t	Maximum depth of true crater
DOB	Depth of burst
E	Youngs Modulus
F	Shape factor ($F = V_a/\pi R_a^2 D_a$)
H_{al}	Apparent lip crest height
H_{el}	Ejecta thickness at crater crest
H_{tl}	True lip crest height
KT	Yield of explosive in kilotons (1 KT = 4.2×10^{12} Joules)
L:1	Crater lip station 1 (also L:2, 3, ..., 40)
M_a	Mass of apparent crater
M_c	Mass of continuous ejecta
M_d	Mass of discontinuous ejecta
M_e	Mass of total ejecta
M_f	Mass of fallback
M_k	Mass of cloud

KEY TO SYMBOLS AN

V_1 Missing crater

V_2 Mass of true c

V_3 Mass of upthru

V_4 Mass of compac

V_5 Unaccounted ma

M_1 Geomorphic mar

R_1 Radius of app

R_2 Radius of app

R_3 Radius of the

R_4 Radius of ca

R_5 Radius to ou

R_6 Radius of th

R_7 Radius to m

R_8 Radius of

R_9 Radius of

R_{10} Radius of

R_{11} Ray 1 (als

Recart Rubble mo

S_1 Apparent

S_{a1} Apparent

S_2 Displace

S_0 Origina

S_3 Presho

M_m	Missing crater mass
M_t	Mass of true crater
M_u	Mass of upthrust
M_β	Mass of compacted zone
M_Δ	Unaccounted mass
M:1	Geomorphic mapping area (also M:2, 3, ..., 559)
R_a	Radius of apparent crater
R_{al}	Radius of apparent lip crest
R_b	Radius of the continuous block boundary
R_c	Radius of cavity below ZP
R_{ds}	Radius to outer displaced boundary
R_{eb}	Radius of the continuous ejecta boundary
R_m	Radius to maximum ejecta range
R_r	Radius of "R" boundary
R_t	Radius of true crater
R_{tl}	Radius of true crater lip
R-1	Ray 1 (also R-2, 3, ..., 11)
Retarc	Rubble mound (crater spelled backwards)
S_a	Apparent crater surface
S_{al}	Apparent lip surface
S_d	Displaced ground surface
S_o	Original ground surface
S_p	Preshot ground surface

KEY TO SYMBOLS A

A_t True crater su

A_u Upthrust surfa

SL Surface ground

TD Total depth of

TL Trough l (also

TS Trench station

V_a Apparent crate

V_c Continuous ej

V_d Discontinuous

V_e Total ejecta

V_f Fallback volu

V_k Cloud volume

V_l Apparent lip

V_m Missing crate

V_p Compressional

V_t True crater v

V_u Upthrust volu

VL Valley l (al

W Yield of ex

ZP Zero Point

μ Shear modul

μ_c Continuous

μ_d Discontinu

μ_f Fallback

KEY TO SYMBOLS AND ABBREVIATIONS (cont'd)

S_t	True crater surface
S_u	Upthrust surface
SGZ	Surface ground zero
T.D.	Total depth of a drill hole
T-1	Trough 1 (also T-2, 3, ..., 112)
T:1	Trench station 1 (also T:2, 3, ..., 11)
V_a	Apparent crater volume
V_c	Continuous ejecta volume
V_d	Discontinuous ejecta volume
V_e	Total ejecta volume
V_f	Fallback volume
V_k	Cloud volume
V_l	Apparent lip volume
V_m	Missing crater volume
V_p	Compressional wave velocity
V_t	True crater volume
V_u	Upthrust volume
V-1	Valley 1 (also V-2, 3, ..., 11)
W	Yield of explosive
ZP	Zero Point - effective center of explosive energy
μ	Shear modulus
ρ_c	Continuous ejecta density
ρ_d	Discontinuous ejecta density
ρ_f	Fallback density

KEY TO SYMBOLS A

γ_t True crater de

γ_u Upthrust densi

$\bar{h}$ Average overbu

ρ_t	**True crater density**
ρ_u	**Upthrust density**
$\overline{\rho}$	**Average overburden density**

CH

INTR

A Statement of the P

explosion beneath t

shallow enough

the upward and ou

produced by the

surrounding ground sur

meteorite or a

ing craters and e

and structural

Oberbeck, 1971).

principal object

ence of the geolog

explosive ev

fields are i

planetary ex

ing. Meteorite i

on the Moon (Ba

(Danielson, 1

also known. T

which has be

opportunity to

CHAPTER I

INTRODUCTION

A. Statement of the Problem

An explosion beneath the ground surface of sufficient magnitude and shallow enough depth of burst results in a crater produced by the upward and outward ejection of material and an ejecta field produced by the subsequent deposition of that material on the surrounding ground surface. Whether an explosion is due to an impacting meteorite or a buried chemical or nuclear detonation, the resulting craters and ejecta fields exhibit a number of morphological and structural similarities (Shoemaker, 1963; Roddy, 1968; and Oberbeck, 1971).

The principal objective of this investigation is to determine the influence of the geologic setting on the crater and ejecta field from a buried explosive event.

Ejecta fields are important to at least three geotechnical disciplines: planetary exploration, weapons effects, and excavation engineering. Meteorite impact structures are important planetary features on the Moon (Baldwin, 1963), Mars (Mutch and Head, 1975), and Mercury (Danielson, 1975). Several impact structures on the Earth are also known. The ejecta fields of these structures consist of material which has been excavated from the crater, thus providing a unique opportunity to sample depths otherwise inaccessible.

...ejecta distribut...

...logic settings.

...distributions a...

...fects for military ...

...ejecta. Additiona...

...serve as effective ...

... This, for a partic...

...estimate ejecta thi...

...size of ejecta im...

...azimuth from th...

...portant in excava...

...construct harbo...

...ms, etc. (Vort...

...ment ejecta pred...

...the geologic ...

...soil and rock, ...

...For example, the pr...

...from an explosiv...

...azimuthal varia...

...event is more typi...

...rounding, and oth...

...reduction of th...

1. Previous Rese...

...ile research ha...

...relatively l...

Furthermore, ejecta distributions provide a means of examining subsurface geologic settings.

Ejecta distributions are also important in the assessment of weapons effects for military targets vulnerable to impact and/or burial by ejecta. Additionally, critically placed accumulations of ejecta can serve as effective barriers to troop and vehicular movement. Thus, for a particular geologic setting relationships are needed to estimate ejecta thickness, ejecta mass per unit area, and number and size of ejecta impacts per unit area as a function of distance and azimuth from the crater. Ejecta distributions are likewise important in excavation engineering where buried explosives are used to construct harbors, canals, railroad or highways cuts, earth-fill dams, etc. (Vortman, 1970).

Current ejecta prediction techniques do not take into consideration the geologic setting, except to differentiate between wet or dry soil and rock, thus leading to large prediction uncertainties. For example, the prediction of ejecta thickness at a given distance from an explosive detonation incorporates a 2 to 3 order of magnitude azimuthal variation while the azimuthal variation for a single event is more typically an order of magnitude. By relating raying, mounding, and other distributional features to the geologic setting, reduction of these uncertainties should be possible.

B. Previous Research

While research has been prolific in the general field of cratering, relatively little attention has been given to ejecta

...ctions and most is unre...

...s reviewed here.

...Terrestrial Impact ...

...early 100 "possible" ...

...chnery (1966) of which 5...

...in 1961 based on their a...

...ural, geophysical, and ...

...ctures have been studied, ...

...ture has been mapped in a...

...ap of this crater and e...

...nal structure of the cr...

...ragmata blanket. Roddy ...

...more examination of thi...

...determine the nature and ...

...ion of the ground surface ...

...the overturned flap to co...

...to crater radii.

Moore (1976) publishe...

...with missile impact str...

...ture. Craters ranging fr...

...ures were mapped with inv...

...ntrance of material prop...

...ctering and characterist...

...ructures.

distributions and most is unrelated to the stated problem. Applicable research is reviewed here.

1. Terrestrial Impact Structures

Nearly 100 "possible" terrestrial impact structures were listed by Freeberg (1966) of which 52 were considered "probable" by Short and Bunch (1968) based on their analysis of relevant morphological, structural, geophysical, and petrological data. While many of these structures have been studied, only the ejecta field of Meteor Crater, Arizona, has been mapped in any detail. Shoemaker (1963) mapped the geology of this crater and ejecta field demonstrating the overturned synclinal structure of the crater lip and the inverted stratigraphy of the ejecta blanket. Roddy, et al. (1975) recently concluded an extensive examination of this ejecta blanket, drilling some 160 holes to determine the nature and thickness of its stratigraphy and related uplift of the ground surface. They found the inverted stratigraphy of the overturned flap to consist of continuous layered units out to near 3 crater radii.

Moore (1976) published an analysis of over 50 high to hypervelocity missile impact structures at White Sands Missile Range, New Mexico. Craters ranging from 2 to 10 m in diameter and their ejecta fields were mapped with inverted stratigraphy observed. The importance of material properties of the ground surface on the dimensions and characteristics of the craters and ejecta fields was demonstrated.

2. Laboratory Cratering Experiments

Laboratory impact and explosive cratering experiments are useful in studying source parameters (charge size and position, projectile impact mass, angle, and velocity, etc.) and site parameters (material properties, layering, terrain, etc.) since these can be varied in a controlled manner and the resulting crater and ejecta fields are readily measured. The primary limitation of these experiments is in scaling up the results to "real world" structures. Nevertheless, a significant amount of experimentation has been performed, but unfortunately with little emphasis on ejecta.

Johnson, et al. (1971) using gram-size charges in a homogeneous, dry sand demonstrated that ejection processes were orderly. Ejecta exit angles increased and velocities decreased regularly as depth of burst increased while at the same scaled depth of burst exit angles were nearly identical.

Vesic, et al. (1967, 1972) detonated gram-size charges in a specially designed test bed with a vertical window to obtain high-speed cinema records of the events. They determined that material properties, layering, and terrain have important effects on the formation of craters and presumably ejecta fields, although the latter were not measured. Piekutowski (1974) and Andrews (1975), using similar techniques, studied the formation of craters and ejecta fields in dry and wet sand. They identified zones of ejecta origin and observed ejection processes to be orderly. Beyond the crater lip individual sand grains, traveling ballistic trajectories, were

xxx a steadily outwar

xxxxx of the lip was o

xx inwardly to ton-siz

xxxs were used (Post, 1

Xx Sault, et al. (19

xxxly ejection and depo

xx xx quartz-sand targ

x xx structural features

xx xxxels with laborat

xxxxl impact and burie

1. High-Explosive a

Xxxg the past 30 y

xxplosive and nuclear

xxx charge positions

xx of burst (Vaile, 19

xxlson and Jones

xxl nuclear and high-

xx mass distributions

xxxx R/R_a)* and near

xx of burst (DOE/wl/3

In addition, a nu

xx. (1959), Chabai (1

xxlson and Newell (

xx xxcers preplaced

xx key to Symbols and

deposited in a steadily outward progressing pattern. Inverted stratigraphy of the lip was observed and ejecta distributions compared favorably to ton-size field events when appropriate scaling techniques were used (Post, 1974).

Both Gault, et al. (1968) and Stoffler, et al. (1975) observed the orderly ejection and deposition of ejecta from hypervelocity impacts into quartz-sand targets. Many of the resulting morphological and structural features of their craters and ejecta fields have close parallels with laboratory explosive events, as well as larger terrestrial impact and buried explosive events.

3. High-Explosive and Nuclear Field Tests

During the past 30 years there have been a large number of high-explosive and nuclear field tests ranging from 1/4 kg to 15 MT and with charge positions varying over a wide range of heights and depths of burst (Vaile, 1961; Vortman, 1969; and Circeo, 1969).

Carlson and Jones (1965) analyzed ejecta distributions from several nuclear and high-explosive events in desert alluvium. They found mass distributions of ejecta similar at the same scaled distance (R/R_a)* and nearly identical for events at the same scaled depth of burst ($DOB/W^{1/3}$).

In addition, a number of investigators including Sakharov, et al. (1959), Chabai (1962), Ahlers (1962), Diehl and Jones (1964), and Carlson and Newell (1970) have studied ejecta mechanisms (origins) using tracers preplaced in the region to be cratered. In nearly all

*See Key to Symbols and Abbreviations for definitions of terms.

were distribute

rimental dispersion e

ed to benchmark t

), Cherry (196

ness, especially for

examined the effec

of their size and ve

ejecta distributio

ejecta distrib

Shoemaker (1963) was

of a buried nuclear

gy and structural

. Since then crater

mapped; Sedan (R

ton and Girucky,

exhibited an overtur

deformations d

ences in the geolog

and 1973) has mapp

00 tons) favorab

logical, and strat

terrestrial impact

Johnson (1962) a

. He observed th

increasingly inf

cases tracers were distributed radially outward from SGZ with only limited azimuthal dispersion even for sand-size tracers. These data have been used to benchmark theoretical calculations by Hess and Nordyke (1961), Cherry (1967), and Terhune and Stubbs (1970) with some success, especially for relatively homogeneous media. Sherwood (1967) has examined the effect of drag on ejecta fragments as a function of their size and velocity and applied corrections to calculated ejecta distributions bringing them closer to agreement with measured ejecta distributions.

Shoemaker (1963) was first to map the structure and stratigraphy of a buried nuclear event and favorably compared the inverted stratigraphy and structural deformation of the crater lip to Meteor Crater. Since then crater lips of several other buried nuclear events have been mapped; Sedan (Richards, 1964), Danny Boy (Short, 1964), Sulky (Lutton and Girucky, 1966), and Cabriolet (Fransden, 1970). Each exhibited an overturned flap with inverted stratigraphy and structural deformations differing only in detail, presumably due to differences in the geologic setting. During the past 10 years Roddy (1970 and 1973) has mapped a number of high-explosive surface events (20 to 500 tons) favorably comparing their deformational, morphological, and stratigraphic characteristics to terrestrial and extraterrestrial impact structures.

Johnson (1962) studied 12 buried high-explosive events in basalt. He observed that as crater size decreased crater shape became increasingly influenced by joint spacing. On several events one

rays were align

of the jointing p

) correlated e/e

basalt with major j

. The Schooner Event

The Schooner event, a

KT on 8 December 19

by the University o

U.S. Energy Research

program for the dev

ones. The Schooner de

specially designed f

of 11 ± 4 KT. The dev

that the zero poi

. The device was st

to detonation to ensu

The primary objectiv

crater growth and d

ations and to determ

ologies. Site geolo

sequence of welded

ed to resemble the

of previous buried

ing individual exper

or two ejecta rays were aligned with joint trends; but local variability of the jointing produced conflicting results. Henny and Carlson (1968) correlated ejecta rays from surface high-explosive events in basalt with major joint trends.

C. The Schooner Event

The Schooner event, a buried nuclear experiment, was detonated at 0800 PST on 8 December 1968 at Nevada Test Site. Schooner was executed by the University of California Lawrence Livermore Laboratory for the U.S. Energy Research and Development Agency as part of the Plowshare Program for the development of nuclear excavation techniques. The Schooner device was a thermonuclear (fission-fusion) source, specially designed for Plowshare excavation, with a measured yield of 31 $\pm$ 4 KT. The device canister was implaced in an encased hole such that the zero point (ZP) or depth of burst (DOB) was at 108.2 m. The device was stemmed with a grout-gravel mix several weeks prior to detonation to ensure compatability with the surrounding media.

The primary objectives of the Schooner experiment were to acquire crater growth and dimensional data to benchmark theoretical calculations and to determine the fractional release and transport of radionuclides. Site geology, consisting of a partially saturated, layered sequence of welded and nonwelded tuffs, was specially selected to resemble the Transisthmian Canal Region more closely than sites of previous buried nuclear events. Lessler (1968) has described individual experiments and a summary of results has been

...n Eaves (1970). Ea...

...ejecta field.

...Approach to the P...

...The research to dat...

...rally produced ejecta ...

...asses: there is litt...

...ology and structure of ...

...ountered data relation...

...ion.

...The Schooner event is ...

...ion. The geologic sett...

...the surface is relative...

...ring Schooner result...

...consecutive steps. F...

...thematically mapped and a...

...ologically (Chapter V)...

...pters VI and VIII). Se...

...ta field are compared t...

...establish cause and effe...

...e features and relation...

...former data (Chapter II...

...e processes responsibl...

...ure ash ejecta field (...

reported by Tewes (1970). Henny (1970) presented general data on the crater and ejecta field.

D. Approach to the Problem

While research to date indicates that to a first degree explosively produced ejecta fields are the result of an ordered set of processes; there is little specific information available on the morphology and structure of any large crater and ejecta field and only scattered data relating the geologic setting to their formation.

The Schooner event is uniquely qualified to address this problem. The geologic setting has been well documented (Chapter II) and the surface is relatively level and free of vegetation.

Using Schooner results, the stated problem is addressed in three consecutive steps. First, the crater and ejecta field are systematically mapped and analyzed; dimensionally (Chapter IV), morphologically (Chapter V), and stratigraphically and structurally (Chapters VI and VIII). Second, major features of the crater and ejecta field are compared to key parameters of the geologic setting to establish cause and effect relationships (Chapter VIII). Third, these features and relationships are assessed against available transient data (Chapter III) to construct a time history of, and to infer processes responsible for, the formation of the Schooner crater and ejecta field (Chapter IX).

CHA

GEOLO

A. Physiography

The Schooner site is l

Nevada Test Site ar

Nevada (Fig. 1). Scho

level and geodetic c

", is approxim

dissected plateau al

The plateau has a

to fully contain

extends beyond

rims (Fig. 3).

The topographic gradi

to 135° with a

across the crater

Stream valle

produce local ele

The ground surface

on the south and

where bedrock is exp

and small bushes n

CHAPTER II

GEOLOGIC SETTING

A. Physiography

The Schooner site is located on Pahute Mesa in the northwest corner of Nevada Test Site approximately 200 km northwest of Las Vegas, Nevada (Fig. 1). Schooner SGZ, with elevation 1695.4 m above mean sea level and geodetic coordinates of N 37°20'36.3187" and W 116° 33'57.1419", is approximately centered on a gently undulating, slightly dissected plateau along the northwestern edge of Pahute Mesa (Fig. 2). The plateau has a minimum radius of 800 m about SGZ, sufficient to fully contain the continuous ejecta blanket while to the south it extends beyond 2.4 km, sufficient to contain maximum ejecta ranges (Fig. 3).

The topographic gradient is constant across SGZ curving from azimuth 295° to 135° with an average 1 1/2° slope. Maximum elevation decrease across the crater and continuous ejecta blanket is 7 and 25 m, respectively. Stream valleys approximately 450 m to the east and southeast produce local elevation changes up to 18 m.

The ground surface is covered by soil ranging from 2 m in thickness on the south and east to less than 1/3 m on the west and north where bedrock is exposed locally. The soil unit supports some grasses and small bushes not exceeding 1 m in height.

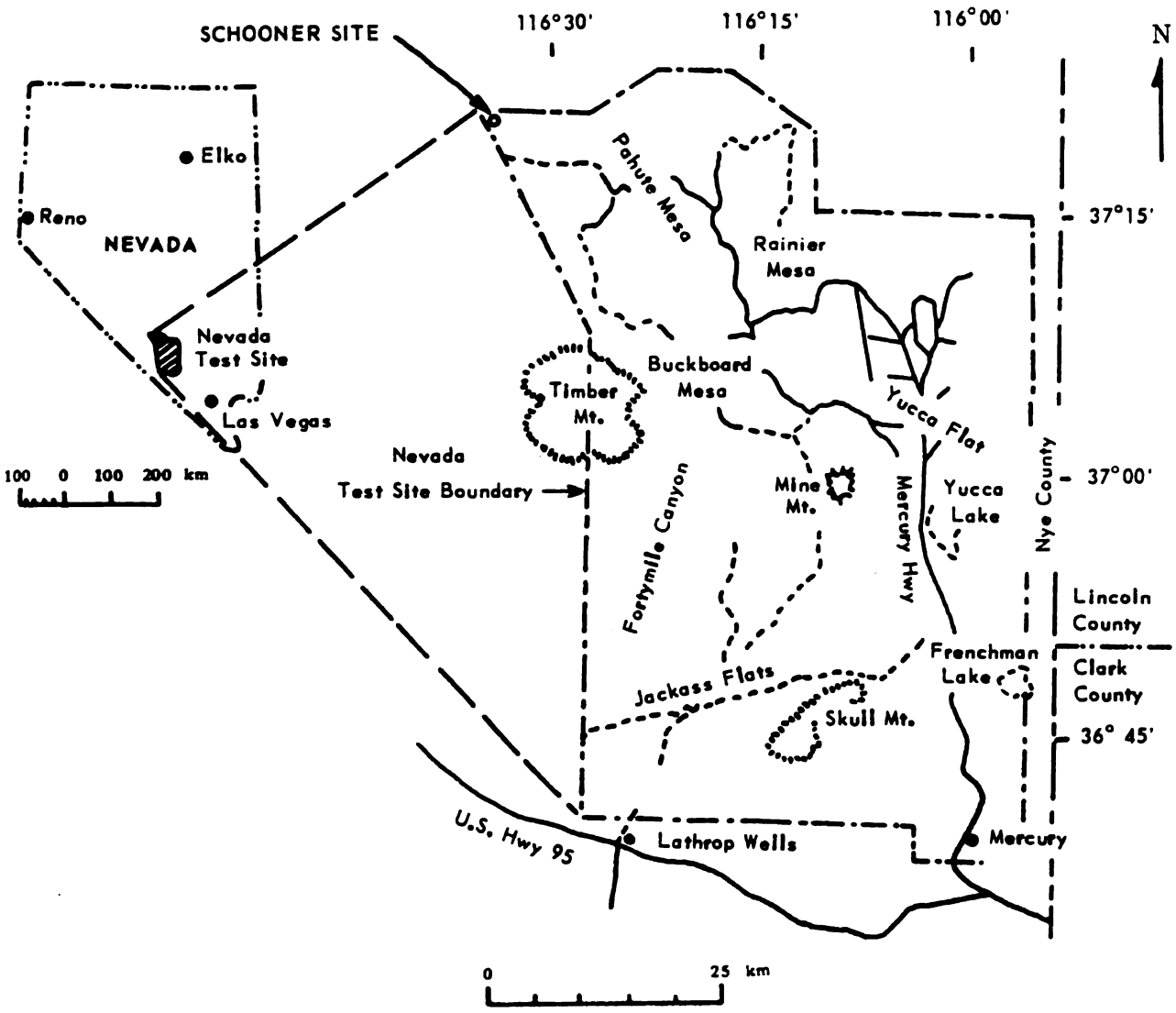

Figure 1. Index Map - Nevada Test Site, Pahute Mesa, and Schooner Site

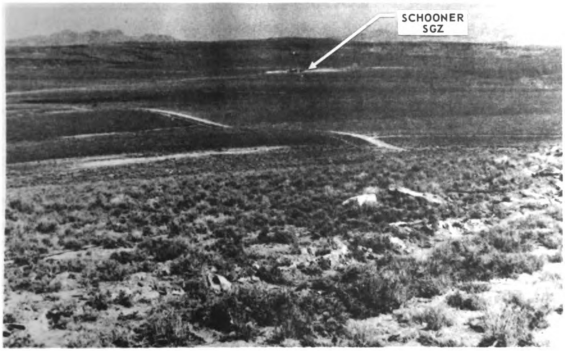

From Five Kilometers Southeast

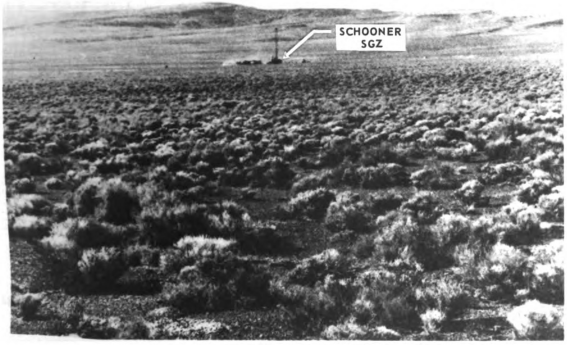

From Four Hundred Meters Northeast

Figure 2. **Two Views of Schooner SGZ Area (Lawrence Livermore Laboratory Photos)**

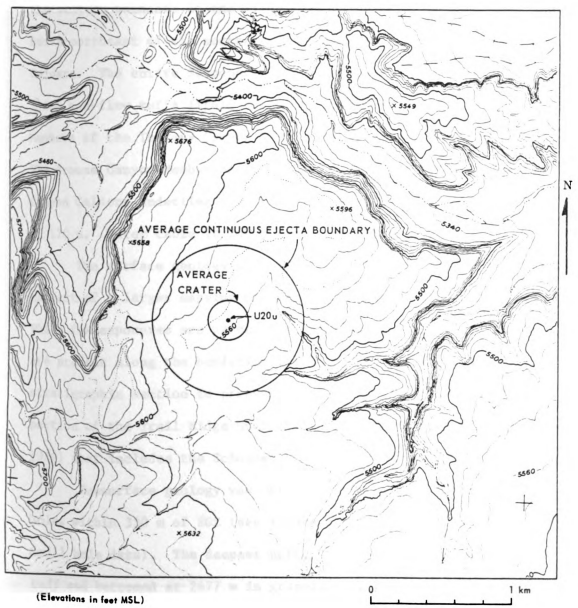

Figure 3. **Topography of Schooner Plateau with Average Crater and Continuous Ejecta Boundary Indicated**

1. Stratigraphy

The Schooner site is
eastern boundary of the
northeast of the north
Mtn. The entire Schoone
ignimbrite tuffs (Trail
west of the Thirsty Canyo
Tiva Canyon Member of
rhyolites underlies the
The water table is
The surface geology
part of a larger mapping
Outcrop exposures are pr
pavement along the bord
stratigraphic section is
Tuff of the Trail Ridge
Unit that includes the S
Subsurface geology
was within 350 m of SC
drillhole data). The d
was bottomed at 267
Mtn. 365). Two other
geologic and physical pr
distance from the Sc
Five additional holes

B. Stratigraphy

The Schooner site is located approximately 6 km northwest of the western boundary of the Silent Canyon Caldera and less than 5 km north-northeast of the northeastern boundary of the Black Mountain Caldera. The entire Schooner plateau is underlain by nearly flat-lying ash-flow tuffs (Trail Ridge, Spearhead, and Rocket Wash Members of the Thirsty Canyon Tuff) from the Black Mountain Caldera. The Grouse Canyon Member of the Belted Range Tuff from the Silent Canyon Caldera underlies the Thirsty Canyon Tuff to an average depth of 170 m. Water table is 260 m below the surface.

The surface geology was mapped by the U. S. Geological Survey as part of a larger mapping program covering most of Pahute Mesa. While few exposures are present on the plateau surface, good exposures are present along the bordering cliffs and a particularly good stratigraphic section is present 1 km southwest of Schooner SGZ. A portion of the Trail Ridge Quandrangle Map (Christiansen and Noble, 1968) that includes the Schooner site is reproduced in Figure 4.

Subsurface geology was obtained primarily from eight drill holes within 350 m of SGZ (see Figure 5 for locations and Table 1 for drill hole data). The deepest hole, PM #2, penetrated over 1260 m of tuff and bottomed at 2677 m in granodiorite porphyry (Hasler and Byers, 1965). Two other holes, Ue20u-1 and 3, examined the subsurface geology and physical properties of the media over predicted depths of disturbance from the Schooner event (Sargent and Jenkins, 1968). Four additional holes (U20u-1, 2, 3, and 4) were drilled for the

Geologic Map
and Noble, 19

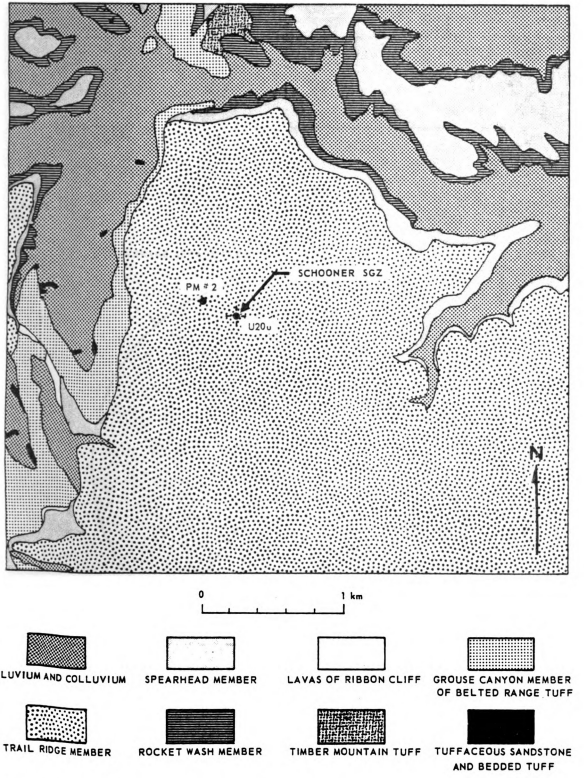

Figure 4. Geologic Map of the Schooner Plateau (After Christiansen and Noble, 1968)

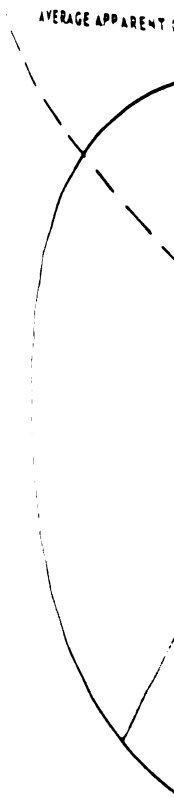

Fig. Location o

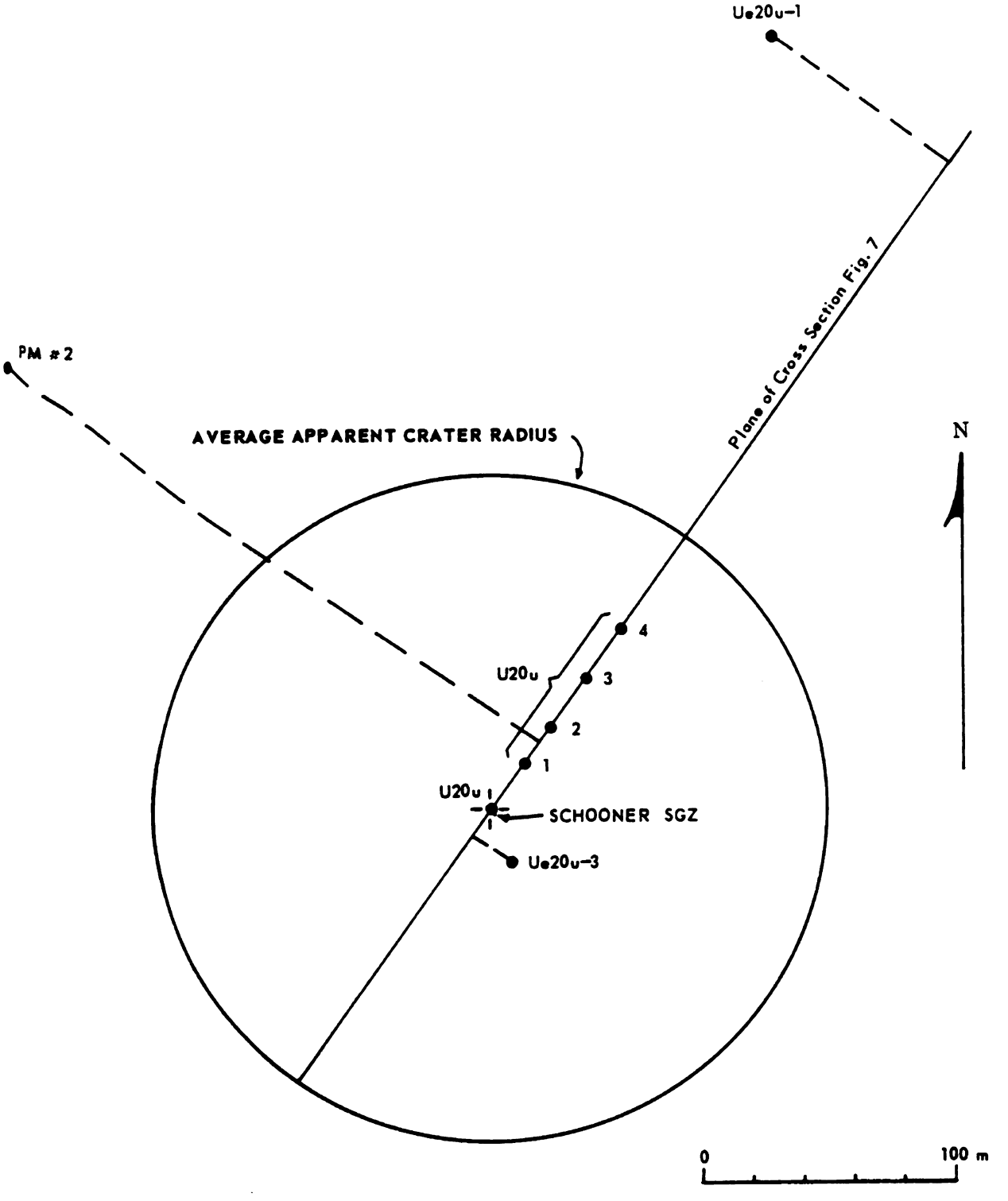

Figure 5. Location of Exploratory Drill Holes Near Schooner Site

T

SCHOONER

[illegible]	[illegible] Elev. MSL (m)	Distance From Schooner SGZ (m)	Hole Dia (in)
[illegible]	[illegible]	263	[illegible]
[illegible]	1695.6	0	52
[illegible]	1697.6	322	[illegible]
[illegible]	1695.2	21	[illegible]
[illegible]	1695.3	21	[illegible]
[illegible]	1695.2	43	[illegible]
[illegible]	1695.3	64	[illegible]
[illegible]	1695.6	88	[illegible]

[illegible] used for geophysical [illegible]

[illegible] Caliper

[illegible] Directional

[illegible] Density

[illegible] velocity

[illegible] velocity

TABLE 1

SCHOONER DRILL HOLE DATA

Hole Designation	Location (Nevada State Coord.)	Collar Elev. MSL (m)	Distance From Schooner SGZ(m)	Hole Dia. (in.)	Total Depth (m)	Date Begun	Drill Method	Sample Method	Geophysical Logs (1)	Reference
PH #2	N944,582 E528,655	1703.5	263	26 to 6 1/8	2677	5/64	Rotary air, soap & water mud below 1981 m	Cuttings & intermittant coring (38 runs, total 64 m)	C,E,D,V, 3D,F,Y	Hasler & Byers (1965)
U20a	N944,009.4 E529,300.0	1695.4	0	52	137	8/68	Dry air w/vacuum	Cuttings at 3 m intervals	C,D,P,Y	Ramspott (1968)
Ue20a-1	N945,005.7 E529,645.9	1697.6	322	3 5/8	229	6/68	Mud	Continuous core to TD	C,D,3D* SU,N,T,E	Sargent & Jenkins (1968)
Ue20a-3	N943,942.8 E529,284.1	1695.1	21	9 7/8	152	7/68	Dry Air w/vacuum	Cuttings plus 13 core runs nominally 1.5 to 3 m in length, 17 m recovered	C,D,DL, SU,SD, P,N	"
U20a-1	N944,066.7 E529,340.0	1695.3	21	6 3/4	124	10/68	Rotary with Davis Mix	Cuttings at intervals 3 m	C,D,Y	Purtymun, Harrill, & Rush (1969)
U20a-2	N944,123.9 E529,380.4	1695.2	43	6 3/4	112	10/68	Rotary with Davis Mix	Continuous core to TD	C,D,Y, 3D+,V+,N	"
U20a-3	N944,181.5 E529,420.6	1695.3	64	6 3/4	79	10/68	Rotary with compressed air to 30 m Davis Mix below	none	C,D,Y	"
U20a-4	N944,246.8 E529,466.5	1695.4	88	6 3/4	46	10/68	"	none	C,D,Y	"

Notes: (1) Symbols used for geophysical logs

C :	Caliper	N :	Gamma neutron	F :	Fluid density
Y :	Directional	DL:	Interval density	SU:	Seismic uphole
D :	Density	P :	Bore hole photography	SD:	Seismic downhole
3D:	3D velocity	T :	Neutron-neutron	* :	Partial logs obtained
V :	Continuous velocity	E :	Electric	+ :	Suitable logs not obtained

present study to examine detailed variations in stratigraphy across the crater region (Purtymun, et al., 1969). The Schooner emplacement hole (U20u) was also sampled and geologically studied (Ramspott, 1968). In addition 5 other deep holes within 6 km east and southeast of Schooner were drilled for other projects; but provide areal stratigraphic correlations (U20m to 1264 m, Orkild, 1969; Ue20j to 1734 m, Hasler, 1965; Ue20p to 1524 m, Jenkins, 1969; U20p to 998 m, Jenkins, 1969; and Ue20u-2 to 381 m, Ramspott, 1968).

The geology at Schooner site is subdivided into four overlapping systems of units (Fig. 6): stratigraphic units for correlation with the areal geology, mapping units for detailed geologic mapping of the crater and ejecta field, physical property units for examining their effect on cratering, ejection, and depositional processes, and ejecta units for describing the surface morphology of the ejecta field.

Listed below are brief descriptions of the five major stratigraphic units encountered at Schooner from Christiansen and Noble (1968) and Orkild, et al. (1969).

Trail Ridge Member (0 - 43.3 m): Multiple-flow simple cooling unit of metaluminous to peraluminous silicic ash-flow tuff underlain by pumice-rich air-fall tuff at base. Ash-flow tuff densely to moderately welded, mainly devitrified, but with glassy base.

Spearhead Member (43.3 - 60.7 m): Simple cooling unit of comenditic to trachytic soda rhyolitic ash-flow tuff underlain by pumice-rich air-fall tuff. Ash-flow tuff ranges from nonwelded to

Correlation betw
Property, and ge

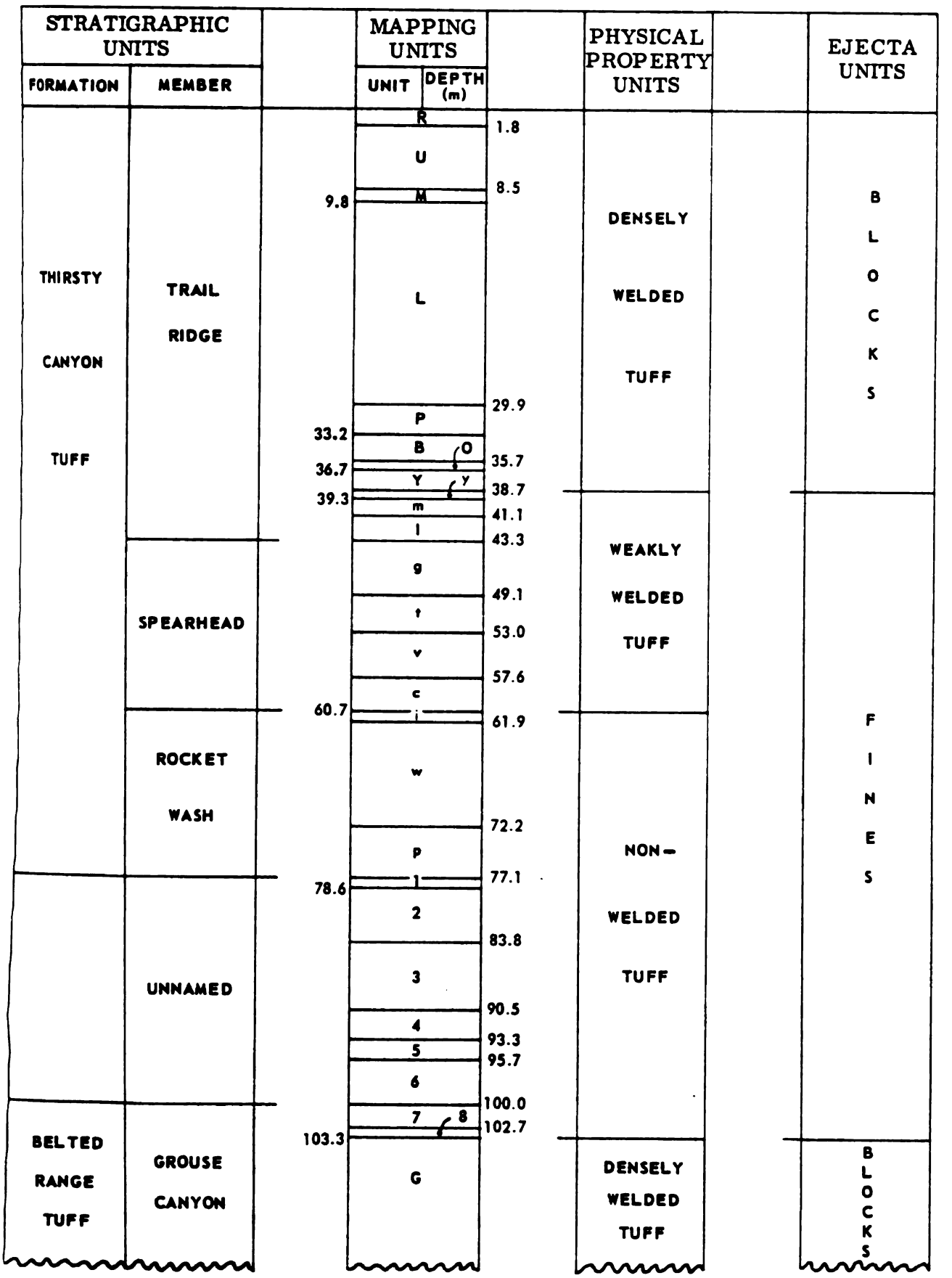

Figure 6. Correlation between Stratigraphic, Mapping, Physical Property, and Ejecta Units at Schooner Site

devitrified a

at top and base

Wash Member (

rhyolitic to

air-fall tuff.

zones, vitric

and base.

Member (77.1

sediments with

Canyon Member

ash-flow tuff

glassy base. Pro

gas cavities con

lation of strat

Schooner SGZ is p

ater profiles s

at PM #2, the ma

ted. Variations i

for the Tra

ity of the varia

tuff horizons.

Sargent and Jenkin

the remaining

Canyon topogr

weakly welded, devitrified and in part vapor-phase altered, thin glassy zones at top and base.

Rocket Wash Member (60.7 - 77.1 m): Compound cooling unit of trachytic soda rhyolitic to comenditic ash-flow tuff underlain by pumice-rich, air-fall tuff. Ash-flow tuff primarily nonwelded, some weakly welded zones, vitric, in part vapor-phase altered, thin glassy zones at top and base.

Unnamed Member (77.1 - 100.0 m): Reworked bedded tuff and tuffaceous sediments with minor nonwelded ash-flow (and air-fall?) tuff layers.

Grouse Canyon Member (100.0 - 148.1 m): Compound cooling unit of comenditic ash-flow tuff, moderately to densely welded, devitrified with glassy base. Prominent compaction and flow foliation; lenticular gas cavities containing vapor-phase crystals.

Correlation of stratigraphic units between drill holes within 350 m of Schooner SGZ is presented in Figure 7 with average apparent and true crater profiles superimposed for reference. With the exception at PM #2, the major units are continuous and uniformly distributed. Variations in thickness across the cratered region range from $\pm$6% for the Trail Ridge to $\pm$16% for the Spearhead, with the majority of the variation contained within the weathered and reworked tuff horizons.

Sargent and Jenkins (1968) maintain that differences between PM #2 and the remaining sections are real and probably the result of pre-Thirsty Canyon topography. The original interpretation for the

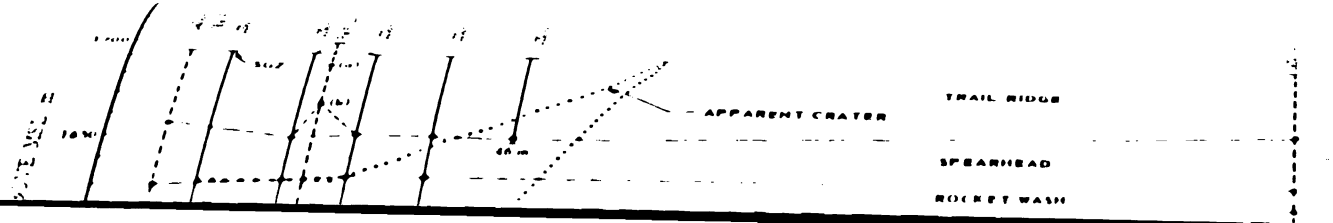
APPARENT CRATER
TRAIL RIDGE
SPEARHEAD
ROCKET WASH

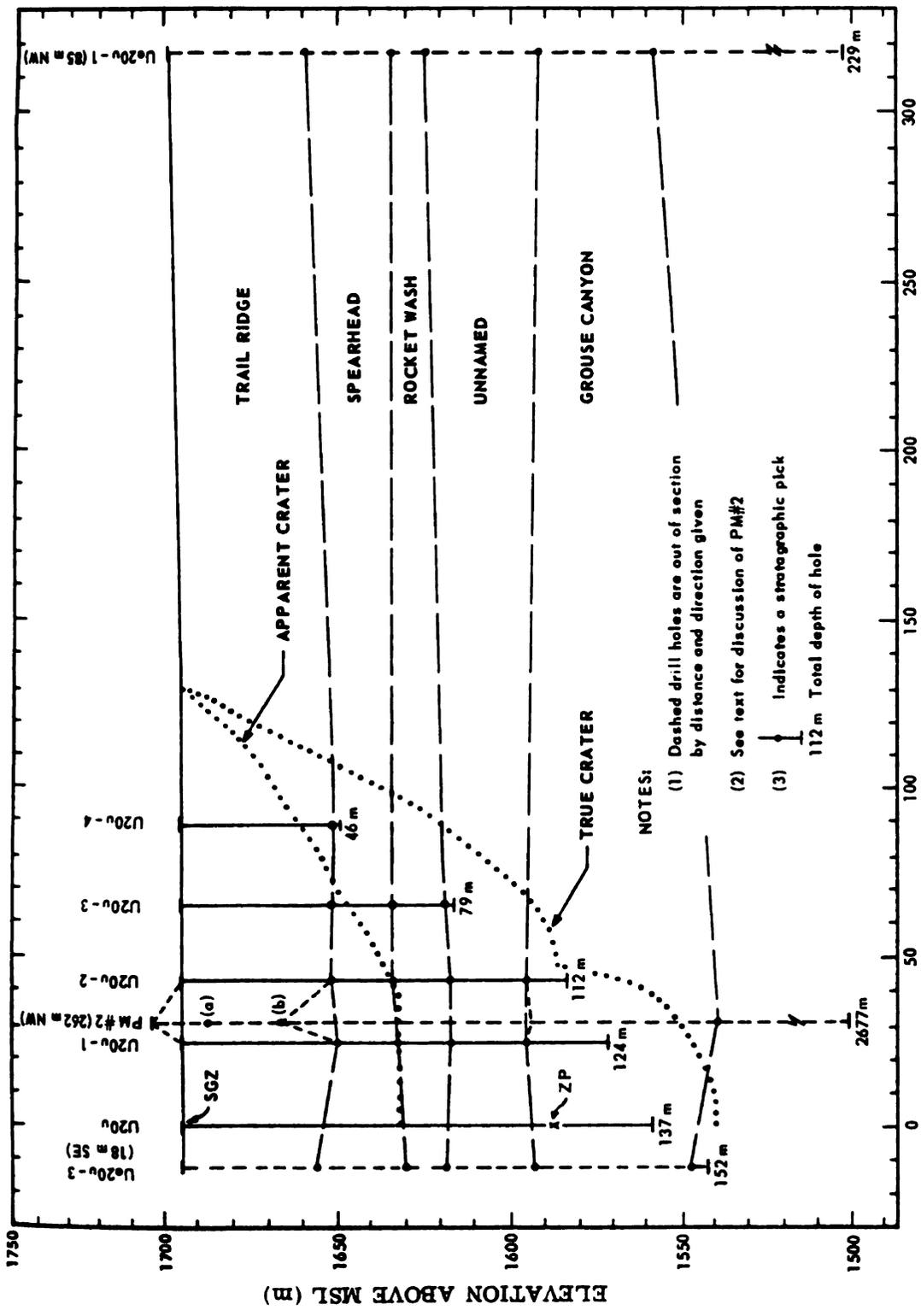

Figure 7. Correlation of Stratigraphic Units Across Schooner Site

...spearhead conta...

...'. An alternate ...

...ming their lithi...

...material at a...

...with the vitrophy...

...portant, examination...

...together with e...

...stratigraphic diff...

...and ejecta field...

..., if they exist,

...in studying the S...

...geologically map...

...) the stratigraph...

...units each rea...

...for description...

...primarily on me...

...followed by close...

...considered wer...

...of inclusions.

Figure 8 presents ...

..., 2, 3, and 4. Ma...

...density log signatu...

...region using simi...

...holes. Results in...

...are distributed co...

Trail Ridge-Spearhead contact (Hasler and Byers, 1965) is marked (a) in Figure 7. An alternate interpretation marked (b) is preferred after examining their lithologic log, especially the comment, "Much glassy material at about 37 m." This glassy material may correlate with the vitrophyre observed in U20u-2 from 33.2 to 38.7 m. More important, examination of the crater wall half-way between U20u and PM #2 together with ejecta deposits in that direction indicates no basic stratigraphic differences with respect to other portions of the crater and ejecta field. Therefore, differences in stratigraphy above 70 m, if they exist, occur beyond the crater and are thus not important in studying the Schooner crater and ejecta field.

To geologically map the crater and ejecta field in detail (see Chapter VI) the stratigraphic column to 112.2 m was subdivided into 28 distinct units each readily identifiable in the field (see Appendix A for descriptions of mapping units). Definition of units was based primarily on megascopic examination of the U20u-2 continuous core followed by close correlation with ejecta deposits. Properties considered were degree of welding, porosity, color, texture, and types of inclusions.

Figure 8 presents traces of continuous density logs for U20u-1, 2, 3, and 4. Mapping units delineated above were correlated with density log signatures of U20u-2 and then traced across the crater region using similar density log signatures from the other drill holes. Results indicate that mapping units like stratigraphic units are distributed continuously and uniformly across Schooner

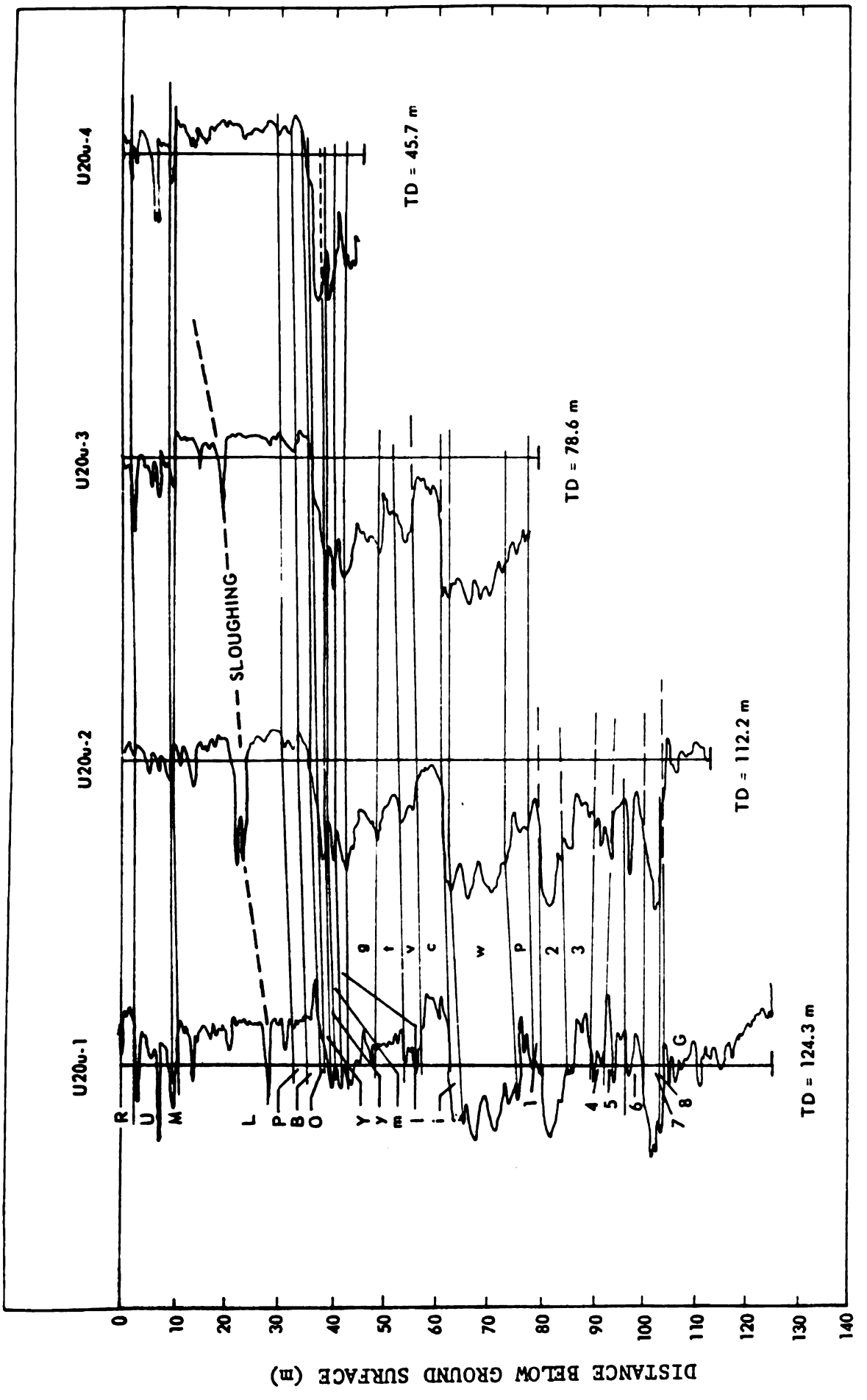

Figure 8. Correlation of Mapping Units across Schooner Crater Area Using Continuous Density Logs from Drill Holes U20u-1, 2, 3, and 4

rrain. Thicknesses

from their means; but

times exhibit variation

Structure

In the vicinity of t

rally uncomplicated.

ime strikes roughly no

s. The previously dis

erally follows this d

ion.

The few fold struc

ary deposition over t

consolidation of wa

ion. The nearest fol

to the east. It tr

mapped as a surfac

(L, 1963).

In Paiute Mesa a

down dropped side

ained within 1.3 km

Ridge line, would p

ion, 1.8 km north

displacements within

ridge south onto t

crater region. Thicknesses of mapping units vary, on the average, ±15% about their means; but oxidized zones, reworked ash-flows, and soil zones exhibit variations up to ±50%.

C. Structure

In the vicinity of the Schooner site the tuff units are structurally uncomplicated. The Trail Ridge, capping the Schooner plateau, strikes roughly northeast with southeast dips averaging 2° to 5°. The previously discussed topographic gradient across SGZ essentially follows this dip and probably reflects the depositional surface.

The few fold structures observed on Pahute Mesa are related to primary deposition over topographic irregularities or to subsidence from consolidation of water-carrying units rather than compressional forces. The nearest fold to the Schooner site is a synclinal flexure 3 km to the east. It trends north-south for 10 km and has been interpreted as a surface expression of a buried fault scarp (Orkild, et al., 1969).

On Pahute Mesa all faults are normal and nearly vertical with the down dropped side commonly to the west. No exposed faults are observed within 1.3 km of SGZ and only two faults, if extended in a straight line, would pass nearer (~300 m south of SGZ). These two faults, 1.8 km north of Schooner on an adjoining butte, show displacements within the Spearhead of 9 m, but are not observed to continue south onto the Schooner plateau.

nature of their e

near vertical dips a

ism of shrinkage joi

ne Ridge ("R" and

nearest outcrops surr

mately 100 joints we

mmm the major joi

ge ranges east-west,

55 m station #2 (E-

ment probably refl

across Pahute

ural variation, pos

ain tuff units.

Examination of t

ert stream cuts, cli

joints are near ve

ints are almost al

joint surfaces are

with joints dis

ocated near the

Rainier Mesa, the Grouse

fault scarps indicate

ion, throughout t

the 95 m of U2bu-

interconnected

By nature of their emplacement welded tuffs are well jointed. Their near vertical dips and slightly curved plan view trends are diagnostic of shrinkage joints due to cooling. Near surface joints in the Trail Ridge ("R" and "U" mapping units) were mapped at the three closest outcrops surrounding Schooner SGZ (Fig. 9). Approximately 100 joints were counted at each 500 m^2 location. At each location the major joint trend is nearly north-south. The minor trend averages east-west, but varies with location from station #1 (NE-SW) to station #2 (E-W) to station #3 (NW-SE). The major north-south trend probably reflects the dominant north-south structural alignment across Pahute Mesa. The minor east-west trend, particularly its areal variation, possibly reflects local flow patterns of the ash-flow tuff units.

Examination of the U20u-2 core together with observations of nearby stream cuts, cliff faces, and the crater wall shows that almost all joints are near vertical while fractures dip 45^{o} to 60^{o}. Joint surfaces are almost always coated with secondary deposits while fracture surfaces are fresh. Both are observed only in the welded units with joints distributed uniformly throughout and fractures concentrated near the upper boundaries of the Trail Ridge and more strongly the Grouse Canyon. Caliper and density logs from nearby drill holes indicate sloughing, probably along open joint and fracture zones, throughout the Trail Ridge. The inability to hold mud in the upper 39 m of U20u-2 during logging suggests that many of these zones are interconnected as does the slough zone pattern observed in

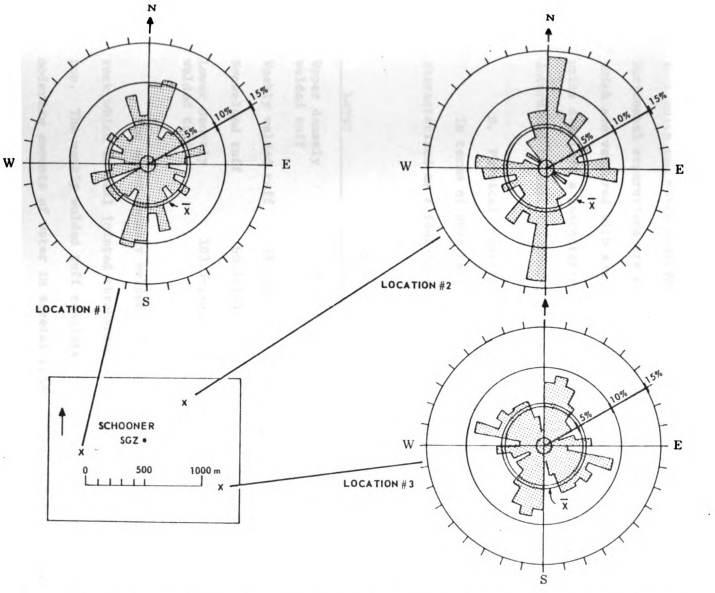

Figure 9. **Orientation of Joints in the Trail Ridge Member (Mapping Units "R" and "U") of the Thirsty Canyon Tuff at Three Locations Surrounding Schooner SGZ (After Purtymun, et al., 1969)**

...bbliations are a...

...m ml where observe...

...ml separations are ...

...mmeered with sec...

...splays a characteris...

...ly unit thickness...

...Physical Propert...

...terms of physical...

...rmed as a four-lay...

...ne	De...
...ely ...uff	
...welded tuff	38
...ded tuff	60
...ely ...uff	103

...he upper densely ...

...ich is well joint...

...he weakly welded ...

...ome amounts of wate...

...he nonwelded tuff...

...al zones of high wa...

...ilar to the upper ...

Figure 8.

Flow foliations are also common within many of the welded tuff units and where observed, parallel the present ground surface. Horizontal separations are mostly along foliation planes, some of which are veneered with secondary deposits. Each of the welded tuff units displays a characteristic set of in situ block sizes and shapes determined by unit thickness, jointing, and foliation.

D. Physical Properties

In terms of physical properties the Schooner site can be characterized as a four-layer system (Fig. 6):

Layer	Depth (m)	Mean Density (g/cc)	Seismic Velocity (m/sec)	Bulk Modulus (GPa)
Upper densely welded tuff	0-38.7	2.3	2200	6.3
Weakly welded tuff	38.7-60.7	1.6	1170	2.8
Nonwelded tuff	60.7-103.3	1.5	1340	1.5
Lower densely welded tuff	103.3-148.1	2.2	2030	7.9

The upper densely welded tuff consists of dry, dense, strong rock which is well jointed throughout and slightly fractured near the top. The weakly welded tuff consists of porous, weak rock containing moderate amounts of water in several zones, especially in the upper 7 m. The nonwelded tuff is a very porous, very weak rock with several zones of high water content. The lower densely welded tuff is similar to the upper unit except that it is more fractured.

…ner densely we…

…rations in their …

…correlate with th…

…ed tuff unit var…

…ly with gross p…

…rence Livermore …

…er media using bo…

…contains a sum…

The upper densely welded tuff and the weakly welded tuff units display variations in their physical properties with depth which generally correlate with the mapping units. Physical properties of the nonwelded tuff unit vary greatly with depth and mapping units correlate only with gross property changes.

Lawrence Livermore Laboratory measured physical properties of the Schooner media using both in situ and laboratory techniques. Appendix A contains a summary of their results.

TRANSIENT

sented are major

rmal and side-on c

mation of the resu

m detailed discuss

ing ejecta masses

re presented f

A. Major Processe

1. Mounding

The ground surfac

m detonation wit

e, Lorer (1972).

relatively cons

cration phase) to

e mound grew, lar

ion (Fig. 10a, b

from the ground

e mound growth

the ratio of maxi

Fig. 11). Maximum v

ching 65 m/sec or

ec.

CHAPTER III

TRANSIENT CRATERING PHENOMENA

Presented are major transient cratering processes observed from overhead and side-on cinema records that are important in the interpretation of the resultant crater and ejecta field, followed by a more detailed discussion of the distribution and time sequence of impacting ejecta masses. Selected photographs of the Schooner detonation are presented in Figures 10 and 11.

A. Major Processes

1. Mounding

The ground surface at SGZ began to rise (spall phase) at 0.08 sec after detonation with upward velocity increasing to 50 m/sec by 0.2 sec, Rohrer (1972). From 0.2 to 0.6 sec the upward velocity remained relatively constant followed by a second increase (gas acceleration phase) to 58 m/sec by 1.7 sec, just prior to venting. As the mound grew, large circumferential cracks formed in the soil overburden (Fig. 10a, b). Mound growth was reasonably symmetrical viewed from the ground surface southeast of SGZ. Viewed from overhead the mound growth was elongated in a northeast-southwest direction with the ratio of maximum to minimum radii ranging from 1.7 to 2.2 (Fig. 12). Maximum vertical mound velocity occurred southwest of SGZ, measuring 65 m/sec or 12% greater than the peak velocity recorded above SGZ.

a.
(0.8 sec)

b.
(1.9 sec)

c.
(2.6 sec)

d.
(4.0 sec)

0 300
Meters

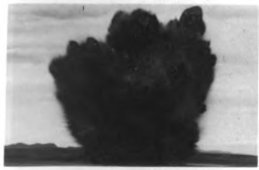

e.
(6.0 sec)

f.
(13.0 sec)

Figure 10. **Schooner Detonation Sequence from 0.8 to 13.0 Seconds after Detonation as Observed from Ground-Based High-Speed Cinema Located at Azimuth 145° and 5,738 m from SGZ**

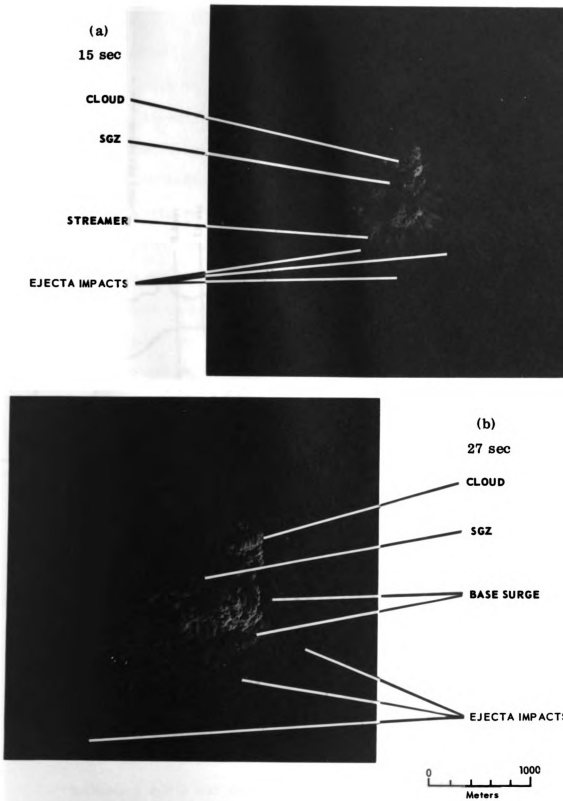

Figure 11. Overhead Views of Schooner 15 and 27 Seconds after Detonation


MOUND PATTERNS
VENT PATTERNS
0.5 sec
1.0 sec

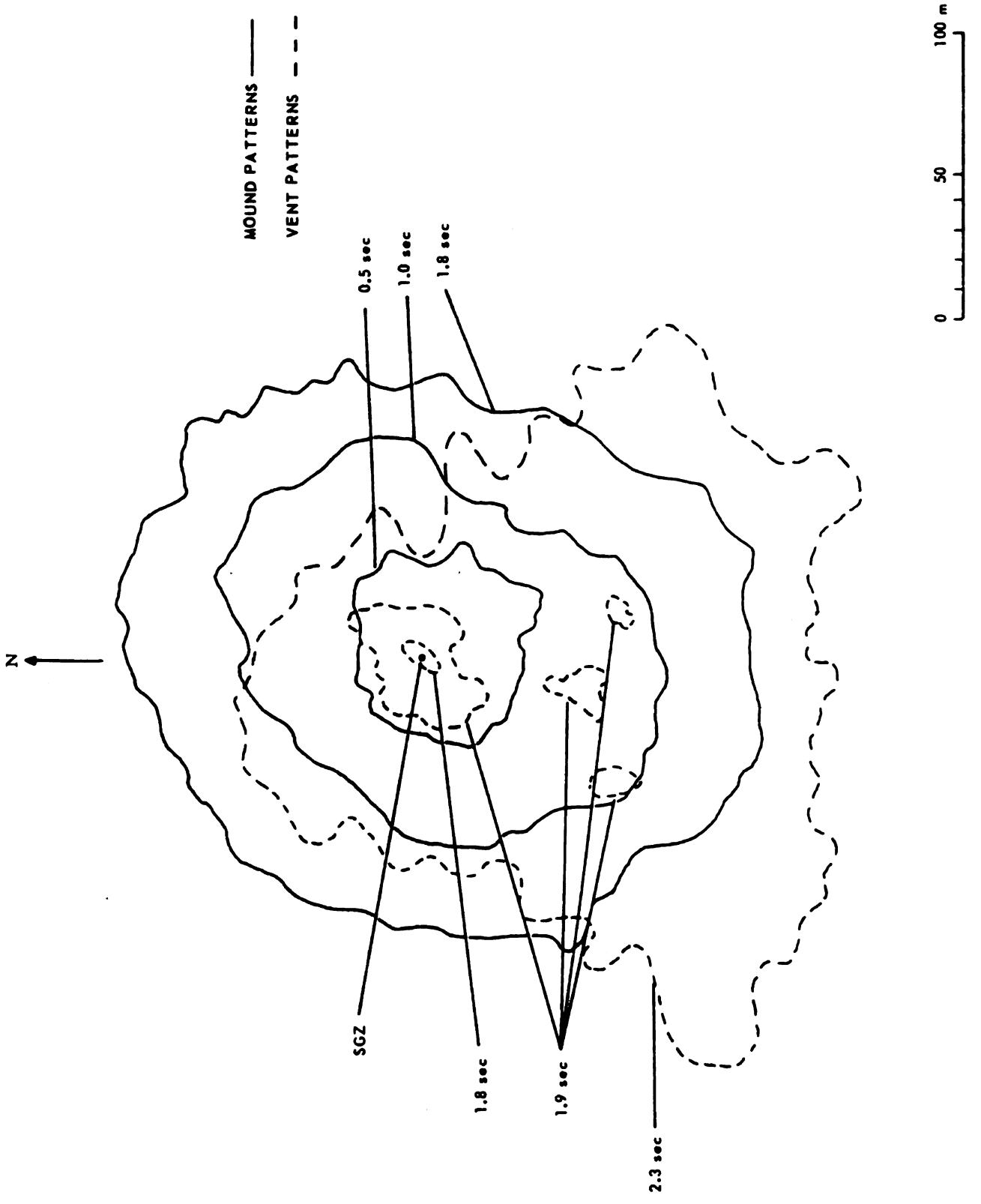

Figure 12. Mound Development and Venting Patterns from 0.5 to 2.3 Seconds after Detonation as Observed from Overhead High-Speed Cinema

1 Ejection

ering began at 1.

ntially above SGZ

ge and still risi

ove SGZ followe

ed along an ar

The four cente

e mound area

minous ejecta

by Rohrer (1972)

rtheast-southwest mo

1.1 sec a broad

ined centered app

persisted until 5.

minous jet approx

ing to 600 m from SG

also observed; but no

only one vertical v

served at 1.9 sec pr

ee Fig. 10b, c). Th

with the southeas

ent remained visible

ominated mound was ov

between 3 and 5 se

) m across exited i

2. Ejection

Venting began at 1.75 sec (Fig. 10b) with the mound surface 88 m vertically above SGZ and approximately 9 m high at the final crater edge and still rising at 2 m/sec. First venting occurred directly above SGZ followed at 1.88 sec by three new centers equally spaced along an arc approximately 60 m southwest of SGZ (Fig. 12). The four centers had coalesced by 1.96 sec and by 2.10 sec the entire mound area was engulfed in a plasma of incandescent gases and luminous ejecta fragments with highest temperature recorded by Rohrer (1972) of 2590°C. Early vent patterns paralled the northeast-southwest mound elongation.

By 2.1 sec a broad three-lobed triangular blanket of plasma had developed centered approximately 60 m southwest of SGZ. This pattern persisted until 5.4 sec with the southwest lobe developing into a luminous jet approximately 60 m above the ground surface and extending to 600 m from SGZ by 7.9 sec (Fig. 10c). A few other jets were also observed; but none extended out as far nor persisted as long. Only one vertical vent not obscured by the mound disassembly was observed at 1.9 sec propagating downward towards the ground surface (Fig. 10b, c). This vent between 115° and 125° was closely aligned with the southeast plasma lobe of Figure 12. The plasma blanket remained visible until 8.5 sec at which time the partially disassembled mound was over 500 m high.

Between 3 and 5 sec several thousand luminous masses of ejecta up to 3 m across exited in ballistic trajectories from the upper

...of the mound throu...

...ally, exit angles ver...

...of 300 to 400 m/sec.

...rease to near 45° whil...

...of these ejecta masse...

...flight and some impa...

...from the last luminou...

...idence presented

...ejecta masses apparent...

...ere with fused glass (s...

...ured at later times,

...or more probably f...

...ized by the plasma; i...

...plasma blanket or fro...

Another type of e...

...from the partially di...

...ring at 4 sec. The...

...ased in number and r...

...ta masses in that th...

...ed, some up to 50 m...

...ments were luminous.

...to 30 and 60 to 90...

...sequently behind the...

...from observed impact...

portion of the mound through the plasma blanket (Fig. 10d, e). Initially, exit angles were near vertical with velocities on the order of 300 to 400 m/sec. With time, exit angles gradually decreased to near 45° while velocities quickly decreased to 100 m/sec. Many of these ejecta masses remained luminous for up to one-half of their flight and some impacted in this condition. Viewed from the southeast the last luminous impact was recorded at 22 sec.

Evidence presented in Chapter VII indicates that most impacting ejecta masses apparently were nonluminous; i.e. they were not coated with fused glass (solidified plasma). Either they exited from the mound at later times, presumably when plasma temperatures were lower, or more probably from portions of the mound which were not affected by the plasma; i.e. from the outer mound surface beneath the plasma blanket or from fringes of the flap segments.

Another type of ejecta mass, termed streamers, were observed to exit the partially disassembled mound in ballistic trajectories beginning at 4 sec. These masses, several hundred to perhaps a thousand in number and ranging up to 3 m across, differed from other ejecta masses in that they formed thick contrails of dust (ejecta fines), some up to 50 m in diameter (Fig. 10e, f, and 11a). Some streamers were luminous. Exit angles and velocities averaged between 60° to 70° and 60 to 90 m/sec, respectively. Streamers impacted consistently behind the previously discussed welded blocks with maximum observed impact at 700 m and 19 sec.

h high resolution

ium of ejecta, belie

ne of streamers stoppe

ue to having cor

ming unit "c".

l. Deposition

ion after initial

ne occurred first by t

generated during the

ase of the base surge

ome crater nor the m

several minutes aft

ad ceased. Data

of the ejecta w

organized radially

ections were probabl

erations of the base

Individual ejecta

ths in front of the

to 2150 m (Fig

ons resulted with cl

m. These ejecta

tonary craters and

On high resolution photography streamers are seen to consist of a core of ejecta, believed to be compressed, nonwelded tuff. A number of streamers stopped forming contrails prior to impact, possibly due to having cores of a more denser, weakly welded tuff; i.e. mapping unit "c".

3. Deposition

Soon after initial venting, details of the mound disassembly became obscured first by the plasma, second by the large quantity of dust generated during the mound breakup, and third (and later) by the buildup of the base surge and cloud. As a result, neither the Schooner crater nor the majority of the ejecta field were observable until several minutes after detonation by which time all movement of ejecta had ceased. Data presented in Chapters IV-VII will show that over 90% of the ejecta was deposited in a series of overturned mound flaps arranged radially outward like spokes about a hub (the crater). These flaps were probably emplaced by 15 sec as inferred from observations of the base surge.

Individual ejecta masses were observed impacting the ground surface in front of the base surge from 11 to 71 sec over ranges from 380 to 2150 m (Fig. 11). Upon impact large secondary ejecta sprays resulted with cloud heights and diameters growing as large as 100 m. These ejecta masses are typically associated with the secondary craters and secondary ejecta fields which they produced.

ge Formation

base surge, a do

by the flap segme

ssumed breaking thr

. The leading ed

mum velocity of 12 t

(See Fig. 13). Initi

ed number of lobes

ng edge. Afte

ensal cauliflower-l

ere line up with fla

ese lobes tended to li

Vertical stabilizat

ge of 670 and 4220 m

(See Fig. 13), photogr

shows that after stab

the spreading along t

deposits were pushe

deposits.

5. Cloud Formatio

The cloud began t

ceded by 4 min at a

pectively (Cudiksen,

ed up to 700 m move

ud above moved ze

ded from the clou

4. Base Surge Formation

The base surge, a doughnut-shaped cloud of fines formed primarily by the flap segments impacting the ground surface, was first observed breaking through the disassembled mound area at 13 sec (Fig. 10f). The leading edge of the base surge traveled forward at an average velocity of 12 to 18 m/sec, with forward progress ceasing by 71 sec (Fig. 13). Initially the leading edge of the base surge exhibited a number of lobes extending 150 to 200 m in front of the average leading edge. After 21 sec these protrusions became muted and a general cauliflower-like pattern developed. Early lobes tended to line up with flap segments, while the latter-time and broader lobes tended to line up between flap segments.

Vertical stabilization occurred by 4 min at a mean height and diameter of 670 and 4220 m (Gudiksen, 1970). The final base surge pattern (Fig. 13), photographed several days after the event, indicates that after stabilization southerly surface winds inhibited further spreading along the south. To the north and northeast, base surge deposits were pushed downwind and are indistinguishable from cloud deposits.

5. Cloud Formation

The cloud began to develop soon after venting and had stabilized by 4 min at a mean height and diameter of 3960 and 2400 m respectively (Gudiksen, 1970). The base of the cloud from ground surface up to 700 m moved generally north at 1 to 5 m/sec while that portion above moved generally northeast at 7 to 18 m/sec. Surface deposits from the cloud were contained within the base surge pattern

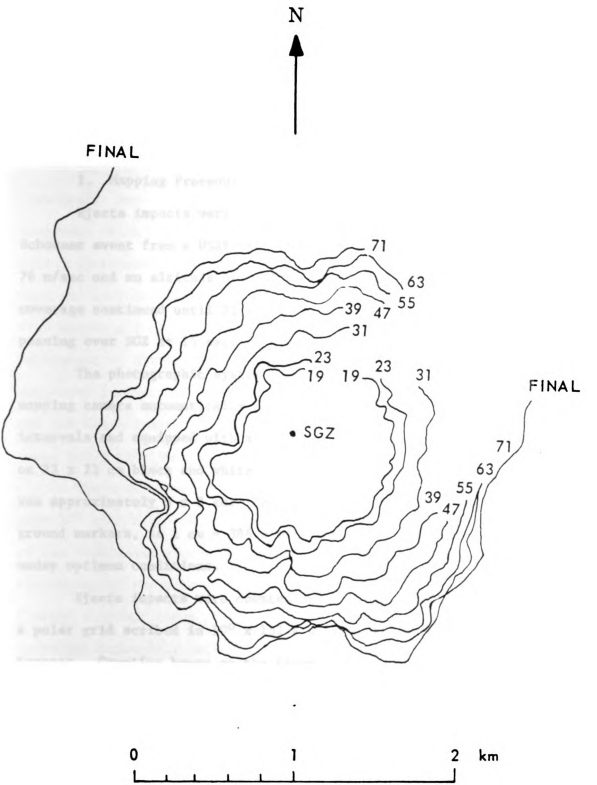

NOTE: Numbers are seconds after detonation

Figure 13. Base Surge Patterns as a Function of Time as Observed from Overhead Time Sequencing Photography

...the northeast q...

...1

...1. Ejecta Impacts

...2. Mapping Proced...

...Ejecta impacts were...

...ment from a USA...

...and an altitude o...

...continued until 7...

...over SGZ at 15 sec...

...The photographic sy...

...camera automatical...

...rolls and equipped wi...

...x 12 cm black and w...

...approximately 8 x 8 k...

...meters, is 1 cm =...

...optimum conditions.

...Ejecta impacts wer...

...grid scribed in l...

...Counting began...

...(11 sec) and conti...

...were observed. T...

...photograph using...

...photographs are...

except in the northeast quadrant where they extended well beyond to 9000 m.

B. Ejecta Impacts

1. Mapping Procedures

Ejecta impacts were photographically recorded during the Schooner event from a USAF C-130 aircraft tracking east to west at 76 m/sec and an altitude of 7620 m above ground surface. Photo coverage continued until 71 sec after detonation with the plane passing over SGZ at 15 sec.

The photographic system consisted of a standard KC-1(B) mapping camera automatically sequenced at approximately 4 sec intervals and equipped with a 150.895 mm Planigon lens for recording on 23 x 23 cm black and white film. Area covered by a single photo was approximately 8 x 8 km. Photo scale, determined from a set of ground markers, is 1 cm = 386 m with a minimum resolution of 3 m under optimum conditions.

Ejecta impacts were counted on each photograph by overlaying a polar grid scribed in 10^{o} x 152.4 m areas and marking all new impacts. Counting began on the first photograph exhibiting a visible impact (11 sec) and continued through successive photos until no new impacts were observed. The scribed grid was accurately repositioned on each photograph using recognized terrain markings. Portions of two such photographs are reproduced in Figure 11.

...Distribution of...

...total of 4383 im...

...ions from 380 to 21...

...11, and 47 sec. D...

...ined. Dominating was...

...ower which by 23 sec...

...Correspondingly, t...

...ar particularly to...

...numerous local conc...

...ment of these was...

...ined luminous jet.

...the depositional pa...

...being partially f...

The cumulative n...

...0 sector is pres...

...the continuous ejec...

...ation of the cont...

...ner concentrations...

...ulate reasonably w...

...better correlatio...

...ry and valley ar...

...ated by dashed...

...ning sectors selde...

...of the concentra...

...ulated by 15 sec...

2. Distribution of Impacts

A total of 4383 impacts were counted from 11 to 71 sec over distances from 380 to 2100 m. Figure 14 presents observed impacts at 15, 31, and 47 sec. During the first 31 sec two basic patterns developed. Dominating was the strong concentration of impacts to the southeast which by 23 sec had broadened to include most of the east side. Correspondingly, there was a noticeable lack of impacts to the west and particularly to the northwest. Superimposed on this pattern were numerous local concentrations which changed with time. The most persistent of these was to the southwest in line with the previously mentioned luminous jet. After 31 sec number of impacts decreased and the depositional pattern become more symmetrical with low density areas being partially filled in.

The cumulative number of impacts as a function of time for each 10^{o} sector is presented in Figure 15 with ray and valley axes of the continuous ejecta blanket indicated (see Chapter IV for a discussion of the continuous ejecta blanket). There are 8 major and 2 minor concentrations of impacts with intervening lows which correlate reasonably well with valley and ray axes, respectively. That better correlation is not present is possibly due to the fact that ray and valley axes are typically skewed over their total range (indicated by dashed lines in Figure 15) such that the 10^{o} impact-counting sectors seldom match 1:1 with an entire ray or valley axis. Most of the concentrations (with a notable exception at 315^{o}) are recognized by 15 sec and all are well defined by 27 sec, when most

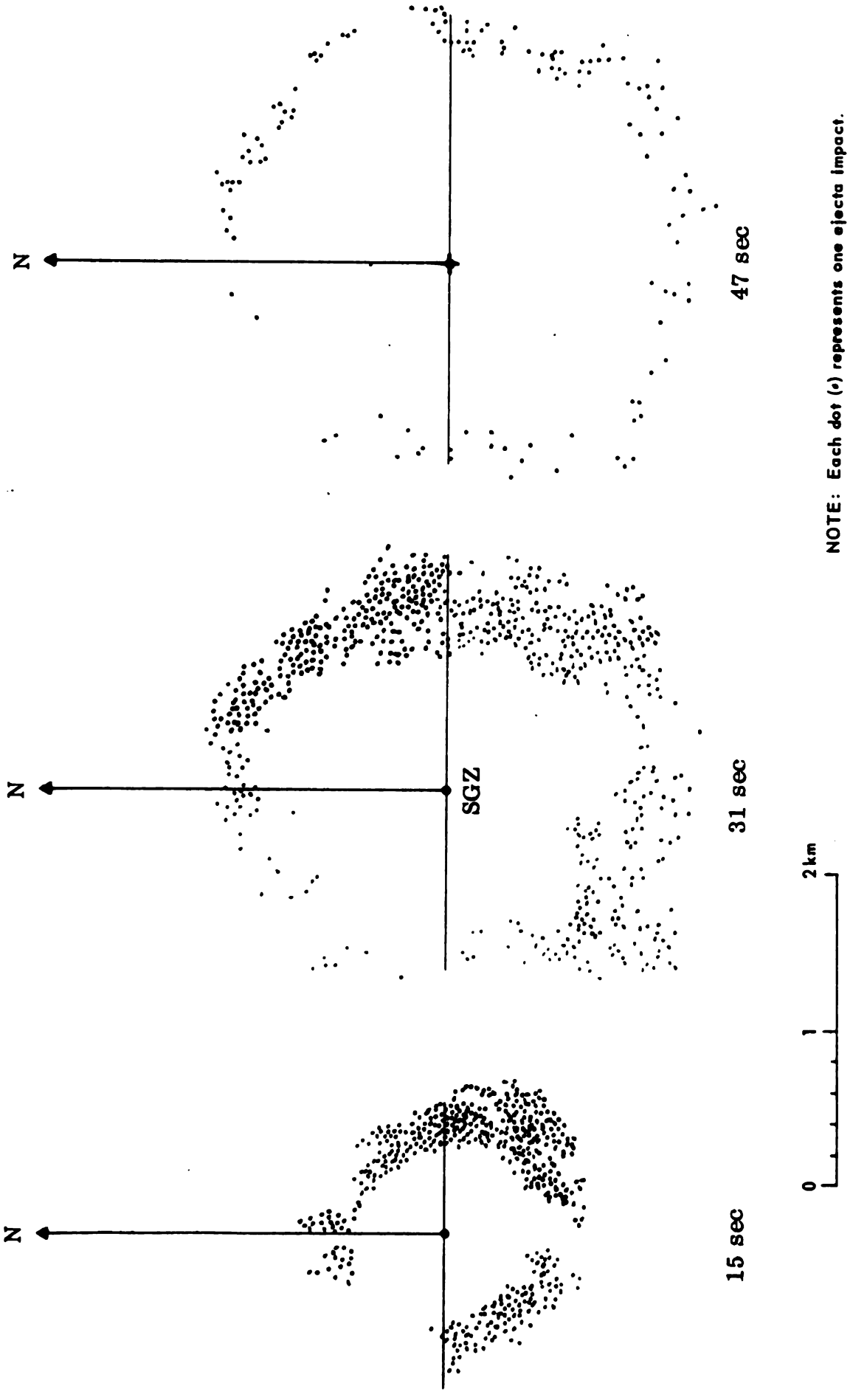

Figure 14. Ejecta Impact Distributional Patterns Observed from Overhead Time Sequencing Photography

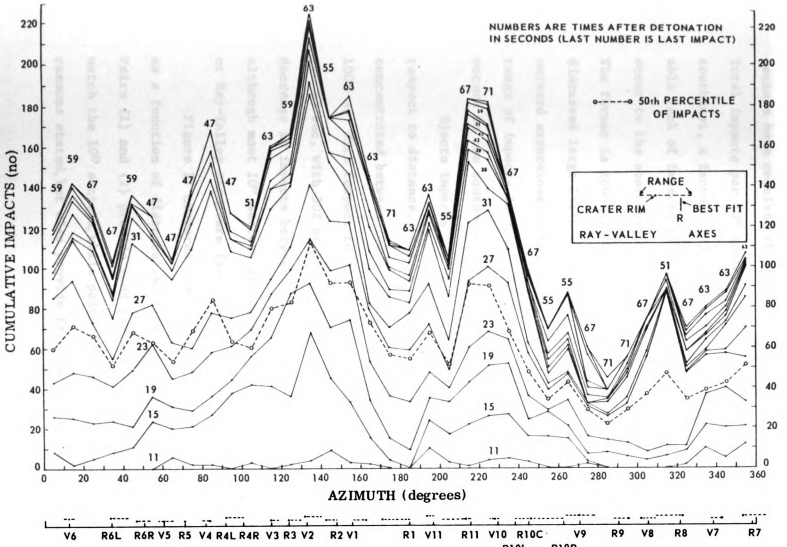

RAY (R) AND VALLEY (V) AXES WITH RANGE OF SKEWING (- - - -)

Figure 15. Cumulative Number of Ejecta Impacts at Four-Second Intervals as a Function of Azimuth

ers have received at

l impacts per 10^{0} sec

ntast, a factor of 5

ber of impacts to t

er to the southeast (1

ber is downhill wh

ased large luminous

ner excursions in the

er of impacts is uphil

er to the southwest (

Ejecta impacts are

ect to distance, impa

centrated between 700

km. With respect to

km sec, with 50% of t

rease in impacts betwe

ough most 10^{0} sectors

ge-valley structure

Figure 17 compares

a function of distanc

ion 2) and (2) provid

ver the 10^{0} sectors, wh

bases stated, but also

sectors have received at least 50% of their total accumulation. Total impacts per 10° sector range from 45 on the west to 226 on the southeast, a factor of 5 variation. In general, there is a noticeable lack of impacts to the west, which is uphill. Most impacts occur to the southeast (135°) and secondly to the southwest (225°). The former is downhill while the latter is aligned with the previously discussed large luminous jet in that direction. Both are aligned with outward excursions in the early venting pattern (Fig. 12). Minimum range of impacts is uphill to the west (295°) and maximum range occurs to the southwest (225°).

Ejecta impacts are not evenly distributed (Fig. 16). With respect to distance, impacts are peaked near 1200 m and heavily concentrated between 700 m and 1500 m with the 50th percentile near 1000 m. With respect to time, impacts are concentrated between 15 sec and 35 sec, with 50% of the impacts occurring by 25 sec. The slight decrease in impacts between 15 sec and 27 sec is not understood although most 10° sectors are similar, irrespective to either azimuth or Ray-Valley structure (see Chapter IV).

Figure 17 compares cumulative distributions of ejecta impacts as a function of distance and time for four pairs of 10° sectors. Pairs (1) and (2) provide good ray and valley contrasts; i.e. axes match the 10° sectors, while pairs (3) and (4) were selected for reasons stated, but also provide fair ray and valley contrasts.

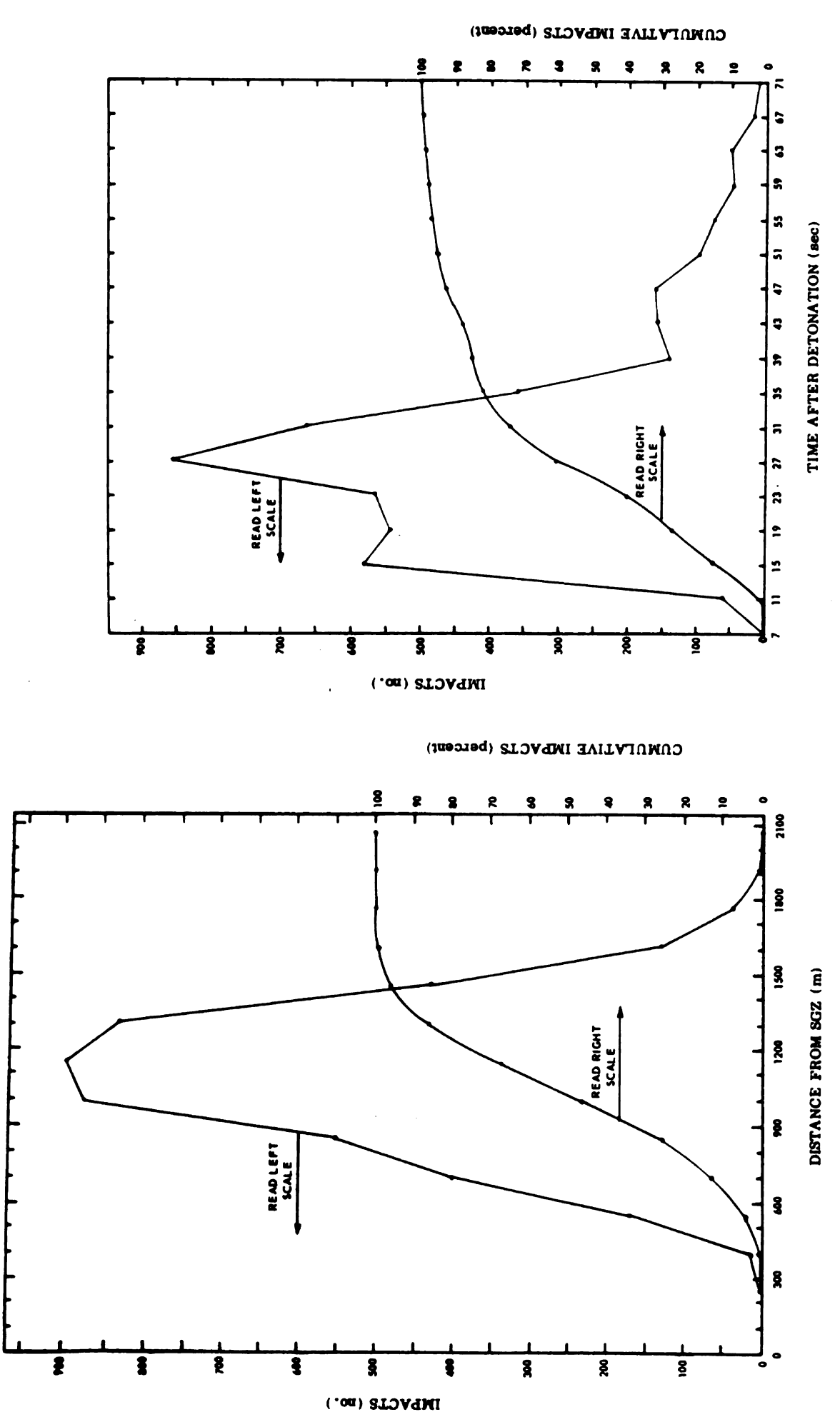

Figure 16. Number and Cumulative Number of Ejecta Impacts as a Function of Distance and Time

Figure 17.

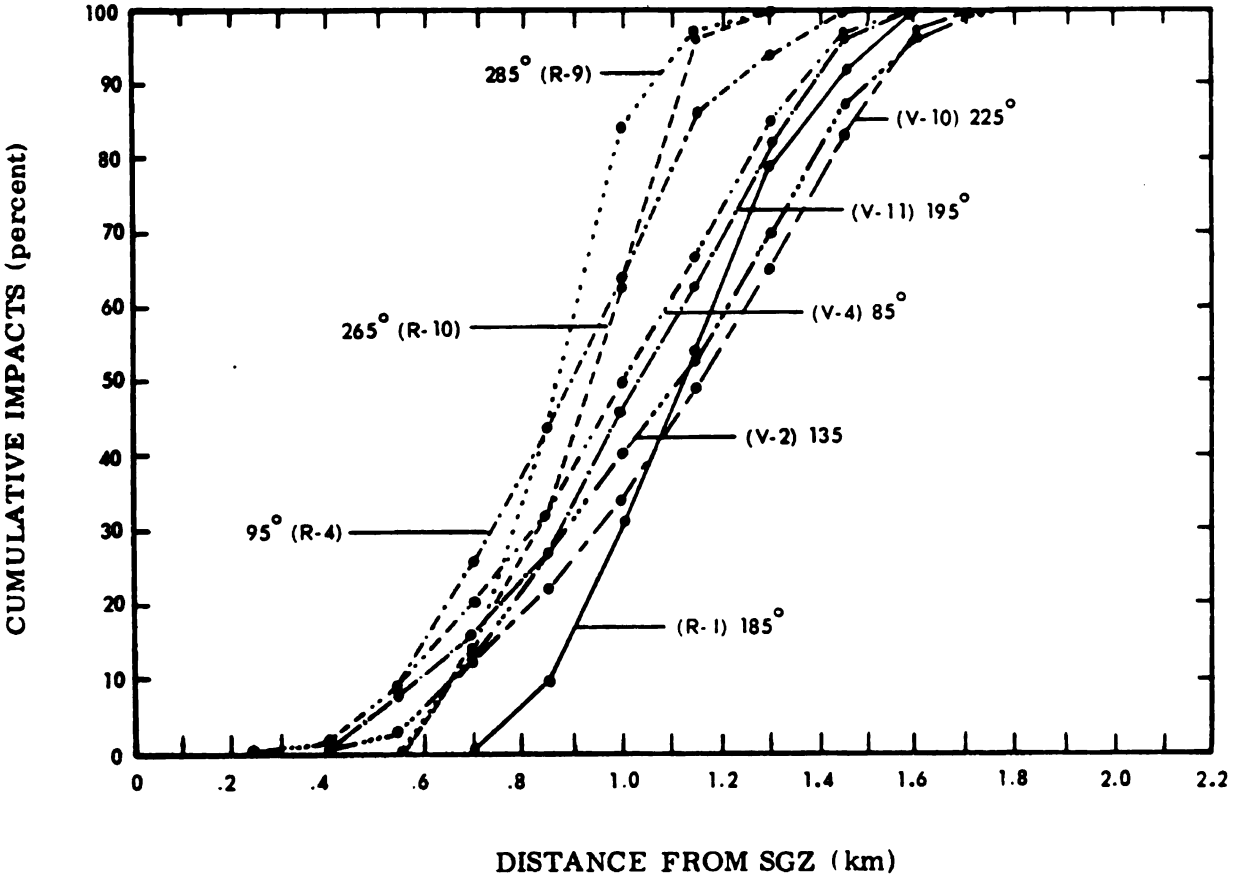

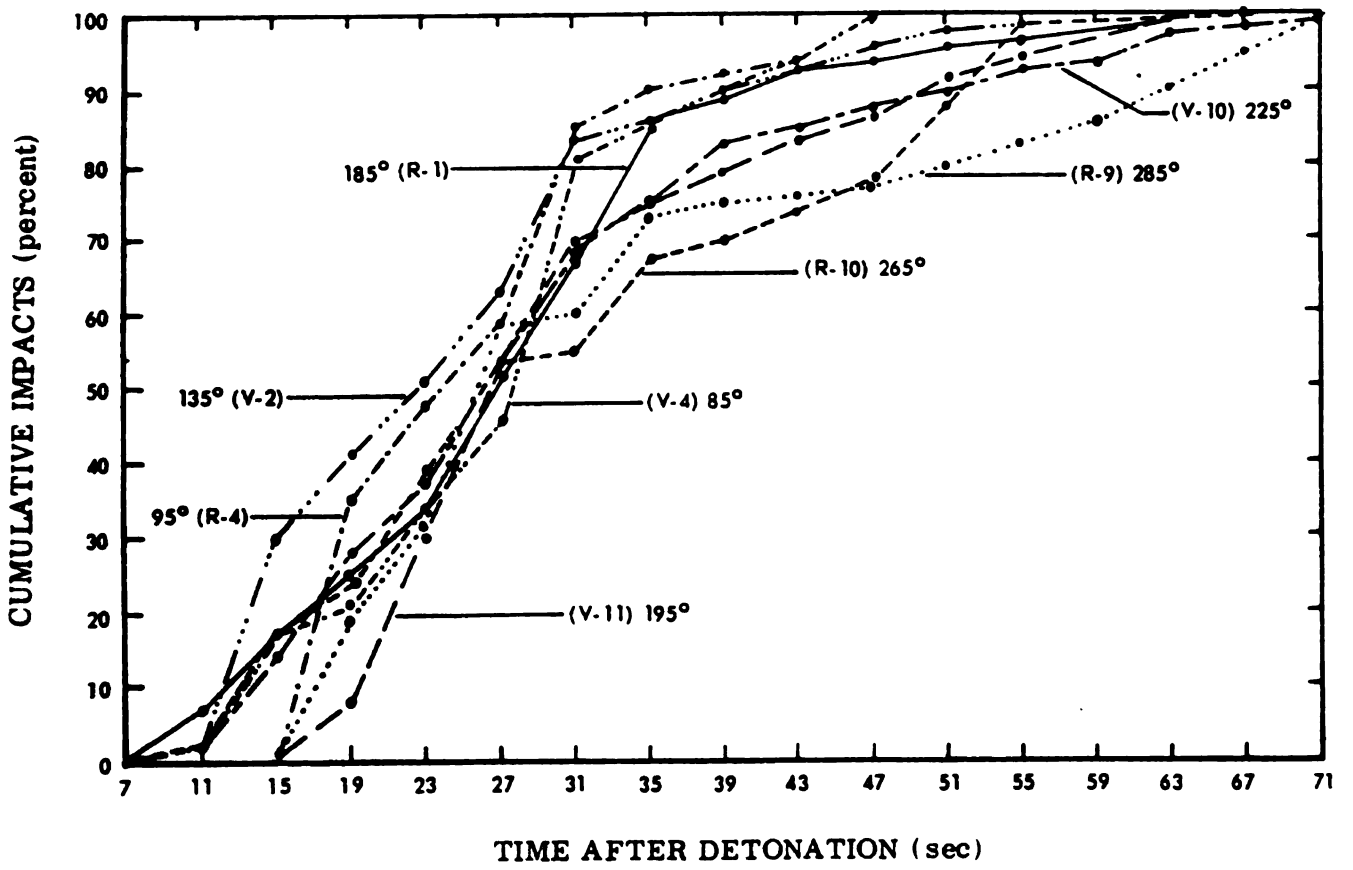

Figure 17. Cumulative Distributions of Ejecta Impacts for Selected Azimuths as a Function of Distance and Time

(3)

(2)

(3)

(4)

The distribution o

valley axes exami

ear range. Maximum r

which is alligne

while overall, imp

ment with either

rest uphill. Th

maller and farthe

masses on the we

the mound later

the higher traject

1. Time Sequen

There were two

ber of ejecta as s

for all impacts

ance [2/number x

ented of a stead

an average ground

and 3-4 are sy

(1)	85°	V-4*
	95°	R-4
(2)	195°	V-11
	185°	R-1
(3)	135°	Downhill (V-2)
	285°	Uphill (R-9)
(4)	225°	Maximum impact range (V-10)
	265°	Minimum impact range (∿R-10)

The distribution of impacts is basically different for those ray and valley axes examined, with valley impacts distributed over a greater range. Maximum range is generally greatest downhill, except for V-10 which is aligned with the previously discussed southwest jet. While overall, impacts as a function of time appear insensitive to alignment with either ray or valley axes, the last 25% of impacts is greatest uphill. Thus, it appears that impacts downhill occurred both earlier and farther out than those uphill. This suggests that ejecta masses on the west did one or more of the following: (1) exited the mound later, (2) exited with lower velocities, or (3) traveled higher trajectory paths.

3. Time Sequence of Impacts

There were two characteristically different phases in the impact of ejecta as shown in Figure 18. Plotted are time-distant data for all impacts in terms of the range and the weighted mean distance [Σ(number x distance) ÷ total number]. The first phase consisted of a steadily outward progressing curtain of impacts moving at an average ground speed of 42 m/sec to 1200 m. The second phase,

*V-4 and R-4 are symbols for Valley 4 and Ray 4 respectively.

Fig 13. Freq
Dist

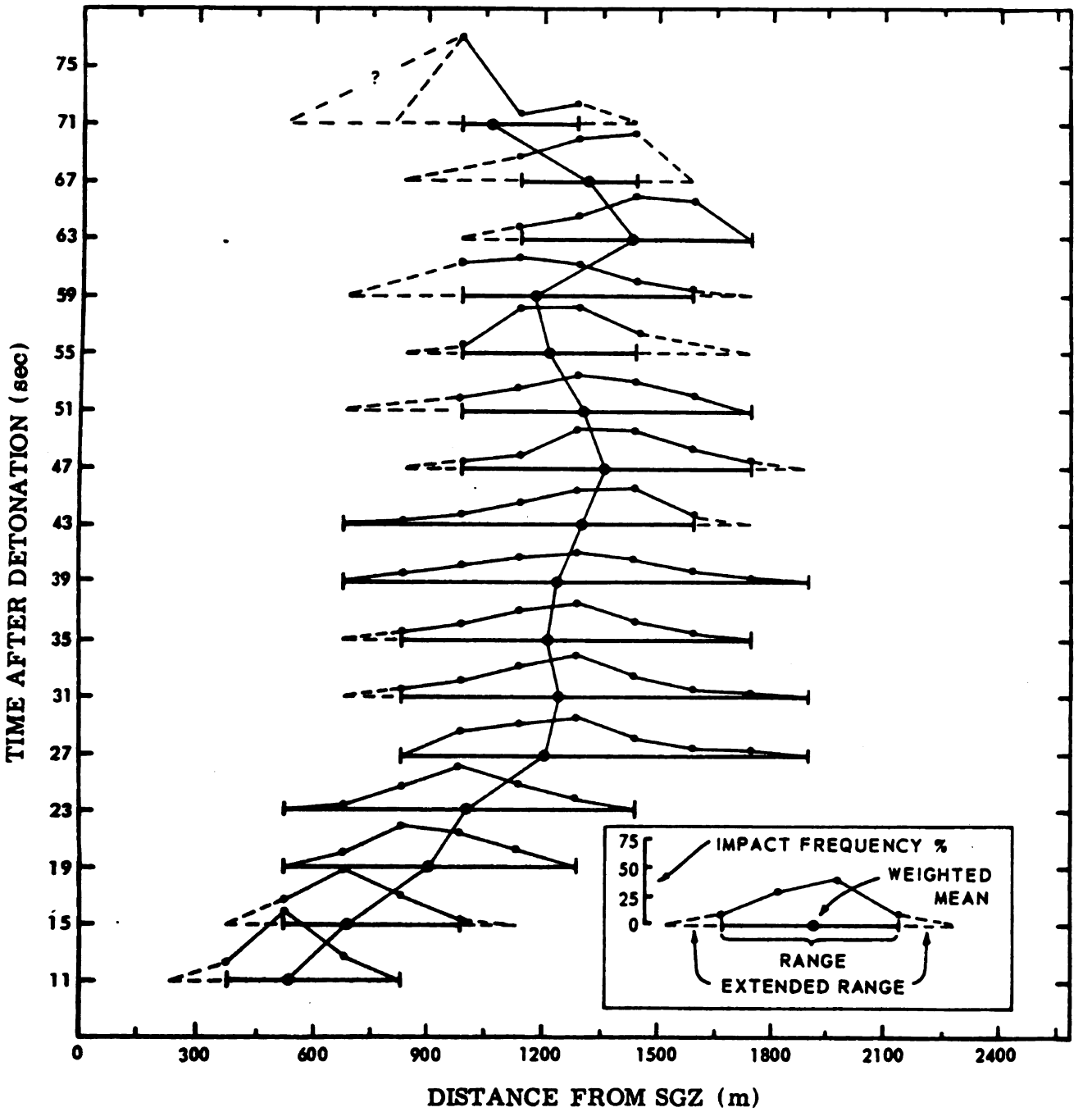

Figure 18. Frequency of Ejecta Impacts as a Function of Distance and Time

ximately 17 sec, cons

ion progress of the c

ns substantially char

ion. Note that the i

roximately when 50% of

During a given tim

ccurring from a mini

ximum 38 sec. Maxim

ent occurred near t

ately to either side

ion data are estima

ximal and base surg

ions reach 20% of t

beginning by 27 sec, consisted of a series of oscillations in the forward progress of the curtain with neither mean nor maximum range values substantially changing throughout the remaining depositional history. Note that the initiation of the second phase occurs approximately when 50% of all impacts have occurred (Fig. 16).

During a given time interval impacts occurred over a distance range varying from a minimum of 600 m at 11 sec to a maximum of 1220 m at 39 sec. Maximum number of impacts during a given time interval occurred near the weighted mean distance and decreased smoothly to either side. Extended ranges on either side of the plotted data are estimates to account for those impacts obscured by the cloud and base surge. Only beyond 50 sec do the number of these impacts reach 20% of the total.

TIONAL CHARACTE

A. Definition of

By definition, the

original ground sur

portion above is

known crater and

an oblique photogr

from averaged pro

ured from the isopac

ical. Terms are mod

the Key to Symbols a

1. Crater

The apparent cra

ering processes mo

by water and wind

ion, consolidation

the crater rim,

crater sides. Th

ere being the bou

rial has occurre

upper sides of t

between the

result of a num

CHAPTER IV

DIMENSIONAL CHARACTERISTICS OF THE CRATER AND EJECTA FIELD

A. Definition of Major Features

By definition, the visible portion of the Schooner crater below original ground surface is termed the apparent crater while the visible portion above is termed the apparent lip. Major features of the Schooner crater and ejecta field can be seen in the aerial overhead and oblique photographs of Figures 19 through 22. Figure 23 presents an averaged profile of the Schooner crater and ejecta field prepared from the isopach map of Figure 24 with major features defined. Terms are modified from Hansen, et al. (1964) and listed in the Key to Symbols and Abbreviations.

1. Crater

The apparent crater is the void resulting from the sum of the cratering processes modified to a minor extent by post-event processes such as water and wind transport of ejecta fines into and within the crater, consolidation of the bulked fallback, mass slumping of ejecta from the crater rim, and tumbling of individual ejecta blocks down the crater sides. The true crater lies outside and below the apparent crater being the boundary beyond which no significant dislocation of material has occurred. On Schooner, the true crater is exposed along the upper sides of the apparent crater.

Between the true and apparent crater lies the fallback which is the result of a number of cratering processes including displacement

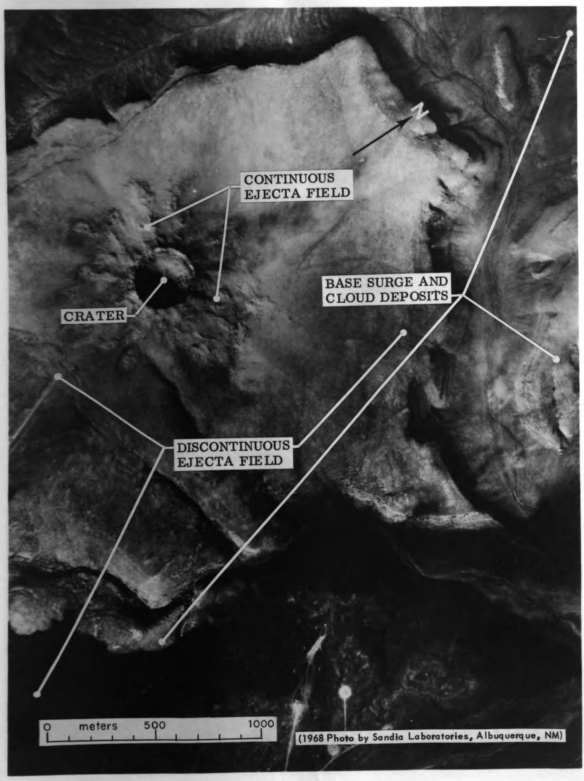

Figure 19. High Altitude Aerial Photograph of the Schooner Crater and Ejecta Field

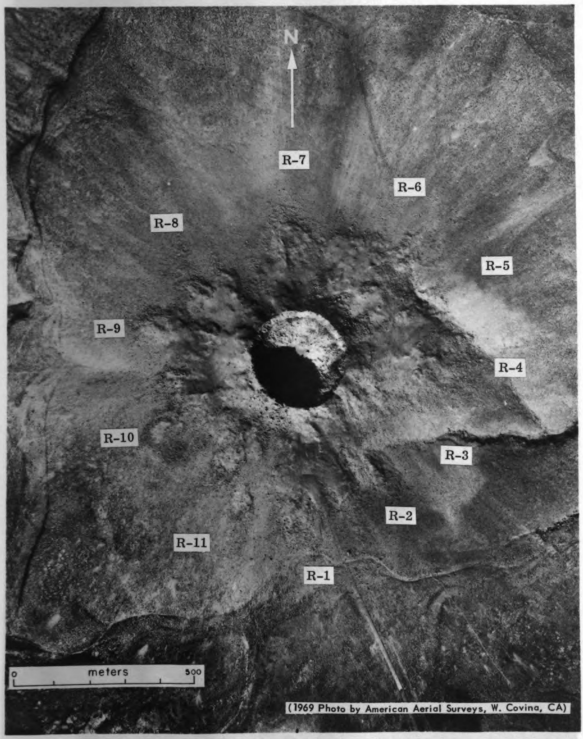

Figure 20. Intermediate Altitude Aerial Photograph of the Schooner Crater and Ejecta Field

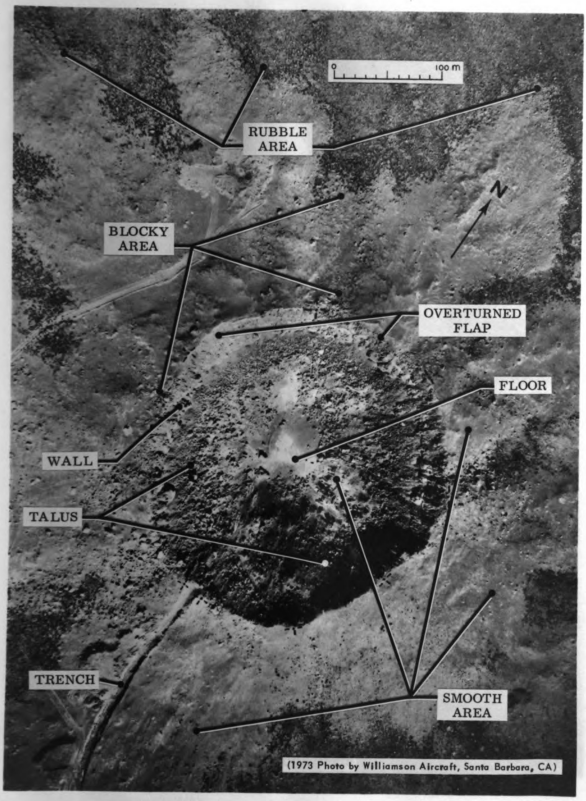

Figure 21. Low Altitude Aerial Photograph of the Schooner Crater and Ejecta Field

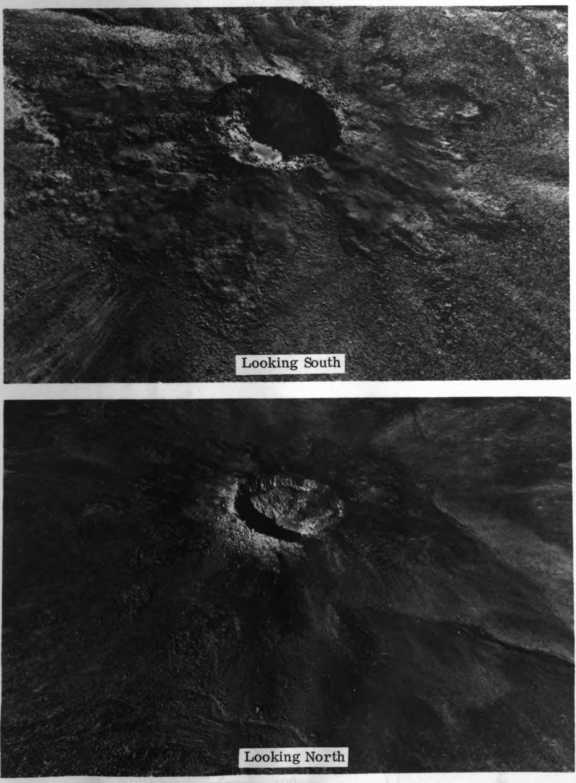

[Crater is 292.6 m Rim to Rim] (1969 Photos by American Aerial Surveys, W. Covina, CA)

Figure 22. Aerial Oblique Photographs of the Schooner Crater and Ejecta Field

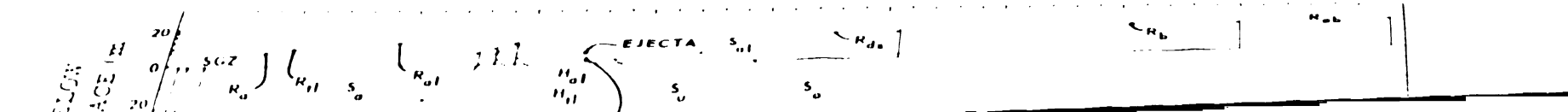
EJECTA

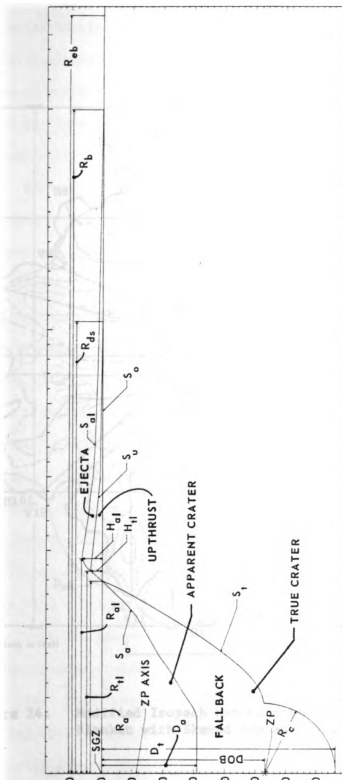

Figure 23. Averaged Profile of the Schooner Crater and Ejecta Field (See Key to Symbols and Abbreviations)

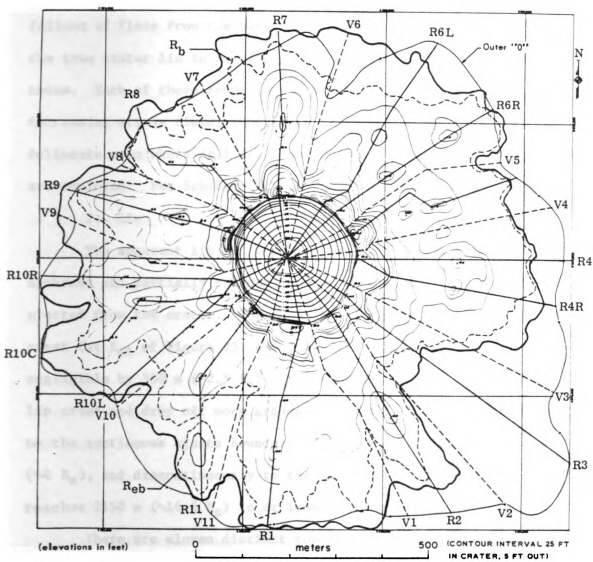

Figure 24. Modified Isopach Map of Schooner Crater and Ejecta Blanket with Skewed Ray and Valley Axes Indicated

of material within the crater, ballistic return of material originally ejected, collapse of portions of the mound after venting, failure of portions of the overturned flap along the crater rim, and fallout of fines from the base surge and cloud. Outside and below the true crater lie in succession the rupture, plastic, and elastic zones. Each of these zones is the imprint of a continually decreasing stress field; thus, each is imprecise and difficult to delineate even where drilling, excavation, and geophysical techniques are employed. For Schooner, these zones remain undefined.

2. Lip

The apparent lip is composed of the true lip, formed by the upthrust and partially relaxed ground surface, overlain by material ejected from the crater. The true lip peaks inside the crater lip crest (at R_{a1} of Figure 23) and drops off rapidly, becoming negligible by 300 m ($\sim$2.5 R_a). Ejecta deposits peak at the crater lip crest and drop off more gradually. They extend continuously out to the continuous ejecta boundary (R_{eb}), which averages 510 m ($\sim$4 R_a), and discontinuously to the maximum ejecta range (R_m), which reaches 2150 m ($\sim$16.5 R_a) in at least one direction.

There are eleven distinct topographic highs (crests) and intervening topographic lows (troughs) spaced unevenly along the crater rim. Each crest and trough gives way outward on a 1:1 basis to radial concentrations of ejecta (rays) and intervening sectors with little ejecta (valleys) (Fig. 20). Rays and valleys extend out to the continuous ejecta boundary and, as will be demonstrated in

Chapter VII, can be traced well into the discontinuous possibly leaving their imprint as far as the maximum ejecta range. This Ray-Valley structure is a key feature of the Schooner ejecta field against which the dimensional (Chapter IV), geomorphic (Chapter V), and geologic (Chapter VI) characteristics are compared.

The continuous ejecta field, also called the ejecta blanket, is comprised primarily of material from the overturned mound sections (flaps) overlain by discrete masses of ejecta that have impacted ballistically. The discontinuous ejecta field is comprised primarily of ballistic impacts together with some material from the ejecta blanket that has moved outward along the ground surface after initial emplacement. Secondary craters, formed by ballistic impacts of ejecta masses, are observed from the crater rim out to maximum ejecta range; but are concentrated between 3 and 6.5 R_a (400 and 850 m). The entire ejecta blanket and much of the discontinuous ejecta field is covered by thin, late-time, fallout deposits from the base surge and cloud.

Ejecta sizes are strongly bimodal, consisting of boulder-size blocks up to 9 m in length and sand-size fines. Blocks are derived from the upper densely welded tuff unit (0 to 38.7 m) with sizes and shapes varying about the crater radially, and to a lesser extent azimuthally. Blocks retain, to a large degree, their in situ shapes and are usually bounded by joint and foliation surfaces or by new surfaces paralleling these in situ surfaces. There are two notable exceptions, secondary craters and their associated secondary ejecta

fields and more significantly the rubble zones that make up portions of the rays. In both cases, block sizes are significantly comminuted downward with most in situ surfaces destroyed. In no case were blocks observed joined together as a result of the cratering processes.

Fines were derived from the weakly welded tuff and the upper portion of the nonwelded tuff (38.7 to ~75 m) and remain a consistent coarse to fine-sand size wherever observed. There are two minor exceptions. A small percentage (less than 1%) of fines was shock lithified into light frothy fragments a few centimeters up to one-half meter in size. Another equally small percentage of fines was melted and subsequently cooled to form the thin coating (up to a few centimeters) of fused glass encasing many blocks observed beyond the continuous ejecta boundary. Although portions of the weakly welded tuff were lightly cemented in situ, except for the "c" unit, no cemented ejecta masses were observed in the ejecta field.

B. Dimensional Relationships

The dimensional characterization of the Schooner crater and ejecta field was accomplished by aerial stereophotography and photogrammetric analysis, details of which are presented in Appendix B1. The resulting isopach map (Fig. 24) was used to generate most of the numbers and profiles presented in this chapter. Table 2 presents dimensions for major features of the Schooner crater and ejecta field. Those dimensions enclosed in parentheses were originally reported by Tewes (1970) based on initial work by American Aerial Surveys.

TABLE 2

SCHOONER DIMENSIONS

FEATURE	AVERAGE (m or m^3)	RANGE (m or m^3)
Apparent Crater Radius (R_a)	129.8 (129.9)*	111.6-147.5
Apparent Crater Depth (D_a)	63.4 (63.4)	-
Modified Crater Depth (D_a')	$\geq$ 76.0	71-82
Apparent Lip Radius (R_{al})	146.3 (147.2)	125.9-167.0
Apparent Lip Height (H_{al})	13.1 (13.4)	9.4-18.0
True Crater Radius (R_t)	129.8	111.6-147.5
True Crater Depth (D_t)	155.1	-
Ejecta Lip Height (H_{el})	6.4	2.1-12.2
True Lip Height (H_{tl})	6.7	3.0-8.2
Upthrust Radius (R_{ds})	304.8	-
Continuous Block Boundary (R_b)	447.5	243.8-563.9
Continuous Ejecta Boundary (R_{eb})	510.9	381.0-609.6
Cavity Radius (R_c)	46.9	-
Maximum Missile Range (R_m)	-	$\geq$ 2150
Apparent Crater Volume (V_a)	1,745,433 (1,745,433)	-
True Crater Volume (V_t)	3,840,130	-
Upthrust Volume (V_u)	383,538	-
Apparent Lip Volume (V_l)	1,895,063 (2,099,032)	-
Fallback Volume (V_f)	2,094,697	-
Continuous Ejecta Volume (V_c)	1,511,525	

*Values in parentheses were reported by Tewes (1970).

1. Apparent Crater

The apparent crater, bounded by the inner "0" contour of the isopach map (Fig. 24), is moderately asymmetric with largest radius and shallowest slope on the southeast and smallest radius and steepest slope on the west. The apparent crater radius gradually increases to a maximum of 147.5 m (14% above the mean of 129.8 m) on the southeast and then gradually decreases to a minimum of 111.6 m (14% below the mean) on the west (Fig. 25).

The crater wall dips an average of 65° (range 50° - 80°) on the north and west where it is exposed to a depth of 23 to 30 m and an average of 55° (range 40° - 65°) on the east where it is exposed to a depth of 8 to 15 m. The average dip of the fallback is near 33°; but locally reflects differing concentrations of blocks and fines together with local slump features which continue to develop and change with time.

2. Apparent Lip

The apparent lip lies between the inner "0" contour and the maximum ejecta range. The apparent lip radius (R_{al}), measured from SGZ to the crater lip crest, is moderately asymmetric ranging $\pm$ 14% about a mean of 146.3 m and closely paralleling R_a (Fig. 25). The apparent lip height (H_{al}) is asymmetric ranging from 9.4 to 18.0 m with a mean of 13.1 m and reflects the 11 crests and intervening troughs (Fig. 25). While the primary trends of R_a and R_{al} are independent of the Ray-Valley structure, secondary perturbations of

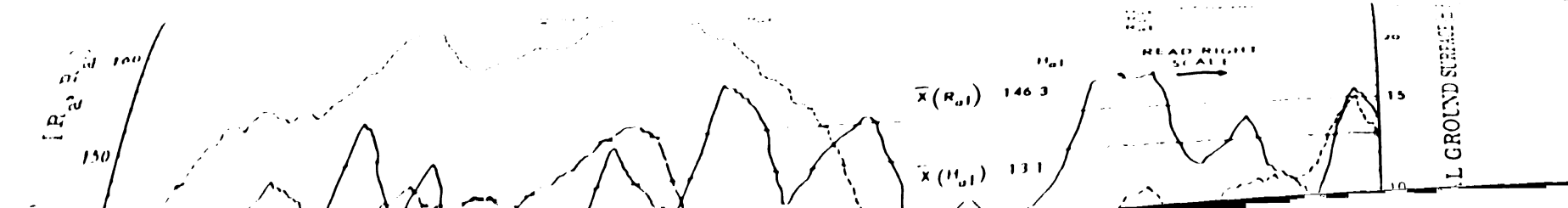
100
150
$\bar{x}(R_{al})$ 146 3
$\bar{x}(H_{al})$ 13 1
HEAD RIGHT SCALE
15
L GROUND SURFACE

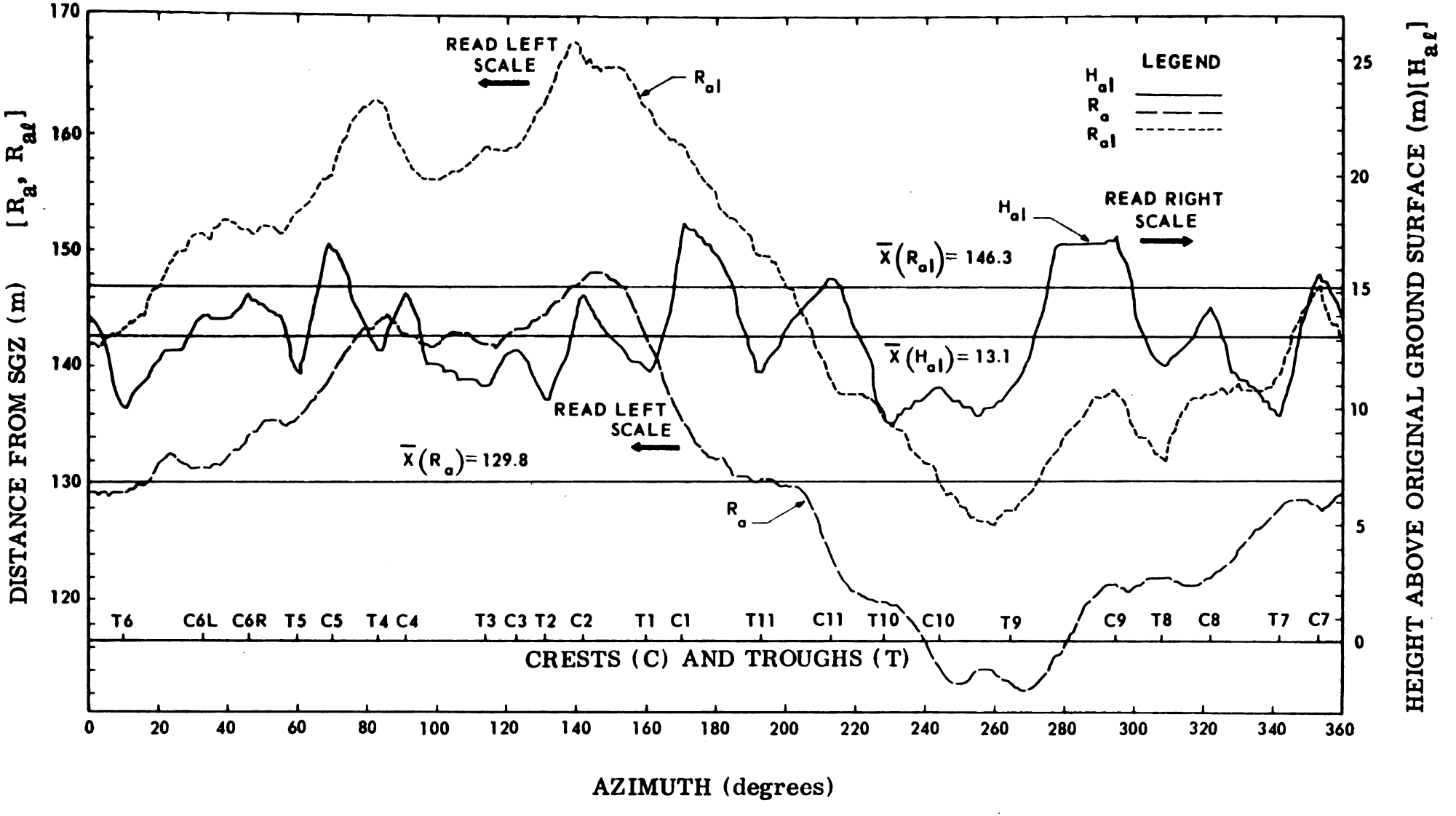

Figure 25. Apparent Dimensions . . . Crater Radius, Lip Radius, and Lip Height as a Function of Azimuth

R_{al} appear to line up with some crests and troughs; e.g. C-2*, 6, 7, 8, 9, and T-5, 7, 8, and 9.

a. Crests

Crests, bound by the inner "0" and approximately the outer 25 ft (7.6 m) contours, are composed of one or more segments of an overturned flap, each roughly semicircular in plan view. When viewed from the ray side, crests appear as a series of irregularly descending plateaus while on the crater side, they slope evenly down to the original ground surface with dips ranging from 20° to 40°. Note that prior to the failure along the hinge zone of the overturned flap, crater-side slopes were probably nearer vertical.

While crests are to a first degree similar in detail, they exhibit differences in shape, structure, and geology (see Chapter V. A). Crest peaks occur along the crater lip crest, except C-10 which is displaced over 30 m outward. Crest peaks are usually not symmetrically positioned with respect to the crest. Most crests contain a singularly distinct peak (C-1 and 7); but one is without a peak (C-3), and another is double peaked (C-6). As shown in the H_{al} plot of Figure 25, Crest 4 contains a poorly developed second peak, Crest 6 contains a poorly developed third peak, and Crest 9 contains a single peak that maintains a near constant elevation over 17° azimuth (~43 m).

In plan view, crest shapes vary from long (with respect to circumference) and narrow (C-11) to short and wide (C-7). Crest

*C-2, R-2, T-2, and V-2 are symbols for Crest 2, Ray 2, Trough 2, and Valley 2, respectively.

lengths, measured from trough to trough, range from 41 to 133 m ($\bar{x}$ = 92 m); while widths, measured perpendicular to the length, range from 48 to 88 m ($\bar{x}$ = 68 m). Spacing of crests is uneven about the crater varying from 17° to 51°.

The inner slopes (towards SGZ) average 33° for the overlying fines and 40° for the underlying blocks. It is these inner slopes, particularly the fines, which are being slowly eroded into the crater. Outer slopes average less than 10°, but approach 50° to 70° at plateau boundaries. Slopes between crests and troughs range up to 60° depending on the type (fines or blocks) and quantity of ejecta.

b. Troughs

Troughs, unlike crests, do not contain large concentrations of ejecta. They are therefore structurally and geologically simpler. They vary in shape from narrow (with respect to circumference) deep features (T-6 and 11) to broad shallow features (T-2) depending upon crest spacing and the degree of "flooding" (downward movement of ejecta) from crests. Trough widths vary from 1/4 to 1/2 that of the bounding crests; while inward and outward slopes are typically 25% and 50% steeper. Crests and troughs differ primarily in the amount of ejecta they contain.

Figure 26 presents a plot of the apparent lip height (H_{al}) and its two components, the upthrust or true lip height (H_{tl}) and the ejecta lip height (H_{el}) obtained from Figure 37 and adjusted for slope of the crater lip. The constant elevation lines are means for crests, troughs, and crests and troughs combined.

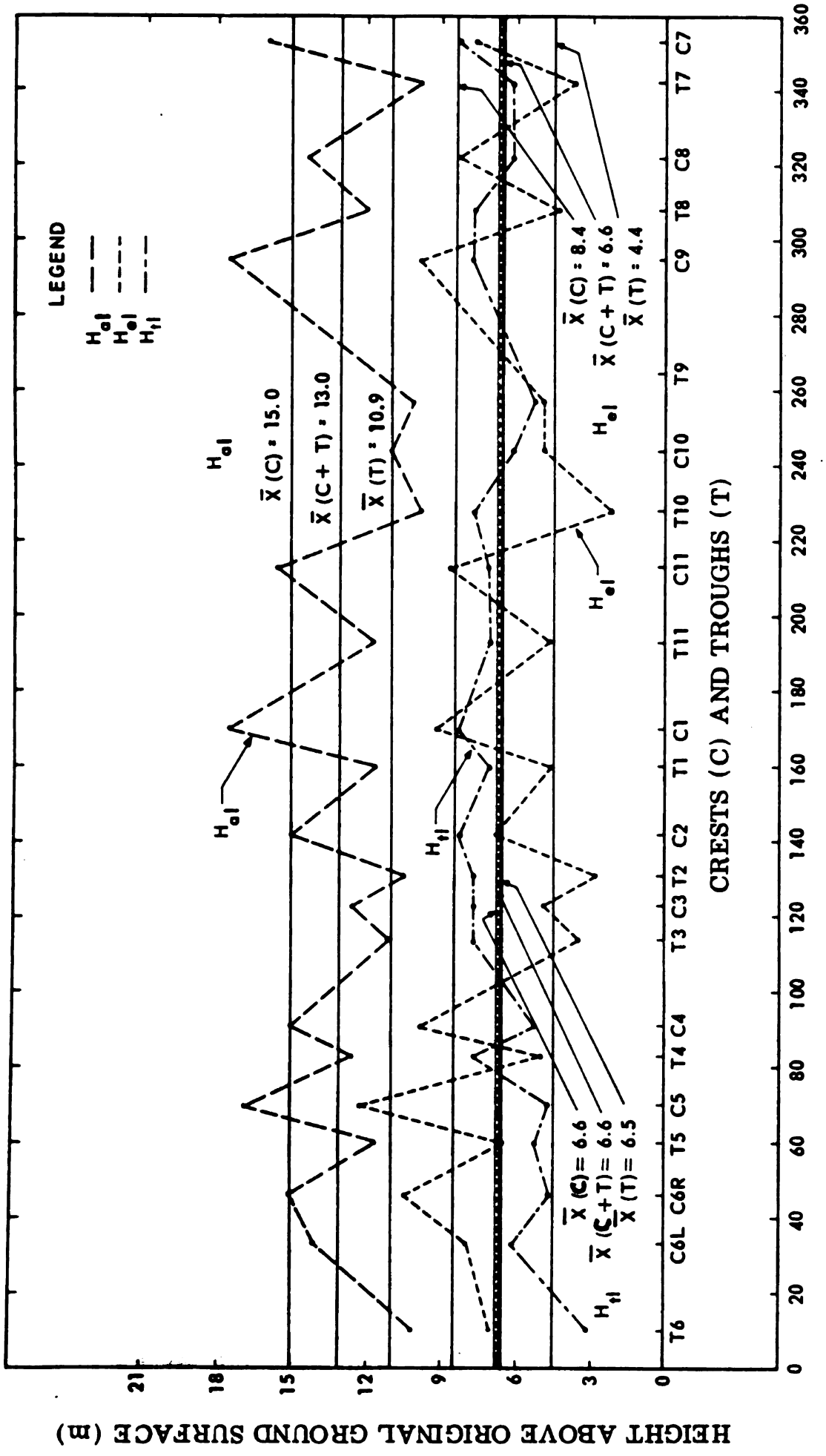

Figure 26. Apparent, True, and Ejecta Lip Heights at Crests and Troughs along the Crater Rim

While ejec

ay vary ab

ne structure

ills (7-6)

difference

ms 6.6 a vs

ening in t

.6 and slig

ne thickness

erally, ej

ard th

t. Rays

Rays con

ne out to t

ically o

al, a smoo

al rubble

ening inte

ral ejecta

ese highs

ally outwa

ese range u

surrounding

Rays 1,

ys are in l

While ejecta and upthrust heights have nearly identical means and both vary about the crater, only ejecta heights reflect the Ray-Valley structure of the lip. In detail, while the upthrust ranges from 3.0 m (T-6) to 8.2 m (C-1, 2, and 7), there is little preferential difference between crests and troughs as illustrated by their means (6.6 m vs 6.5 m). Azimuthally, there is slightly greater upthrusting in the southwest through southeast (T-10 counterclockwise to T-3) and slightly less upthrusting in the northeast (C-5 to T-6). Ejecta thicknesses of crests average twice those of troughs. Azimuthally, ejecta increases toward the northeast (C-4 to C-7) and thins toward the south (T-1 to T-3) and west (T-9 to T-10).

c. Rays

Rays consist of concentrations of ejecta extending from the crater out to the continuous ejecta boundary. Beyond the crest there are typically one or more topographic highs (concentrations of ejecta), a smooth flat area between 1 3/4 and 2 1/2 R_a, and a terminal rubble zone of brecciated blocks. Ray 3 is the only ray not containing intermediate ejecta concentrations. Ray 11 contains an isolated ejecta mass beyond the continuous block boundary. Topographic highs are typically lens shaped in plan view with long axes radially outward, but skewed slightly with respect to SGZ. Ejecta masses range up to 9×10^3 m^2 in area and rise as much as 4.6 m above the surrounding ejecta blanket.

Rays 1, 7, and 9 are best delineated because their topographic highs are in line with each other, their crest peaks, and SGZ. This

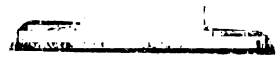

is not the case with other rays where topographic highs do not line up, particularly Rays 5, 8, and 10. Beyond the 25 ft (7.6 m) contour, rays typically slope toward preshot ground surface at less than 5^{o} except in the vicinity of topographic highs where slopes can approach 50^{o} to 70^{o}.

d. Valleys

Valleys, beyond 100 m of the crater rim, contain little ejecta that have not been derived from adjoining rays, either by tumbling of blocks or "flooding" by fines. The amount of flooding ranges from extensive (V-1 and 9) to slight (V-11). Valleys are skewed to the degree to which they are flooded from adjoining rays.

The axis of each ray and valley has been drawn on the modified isopach map (Fig. 24). Each axis is skewed to some extent since no single straight line can adequately represent an entire ray or valley. These skewed axes are obviously not unique; but were drawn as best representing actual field conditions. Each skewed ray axis consists of a straight line from SGZ to the crest peak followed by a minimum set of straight lines connecting the topographic highs out to the R_{eb}. For Rays 4 and 6 (C-6 has two crest peaks) two axes were required to adequately represent the topography. Similarly, Ray 10 required three axes. Valley axes were constructed in the same manner except they follow the topographic lows. In this sense, valley axes bound the ejecta mass of the enclosed rays.

Of the 15 ray and multiple ray axes, 9 are skewed clockwise (with respect to SGZ) and 4 are skewed counterclockwise (all on the

gs 1-3, 9, 10

g. Valley axes

ning of 5°. I

ained troug

ment for ra

C. Areal

The asym

n be seen in

mal contour

n corresponds

nference

ference the

ent eleva

1. Ap

The lo

contour (-

ght but po

ming to

n be attri

ds of talu

ers and so

On th

ntour (-22

ongated to

ms that t

west: R-8, 9, 10L, and 11). Average net skewing is 7°, maximum is 15°. Valley axes are evenly skewed to either side with an average skewing of 5°. Note the near-mirror imagery with respect to SGZ of the paired trough axes 11-6, 1-7, and 2-8. Similar relationships do not exist for ray axes.

C. Areal Relationships

The asymmetries of the apparent crater and lip described above can be seen in plan view. Figure 27 presents traces of selected isopach contours from Figure 24. Each isopach contour is compared to its corresponding mean contour (a circle), constructed such that its circumference is equal to the perimeter of the isopach contour. The difference then is a measure of the asymmetry of the crater or lip at that elevation.

1. Apparent Crater

The lower one-half of the crater, -75 ft contour down to -208 ft contour (-22.9 m to -63.4 m), is nearly symmetric with only a slight but persistent elongation to the north and a less and varied shortening to the south and southwest. These small perturbations can be attributed to differences in fallback distribution; i.e. the lack of talus trains on the north and broad talus trains on the south and southwest.

On the other hand, the upper one-half of the crater, -75 ft contour (-22.9 m) up to zero ft contour (1 R_a), is asymmetric, being elongated to the east and southeast while shortened to the west. Note that the elongation occurs along the direction of the preshot

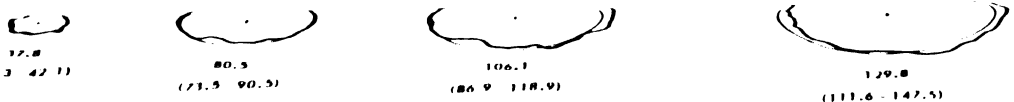
MEAN (m)
RANGE (m)
37.8
(32.3 - 42.1)
80.5
(73.5 - 90.5)
106.1
(86.9 - 118.9)
129.8
(111.6 - 147.5)

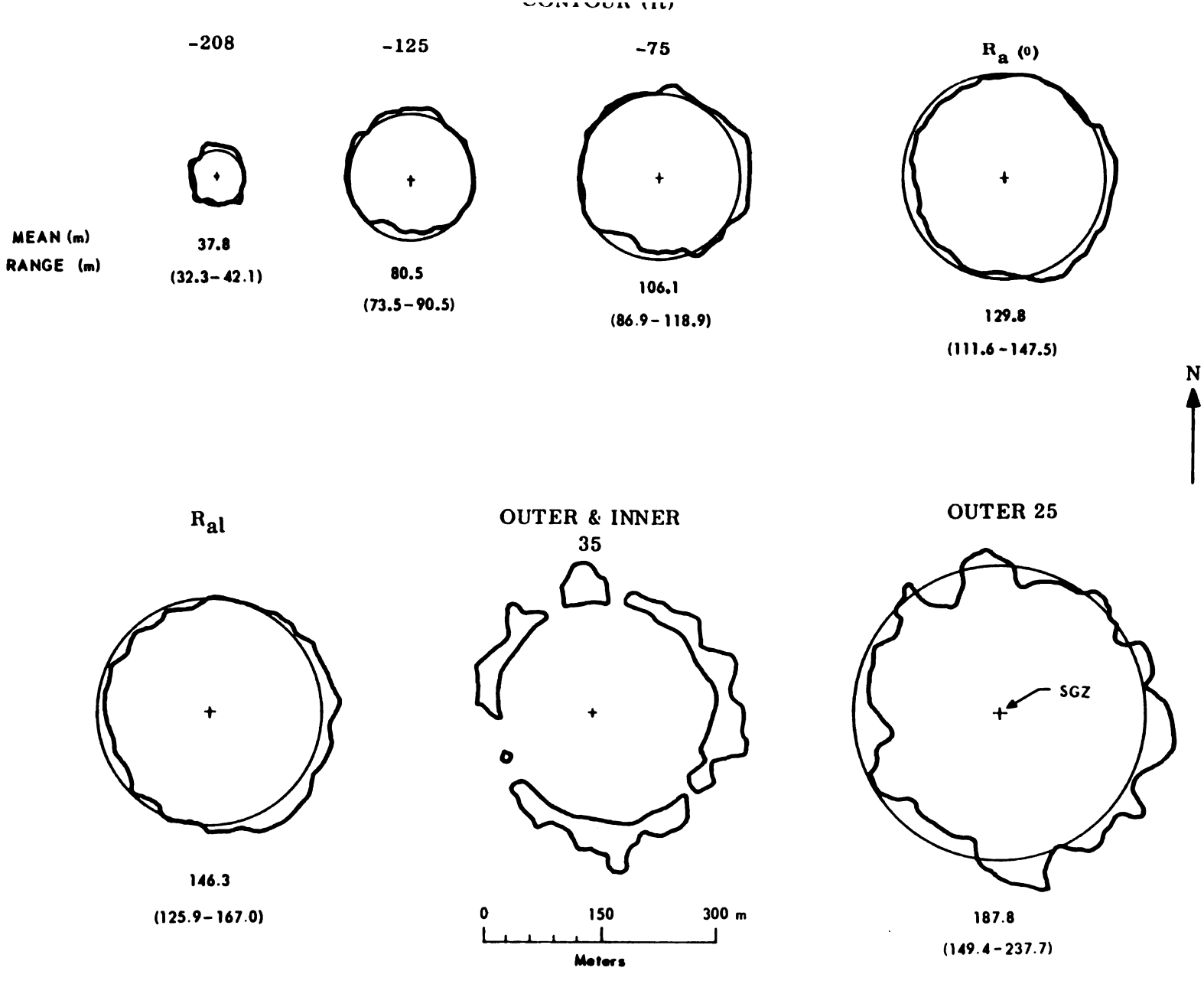

Figure 27. Comparison of Selected Isopach Contours with Their Mean Contours

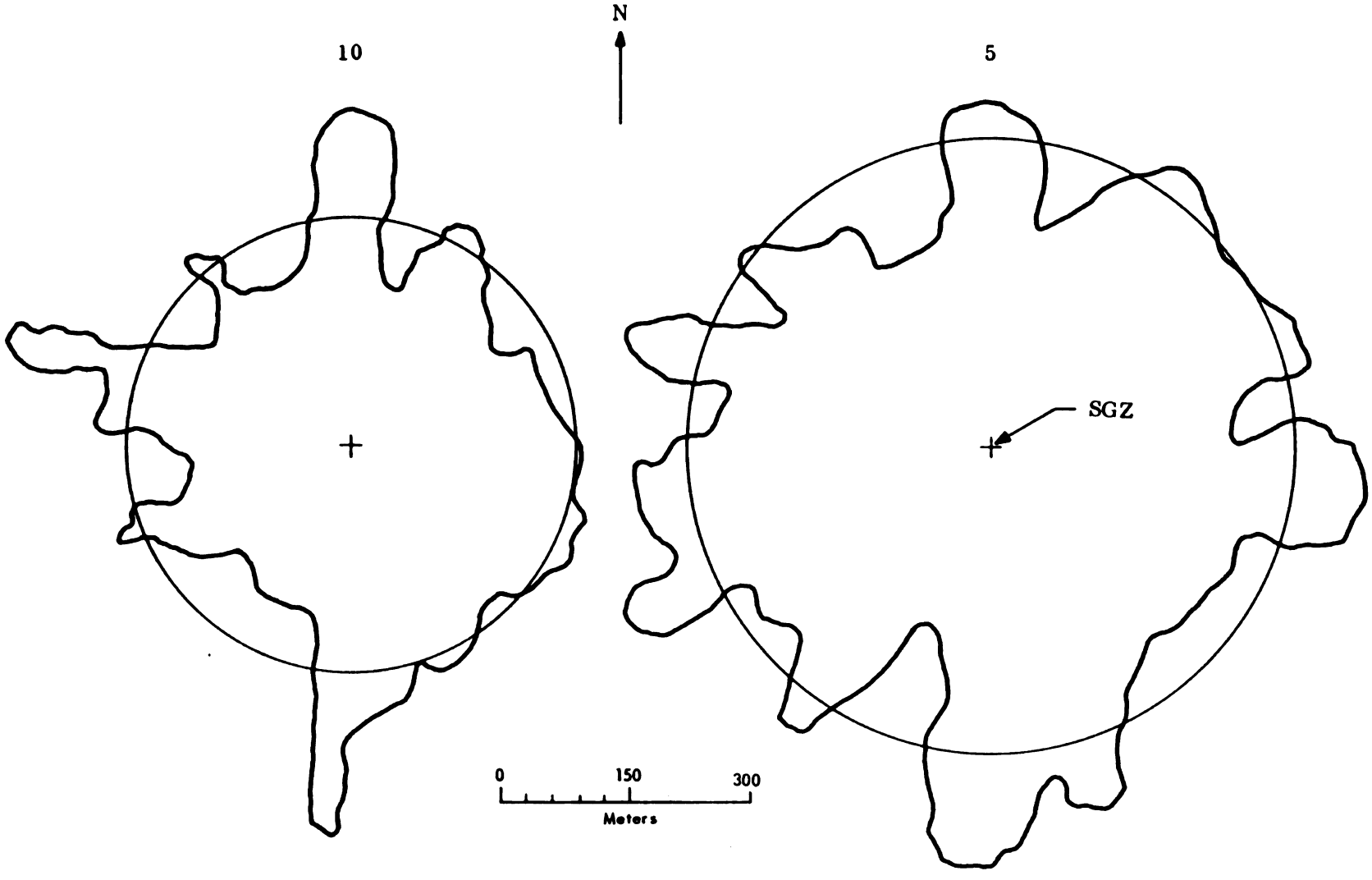

	10	5
MEAN (m)	272.5	367.3
RANGE (m)	(189.0 - 472.4)	(227.1 - 502.9)

Figure 27. (cont'd)

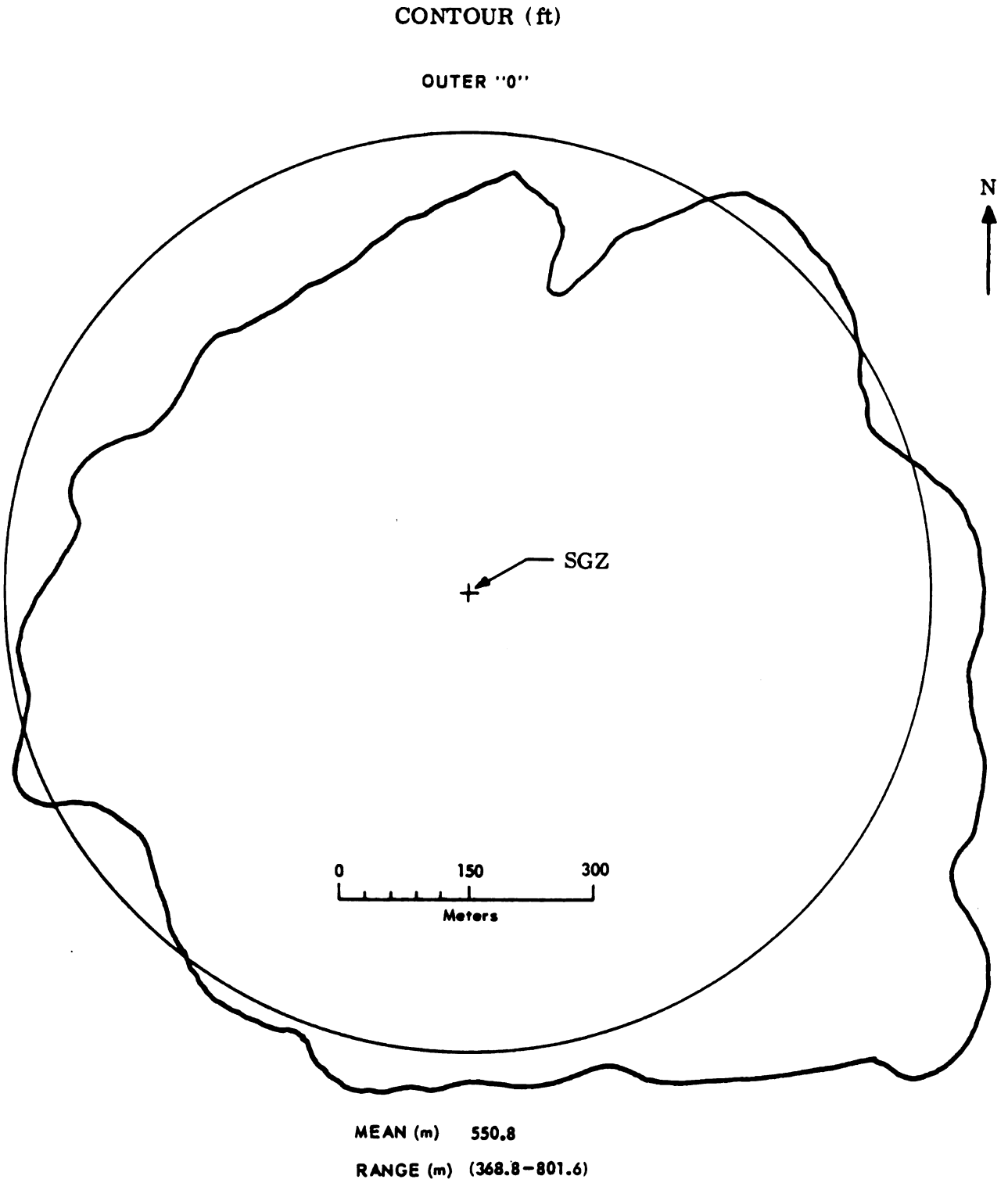

Figure 27. (cont'd)

topographic down-gradient; but not along the local preshot topographic low which is over 30° further clockwise (Fig. B1). Similarly, the shortening on the west follows the preshot topographic up-gradient rather than the local preshot topographic high which is 30° further clockwise. Examination of the crater and ejecta field indicates that the elongation and shortening are the result of excavation and not fallback.

2. Apparent Lip

As mentioned previously, the apparent lip is composed of an upthrusted surface overlain by the ejecta blanket. It is assumed that the upthrust is symmetrical around the crater with respect to SGZ and that it decreases uniformly from the crater rim outward. This is reasonable since, as demonstrated in Figure 26, the upthrust is nearly uniform in height about the crater. Also, work on other buried craters, where sufficient excavation and/or drilling has been accomplished, shows upthrusted surfaces decreasing rapidly and continuously from their highs near the crater rim to virtually zero at 2 1/2 R_a (Fisher, 1968). While undulations may occur, amplitudes are always small fractions of the mean. Thus, relief on the isopach map is primarily a reflection of ejecta deposits.

The ejecta blanket, distributed asymmetrically about the crater, can be divided into a least four distinct but overlapping patterns. The first comprises the ejecta mass of the crests and troughs (1 R_a to the outer 25 ft (7.6 m) contour) and follows the same southeastward-elongated, westward-shortened pattern exhibited by the upper one-half of the crater. Each of the 11 crests are

distinguishable in the 35 ft (10.7 m) contour. The largest and most pronounced peaks are in Crests 1, 5, 7, and 9 while the smallest peaks are in Crests 3 and 10.

The second pattern, comprising the ejecta mass of the rays, is best delineated from the outer 25 to the 10 ft (7.6 to 3.0 m) contours although rays and valleys are recognized across the entire ejecta blanket. The R_b and R_{eb} contours follow the basic Ray-Valley structure, but become increasingly "blurred" with distance. Overall, the most prominent and best developed rays are R-1, 7, and 9. The least developed is Ray 3. The isolated topographic highs concentrated on the east and west give these rays a visual dominance that volumetrically they do not have.

The third pattern is exhibited singularly by the outer "0" contour which does not follow the Ray-Valley structure, but is instead strongly elongated to the southeast. As discussed previously, this pattern is believed related to heavier than average base surge deposits associated with an elevation drop-off and southerly surface winds.

The fourth pattern consists of fallout, deposited at late times from the base surge and cloud, and strongly skewed to the north and northeast.

D. Volumetric Relationships

1. Apparent Lip

Figure 28 presents apparent crater volume (V_a) and apparent lip volume (V_l) for each of the 11 rays delineated in Figure 24.

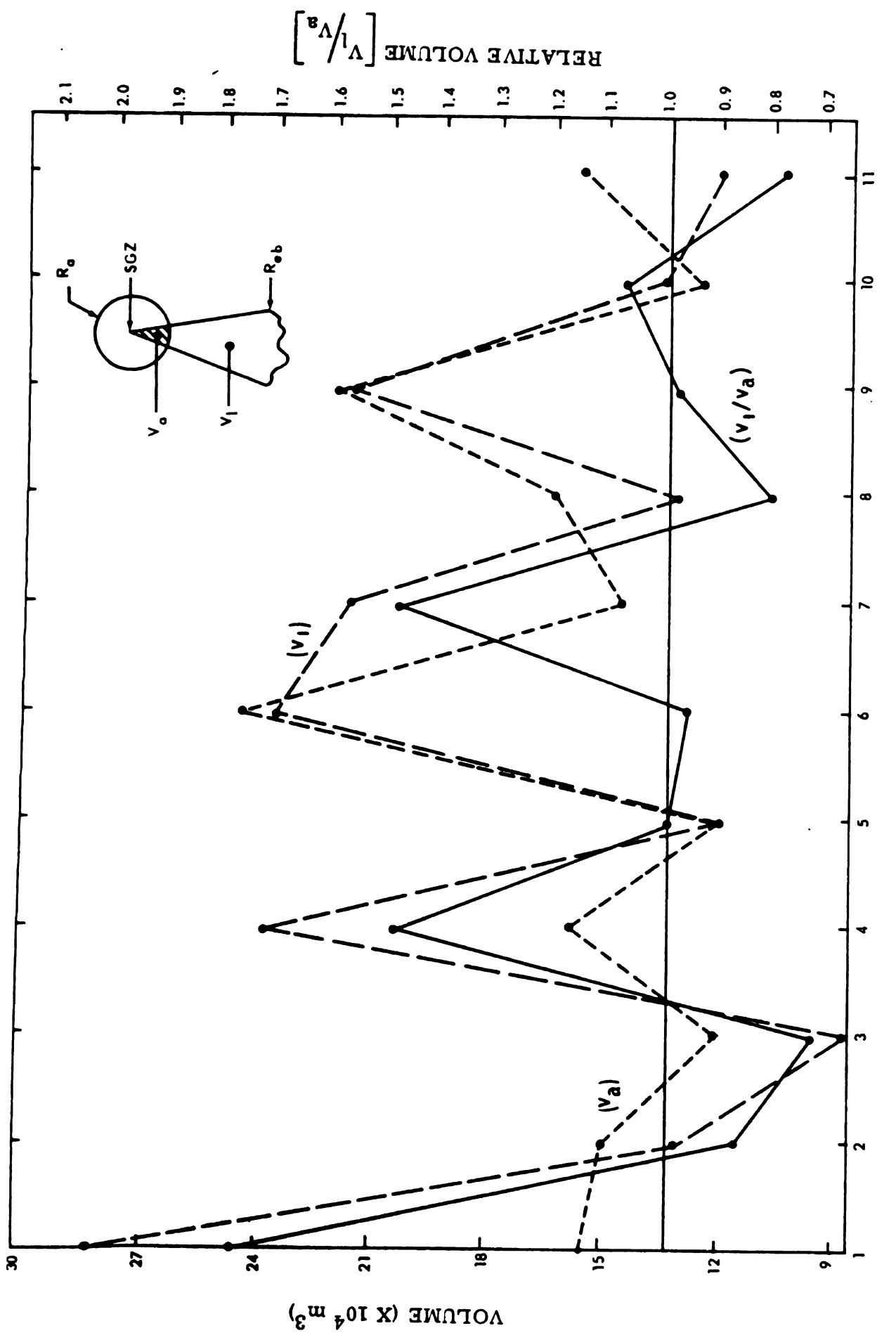

Figure 28. Apparent Crater, Apparent Lip, and Normalized Lip Volumes for Each of the Eleven Rays

Volumes were computed by determining areas between contours with a compensating polar planimeter and multiplying by the appropriate thickness, see Appendix B3 for details.

To obtain relative volumes for each ray, lip volumes were divided by their corresponding crater volumes (Fig. 28). The assumption used is that material was ejected from the Schooner crater in a radial manner. Previous workers have shown this to be the case for buried bursts (Sakharov, et al., 1959 and Carlson and Newell, 1970). When normalized in this manner (i.e. V_l/V_a) Rays 1, 4, and 7 are largest while Rays 3, 8, and 11 are smallest. The greatest enhancement factor is for Ray 1 (1.82) and the smallest enhancement factor is for Ray 3 (0.73).

2. Ray-Valley Comparisons

Volumes of the apparent crater (V_a), true crater (V_t), apparent lip (V_l), and upthrust (V_u) were computed for each ray and valley from profiles constructed along their respective skewed axes of Figure 24. Profiles for Rays 1 (largest), 3 (downhill), 10C (uphill), and 7 (second largest) are presented in Figure 29. See Appendix B4 for methods used.

The true crater volume (V_t) and its two components, apparent volume (V_a) and fallback volume (V_f) (where $V_f = V_t - V_a$), do not reflect the Ray-Valley structure of the lip (Fig. 30). The true crater volume exhibits generally the same asymmetric pattern about SGZ as V_a, both of which follow closely R_a and R_{al} (Fig. 25), True crater volumes deviate slightly more about their mean than apparent

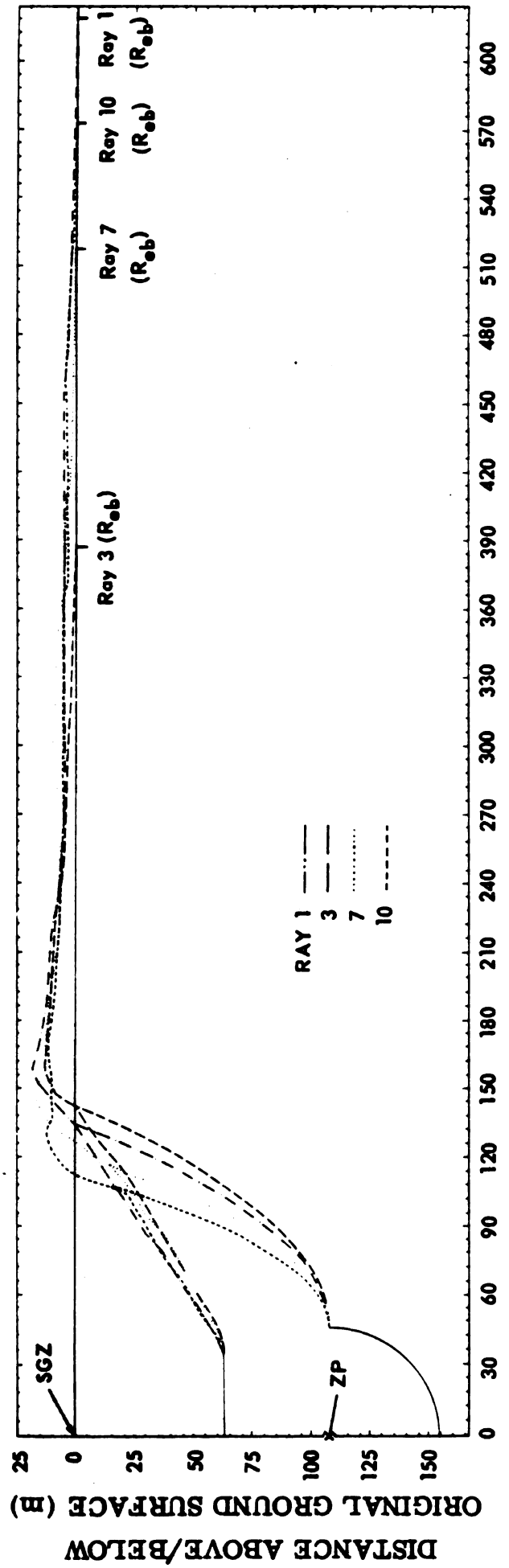

Figure 29. Apparent and True Crater Profiles for Ray Axes 1, 3, 7, and 10

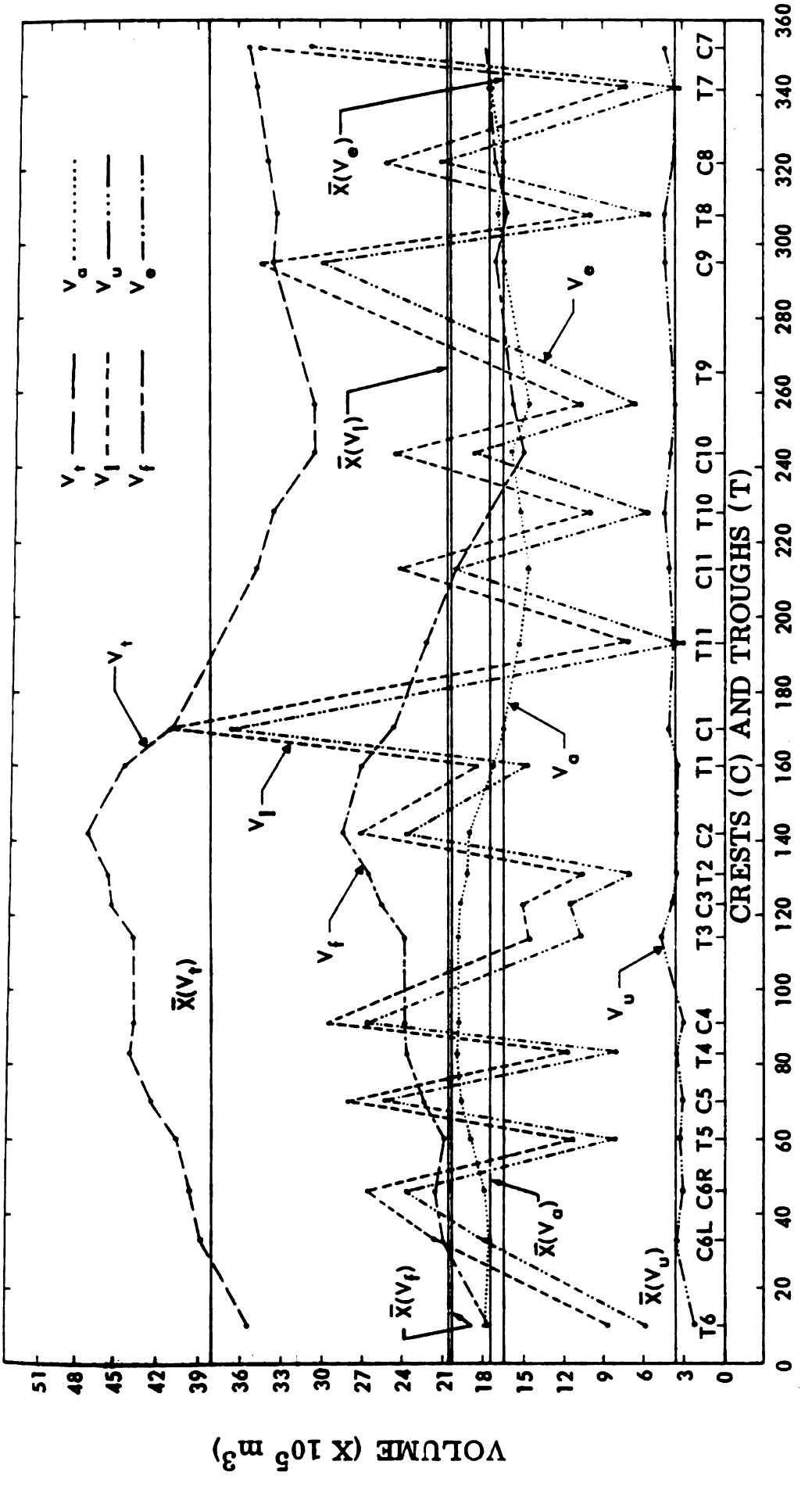

Figure 30. Crater and Lip Volumetric Comparisons for Rays and Valleys

crater volumes ($\pm$ 23% vs $\pm$ 16%) and there are slight azimuthal shifts in maximum and minimum values. Apparent crater and fallback volumes average 46% and 54% of the true volumes, respectively for both rays and valleys. Only where V_t is a minimum (T-6 to C-10) does $V_a = V_f$; elsewhere, $V_f > V_a$.

Apparent lip and ejecta volumes, on the other hand, do reflect the Ray-Valley structure (Fig. 30). The upthrust volume comprises 20% of the apparent lip volume and remains relatively constant (+ 20% to - 28% about the mean). This is a direct consequence of the relatively constant upthrust observed along the crater lip (Fig. 26) and the assumed uplift profile. Ejecta volume makes up 85% and 66% of the apparent lip volume for rays and valleys, respectively. It is this ejecta volume ($V_e = V_l - V_u$), varying + 122% (R-1) to -81% (V-11) about its mean, that is responsible for the relief of the ejecta blanket. Thus, ejecta-lip asymmetries observed along the crater rim (Fig. 26) are continued outward over the ejecta blanket as ejecta-volume asymmetries (Fig. 30).

3. Ray 1 Variations

Ray 1, from the V-1 axis (153°) clockwise to the V-11 axis (194°), was examined in detail by constructing radial profiles in one-degree increments from SGZ out to the R_{eb}. Volume calculations were made for 360° with the computer routine discussed in Appendix B4. Apparent crater volumes (V_a) and apparent lip volumes (V_l) are shown in Figure 31. V_a is independent of the Ray 1 structure, gradually increasing from V-11 (194) to V-1 (153°) following a pattern similar

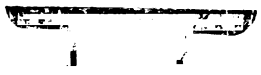

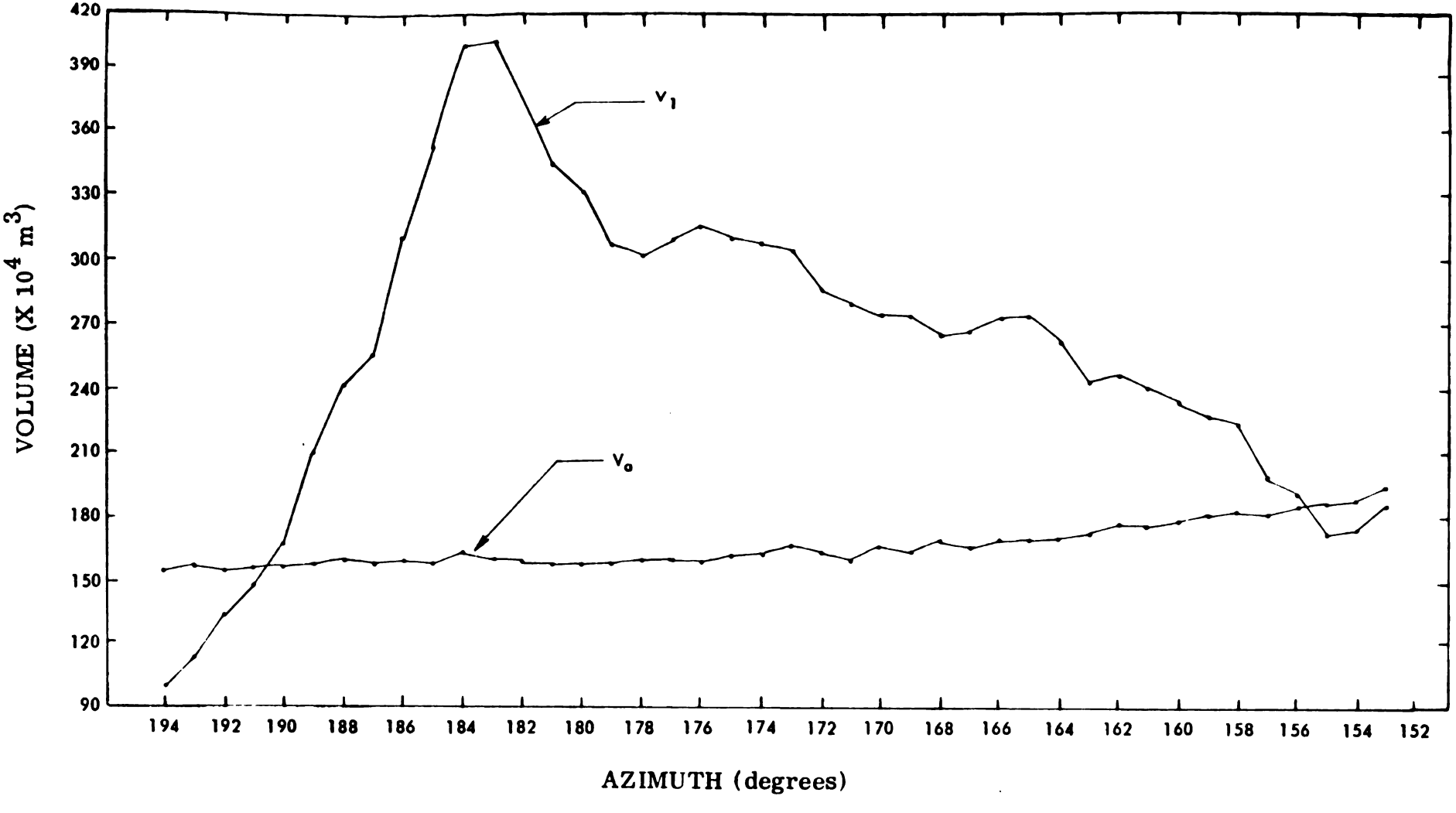

Figure 31. Apparent Crater and Lip Volumes for Radials Spaced in One Degree Increments Across Ray 1

to R_a (Fig. 25). The apparent lip volume (V_l) reflects the Ray 1 structure, rising from 194° to 183°.

From 183° to 153° the lip volume gradually decreases. This gradual and lower net decrease reflects the flooding of ejecta from R-1 into V-1, whereas V-11 is relatively devoid of ejecta.

4. Cumulative Distributions

Cumulative distributions of V_l, V_e, and V_u as a function of distance from SGZ for Ray 9 and Valley 1 axes are presented in Figure 32. Volumes were computed by revolving skewed profiles through a one-degree arc and agree within 2% of the volumes computed by the previously discussed area moment technique. Uplift volume is distributed close to the crater where for both R-9 and V-1, 50% and 90% of the volume is located within 1.4 and 2.0 R_a. Contrast this to the distribution of V_e, where 50% and 90% of the volume is at 2.2 and 3.2 R_a for R-9 and 2.0 and 3.1 R_a for V-1.

Figure 33 compares cumulative distributions of V_e for R-9 (a large volume ray), V-1 (a flooded valley), R-1 (the largest volume ray), R-3 (the smallest volume ray), and V-11 (a valley with very little ejecta). In each case, the distribution of the majority of the ejecta (between cumulative 20% and 80%) is a strong function of the total ejecta volume present; i.e. the larger the total volume the farther away from the crater it is distributed. Distribution of the far-out ejecta is not a strong function of the total ejecta volume.

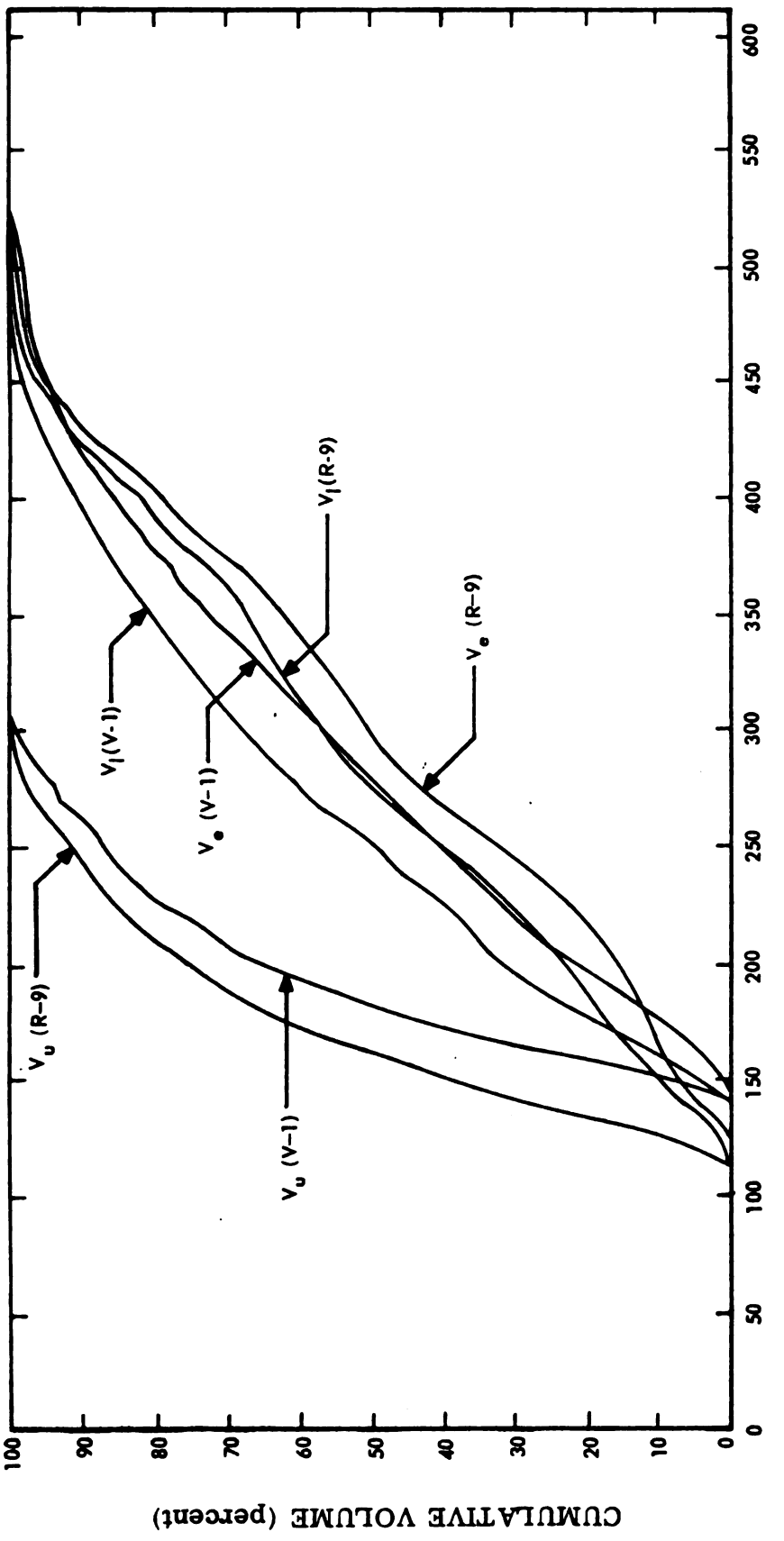

Figure 32. Distribution of Lip, Upthrust, and Continuous Ejecta Volume for Ray 9 and Valley 1 as a Function of Distance from SGZ


80
70
60
V-11
V-1

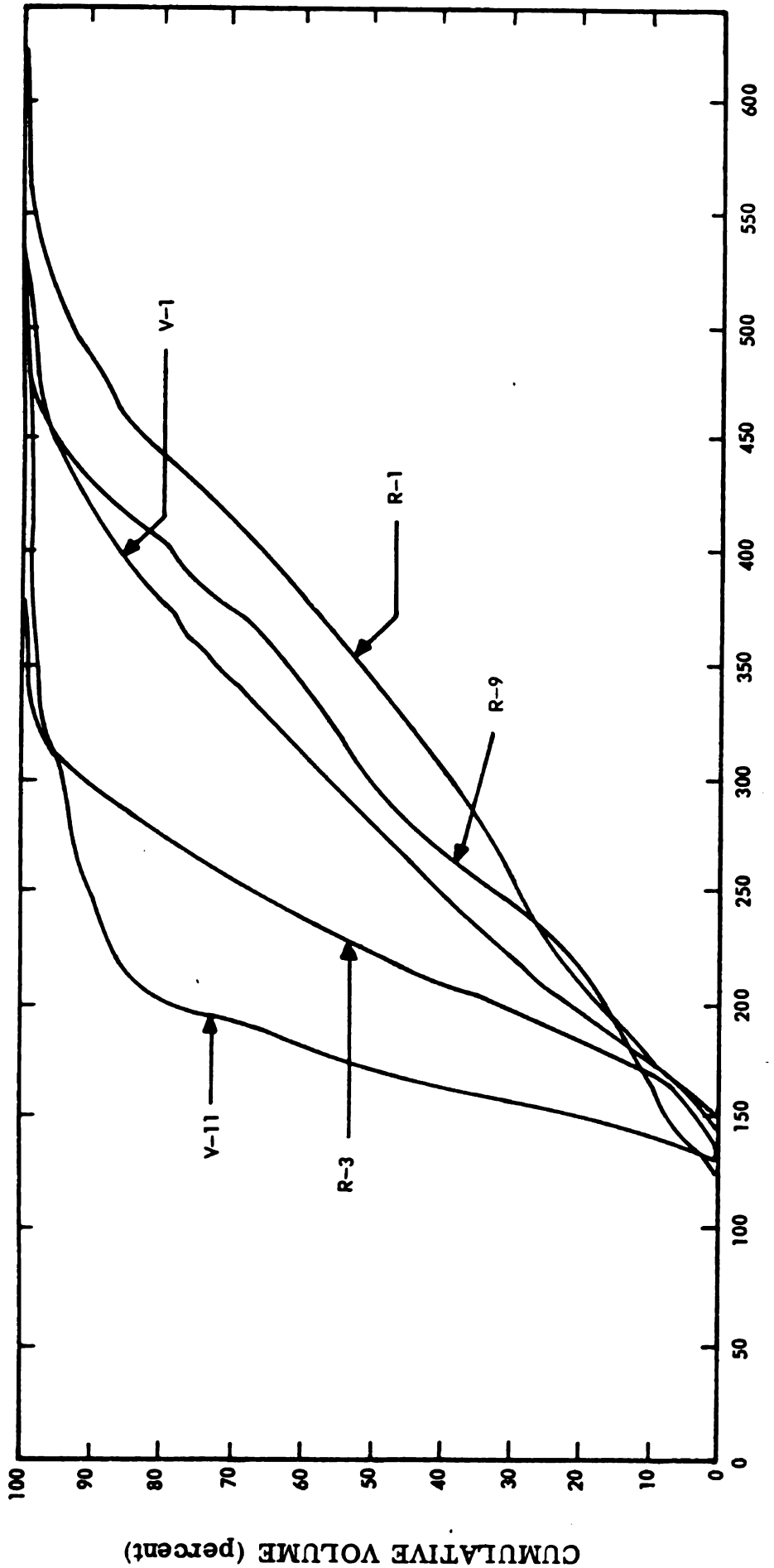

Figure 33. Distribution of Continuous Ejecta Volume as a Function of Distance from SGZ for Selected Rays and Valleys

CHAPTER V

GEOMORPHIC CHARACTERISTICS OF THE CRATER AND CONTINUOUS EJECTA FIELD

A. General

Although used in extraterrestrial studies, geomorphic mapping of terrestrial craters and ejecta fields has received little attention by investigators. Nonetheless, such a study is ideally suited for Schooner because of its distinctive and varied set of surface features.

The ejecta field exhibits an inverted stratigraphic order with fines from the weakly welded and nonwelded tuffs overlying blocks from the upper densely welded tuff. In the crater, on the other hand, fallback exhibits a complex, but apparently normal stratigraphic order with blocks overlying fines. The initial distribution of blocks and fines followed by post-depositional movement gives rise to a large variation of surface morphologies (Fig. 21) which for this study have been grouped into seven distinct regimes: blocky, rubble, smooth, drowned, hummocky, mixed, and transitional. Appendix C presents a description of the morphological regimes and discusses procedures used in their mapping.

Over 550 separate areas were required to map the crater and continuous ejecta field. The data accumulated are listed in Table C1 and presented in three geomorphic maps: a surface feature map, a block size map, and a block areal density map. Maps are provided in the map pocket and reduced to page size in Figures 34, 35, and 36.

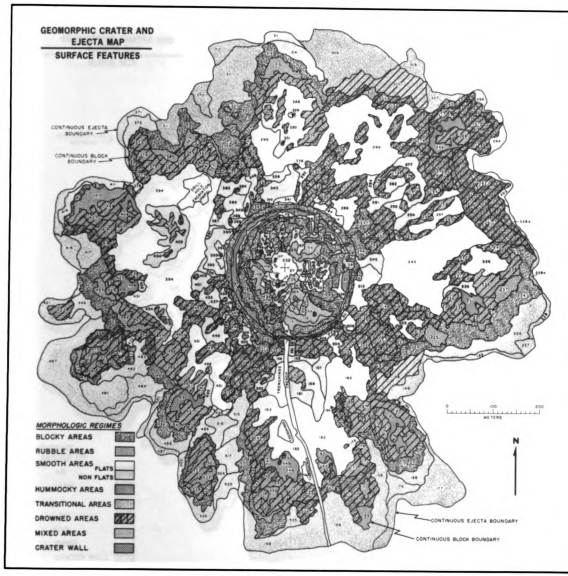

Figure 34. Geomorphic Crater and Ejecta Map - Surface Features

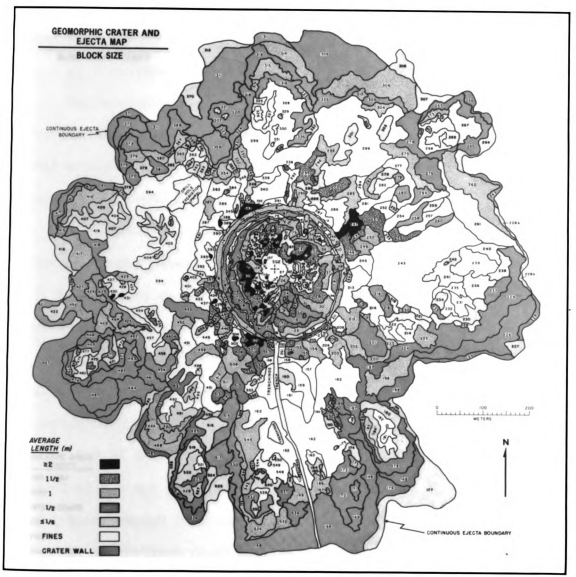

Figure 35. Geomorphic Crater and Ejecta Map - Block Size

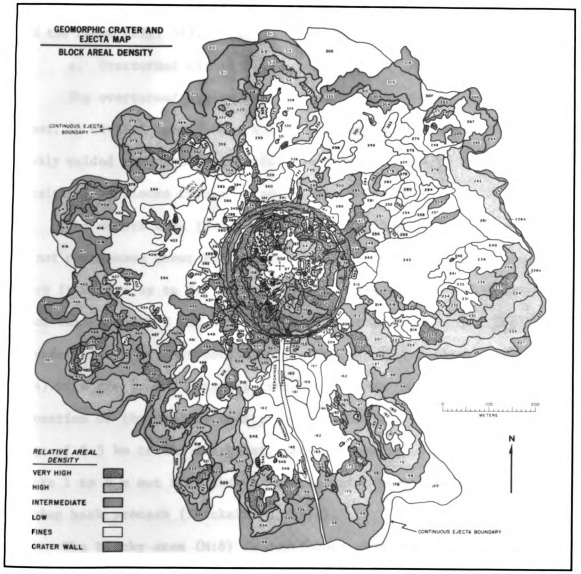

Figure 36. Geomorphic Crater and Ejecta Map - Block Areal Density

pparent Crater

1. Surface

The major fe

overturned ejec

the floor (Fig.

a. Overturn

The overturn

m, is divided

ally walled and

sisting of block

The smooth

ar continuous

ch it ranges up

the Rille Crests

undergoing slow

ft with the ero

ration of the

ge of 5.5 km to

km, to 6 m o

ring back proc

The blocky

1.2 m in thi

ter on the sou

ividual blocks

northeast (W.

B. Apparent Crater

1. Surface Morphology

The major features of the crater from the rim crest down are the overturned ejecta flap, the soil horizon, the wall, the fallback, and the floor (Fig. 34).

a. Overturned Ejecta Flap

The overturned ejecta flap, exposed below the crater rim crest, is divided into a smooth area consisting of fines from the weakly welded and nonwelded tuffs underlain by a blocky area consisting of blocks from the upper densely welded tuff.

The smooth area (M:1-7, Geomorphic Mapping Units 1 thru 7) is not continuous about the crater, being confined only to crests where it ranges up to 2.7 m in thickness. Crests 5 and 10 contain no fines while Crests 3 and 4 contain only scattered amounts. This area is undergoing slow, but continual erosion (up to 1 m between 1969 and 1974) with the eroded material transported down into the crater. Detonation of the Handley event, a 1.2 MT buried event with a slant range of 5.5 km to the southeast, caused a number of circumferential cracks 1 to 6 m out from the crater rim which have accelerated the wearing back process (Shackelford, 1971).

The blocky area (M:8) is continuous about the crater ranging up to 12 m in thickness. There have been no large slope failures, except on the south; but there has been a continual movement of individual blocks into the crater. A typical blocky talus train on the northeast (M:61) is carrying blocks from this area into the crater.

b. Soi

The soi

ne compone

ria. It d

s to meet a

ve thicknes

ructil.

c. Wa

The wa

architectur

ve the cra

ended cul

ons from

ve degrad

d. F

Falli

ments of

ights tha

ches inc

ntrolled;

ns. Bec

ch

ch. Wit

ches tha

ches tha

b. Soil Horizon

The soil horizon (M:9-14), consisting of in situ and overturned components, marks the present location of the uplifted ground surface. It decreases in thickness from a maximum of 3.5 m on the east to near zero on the west and southwest. On the east (M:10) where thickest, it is slowly eroding into the crater, e.g. fine talus train M:51.

c. Wall

The wall (M:40, 60, and 87), consisting of the uplifted and blast-fractured upper densely welded tuff, is exposed continuously about the crater except where covered by fallback. Weakly welded and nonwelded tuffs are not exposed along the crater wall. Wall thickness ranges from 7 to 15 m on the east and 15 to 23 m on the west. Only minor degradation of the wall has occurred since crater formation.

d. Fallback

Fallback, including material eroded postshot from above, consists of blocks and fines distributed continuously from where it overlaps the crater wall down to the crater floor. Morphologic regimes include blocky, smooth, and mixed areas. Rubble areas are not identified; but broken blocks contribute to both the blocky and mixed areas. Because fines do not in general cover blocks, neither drowned nor hummocky areas are present. The distribution of morphologic units, while controlled primarily by the shape of the crater, also reflect the Ray-Valley structure of the lip; e.g. portions of the crater rim that failed during overturning, material eroded postshot

from above units, and the distribution of the large smooth areas containing the weakly welded and nonwelded outcrops.

Blocky areas dominate almost down to the - 100 ft (-30.4 m) contour while smooth areas dominate below. Overall, the distribution of fallback reflects a normal stratigraphic order with blocks overlying fines. There are exceptions, one on the east where fines locally overlie blocks (M:41, 43, and 45), another on the southwest (M:112 and 128). While blocks are observed overriding the perimenters of the five smooth areas (M:47, 67, 80, 84, and 125), few blocks cross the interiors apparently due to the slight outward bulging (toward the ZP axis) of these areas.

Fine unit outcrops (M:46, 71, 94, 130, etc.) discussed in Chapter VI. C are contained within these smooth areas. The large smooth area on the east (M:47) is aligned with Crests 3, 4, and 5 which contain few fines. Similarly, the smooth area on the southwest (M:125) is aligned with Crests 10 and 11 which are also deficient in fines. The smooth areas, particularly the outcrops, are slowly being eroded with the detritus washing down the crater and onto the floor.

This distributional pattern of blocks and fines is modified by a number of talus and slump structures. On the south, a large slump structure extends from near the crater rim down to the floor and consists of a mixture of blocks and fines (M:17-29). Other slump structures exist on the west (M:104, 106, 108) and north (M:68 and 69). On the east (M:55) and northeast (M:61) small talus trains are forming near the rim. Trenching operations in 1969 are probably

responsible for the mixed zone on the south. Where fallback begins along the wall, there is commonly a 1 to 6 m wide band of fines (M:36, 75, 88) presently accumulating from erosion of the overturned fine ejecta units in the flap. The Handley event probably accelerated the growth of these features.

e. Floor

The nearly circular floor (M:27) is clearly anomalous. It is shifted to the northwest with respect to SGZ reflecting encroachment from the east and south. The floor contrasts sharply with the fallback in composition and morphology. Its surface has many of the characteristics of a playa; i.e. flatness, dissection cracks, very fine grain composition, and complete lack of blocks (except those that have obviously rolled or slumped on at post-crater times). Probing has shown that the thickness of the floor unit at SGZ is at least 8 m with composition and grain size unchanged from the surface down (Day, 1972).

There has been a slow, but apparently continuing encroachment of fallback onto the crater floor. The floor is covered by a thin sheet (2 to 10 cm) of fines washed out of the fine outcrops above. Centimeter-size shocked pumice fragments, washed and rolled down the crater, thinly cover outer portions of the floor. Coarser fragments (up to 1/3 m) are collecting at two cresent shaped ridges on the west and northwest perimeter. On the west there are two talus trains (M:106), 3 to 6 m wide by 1.5 m high and composed of mixed blocks and fines, that have moved over 8 m out onto the floor. On the south a large irregular mass (M:26) 30 m across and 3 m high has moved 9 m

n the floo

A numb

ri i 6 m (

nid into

ns at the

ng the Ha

nutes tha

he has bee

1. Bl

The s

the elect

The s

ectly by

e Fig. 3

ents. I

ch) elec

ch the s

hat eff

the perc

Cm/s),

the are

A metho

A mod pr

onto the floor.

A number of large blocks, one 9 x 6 x 6 m (M:134), another 6 x 6 x 6 m (M:10), and several smaller ones on the northeast have tumbled onto the floor; again all postshot. The two equi-dimensional blocks on the northwest portion of the floor (M:107) tumbled there during the Handley event. Observation of their impact craters indicates that in 5 years (1969 to 1974) infilling of the crater floor has been less than 15 cm.

2. Block Size

The size distribution of blocks in the wall and the overturned ejecta flap is discussed in Chapter VI. A.

The size distribution of blocks in the fallback is controlled primarily by the shape of the crater with block size increasing downward (Fig. 35). This pattern is modified by talus trains and slump features. Transportation of blocks down the crater via talus trains locally decreases block size in the blocky areas (M:30) and increases block size in the smooth areas (M:106). Slump features produce a similar effect, but in a more complex manner since they involve a larger percentage of fines and some mixing of blocks and fines (M:24-26). The relatively larger block sizes on the east side of the crater are due to a combination of factors, including fewer fines in the overturned flap, more postshot slope failures along the crater rim, and probably larger in situ block sizes.

1. Block

Block area

ape of the

). Bloc

creases sh

ay for the

s and slum

-30 ft (-3

ntinuous

1. Sur

The gen

nuous e

lp. Whe

ral stra

ting. T

ed thi

In gen

rtly alo

ing va

most c

, but

flap

ock an

central

3. Block Areal Density

Block areal density, like block size, is primarily controlled by shape of the crater modified by talus trains and slump features (Fig. 36). Block areal density is obviously high in the blocky areas and decreases sharply with the onset of the smooth areas. Areal density for the mixed areas is intermediate. As a consequence, talus trains and slump features generally reduce block areal density above the -100 ft (-30 m) contour (M:51) and increase areal density below (M:70).

C. Continuous Ejecta Field

1. Surface Morphology

The general spatial distribution of blocks and fines in the continuous ejecta field closely reflects the Ray-Valley structure of the lip. Wherever blocks and fines are observed, they exhibit an inverted stratigraphic order (fines over blocks) with little evidence of mixing. The only exception is where secondary cratering has destroyed this order by inverting the order once again.

In general, blocky areas are observed where fines are thin, primarily along ray perimeters and in partially drowned troughs and connecting valleys. Within ray interiors blocky areas are observed along most topographic breaks. Rubble areas are concentrated at ray termini, but are also associated with several of the topographic highs (flap segments) within rays. With few exceptions, fines cover all block and rubble areas to some degree; but are concentrated in the central portions of rays where they formed extensive smooth areas.

a. Bloc

Blocks a

b. Blocks a

ble areas or

e morphs al

ally covere

erating val

In ray

ern topograp

e USGS stee

ween most

ge exposed

156, 178,

Althou

ese blocks

ble contin

ll indica

ere is at

ere are no

ations of

ks on alac

ntributed

A nu

ble for

ble exca

a. Blocky Areas

Blocks are best exposed along ray perimeters where fines are thin. Blocks are concentrated at ray termini where they surround rubble areas on the outer three sides. Blocks underlie all crests and troughs along the crater edge (Chapter VI. A) and are only lightly covered by fines in several troughs (T-5, 6, 7, and 11) and connecting valleys.

In ray interiors, blocks are exposed wherever there is a sharp topographic break; e.g. crest plateau boundaries (M:388, 395, and 505), steep slopes bounding crests (M:251, 385, and 499), and between most crests and troughs (M:212, 293, and 397). Blocks are also exposed along many topographic highs; e.g. R-4 (M:241), R-5 (M:256, 278, and 283), R-6 (M:301-303), and R-10 (M:409).

Although blocks are observed seemingly wherever fines are thin, blocks are not deposited continuously from the crater rim out to the continuous block boundary. Examination of the trench (Chapter VI. B) indicates that while blocks provide the foundation for Ray 1, there is at least one interval, 250 to 300 m (2 to 2 1/4 R_a), where there are no blocks. This location in the trench coincides with portions of the smooth area of Ray 1 (M:162) which in turn is aligned with an almost continuous circumferential band of smooth areas distributed around the crater.

A number of other locations along this circumferential band provide further evidence for a discontinuous deposition of blocks. At the excavation surrounding drill hole PM #2 (R-8, M:394) very few

blocks are observed. Also, at several locations where fines from rays enter valleys, field examination indicates a discontinuous deposition of blocks; e.g. R-1 (M:529) and R-11 (M:496). Thus the symmetry and persistence of this circumferential band argues that the lack of a continuous layer of blocks is a basic depositional feature of the Schooner ejecta blanket.

Morphology of the blocky areas suggests movement of ejecta after deposition. The outward spreading pattern of many ray termini accompanied by broad protruding masses (R-1, M:534 and 536; R-4 M:224; R-8, M:369; and R-9 M:415) points to both forward and lateral movement of ejecta on the ground. Along the leading edge of ray perimeters, there are numerous small blocky lobes which protrude up to 5 m beyond the average boundary; e.g. on R-2 (M:179), R-7 (M:313), and R-11 (M:518). Along lateral ray perimeters, similar blocky lobes are present, skewed from perpendicular to the perimeter to radially outward from the crater; e.g. on R-1 (M:530), R-2 (M:179), and R-11 (M:486). Finally, most troughs and connecting valleys contain accumulations of blocks that have obviously tumbled down from surrounding crests and connecting rays.

In cross section many of the ray termini contain low areas 10 to 30 meters behind the leading ray perimeters. Outward the surface is typically "stair-stepped"; i.e. the surface rises gradually for 1 to 2 meters and then drops off quickly. This "stair-step" is repeated several times with the net surface sloping gradually down to the original ground surface. "Stair-steps" are not well developed, if

they exist at all, along lateral ray perimeters.

b. Rubble Areas

Rubble areas are associated with four physiographic features: ray termini, outer ray segments, interior topographic highs, and isolated masses near the continuous ejecta boundary. With depth some rubble, actually broken blocks, are observed beneath crests and troughs (Chapter VI. A). Rubble areas are observed locally within flap segments along the trench (Chapter VI. B) where they tend to be localized and surrounded by unbrecciated blocks. With distance from the crater, brecciation increases.

Rubble areas are observed neither along ray perimeters nor on the surfaces of crests, troughs, or valleys. The largest concentrations of rubble are observed near ray termini where they are surrounded by blocks on the outer three sides and overlapped by fines, the hummocky areas, on the interior side. In plan view rubble areas follow the general pattern of rays ranging up to 2×10^4 m^2 in area. In cross section rubble areas typically consist of a broad topographic high rising 1.5 to 4 m above the surrounding ejecta blanket followed outward by a broad shallow area that is often slightly depressed below the surrounding ejecta blanket.

Rubble areas typically occupy major portions of ray termini particularly those containing large outward protrusions (R-1, 4, 7, 9, and 11). On Ray 1 there are three terminal rubble areas, two associated with protrusions (M:531-533 and M:172-174) and one not (M:164). Along portions of R-10, there is a band of rubble roughly

paralleling the ray perimeter (M:424-426, 458-460, and 464), while along the eastern side of the ejecta blanket there appears to be significantly less rubble. The extent to which rubble areas are covered by fines is a question that only further excavation can answer. The trench shows that two of the rubble areas on R-1 (M:164 and 541) are not connected.

Rubble areas are observed within the outermost segments of Rays 2, 6, 10, and 11. These are similar to terminal rubble areas; but smaller in area. They contain interior hummocky areas (M:182, 268, 476, and 521) indicating that the fines and blocks traveled together in inverted stratigraphic order with little mixing on or after impact.

Rubble are also observed on top of several topographic highs within ray interiors; e.g. R-1 (M:160), R-5 (M:259), R-7 (M:327), R-9 (M:405), and R-10 (M:455). This rubble is smaller in size than in the terminal rubble areas, at least in part due to a difference in lithology; i.e. "PBO" mapping units rather than "RUL" mapping units (see Fig. 51). Study of the trench (Chapter VI. B) suggests that some of these topographic-high rubble areas may be only the "tip of the iceberg" of larger rubble masses below; but excavation is required to substantiate this.

A number of isolated masses, up to 10^3 m^2 in area and located predominately beyond the continuous block boundary, are composed primarily of rubble. These rubble masses range from broad shallow sheets (M:169, 171, 323, and 463) to small compact mounds (M:167, 310,

s mill. T

ar freshn

e deposit

ner but,

The d

n they we

ne secon

rmation.

rtions of

e or brec

ments tha

widely are

e this li

ed in mas

fragment

this seg

c. S

Fines

Water

ions of

ely rema

ntribution

ight sug

Overa

ble to

and 321). The former have mixed slightly on and/or after impact. Their freshness and lack of coverage by fines is indicative of late time deposition. Similar features may well exist closer to the crater; but, if so, are covered by fines.

The distribution and localization of rubble areas indicates that they were formed by brecciation upon impact, although later-stage secondary cratering undoubtedly contributed to further local brecciation. Rubble areas are concentrated within the thicker portions of large ejecta masses (segments) surrounded by blocks that are not brecciated. Since segments probably impacted as a unit, this suggests that the size of the impacting mass together with its impact velocity are important parameters in the brecciation process. Following this line of argument, the isolated rubble mounds, being relatively small in mass, probably impacted at higher velocities than the larger flap-segment rubble areas. In this sense, the mounds are intermediate to flap segments and secondary craters.

c. Smooth Areas

Fines cover the surface of the ejecta field continuously from the crater rim out to the continuous ejecta boundary. Scattered patches of fines observed beyond the continuous ejecta boundary are mostly remnants of base surge and cloud deposits. The spatial distribution of smooth areas and their relationships to blocky areas strongly suggests movement of fines after initial deposition.

Overall, fines and resulting smooth and drowned areas are shifted to the east and northeast (R-4, 5, and 6) resulting in

caused drow

eral dens

mouth area

similarly c

allowing th

ames of "d

ximums on

Pines

ent and th

riously di

ent smoot

h N(0,3),

served in

similariti

Topog

ring degr

ial buri

the large

ear to ha

Where

del; e.g.

N(0,3), and

to very l

ng the m

ween betwe

increased drowning (Fig. 34) and subsequent decrease in block size and areal density (Fig. 35 and 36). Note that there is a sparsity of smooth areas along the southeast side of the ejecta blanket, particularly on Ray 3. Fines cap most of the crests and spill into neighboring troughs and connecting valleys resulting in varying degrees of "drowning"; e.g. T-1, 2, 3, 10. Fines are thin and discontinuous on Crests 3, 4, 5, and 10.

Fines are concentrated within rays reaching their maximum extent and thickness in the middle interiors and aligned with the previously discussed circumferential band of smooth areas. The largest smooth areas (up to 5×10^4 m^2) are located on R-1 (M:162), R-4 (M:243), R-6 and 7 (M:299), R-9 (M:394), and R-11 (M:451). As observed in the trench fines fill in and smooth out the topographic irregularities of the underlying block deposits.

Topographic highs (flap segments) are drowned by fines to varying degrees from complete burial as observed in the trench, to partial burial (R-6, M:301-303), to slight burial (R-7, M:327). Two of the largest topographic highs, R-4 (M:241) and R-9 (M:404-406) appear to have deflected fines to either side.

Where fines lightly cover rubble areas, hummocky areas are formed; e.g. R-1 (M:539 and 548), R-4 (M:231), R-9 (M:408), R-10 (M:427), and R-11 (M:492). Fines thin rapidly toward ray perimeters with very little extending beyond. There are several exceptions, one along the middle of R-1 (near the trench) where a tongue of fines passes between two rubble areas. Other exceptions are on R-6, 7, 8,

and 9. In each case fine deposits appear to have flowed through gaps between earlier block deposits.

Valleys apparently received the bulk of their fines, not from spilling out across the ray perimeters, but by flowing out through such gaps in the ray perimeters, chiefly along the circumferential band between 2 and 2 1/2 R_a. On some of the larger rays, fines apparently overwhelmed these gaps and drowned the neighboring valleys; e.g. (R-1 into V-1, R-4 into V-4, R-7 into V-6, R-9 into V-8 and 9, and R-11 into V-11).

2. Block Size

Block sizes on the surface of the ejecta blanket follow the Ray-Valley structure of the apparent lip (Fig. 35). Radially, block size decreases rapidly from the crater out to near the continuous block boundary. Beyond, the decrease is more gradual to the continuous ejecta boundary. The exceptions to this trend are in the various rubble areas where a local decrease in block size occurs due to more brecciation and between the continuous block and ejecta boundaries where local increases occur due to less brecciation.

Azimuthally, the largest blocks are exposed in the troughs, connecting valleys, and along ray perimeters. While maximum block sizes in the trench are comparable to those along ray boundaries at the same distances, the amount of brecciation in the trench is greater. Thus, while the observed smaller block sizes on rays is due in part to coverage by fines, there appears to be a basic difference in the mechanisms of deposition and perhaps post-depositional

rent within

ne to which

greater the

the less br

In addit

to be slig

similar obse

ar in situ

Observed

ection of F

ar for "PS

ne first ar

(1 vs 202),

at that blo

ch such dif

The obse

ically, as

ent and ave

larger blo

, there i

6]. More

5]. The

(62) or

movement within a ray segment. This difference may reflect the degree to which a flap segment is dispersed prior to impact; i.e. the greater the dispersion the less mass impacting per unit area and the less brecciation.

In addition to these Ray-Valley related patterns, block sizes tend to be slightly larger on the east (R-4 thru V-5) which corresponds to similar observations of the fallback and is probably related to larger in situ block sizes.

Observed block size is strongly affected by lithology. Comparison of Figures 35 and 51 shows that average block size is smaller for "PBO" than "RUL" units. Examples, with PBO areas listed first are: R-1 (M:540 vs 537), R-2 (M:184 vs 185), R-3 (M:201 vs 202), R-4 (M:236 vs 237), and R-9 (M:409 vs 410). The reason that block sizes are smaller on rays versus valleys is in part due to such differences in block composition; e.g. (R-3 vs V-2 and V-3).

The observed block size is also affected by drowning from fines. Initially, as drowning begins, the smaller blocks are preferentially covered and average size increases; but later, as drowning continues, the larger blocks are covered and average size decreases. In some cases, there is a clear increase in size; e.g. R-6 (M:306) and R-1 (M:545). More typically, size decreases; e.g. V-7 (M:348) and V-10 (M:443). The larger block sizes on R-3 (M:212 or 201) relative to R-1 (M:162) or R-7 (M:299) are due to the lack of fines on R-3.

An example of both lithology and drowning affecting block size distribution is observed on the outer ray segment of R-2 where large blocks ("RUL"), small blocks ("PBO"), and fines were deposited in an off-lap pattern to the east. A similar example in the opposite direction occurs on the outer ray segment of R-11.

Block size distribution is also affected by preshot topography. In the stream cut to the east of SGZ, block size at the bottom of the cut (M:262) is larger than block size on either side (M:261, 288a, 263, and 264) apparently due to preferential rolling and tumbling of the larger blocks down the hill; but not up the other side. An example of block movement downhill is observed outward from R-4 (M:224 and 226) where blocks are spread downhill beyond the continuous block boundary for several hundred meters. This is in contrast to the west (uphill) where there is an abrupt drop off at the continuous block boundary.

3. Block Areal Density

Block areal density follows the Ray-Valley structure of the apparent lip (Fig. 36). Areal density is primarily a reflection of the amount of drowning by fines; i.e. areal density decreases with increased drowning. Areal density is highest in the undrowned troughs; e.g. T-5 (M:247), T-7 (M:343), and T-11 (M:506) as well as in rubble areas near ray perimeters R-1 (M:532 and 172), R-2 (M:186), R-4 (M:237), R-7 (M:315), R-9 (M:410), R-10 (M:424 and 464), and R-11 (M:490). Local rubble areas also exhibit high areal densities; e.g. R-1 (M:167), V-3 (M:225), V-7 (M:321), and V-11 (M:511).

The previ

northeast (

ecrease in

ness of fi

ayers blan

ely covered

ner out fro

Areal de

viously seen

other side

ger than av

neral lack

The previously mentioned general shift of fines to the east and northeast (R-5 and 6) is noticeably reflected by the corresponding decrease in areal density. Field observations indicate that the thickness of fines is not necessarily greater than on other parts of the ejecta blanket as shown by several low flap segments that are barely covered (M:260, 278, and 303). However, fines are distributed further out from SGZ (M:307 and 309).

Areal density also reflects the preshot topography. In the previously mentioned stream cut (M:262) areal density is higher than on either side. Outward from R-4 (M:224 and 226) areal density is higher than average due to downhill tumbling of blocks coupled with a general lack of fines.

GEOLOG

This sectio

analysis of th

ationships betw

crater lip sho

the processes

ong the

demonstrat

. With th

mapping,

ture of the

ich provides

ass involved.

A. Geolog

1. Overv

The crate

crater rim,

which are the

.

Where exp

ic and stru

CHAPTER VI

GEOLOGIC CHARACTERISTICS OF THE CRATER AND CONTINUOUS EJECTA FIELD

This section presents the results from detailed geologic mapping and analysis of the crater and continuous ejecta field. Geologic relationships between in situ units in the wall and ejecta units in the crater lip show that the material in the lip was overturned and that the processes of overturning were orderly. Comparison of the geology along the trench excavation to that of the surrounding ejecta blanket demonstrates the inverted stratigraphic order of the ejecta blanket. With these first order relationships as a base line, detailed mapping, analysis, and comparison of the stratigraphy and structure of the crater, crater lip, trench, and ejecta blanket surface provides a means for understanding the crater and ejecta process involved.

A. Geology of the Crater Lip

1. Overview

The crater lip, exposed in near cross section inside and below the crater rim, was mapped in detail. The major features above the fallback are the wall, the soil horizon, and the overturned ejecta flap.

Where exposed, the wall provides a good 3-dimensional stratigraphic and structural record of the in situ geology that compliments

drilling and

dition, the

rms of blas

The ejecta

mally insid

ayered. Si

as with littl

t was complet

ne blanket.

The soil

he remains th

s cannot gro

e crimust (w

ower detona

1. Mapp

Mapping

mediately

0.45 m and

ks were t

TEC. From

ained on a

ethod to ei

A base

2.4 station

x 2.4 m a

the drilling and geophysical logging data discussed in Chapter II. In addition, the wall provides an imprint of the cratering processes in terms of blast-induced fracturing and displacement.

The ejecta flap lies above the wall and contains the material originally inside the wall that was compressed, fractured, bulked, and ejected. Since at the crater lip the ejecta was overturned en masse with little post-depositional movement, it contains the simplest yet most complete record of the stratigraphic units comprising the ejecta blanket.

The soil horizon lies between the wall and the ejecta flap and thus contains the hinge line along which overturning occurred. Marking the preshot ground surface, its present position is a measure of the net upthrust (upthrust followed by some relaxation) resulting from the Schooner detonation.

2. Mapping Procedures

Mapping control was established with 40 stations spaced approximately every 25 m along the crater rim and surveyed vertically to $\pm$ 0.15 m and horizontally to $\pm$ 0.3 m. Photographs (35 mm color slides) were taken of each station from the opposite side of the crater. From this distance of approximately 300 m, the field of view, centered on a 2 m stadia rod at the prime station, included the stations to either side.

A base map delineating major features was produced for each of the 40 stations (L:1 thru 40) by projecting the slides at a scale of 1 cm = 2.4 m and mapping the center one-third. Each mapping unit

[illegible] and "A" in

[illegible] is a rep

[illegible] center rim

[illegible] ified a

[illegible] ming uni

[illegible] ination of

[illegible] vation fro

[illegible] into the

[illegible] ently accura

The res

[illegible] ure survey c

[illegible] is present

[illegible] ch is pre

[illegible] ations of th

1. Wa

a. St

Mapping

[illegible] road along

[illegible] ntified, b

The "A

[illegible] consistenc

[illegible] water si

[illegible] the objecta

[illegible] ficiency.

("t" and "v" included with "g") was recorded. Individual blocks were mapped in a representative manner with only the larger blocks along the crater rim mapped 1:1. Base maps were checked in the field and details added as required. Boundaries are accurate to within 1/2 m for mapping units "P" thru "p". Due to inaccessibility, field confirmation of the other units ("s" thru "L") was limited to visual observation from the crater rim, the crater floor, and from along one rope into the crater below L:2. Boundaries for these units are probably accurate to within 1 m.

The resultant Geologic Map of the Crater Lip, compiled with the above survey control, is provided in the map pocket and a generalized map is presented in Figure 37. An enlarged photograph of a portion of Crest 9 is presented in Figure 38 and selected photographs of other sections of the crater lip are presented in Figure 39.

3. Wall

a. Stratigraphy

Mapping units down through most of the "L" unit (~27 m) are exposed along portions of the crater wall. The "P" unit is not identified, but is probably just barely covered by fallback beneath L:31.

The "M" unit can be positively identified (color and texture) intermittently on the west (L:27-37); but must be present throughout the crater since it is observed everywhere along the crater lip and in the ejecta field. Where identified, it ranges from 1.2 to 1.8 m in thickness. The contact between the "U" and "L" units is based

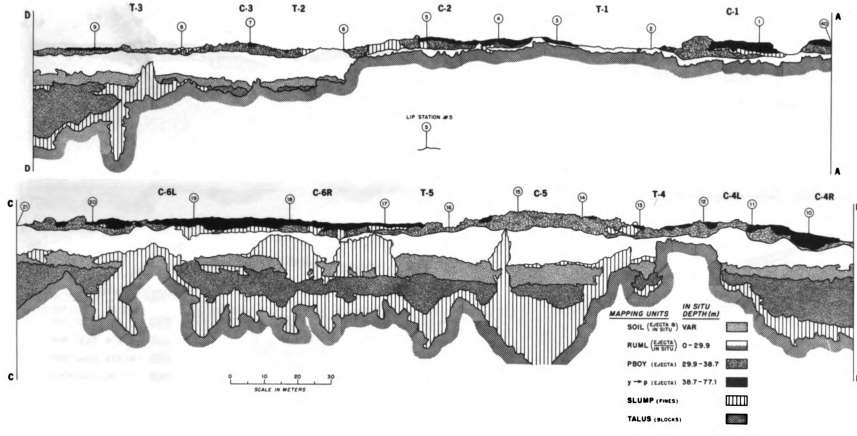

Figure 37. Generalized Geologic Map of the Crater Lip

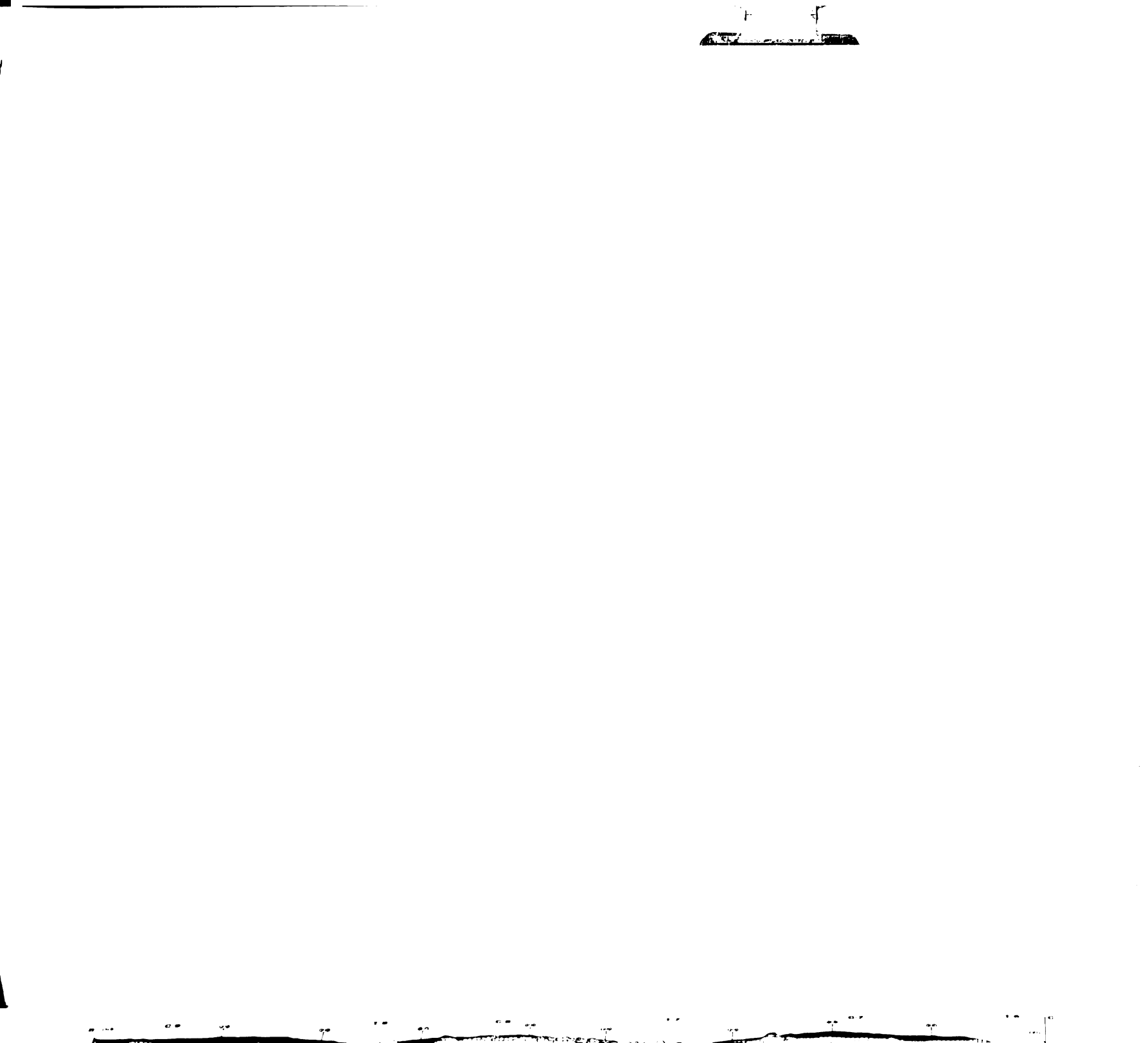

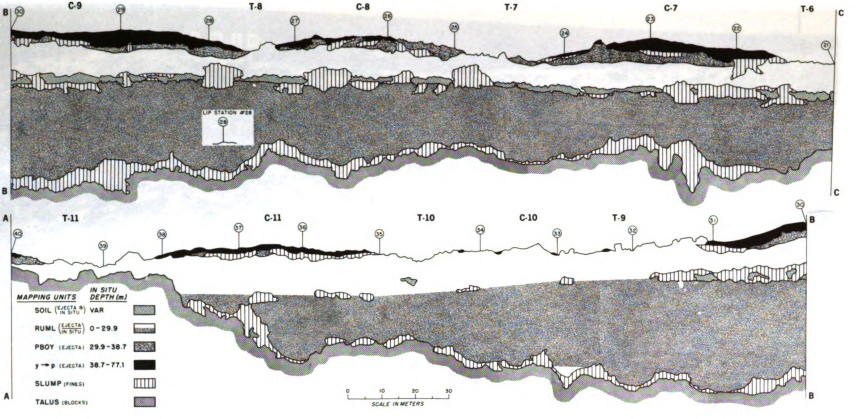

Figure 37. (cont'd)

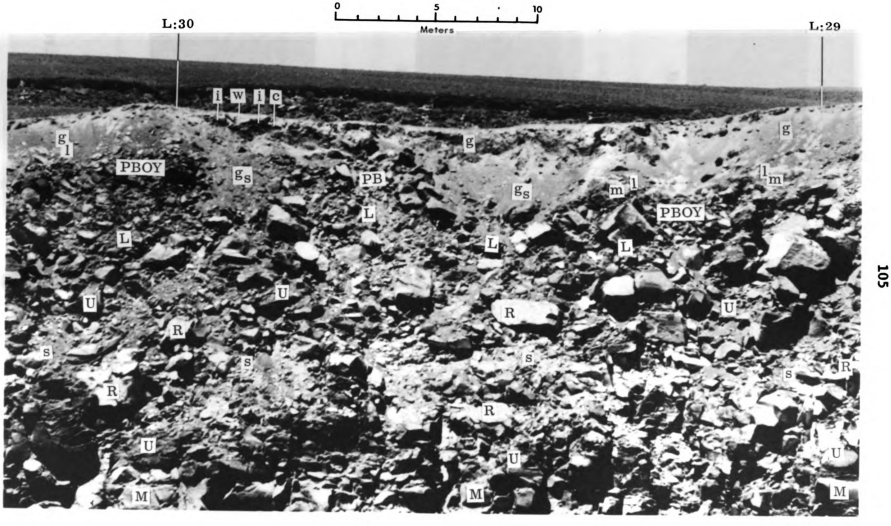

Figure 38. Photograph of a Portion of Crest 9 with Mapping Units Indicated

L:3

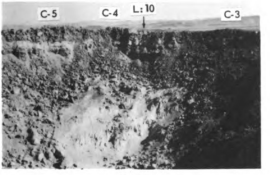

L:10

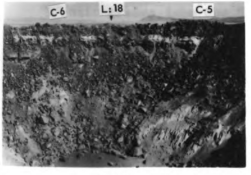

L:18

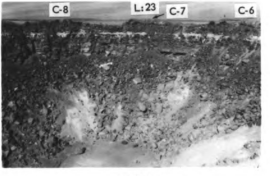

L:23

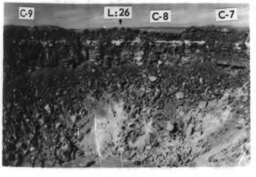

L:26

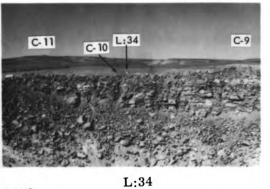

L:34

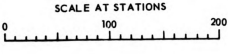

Figure 39. Selected Photographs of the Crater Lip with Lip Stations and Crests Indicated

primarily on the higher degree of fracturing for the "U" unit. In addition, the color of the "U" unit varies from red to purple-gray whereas the "L" unit is a consistent medium gray. Due to poor color contrast and sparsity of fracturing, the contact between the "U" and "L" units beneath L:9-11 is in question.

The upper portion of the "R" unit is easily identified by its dark brick red color on the east changing to pale red on the south and north and by its ever present white caliche coating. With depth the "R" unit grades into the "U" unit with the contact often difficult to pick. Local variations in thickness of the "R" unit are usually at the expense of the "U" unit; e.g. on the west-northwest (L:29-30) the "R" unit doubles its thickness over an 18 m stretch while the thickness of the "R + U" unit remains nearly constant.

While units exposed in the wall are continuous (with the possible exception of "M"), they exhibit considerable variation in thickness about the crater. Figure 40 presents thickness of in situ units in the crater wall below each of the crests and troughs. As expected, thicknesses are independent of the Crest-Trough structure of the crater lip with azimuthal trends different for each of the units; i.e. "U" thickens to the north (C-7 to T-6), R to the west (C-11 to T-10), and "s" to the east (C-6 to C-5). The range in thickness for the "R" and "U" units approaches $\pm$ 50% about their respective means, while for the "R + U" unit the variation is near $\pm$ 20%. The latter is similar to variations observed for the "R" + "U" unit in the four satellite drill holes of U20u (Fig. 8).

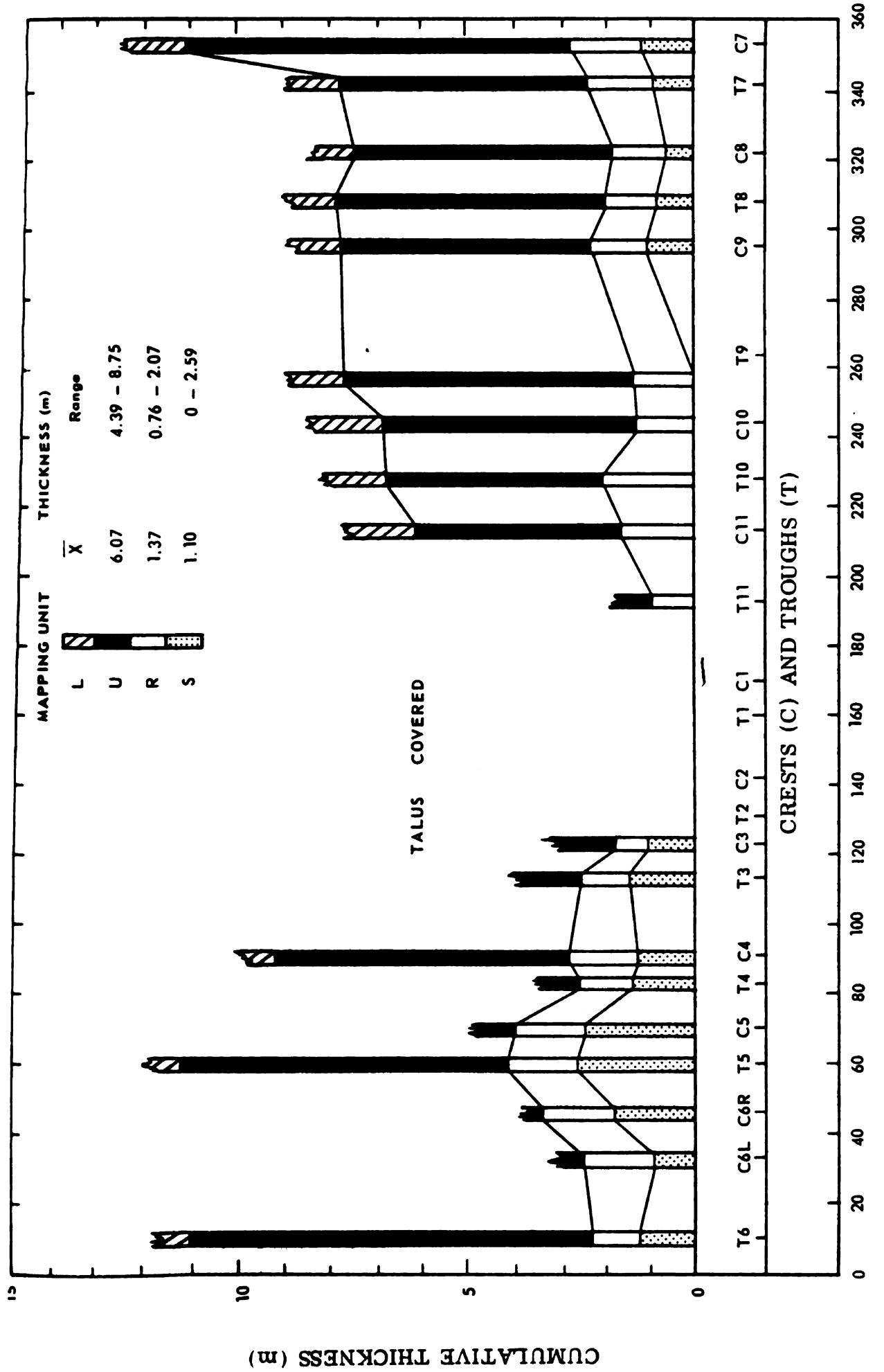

Figure 40. In Situ Mapping Unit Thicknesses in the Crater Wall

These circumferential variations in thickness, color, and texture obviously imply corresponding radial variations which have important implications in interpreting ejecta composition observed in the field; i.e. in determining whether changes in ejecta composition are the result of in situ conditions or crater and ejecta processes.

b. Structure

No faulting, folding, or other significant structural discontinuities in the in situ geology were observed. Each of the welded units is well jointed with all joints near vertical. The "L" unit exhibits hexagonal jointing with columns 5 to 10 m across and 10 to 20 m long. Where close examination was possible, welded units exhibit weak ("U") to strong ("L" and "P") flow foliation. Resulting horizontal partings were also observed in ejecta blocks and in the core. Vertical joints and many of the foliation partings are veneered with secondary deposits.

Joint trends observed along the crater wall are in general agreement with surface mapped joints. Figure 41 presents major and minor joint trends for the "U" and "L" units observed on those crater wall surfaces not covered by fallback. Measurements were made from the same photo set used in mapping the crater lip. Results are somewhat difficult to interpret because the wall is partially covered by fallback, there are numerous jagged reentrants, and local blast fracturing tends to obscure some joint faces (particularly in the "U" unit). In addition, orientation of joints vary with depth and

U UNIT (1.8 - 8.5m)

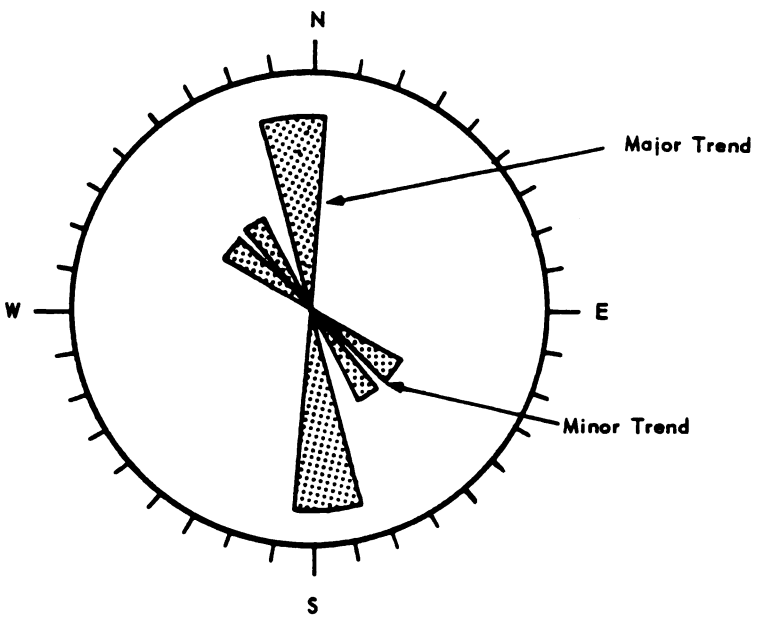

L UNIT (9.8 - 29.9m)

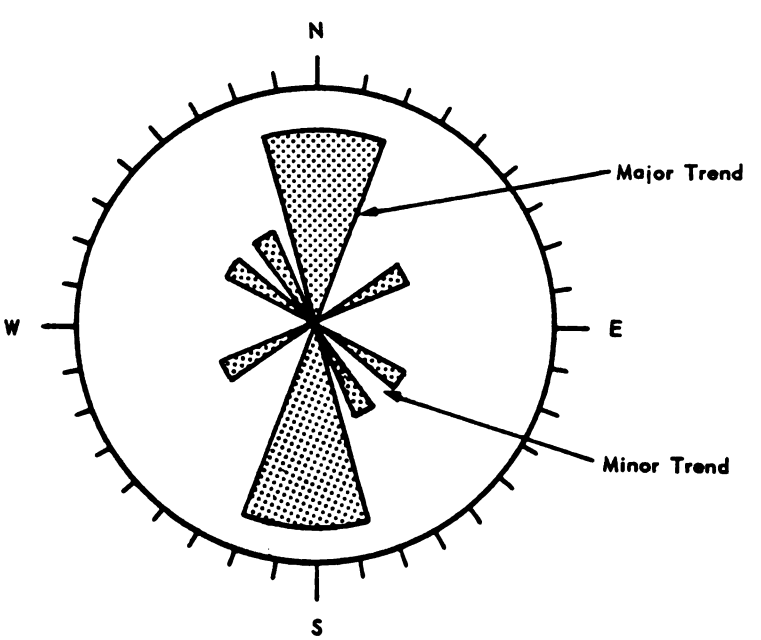

Figure 41. Major and Minor Joint Trends for Welded Units in the Crater Wall

azimuth, similar to surface joints (Fig. 9).

Allowing for these constraints, the major joint trend for the "U" unit is north-south with a minor trend northwest-southeast. With joints in the "U" unit orientated along a rectangular grid, as observed in the "U" ejecta blocks, an east-west joint trend should have been observed. Unfortunately, the south wall is covered by fallback and the north wall is badly fractured. Major trends in the "L" unit are also north-south with minor trends northeast-southwest and northwest-southeast, as might be expected with the observed hexagonal jointing.

c. Cratering Effects

The dominant effect of cratering on the wall was to open up existing joint and foliation separations several centimeters. Blocks were fractured, primarily parallel to horizontal foliation planes and secondarily parallel to vertical joint planes. A new set of diagonal fractures was developed and locally blocks were broken and brecciated. The "L" unit was least fractured and relics of its original columnar structure are visible.

Traces of major through-going vertical joints are drawn on the crater lip maps. Joint paths are offset slightly, probably due to differential uplift and relaxation. Joints are most prominent in the "L" unit with some extending as far as the "R" unit. Major fracture planes, with dips clustered about 51^{o}, are also traced on the crater lip map. Fracture planes are distinguished from joint and foliation planes in that they are fresh, less regular in path, partially

discontinuous, and diagonally cut joint and foliation planes. Displacements along fracture planes do not exceed a meter. The higher concentration of open joints and fractures on the west wall versus the east wall may be related to the greater distance of the east wall from SGZ (148 vs 112 m). Areas of intense brecciation vary locally and do not appear to be related to crests or troughs. Major fracture planes, on the other hand, tend to be concentrated beneath troughs; e.g. T-7, 8, and 9.

Figure 42 presents a trace map of the ejecta flap and crater wall beneath Trough 9 (L:31). Blocks 2/3 m and larger are traced and brecciated zones, slump zones, and mapping units are outlined. Plots of horizontal block lenth (l) versus vertical block thickness (t) are presented in Figures 43 and 44 with data summarized in Table 3.

While the largest blocks in the wall are from the "L" unit, mean 2-D size (l x t) increases only slightly from "R" (1.9 m^2) to "U" (2.0 m^2) to "L" (2.4 m^2). Most of the blocks are rectangular with $l > t$. Mean l/t ratios decrease from "R" (2.1) to "U" (1.5) to "L" (1.4). For a given unit the larger l/t ratios, ranging from 5 to 9, are associated with the larger blocks. Blocks in the ejecta flap are more equidimensional (l/t $\sim$ 30% less) and smaller (l x t $\sim$ 50% less) than blocks in the wall.

4. Ejecta Flap

a. Stratigraphy

All in situ mapping units down through "p" (77.1 m) are present as mappable units somewhere along the crater lip. These units are well

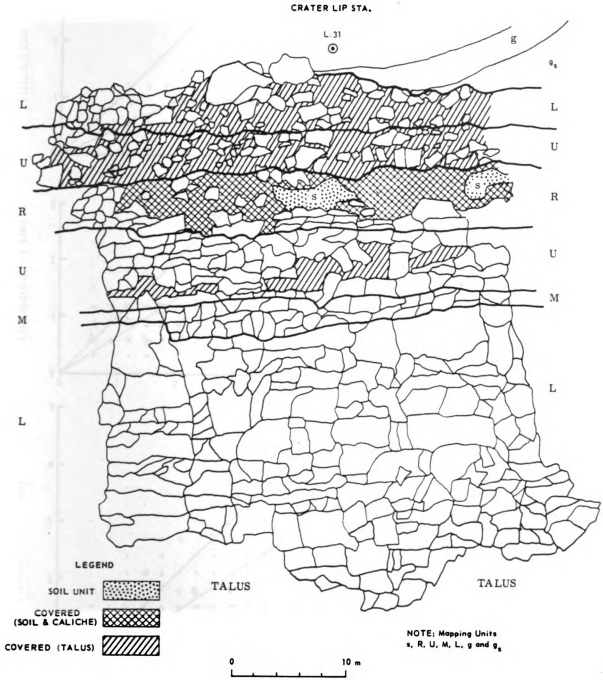

Figure 42. Trace Map of Welded Blocks in the Ejecta Flap and Crater Wall Beneath Trough 9

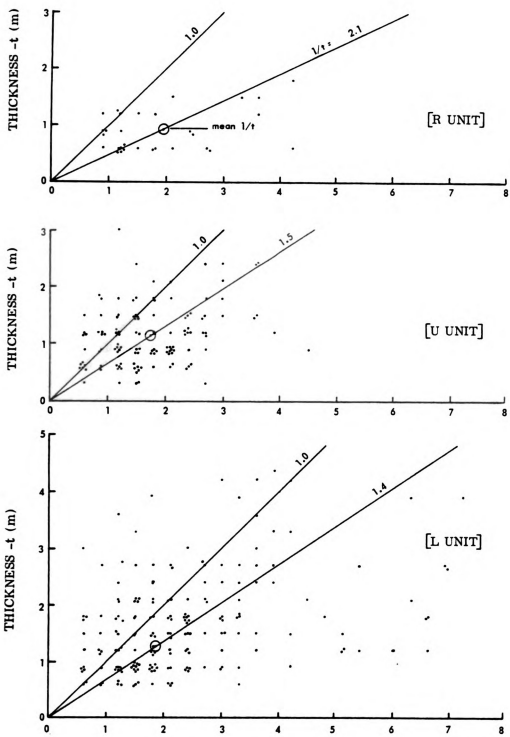

Figure 43. Size and Shape Distributions of Welded Blocks in the Crater Wall - Trough 9

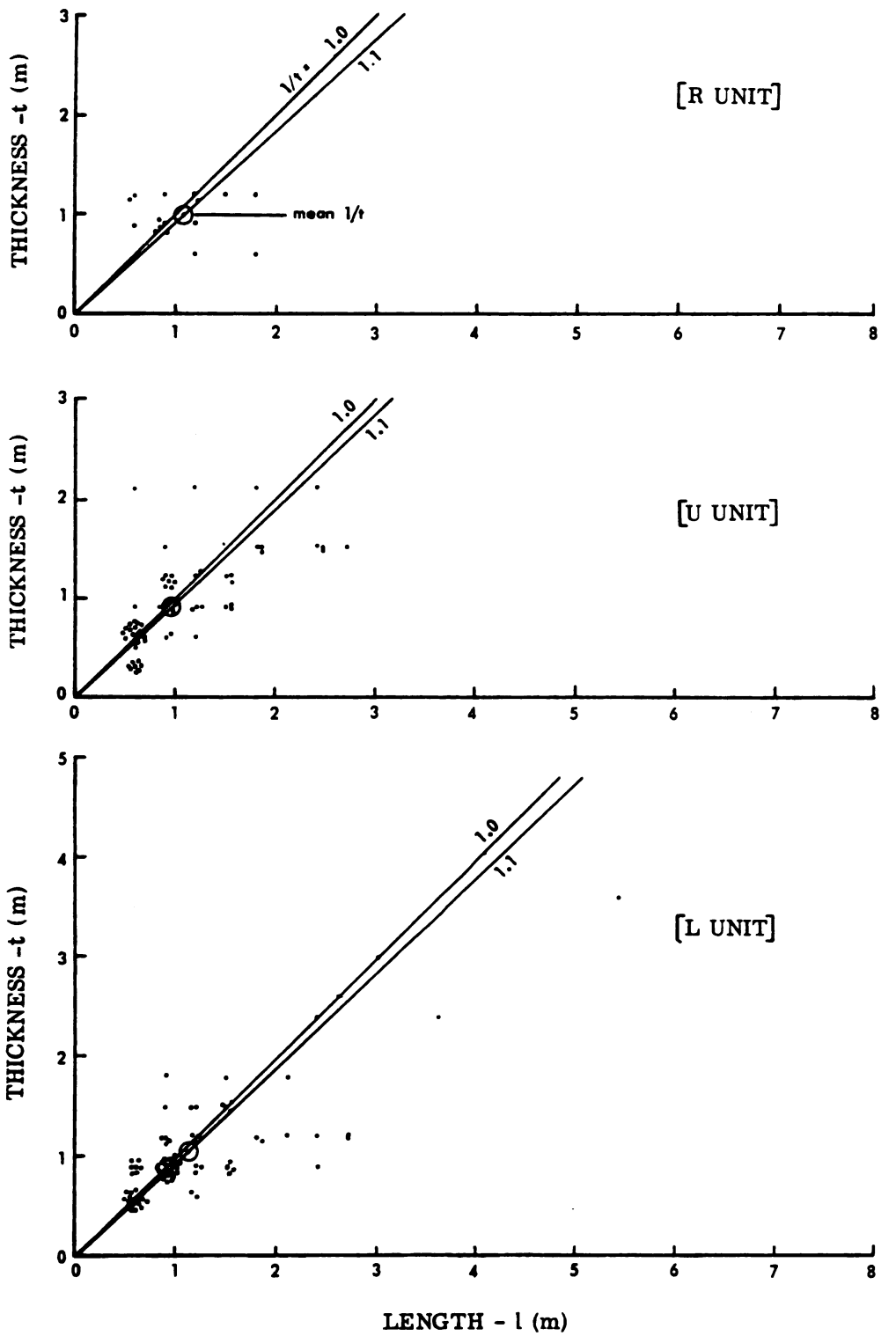

Figure 44. Size and Shape Distributions of Welded Blocks in the Ejecta Flap - Trough 9

TABLE 3

SIZES AND SHAPES OF BLOCKS IN THE CRATER WALL AND EJECTA FLAP AT CREST 9

Unit	Length [l] (m)		Thickness [t] (m)		Area [l x t] (m^2)		Shape [l/t]	
	$\bar{X}$	Max.	$\bar{X}$	Max.	$\bar{X}$	Max.	$\bar{X}$	Range
"L"								
wall	1.86	7.32	1.29	4.27	2.40	28.99	1.44	0.2-2.5
flap	1.12	5.49	1.06	3.66	1.69	20.07	1.06	0.7-2.7
flap/wall	0.60		0.82		0.50		0.74	
"U"								
wall	1.76	4.57	1.15	2.74	2.02	8.92	1.53	0.4-9.0
flap	0.99	3.05	0.91	3.05	0.90	9.29	1.08	0.3-2.0
flap/wall	0.56		0.80		0.45		0.71	
"R"								
wall	1.96	4.27	0.95	2.74	1.87	7.80	2.05	0.4-7.0
flap	1.09	1.83	1.01	1.22	1.10	2.23	1.08	0.5-3.0
flap/wall	0.55		(1.06)?		0.59		0.53	

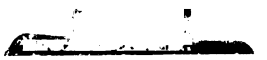

exposed in near cross section and, except for obvious postshot slumping, exhibit inverted stratigraphic order down to the finest detail. None of the mapping units, including brecciated zones within the welded units, are observed to mix with other units to any degree that is not readily explainable by late-time relaxation or postshot slumping. Fallout, while not mapped, covers the entire rim surface to an average depth of several centimeters with local accumulations reaching two to three times that value.

To a first order, in situ units are arranged in an upside-down layer-cake structure with the highest topography containing the thickest sections of ejecta and thus the lowest in situ units. Therefore, distribution of ejecta is not uniform about the crater lip with units down through the upper portion of "L" (~15 m) continuous and units below found primarily in crests (Fig. 45). For example, crests with large accumulations of ejecta (C-1, 7, and 9) contain units down through "w" and "p" (61.9 - 77.1 m) while crests with little ejecta (C-10) contain units only down through "L" (9.8 to 29.9 m). Similarly, troughs with little ejecta (T-10) contain only the very top of the "L" unit (~15 m). Major exceptions to this rule are on the southeast and east. Crests 4 and 5 have the thickest accumulations of ejecta, yet contain units only down through "Y" (36.7 to 38.7 m) while heavily filled troughs (T-5 and 4) contain units down through "P" (29.9 to 33.2 m) and "Y" (36.7 to 38.7 m), respectively.

Superimposed on this first order layer-cake structure are a number of second order features which include: (1) crater wide

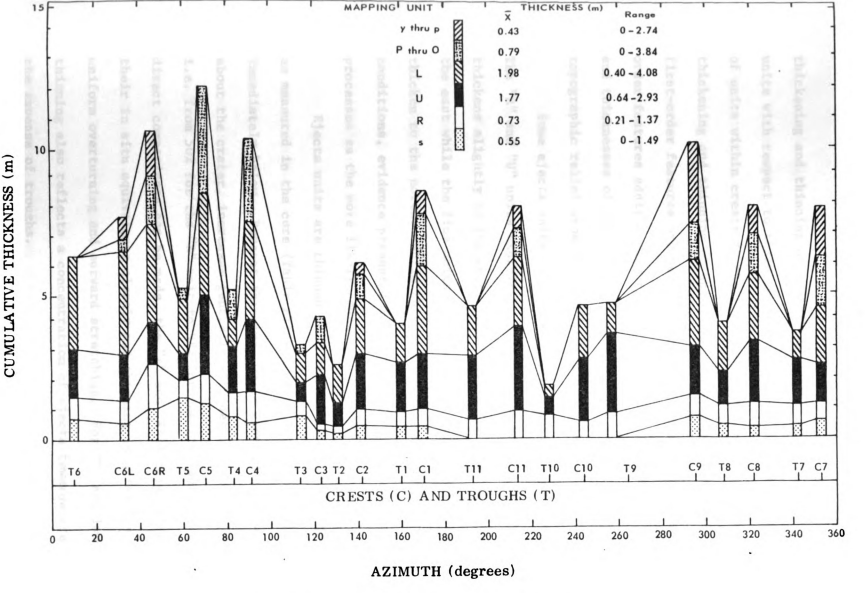

Figure 45. Ejecta Mapping Unit Thicknesses in the Ejecta Flap

thickening and thinning of units; (2) overall thinning of ejecta units with respect to their in situ source; (3) general concentration of units within crests at the expense of troughs; and (4) local thickening and thinning of units within crests and troughs. While first-order features probably reflect simple overturning, second-order features additionally reflect variations in physical properties and thicknesses of the in situ units, further modified by the topographic relief upon which they were deposited.

Some ejecta units thicken and thin across the crater region. The "R" and "U" units exhibit no strong trend while the "L" unit thickens slightly to the east. The "BOY" units thicken strongly to the east while the fine units are noticeably absent on the east, but thicken to the north. While these variations could be due to in situ conditions, evidence presented in Chapter VI. C would suggest ejection processes as the more likely cause.

Ejecta units are thinned with respect to their in situ source as measured in the core (Table A1) and where possible from the wall immediately below. Percent thinning, while varying considerably about the crater, increases generally with depth to the in situ unit; i.e. from 50% for the "R" unit to 98% for the fine units. Where direct comparisons can be made, the "s" and "R" ejecta units track their in situ equivalents closely and thinning is primarily due to uniform overturning and outward stretching. For "U" and lower units, thinning also reflects a concentration of ejecta towards crests at the expense of troughs.

Evidence from the crater rim and trench shows that most in situ units below "L", particularly the fine units "g" through "p", attain their thickest sections beyond the crater rim. The "BOY" units are absent on Crest 10; but do occur some 30 m further out, as though that portion of the flap was sheared outward en masse during overturning.

While inverted stratigraphy is everywhere present, it is not unusual to find one or more units missing in a given section; e.g. L:3 ("w" and "g" on "L"), L:18 ("g" on "B" through "Y"), and L:28 ("g" on "P" and "B").

The weakly welded and nonwelded units, consisting primarily of fines, tend to spread laterally outward, smoothing the surface and where sufficient in volume (especially the "g" unit) dominate crests. Where small in volume they exist as lenticular masses a few meters in size thinly draping underlying blocks or spreading over underlying fines. Lenticular masses of fine units (typically "c" and "i") are found predominantly on the largest crests (C-7 and 9), but are also observed on smaller crests and even some troughs (C-10 and T-9). Large welded blocks along the crater rim are draped by such small masses ($\sim$0.1 m^3), almost always in inverted stratigraphic order; e.g. L:16, L:23, L:33, and L:37. Most of these masses appear to have been deposited in a pliable (wet?) condition.

Individual units locally peak about the crater. Peaks appear to be primarily due to local thickening; but bulking and/or arching may be important in some cases, particularly for the welded units.

Units typically peak beneath crests; but the "L" unit, and sometimes the "U" unit, also peak beneath troughs; e.g. T-2 and 6. Often, total thickness of the "L" unit is greatest beneath neighboring crests. Within crests C-2 and 4, the "L" unit abruptly peaks to the surface.

b. Structure

The foundation of all crests is the "L" unit while major crests are capped by concentrations of the "g" unit. Crests, however, are neither the result of a concentration of any one unit nor of a particular set of units. While units tend to thicken beneath crests, amounts and locations vary. Many units thicken more than once under a crest; but just as many do not thicken at all. Concentrations (peaks) of units are seldom vertically aligned and the overall stratigraphic pattern of crests is seldom symmetric with respect to the crest peak. In addition, the lowest in situ unit present is not necessarily the highest topographic deposit.

Compare C-9, which contains a double peak of "L" and a massive broad cap of "g", to C-7, which contains only a minor "L" peak and a thick cap of "g". Also note that on C-9, the thickest section of "g" occupies the saddle between two "L" peaks. Crest 8 contains a peak of "L" but only a small cap of "g" which is on the left of the crest, while "BOY" units cap the right. Thus, C-8 and 9 are due primarily to peaking of "L" and C-7 is due primarily to peaking of "g". Crests 4 and 5 consist of peaks of "L" and "BOY", but no "g".

The distribution of "BOY" units is neither continuous nor symmetric with respect to a peak. On Crests 1 and 8 they are shifted

to the clockwise while on Crest 7 they are to the center and counter clockwise. Crest 6 is interesting in that it contains three minor peaks of "BOY" and "yml" units, each of which are roughly aligned with rays in the ejecta blanket (see Fig. 51).

Each of the ejecta units observed in the crater lip exhibits a distinct set of characteristics directly related to their in situ properties. The welded units are blocky and form irregular topographic surfaces. Where large in volume, especially the "L" unit, they easily fill underlying topographic irregularities while producing large topographic irregularities themselves. Where small in volume, especially the "BOY" units, they do not completely fill underlying topographic irregularities and are typically observed as thin, discontinuous layers.

The in situ structure of welded units becomes increasingly disorganized above the preshot ground surface. Caliche surfaces are less and less aligned, and major fracture planes become difficult to trace. Mapping units "PBOY" are typically brecciated, but large in situ blocks also are present.

Overall, blocks in the flap relative to the wall are smaller by a factor of 2 to 3. In general, ejecta sizes in the flap are ordered as follows: "L > P > R,U > M > B,O > Y >>> c >> g,y,m,l > p > w". Where brecciation occurs, "P" blocks are typically smaller than "Y" blocks. There are local variations in fracturing; e.g. "L" blocks in T-6 are one-half as large as those in T-7 and "L" blocks in C-9 are twice as large as those in C-8. However, there is little correlation of block

size with crests or troughs.

5. Soil Horizon

The soil horizon thickens and thins about the crater reaching a maximum of 4 m on the east (L:14-17) and thinning to near zero on the west (L:31-38). Where the soil horizon is absent, location of preshot ground surface can be inferred by either the caliche coated "R" unit or by a narrow band of scattered vegetation, both of which are closely associated with the soil horizon elsewhere.

The soil horizon consists of the in situ unit directly overlain by the overturned ejecta unit. Observation of plant roots in the one accessible soil outcrop area beneath T-2 (L:6) indicates that the thickness of the ejecta portion of the soil horizon varies from 1/2 to 2/3 that of the in situ portion. This factor was used as a guide in drawing the hinge line about the crater.

The soil horizon is not continuous about the crater; but segmented with most breaks aligned along the previously discussed diagonal fracture planes in the wall. Vertical and horizontal displacements range up to a meter and soil horizon segments are tilted a few degrees with respect to each other; e.g. L:7, 14, 20, 30, and 38. This tilting suggests differential movement during uplift, relaxation, or both. Since fracture planes extend up into the ejecta flap, these planes were active during the relaxation phase.

Other structural features visible in the crater which may be related to differential upthrust/relaxation movement include: a possible slump covered fault below Trough 4 (L:12-14) with a vertical

offset of 3 m and the displaced soil horizon segment beneath Trough 10 (L:34-35) with a vertical displacement of 1.5 to 3 m. The sharp increase in thickness of the soil horizon beneath L:14-17 is probably the result of local in situ thickening since the underlying "R" unit remains nearly constant.

B. Geology of the Trench

1. Physical Setting

A 350 m trench was excavated along the length of Ray 1 from the crater rim to near the ray terminus, 500 m from SGZ. The trench intersects the crater to the west of C-1 and remains on the west side of the R-1 axis until 340 m, where it crosses the axis and finally terminates 80 m to the east. Along this path the trench transects a number of key features of the Schooner ejecta blanket, exposing their structure and stratigraphy with depth.

The outer half of the trench intersects the preshot ground surface while the inner half bottoms within the overturned "L" unit. The trench has an average width of 5 m. Its walls range up to 4 m, with typically the lower 1/2 to 1/3 covered by debris. The ejecta portions of the trench walls are nearly vertical except for the first 30 m where slopes as low as 45^{o} occur.

The debris, from erosion of ejecta fines along the trench, does not overly detract from the mapping since it is discontinuous and in many places thin enough for ejecta units to show through. In addition, mapping of the trench was supplemented by observations of

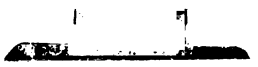

the trench floor and of material excavated from the trench (trenchings). Figure 46 presents an enlarged photograph of a portion of the trench cutting through Crest 1. Selected photographs of other portions of the trench are presented in Figures 47 and 48.

2. Mapping Procedures

The east wall exhibited the best exposures and was mapped in its entirety. Selected areas on the west wall were mapped for 3-D comparison. Stations T:-6 through T:112 were established at approximately 3 m intervals and surveyed to $\pm$ 0.3 m horizontally and $\pm$ 0.15 m vertically. Color photographs (35 mm slides) were taken perpendicular to the trench wall and centered on each station with a field-of-view that included the station on either side. Projecting at a constant scale (1 cm = 0.36m) base maps containing major features were prepared for each station; details were added in the field.

Each mapping unit ("t" and "v" included with "g") and mix unit was outlined in its entirety. Individual blocks over 1/3 m in largest dimension were mapped 1:1. Smaller blocks were also mapped, but only on a representative basis. Fallout, covering the ejecta blanket up to 10 cm thick, was not mapped. A composite map, using the center 1/3 of each base map, was constructed with the established survey control. The resulting Geologic Map of the Trench is provided in the map pocket and a generalized version is presented in Figure 49.

3. Major Features

Five ejecta units are defined: blocks (B), fines (F), slightly mixed fines (A_m), moderately mixed fines (A_x), and well mixed fines

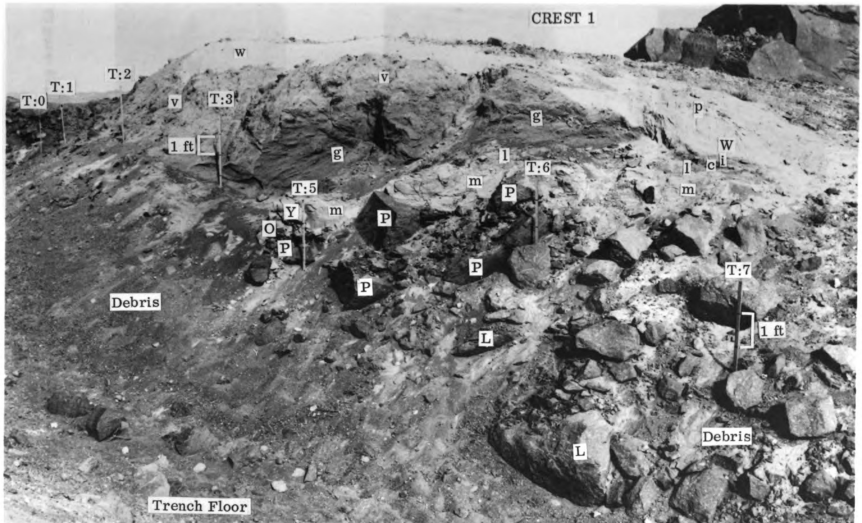

Figure 46. Photograph of the Trench Through Crest 1 with Trench Stations and Mapping Units Indicated

Toward Crater From T:75

T:5

T:19

T:22

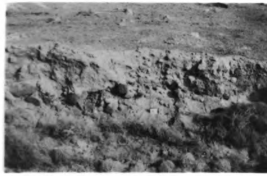

T:32

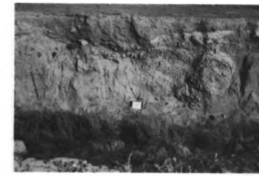

T:40

Figure 47. Selected Photographs of the Trench with Trench Stations Indicated (Clip Board is 35 cm Long)

T:43

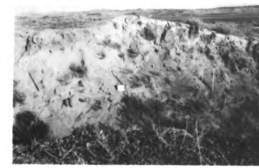

T:56

T:60

T:85

T:87

T:95

Figure 48. **Selected Photographs of the Trench with Trench Stations Indicated (Clip Board is 35 cm Long)**

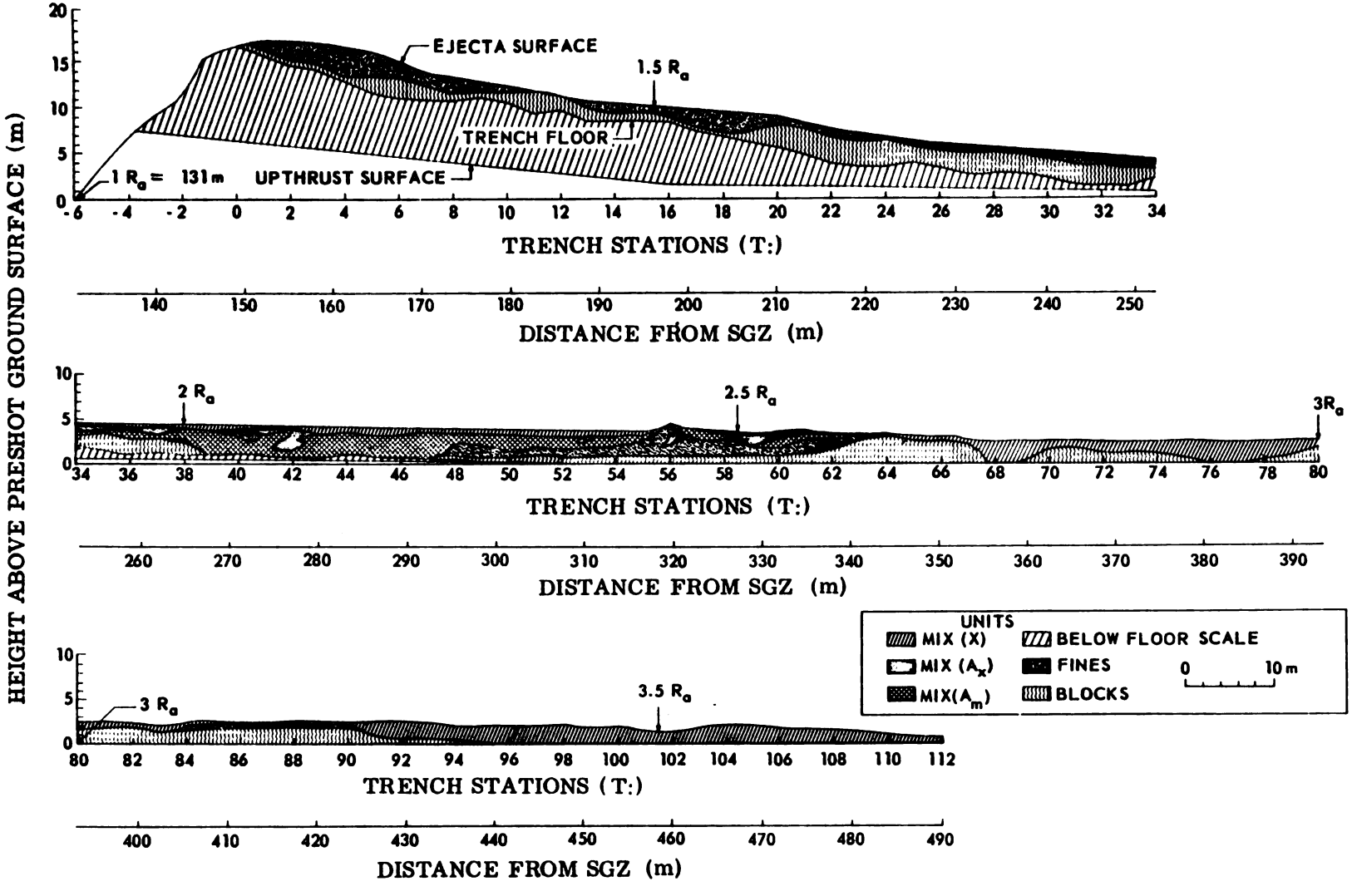

Figure 49. Generalized Geologic Map of the Trench

(X). Block units are from the upper densely welded tuff (mapping units "R" through "Y", 0 to 38.7 m) and fine units are from the weakly welded and nonwelded tuffs (mapping units "y" through "p", 38.7 to 77.1 m). The three mix units consist of fine units that are in various stages of mixing, with unit integrity preserved, partially destroyed, and totally destroyed, respectively.

Major trench features consist of four flap segments composed of block units overlain by fine units. Flap segments are in turn overlain and filled in by the three mix units. Flap segments become smaller, thinner, and more dispersed with distance while the mix units become thicker and more mixed with distance. Only the first segment produces topographic relief observable from the surface. The gap between the first and second segments (T:39 - 46) is filled with mix units and lies within the circumferential ring of smooth areas described in Chapter V.

Each segment and subsegment is composed of mapping units in near perfect inverted stratigraphic order with almost no mixing within or between units. The overlying mix units are also ordered, but mixing increases both upward and outward. Gradations between mix units are predominantly in the outward direction with vertical stratification typically preserved.

Figure 50 presents cumulative thicknesses as a function of distance along the trench for the five ejecta units. Measurements were made at each trench station with interpolation for areas covered by debris and for areas between the trench floor and the upthrusted

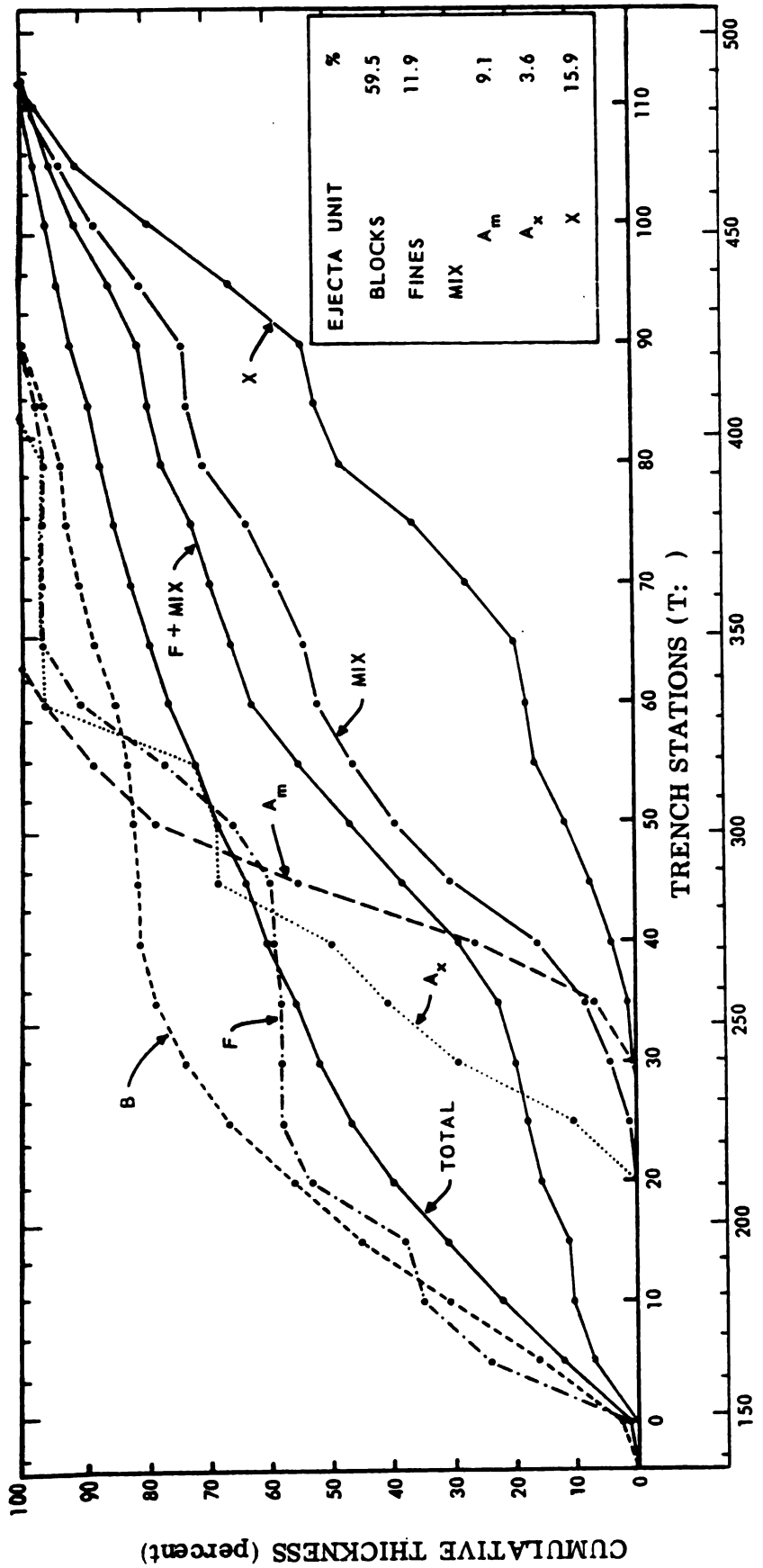

Figure 50. Distribution of Major Ejecta Units along the Trench

ground surface. The ejecta blanket decreases regularly outward with the 50th percentile occuring at 1.8 R_a (235 m from SGZ).

Distribution of individual ejecta units was controlled to a large extent by their in situ position, thickness, and physical properties, which affected their initial deposition and subsequent movement. Block and fine units are distributed closest to the crater, being contained primarily in the flap segments and undergoing little post-impact movement. A_m and A_x mix units, formed by little to moderate mixing of fine units, are concentrated near the middle of the trench in a relatively narrow band. X mix units, formed by the thorough mixing of fine units, overlie all other ejecta units beyond T:28.

Characteristics of the ejecta units are divided into primary, secondary, and tertiary features. Primary features are the result of the initial emplacement of ejecta. Secondary features reflect movement of ejecta after deposition. Tertiary features result from late-time deposition of discrete ejecta masses such as ballistic impacts, secondary cratering, and secondary ejecta deposition. Primary and secondary features are relatively large in areal extent and are observed on both sides of the trench while tertiary features are not.

Each of the five ejecta units is discussed in greater detail below in terms of its primary, secondary, and tertiary features. In any interpretation of these features, one must recognize that there was movement of ejecta in and out of the plane-of-the-trench.

4. Block Units

a. Primary Features

Block units make up 59.5% (by area) of the ejecta along the trench and form the large majority of the four flap segments. Blocks also comprise 10% of the mix unit beyond T:90.

The first flap segment contains four subsegments (T:-4-39, 47-68, 69-75, and 78-95). Each consists of a plateau followed by a drop-off, matching surface expressions on Ray 1 as well as "steps" in the floor of the trench. Along the length of the first segment, the trench floor bottoms within the "L" unit, which when cleaned of debris typically consists of overturned and unbroken hexagonal blocks in partially interlocked positions. Prominent blocks are indicated in the Geologic Map of the Trench; e.g. the 5 m diameter by 1.5 m thick hexagonal "L" block marking the floor at the trench-crater intersection (T:0-1). It appears that within the first segment, the trench floor may separate partially interlocked blocks below from the easier-to-excavate and jumbled blocks above. This corresponds to the decrease in block interlocking with distance above the upthrusted ground surface observed along the crater lip.

The outer three flap segments are separated by distances of 24, 5, and 6 m, respectively, over which there appears to be no continuous deposition of blocks. Whether these segments are connected out of the plane-of-the-trench is not known since surface exposures are absent. The second segment consists of one well exposed subsegment (T:61-68) and another subsegment (T:48-59) with block units covered by slump on

the east wall, but visible on the west wall. The third flap segment is very short and may well be connected to the second out of the plane-of-the-trench. The fourth segment is opposite a topographic high (exposed flap segment) about 50 m to the west and may be related. The outer edge of the fourth segment drops off sharply beyond T:90.

The first six subsegments (first two flap segments) are broadly triangular in radial cross section, with back slopes (towards SGZ) steeper than front slopes (10-30° vs 5-10°). The first subsegment (T:0-7) which can be viewed on both sides of the trench, as well as along the inside of the crater lip, is horseshoe shaped in plan view. In lateral cross section it is convex upward towards both the east and west.

All block units are exposed along the trench in near perfect inverted stratigraphic order. Following the upside-down layer-cake structure viewed in the crater lip, units observed successively outward are from successively higher in situ units. This pattern is partly repeated in each of the segments and subsegments with the most complete and thickest stratigraphic sections located on the back slopes.

Beds of "L" through "Y" are exposed directly in the trench wall, while "R" and "U" units are observed as individual blocks near the floor of the trench and in the trenchings. Each block unit consists of a few large in situ blocks together with a wide range of smaller broken and brecciated blocks.

With distance, maximum block size decreases and degree of breakage and brecciation increases. Block units thicken, thin, and are locally missing, but preserve their integrity with little mixing between. The "L" unit, contributing the largest ejecta volumes and block sizes, dominates all segments. "BOY" units, being both smaller in volume and in block size, tend to fill in the underlying irregularities although locally they dominate. For example, "BOY" units are well represented in the center of the first segment (T:20-30) and in portions of the second segment (T:62-65), poorly represented in the fourth segment, and absent in the third segment.

b. Secondary Features

The triangular-shaped radial cross section of many of the flap segments suggests outward movement (spreading) after initial deposition. That segment cross sections become broader with distance suggests that such movement increases with distance. Observations of the surface morphology of the ejecta field (Chapter V) also supports such movement. Since there is little mixing between units, such movement must either be en masse or less likely between units.

There is evidence for tumbling of individual blocks along present ray surfaces. Presumably such movement could have also occurred along interim surfaces during emplacement of the ejecta blanket. The "Y" blocks incorporated within A_x mix units; e.g. "i + w + ws" (T:20-21), "g + w" (T:22-23), and "m + g" (T:24-38), can be explained in part by tumbling of "Y" blocks downhill from the east. The source is possibly an eastward continuation of the "Y_r" bed at

T:22-25. To the east, "Y" blocks only partially covered by mixed fines are observed on the ray surface and appear to have tumbled to their present positions from uphill near the R-1 axis.

c. Tertiary Features

Almost all individual blocks within the trench can be related to segments, either directly (within beds) or indirectly (separated after deposition and incorporated in the various mix units). Less than 1% of all blocks are proven late-time impacts. Evidence for a late-time impact is of three kinds: (1) blocks encased in fused glass; (2) resultant secondary craters or secondary ejecta deposits; and (3) blocks clearly out of stratigraphic order and for which there is no other satisfactory explanation, such as erosion or tumbling.

Only two blocks encased in fused glass were observed, both "L" blocks approximately 25 cm in length. One impacted late time in a "p" unit (T:56), the other is located within the X_3 mix unit at T:103. Evidence that other such impacts have occurred, out of the plane-of-the-trench, is indicated by scattered fragments of fused glass in the mix units.

The only obvious impact crater is near T:22, where a "B" block (1/3 x 2/3 m) impacted "i" and "g" beds pushing portions of both outward. The impact crater was subsequently covered by a "i + w + ws" mix unit. An example of a secondary ejecta deposit from an impact, presumably out of the plane-of-the-trench, is exposed at T:13 ("B" rubble in "w" and "p" beds). The "P" lenses near T:88

may be of similar derivation.

The "O/B" block (1.5 m x 1.2 m) at T:18-19 is completely enclosed in the "w" bed and is a probable impact. Its undamaged condition and lack of an impact crater or ejecta field argues for an impact out of the plane-of-the-trench with subsequent tumbling to its present position. Several "B" blocks of comparable size are in various stages of burial on Ray 1 just to the east of and uphill from the trench. Smaller blocks, such as the "P" and "L" blocks in the "w" bed at T:52 and the "P" and "O" blocks in the "w" bed at T:19-20 are also good impact-tumble candidates. Less positive are the two "O" blocks in the "m", "y", and "L" beds near T:85-87. Finally, some of the blocks within the X_3 unit may be impacts, but positive proof is lacking.

5. Fine Units

a. Primary Features

Fine units comprise 11.9% of the ejecta along the trench and directly overlie block units on portions of the first, second, and fourth flap segments. Interestingly, fine units always overlie block units (the one exception is at T:40) indicating that both traveled reasonably close together. Small masses ($\leq$ 1/3 m^2) of discrete fines make up to 2% of the various mix units.

All fine units down through "p" (77.1 m) exist as mappable units within the trench. Small centimeter-size fragments of suspected units below "p", in varying degrees of shock lithification, are observed throughout the mix units, but were not mapped. Fine units

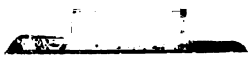

are present in near perfect inverted stratigraphic order with lower in situ units observed successively higher and closer to the crater. This stratigraphic order is partially repeated for each of the segments and subsegments.

While units thicken, thin, and are locally missing, those present exhibit only minor smearing between beds. The most complete stratigraphic sections are observed on the back slopes of segments and subsegments. In addition to locally absent units, there are broad concentrations of units. For example, the "g" unit is concentrated almost exclusively between T:1-5 and 42-49. Similarly, "w" and "m" units are concentrated to the near exclusion of other fine units between T:8-20 and 28-37, respectively.

Local variations within units also exist. The "ws" unit, observed sparsely along the crater lip, is concentrated over one area of the trench (T:16-21) and is present in small centimeter-size fragments scattered throughout the mix units. It is also observed as meter-size masses on the surface of Ray 1. Within the "yml" unit sequence, "y" and "m" units are not differentiable at the mapping scale used, except in the fourth segment (T:84-90). Here "y" deposits correspond in distance and appearance to "y" deposits that make up the hummocky areas of Ray 1. The "m" and "l" units remain differentiable throughout the length of the trench. An interesting observation is that only where the trench cuts the innermost portion of the crest (T:1-4) is the "v" unit (53.0-57.6 m) distinguishable, elsewhere it is undifferentiable from the "g" unit. The "v" unit is

also observed locally along the crater lip where it was mapped with the "g" unit.

As observed in the crater lip, block units attain their thickest sections at the crater rim, but fine units attain their thickest sections beyond the crater rim. The "w" unit is 1.2 m thick at T:56 versus 0.6 m at T:3 and less than 0.3 m along the crater rim. Similarly, local concentrations exist for "g" (T:3, 38, 43, and 60), "c" (T:9, 48, and 57), "i" (T:21, 54, and 58), and "p" (T:9, 13, 51, and 56). This thickening beyond the lip is probably due primarily to unequal stretching of the segments prior to deposition, possibly even during mounding.

b. Secondary Features

Partly because weakly welded and nonwelded in situ units become sand-size ejecta, there is a tendency for movement of fines after deposition resulting in varying degrees of mixing. Thus, some fine units grade laterally with distance, first into A_m and later into A_x mix units. The X mix unit is the result of thorough mixing (strong movement) of fines.

Within fine units, there is some movement and/or adjustment sufficient to fill in and smooth out local topographic irregularities. Also, there are examples where fine units have draped over previously deposited blocks similar to observations on the crater lip; e.g. T:5 where "m" drapes over "Y" blocks and T:12-13 where "p" and "w" drape over "L" blocks. There is also evidence of slight adjustments or slippages within fine units after deposition; e.g. at T:6 the "w"

unit moved slightly downhill as recorded by the doubling up of a thin lense of "p". Also, within the top meter of the "g" unit at the crest (T:3-6) thin barely continuous alignments of small welded fragments may be the result of such post-depositional adjustments.

c. Tertiary Features

There are a large number of fine masses composed of one or more units that impacted late during the deposition of the ejecta blanket. These are preserved at various depths in the trench beyond T:29. Some moved sufficiently after impact to form A_m and A_x mix units. In cross section, sizes range from 5 cm^2 to 75 m^2. Shapes range from equidimensional for the smaller sizes to radially elongated for the larger sizes. Dimensions perpendicular to the trench walls, even for the large masses, are relatively small (probably less than 5 m); i.e. few masses are observed on both sides of the trench.

The largest (75 m^2 in radial cross section) and most spectacular impacting mass occurs at T:54-59. Here a section of fine units ("g" through "p") impacted previously deposited block units. The impact resulted in some post-depositional movement of the impacting units forming A_m units ("g_m", "c_m", "i_m", and "w_m") at T:57, some moderate mixing of the impacting units forming A_x units ("g + c + i") at T:59-60, and secondary cratering and redeposition of previously deposited block units at T:58-60.

A second fine mass (T:50-54) apparently impacted behind and slightly after the first mass with similar movements of units after

deposition including outward flow of "g_m" and "i_m" units up and over portions of the "w" unit. Both masses impacted block units of the second segment from which they probably separated during overturning of the flap segment. The small "w_m and p_m" mass at T:52 appears to have rotated ("w_m" over "p_m") prior to impact.

A third large impacting mass composed of a single "m" unit is located at T:40-41. It is particularly interesting in that it appears to have folded over on itself, either in flight or upon impact. This mass was probably detached in flight from the "m" unit at T:28-39.

Examples of small, fine masses deposited within the mix units are: "i" and "l" masses in "g_m" at T:45, "p" lense in "X_1" at T:53, "m" masses in "X_3" at T:72, and a "p" lense in "X_3" at T:76. In addition, there are hundreds of centimeter-size fragments of all fine units down through at least "p" incorporated in the mix units. Many of these small masses may be the result of erosion of previously deposited units and/or secondary ejecta from impacts. There are also many 1 to 20 cm fragments of shocked pumice, tentatively identified from units below the "p" unit. Examples are present at T:20 in the "i + w + ws" mix and at T:42 in the "g + w" mix.

6. Mix Units

Mix units are defined as those masses where movement between two or more mapping units resulted in mixing or where there was significant movement and distortion within a single unit. Mix units consist predominately of nonwelded fines; but beyond T:90 contain up

to 20% blocks.

Mix units make up 28.6% by area of the ejecta along the trench distributed such that the 50th percentile occurs at T:65 (2.7 R_a). Mix units are divided into three mappable units: A_m - a single fine unit exhibiting internal movement, but little mixing with other units; A_x - two or more fine units moderately mixed, but with individual unit identities preserved; X - two or more fine units strongly mixed such that individual unit identities are lost.

A_m and A_x mix units appear to be mixed in place and typically exhibit gradations with unmixed fine units from which they were derived. X mix units, on the other hand, appear to be mixed prior to reaching their present location since they rarely exhibit gradations with underlying units.

In addition to the fact that they were mixed, mix units exhibit a number of features which strongly suggest movement (flow) after initial deposition. On the crater side of T:90 the majority of these features are laminar in nature with most unit identities preserved. Examples are gentle flow around and over previously deposited blocks, encapsulation and stretching outward of lenticular fine units, and numerous outward oriented S-shaped bands of fines and small welded fragments. Turbulent features are at a minimum being relegated to local erosion of previously deposited units and pick-up and transport of welded blocks. Beyond T:90 the mix is all of the X type which is nearly homogeneous from thorough mixing, probably a consequence of turbulent flow.

a. Slightly Mixed (A_m)

A_m units ("m_m", "g_m", "p_m", etc.) comprise 9.1% of the ejecta along the trench from T:29 intermittently to T:63 with the 50th percentile at T:44. They are closely associated with fine units from which they were derived. Thus, lateral boundaries between A_m and their pure counterparts are gradational and difficult to pick. Boundaries with other units are typically sharp, particularly in the vertical direction. Examples are the boundaries between "g_m" and "w" at T:56 and "p_m" and "X_1" at T:51. While mixing is slight, there are variations within a given unit.

A_m units commonly contain small welded fragments and lenses of discrete fine units; e.g. "g_m" at T:42-48. Some A_m units contain blocks up to a meter in lenth; e.g. "Y" blocks in "m_m" at T:30-36 and "R", "L", and "Y" blocks in "g_m" at T:43-49. A_m units appear most commonly to have been the result of movement after deposition of large masses of fine units. Examples are: "m_m" masses at T:28-40, "w_m" and "p_m" masses at T:52, and "w_m" and "c_m" masses at T:57-58. Typically, encapsulated lenses and bands of discrete fine units are stretched outward and upward in S-shaped patterns indicating increased displacement toward the top of a particular A_m unit; e.g. T:41, 47, and 54.

Some A_m units were apparently formed by masses of ejecta impacting discrete fine units. Examples are at T:22 where a "B" block impacted a "g" bed forming a "g_m" lense and at T:40 where a large impacting mass of "m" was transformed partially into "m_m" while

causing "g" to change to "g_m".

b. Moderately Mixed (A_x)

A_x units ("g + w", "i + w", "m + g", etc.) comprise 3.6% by area of the ejecta along the trench and are distributed intermittently between T:20 and T:84, with the 50th percentile of distribution at T:38. They are closely associated with fine and A_m units from which they were derived. Boundaries are gradational with amount of movement (mixing) ranging from moderate to strong; but with unit identities still preserved.

A_x units were apparently formed similar to A_m units, but with more mixing, which for the most part was laminar. At T:28-37 the "m + g" unit was formed by "m" and "g" units impacting previously deposited block units. A range of mixing is present, general increasing outward and upward. At T:31 "l" and "g" lenticular beds are interlayered with "m" and "m_m" beds. Gradations are best developed laterally with vertical stratifications preserved; e.g. at T:37 the "m + g" unit grades laterally into "g_m", but not upward into "X_l". Near T:43 the "m + g" unit grades laterally into "X_l", but not upward from "g_m".

With movement increasing, the composition of A_x units is modified by incorporation of portions of underlying units; e.g. "i + w + ws" at T:20-21 changes to "g + i + w" by T:23. With even stronger movement, perhaps reaching turbulent levels, A_x units erode, pick up, and transport blocks; e.g. "Y" blocks in the "m + g" mix at T:28-34, "Y" blocks in the "g + w" mix at T:24-28, and "L" and "P"

blocks in the "g + c + i" mix at T:58-60.

There are at least two instances where A_x mixes have been formed or modified by movement of an overlying "X" mix; e.g. "w + p + X_1" at T:53 and "L_r + X_3" at T:85. There are also examples where movement must have been very gentle; e.g. at T:29 where "Y" blocks lying between "m_m" and "m + g" units are relatively undisturbed.

c. Well Mixed (X)

The X units comprise 15.9% of the ejecta along the trench beginning at T:28 and extending continuously to the end. X units cover all other ejecta deposits, except fallout, filling in topographic lows and sweeping around topographic highs to produce a smooth surface. Unit thicknesses gradually increase to a meter by T:67. Beyond T:90, X units comprise the entire trench ranging up to 3 m thick. The 50th percentile of distribution is at T:81.

X units are composed of fine units that were mixed to the extent that individual unit identities were lost. Five X-type mix units were mapped, "X_g", "X_g + w", "X_1", "X_2", and "X_3", grading outward in order while maintaining vertical stratification with most underlying units. The "X_g + w" unit (T:28-32) and the "X_g" unit (T:32-37) are predominately made up of "g + w" and "g" units, respectively and appear to have been derived from underlying units. They differ from their source primarily in degree of mixing and probably were mixed in place.

The outer three X units exhibit only a minor relationship to underlying units. The "X_1" unit (T:37-56) and the "X_2" unit (T:57-64) each have incorporated some fines (slight color variations) from underlying units. Both contain only centimeter-size fragments from all mapping units down through "p". In contrast, the underlying "g_m" unit contains 1/3 m welded blocks.

The "X_3" unit (T:64-112) is more homogeneous in color than "X_1" or "X_2" indicating a greater degree of mixing. It contains, in addition to the small fragments, numerous large blocks and some meter-size masses of weakly welded units. Beyond T:90 blocks are distributed evenly within the trench. Larger blocks are preferentially located near the bottom of the trench; but there is no graded bedding. Many large, rectangular blocks lie with their long dimensions nearly parallel to original ground surface; but the pattern is not pronounced and smaller blocks and fragments are randomly oriented.

The "X_1", "X_2", and "X_3" units were apparently mixed prior to reaching their present positions. This is suggested primarily by the lack of significant gradations from underlying units. Other supporting evidence is found where an X unit truncates, drags, and partially erodes previously deposited fine units; e.g. "w" lens at T:40, "m" lenses at T:42, "i" lens at T:48, and the "i" lens at T:62.

In addition to the thorough mixing of fines, there are numerous examples indicating movement of X units, particularly the "X_3" unit. Beds of "y" and "m" all along the fourth flap segment

have been eroded by the "X_3" unit, especially note the condition at T:85. A "p" lens at T:76 has been stretched outward by the "X_3" unit for more than 10 m. Numerous other such lineaments of both nonwelded fines and welded fragments are present; but are too thin for mapping. The "X_3" unit contains local concentrations of welded blocks (graded upwards from large to small) immediately above the third and fourth flap segments indicating erosion and pickup.

C. Surface Geology

1. Physical Setting

The crater and continuous ejecta field were mapped in detail with all mapping units down through "p" (77.1 m) observed. Each of the units displays a characteristic distributional pattern which is a function of azimuth and distance from SGZ. For the continuous ejecta field, inverted stratigraphy is the rule with mapping units in an upside-down layer-cake structure that closely follows the Ray-Valley structure of the apparent lip. In the crater, mapping units are primarily in a normal stratigraphic order modified by some late-time slumping and talus formation.

2. Mapping Procedures

Mapping was accomplished using transparent overlays on the same set of color aerial photographs used for the geomorphic mapping of Chapter V. Mapping continued over a six-month period in three consecutive steps: (1) bounding the ejecta blanket delineation of the R_b and R_{eb} boundaries; (2) mapping major ejecta units; and (3) filling in the details.

The R_b and R_{eb} boundaries were mapped continuously around the ejecta blanket and are accurate to 5 m. Within the R_{eb} boundary, the ejecta blanket was mapped one ray at a time. Individual blocks were not mapped, rather block fields were outlined such that at least 90% of a given mapping unit was enclosed. Where two or more units overlap, the lowest in situ unit is indicated. "RUL" units were mapped as one, except that a boundary was established delineating first appearance of "R" blocks outward from SGZ. This line is close to a 1/3 m ejecta thickness. The "PBOY" units were mapped separately wherever possible.

Fine units, except near crests, are visible only as small discontinuous masses or outcrops. Outcrops larger than a meter were recorded, although their size on the map may be necessarily exaggerated. The mix units were not differentiated, but underlying units were inferred where possible. On crests, where mix and fallout are thin, undifferentiated fine units were inferred. Fallout, which covers the continuous ejecta field, was not mapped.

The crater was only briefly examined. Geology of the crater lip and underlying wall were presented in Chapter VI. A. Outcrops within the fallback were outlined, the remainder was undifferentiated.

The resulting Geologic Map of the Crater and Continuous Ejecta Field is provided in the map pocket and reduced to page size in Figure 51. Selected photographs of the continuous ejecta field are presented in Figures 52 through 54.

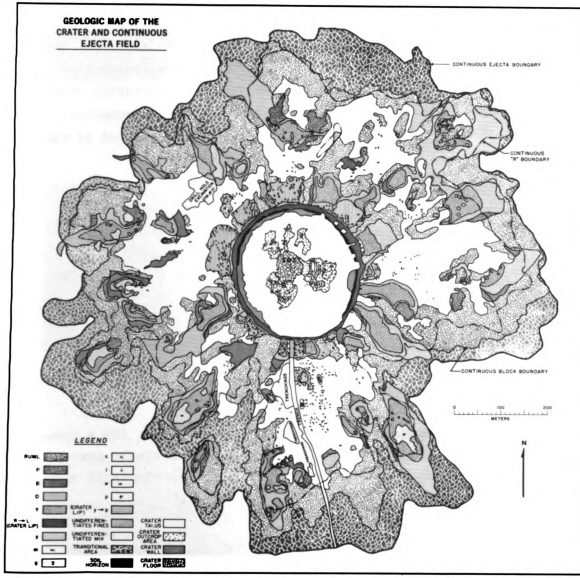

Figure 51. Geologic Map of the Crater and Continuous Ejecta Field

Figure 52

a. Large joint-controlled "L" blocks 60 m off crater edge at 60° azimuth in Valley 4. Man in shadows of center foreground is 1.7 m tall. Photo date: 2/69.

b. Looking south along Ray 1 axis from Crest 1. Smooth area is in foreground with "BOY" blocks protruding. Rubble/block area begins at 470 m from SGZ. Trench has not yet been excavated. Two-meter white structures on right side of road in middle background, beyond main block field, are at 1200 m. Truck at crater-end of road (see Figure 54d) is at 600 m. Photo date: 2/69.

c. Looking towards Crest 1 from near R_{eb} of Ray 1, 600 m, 170°. Near location of truck in Figure 54d. Large block in foreground is 1.5 m across. Photo taken 1 month after event, note fallout covering all surfaces - contrast to Figures 54 and 56 taken several months after event. Photo date: 1/69.

d. Looking away from crater at discontinuous ejecta field from same location as Figure 52c. Note fallout covering. Photo date: 1/69.

e. Looking towards Crest 1 from middle of Ray 1, 270 m from SGZ. Light colored mounds in middle ground are fine ejecta masses "g through p". Block in center background on crater rim is 10 m across. Photo date: 11/74.

f. Looking towards crater rim from Ray 10, 230 m from SGZ. Crests 11 and 1 are to right, Crest 9 is to the far left. Photo date: 11/74.

a.

b.

c.

d.

e.

f.

Figure 52. **Selected Photographs of the Continuous Ejecta Field**

Figure 53

a. Looking outward along Ray 7 from the clockwise side of Crest 7. Snow patches are in shadows of left foreground. Topographic high is 150 m away. Photo date: 2/69.

b. Looking outward along Ray 4 from near Crest 4. Twin topographic highs in background are 190 m away. Large blocks in foreground are "B" and "O", smaller blocks are "Y". Block in center left contains a "B/O" contact and is 1 2/3 m across. Photo date: 6/73.

c. Looking outward along Ray 9 from Crest 9. Topographic high in right middle ground is 110 m away. Drowned secondary crater is in immediate left foreground. Photo date: 11/73.

d. Looking outward along Ray 8 from near Trough 7. People in left middle ground are 1.8 m tall. Large blocks are "L" with several well developed joint faces. Photo date: 6/73.

e. Looking outward along Ray 8 from center of Figure 53d, 60 m from crater rim. Ray 7 is to right. Note flat joint face on large "L" block in center. Man in middle ground is 1.8 m tall. Photo date: 6/73.

f. Looking from Crest 6R left across Ray 6R to the right and Ray 6L to the left. Blocks in foreground are "BOY", larger ones in middle ground are "UL". Photo date: 2/69.

a.

b.

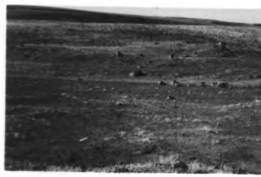

c.

d.

e.

f.

Figure 53. Selected Photographs of the Continuous Ejecta Field

Figure 54

a. Looking at crater from block field 700 m out along Ray 5 radial. Block in middle ground is 1 1/2 m high. Ray 4 is to left. Man is 1.7 m tall. Photo date: 7/69.

b. Close-up of area near Figure 54a. Note caliche covered "R" blocks and secondary deposits capping joint surfaces of "U" and "L" blocks. Man standing is 1.7 m tall. Photo date: 7/69.

c. Looking away from crater 650 m out along Ray 6L radial. Large caliche covered "R" block is 5 x 1 x 1.5 m. Photo date: 7/69.

d. Looking east from 600 m out on Ray 1 at truck (see Figures 52b, c). Snow partially covers ground surface. Note joint controlled block surfaces. Photo date: 2/69.

e. Close-up of a "U" block exhibiting good joint control and partially encased in thick fused glass. Block is same as in lower left corner of Figure 54d. Hammer is 30 cm. Photo date: 2/69.

f. Block field on Ray 1, 500 m from SGZ. Note vertical joint planes and horizontal foliation planes in "L" block with Brunton compass. Area close to that of foreground of Figure 52c - note how fallout has been cleaned up. Photo date: 7/69.

a.

b.

c.

d.

e.

f.

Figure 54. **Selected Photographs of the Continuous Ejecta Field**

3. Continuous Ejecta Field

The continuous ejecta field exhibits inverted stratigraphy that follows the Ray-Valley structure of the apparent lip. Units are arranged in an upside-down layer-cake structure such that traversing outward, either parallel or perpendicular to a ray axis, one encounters progressively higher in situ units. Rays 1, 4, 7, and 9 dominate in both total thickness of the inverted section and in the distance to which it is distributed.

This first-order pattern is complicated with each flap segment partially repeating the sequence. While segments exhibit many similar characteristics, no two segments are identical, either with respect to structure or stratigraphy. The exposed stratigraphy is a function of: (1) initial deposition of segments, followed by partial to complete burial by mix units; (2) movement of portions of segments after deposition; and (3) disruption by late-time impacting ejecta masses. These primary, secondary, and tertiary features are examined below for block, fine, mix, and fallout units.

a. Block Units

(1) Primary Features

Block units were mapped in two groups, the "RUL" group ("M" included) and the "PBOY" group. The "RUL" group was deposited first and, because of its significantly larger volume and block size, comprises the bulk of the flap segments and thus forms the major topographic features of the apparent lip.

Beyond the crest "RUL" deposits are lens-shaped with long axes radially outward from SGZ. Near the crater rim "R", "U", and "L" units are large enough in volume to be continuously exposed in cross section. With distance, "R" units, and farther out "U" units, while maintaining inverse stratigraphic relationships, become discontinuous simply due to low volume. The "L" unit is continuous where exposed, and because of its large relative volume, overwhelms the underlying "R" and "U" units. Thus, the "L" unit dominates all blocks to at least the R_{eb} boundary.

Traversing outward from a ray axis, the relative percentage of "U", and then "R" beginning at the "R" boundary, increases at the expense of the "L" unit (a consequence of inverted stratigraphy). Large variations, however, exist circumferentially. For example, 60 m inside the R_b boundary off Ray 1, a 30 x 30 m area contained the following percentages: R(20), U(40), and L(40) while 60 m westward and still within the R_b boundary the percentages were: R(10), U(75), and L(15). In Chapter VII, data on composition, size, and shape of welded blocks are presented for Ray 1 and Valley 11 radials.

Characteristics of "PBOY" deposits are a function of their location with respect to SGZ and the units and topography on which they were deposited. On crests, "PBOY" blocks are little changed from in situ and are of sufficient size and volume to contribute to crest buildup. "PBOY" deposits are not, however, symmetrically positioned on crests; e.g. C-1, 4, 5, 6, and 11. Crest 5, and to a lesser extent 4, contain an especially large volume of "PBOY"

blocks. Where fine deposits are heavy, "PBOY" blocks are observed at topographic breaks surrounding crests and along crest-trough intersections; e.g. C-2, 6, 7, and 8. On Ray 3, "PBOY" blocks cover the ray surface from the crest out to the R_{eb}. Rays 4 and 10 contain a slightly lesser, but higher than average, distribution of "PBOY" blocks. Lack of fine units that occur on other rays accounts, at least in part, for these observations; but there does appear to be more "PBOY" blocks in the southeast quadrant.

On topographic highs beyond crests, blocks are moderately brecciated and depositional patterns are generally aligned with "RUL" deposits. But volumes of "PBOY" deposits are generally insufficient to contribute more than a thin covering over the underlying "RUL" deposits. Near ray termini "PBOY" deposits are typically lens shaped with long axes directed outward and typically skewed with respect to "RUL" deposits, other "PBOY" deposits, and SGZ. "PBOY" deposits on Rays 7 and 9 are good examples. The "PBOY" deposits on the isolated segment of Ray 11 are skewed with respect to the "RUL" deposit; but radially aligned with SGZ. Where they cross a rubble zone "PBOY" blocks are brecciated; but beyond, blocks return to in situ conditions. In several cases, "PBOY" deposits extend beyond the continuous ejecta boundary; e.g. R-2, 6, 7, 8, and 9. Thus, within flap segments "PBOY" units traveled with "RUL" units but not 1:1. Similar observations were made in the trench.

"PBOY" units are deposited in inverted stratigraphic order, which can be idealized to a lens-shaped "bulls-eye" pattern. When

viewed from above, units lie on top of and are enclosed by the next higher in situ unit. While blocks from each of the units are distributed throughout a given deposit, "Y" blocks are generally concentrated toward SGZ and "P" blocks concentrated away from SGZ. In most terminal deposits and in some intermediate deposits, the fine "y" unit is present. It is concentrated toward the center and associated with the geomorphic hummocky areas. These depositional patterns are rarely perfect, with some shifting and overlapping of units. Such shifting does not significantly increase with distance and appears to be random. In at least two cases, units are shifted in regular manner much like spreading out of a deck of cards; e.g. outer two segments of R-10.

Within a deposit, individual units are observed to thicken, thin, and to be locally missing, similar to observations along the crater lip and in the trench. Block density decreases and block size increases (rubble decreases) outward from a lens center. The relative composition, block size, and areal density of "PBOY" deposits is a function of distance from the crater. Each of the units is typically present; but with a relative decrease in the lower in situ units with distance. For example, the "PBOY" deposit in Crest 5 at the crater edge has the following percentages: "P"(5), "B"(10), "O"(15), "Y"(70), changing 70 m further out to "P"(15), "B"(25), "O"(40), "Y"(20).

Areal density of "PBOY" deposits decreases with distance such that the underlying "RUL" units make up an increasingly larger

percentage of the total. For example, on Ray 1 the percentages are: at the crest--"L"(5), "P"(10), "B"(15), "O"(25), "Y"(45); at the crater size of the ray terminus--"L"(50), "P"(15), "B"(15), "O"(15), "Y"(5); and at the outward size of the ray terminus--"R"(5), "U"(20), "L"(45), "P"(5), "B"(10), "O"(10), and "Y"(5).

Composition, block size, and areal density of "PBOY" deposits are generally similar about the crater at the same distance. The exceptions are the previously discussed block fields on Rays 3, 4, and 10; the heavy concentration of blocks on Crest 5; and the almost complete absence of blocks on Crest 9 (due in part to coverage by thick fine deposits).

(2) Secondary Features

There are several lines of stratigraphic evidence that suggest movement of welded units after initial deposition. The boundaries between "RUL" units observed along ray perimeters are blurred due at least in part to the spreading out of ray segments after initial deposition. Particularly important is the large-volume "L" unit overriding "R" and "U" units.

Tumbling of individual blocks down topographic highs; i.e. from crests into troughs and valleys, is indicated by their lack of stratigraphic order. Blocks of "B" and "Y" that tumbled down the flanks of Crest 1 and were incorporated in and partially covered over by later mix deposits were observed in the trench (Chapter VI. B). The large number of in situ "PBOY" blocks on Ray 3 probably involved some downhill tumbling.

(3) Tertiary Features

Ballistic impacts of welded blocks on the continuous ejecta blanket are evidenced either directly by resulting secondary craters or indirectly by fused-glass encased blocks. There are also undoubtedly a number of impacting blocks not encased in fused glass; but except for those forming secondary craters, there is no ready means of identification. Presented below are observations of secondary craters and fused-glass encased blocks distributed within the continuous ejecta field.

Secondary Craters

Secondary craters are observed from the crater rim out and exist in all stages of burial from fresh craters with no infill, generally near ray termini, to barely recognizable "ghosts" in ray interiors. Many secondary craters that can be seen in aerial photographs cannot be seen from the ground and vice versa. Direction, quantity, and quality of lighting are very important to visual recognition. Some secondary craters can only be inferred by surrounding circular accumulations of secondary ejecta.

The number of observed secondary craters per unit area increases with distance, partially due to increased burial by fines closer to the crater. Secondary craters are preferrential to rays with many secondary craters associated with ray termini rubble zones. It is estimated that on Ray 1 there is one or more secondary crater per 100 m^2 from the crest to the ray terminus.

Secondary craters range from 1 to 15 m in diameter, with most circular suggesting near vertical impact. Most craters exhibit large radius to depth ratios due partially to post-impact filling by mix and fallout units. A large variety of structures is observed, from those with part or all of the impacting block still present to those with none. In the former case, blocks within the crater are in all stages of brecciation. In the latter case, some blocks can be readily traced from their present positions back to secondary craters; but a large number of secondary craters have no obvious blocks associated with them. The absence of blocks in these secondary craters may be due to (1) complete burial of the impacting block, (2) rebound of the block out of the crater, or (3) impact by a mass of fine units.

All welded units down through "O" (35.6 m) were observed to have formed secondary craters. There are few "B" and "O" secondary craters, while "R" and "U" secondary craters become increasingly more common with distance, particularly on the west (Rays 8 through 10). Blocks forming secondary craters are most commonly encased in fused glass; but secondary craters formed by fresh blocks predominate toward ray termini.

During formation of secondary craters, underlying units previously deposited are thrown out resulting in an inversion of the inverted stratigraphy. Impacting times obviously ranged widely as inferred from the wide variations of burial within a small locality. Degree of burial generally decreases with distance beyond the "R"

boundary (as does the amount of fines). Only one case was observed within the R_b where an impacting block cratered the original ground and ejected soil. This occurs near the termini of R-1, 15 m west of the trench.

Fused-Glass Encased Blocks

Fused-glass encased blocks, comprising less than 1% of all blocks in the continuous ejecta field, increase from the crater rim out to the R_{eb}. Each of the welded units is observed encased in fused glass; but "RUL" blocks dominate. Sizes range from fist-size to 3 m across.

The degree of encasement varies from paper thin to several centimeters thick and from partial to complete coverage. There are examples where the fused-glass envelope has been broken loose upon impact and is lying on the ground about the block. Where fused glass has been broken loose, it pulls with it a thin slice (few mm or less) of the block.

b. Fine Units

(1) Primary Features

Fine units down through "p" are present as large continuous deposits only on the crests. Like block units, they are always in an inverted stratigraphic order. Fine units are not distributed evenly about the crater rim with largest deposits (covering up to 10^4 m^2) located at Crests 6, 7, 8, and 9. Crest 5 contains none and Crests 3, 4, and 10 contain only scattered amounts. Thickness of the inverted section, as well as individual units, varies greatly. Only

Crests 1 and 2 contain the "p" unit while Crests 1, 2, 7, and 9 contain the "w" unit. Fine units thicken, thin, and are often missing over portions of a crest. As suggested all along the crater lip and confirmed for Crest 1 in the trench, fine units are thickest beyond the crater rim.

While continuous fine deposits are not observed on the surface beyond crests, observations in the trench indicate that large fine deposits associated with welded flap segments extend out to 2 1/2 to 3 R_a, but are covered by mix and fallout units. Some of the isolated fine deposits, tertiary features discussed below, are probably surface expressions of these covered deposits.

(2) Secondary Features

Only in the vicinity of crests are there sufficient surface exposures of fine units to examine for possible post-depositional movement. Most evidence is of an indirect nature and indicates only minor movement. The fact that fine units peak beyond the crater rim may be partially due to movement after deposition (stretching while overturning is probably the primary cause) particularly with regard to the outward and downward elongation of some crests; e.g. C-1 and 4. Late-time movement along the steeper slopes is suggested by a feature similar to those observed in the trench; i.e. shuffling within units marked by welded fragment or color lineations. Continued late-time slumping of fine units into the crater was discussed in Chapter V.

(3) Tertiary Features

Beyond the crests, isolated deposits of fine units are observed at the surface in varying degrees of burial by mix and fallout units. Some deposits, as observed in the trench, probably are associated with buried fine units capping flap segments. Outcrops range from 1 to 30 m^2 in surface area; but observations from the trench suggest that with depth some deposits may reach 100 times this. Such partial burial is indicative of deposition after the flap segments; but during emplacement of the mix units.

Fine deposits are concentrated along ray axes. Deposits commonly consist of two or three integral fine units unmixed and in stratigraphic order. Deposits are distributed outward in a general inverted stratigraphic sequence with "y" and "m" units farthest out and "w" and "p" units closest in.

There is a large variation in the distribution of fine units from ray to ray. Ray 1 contains the largest number and most distant deposits. Rays 1 and 2 are the only rays with "p" deposits. Rays 6, 7, and 8 contain units down through "w" while Rays 3, 4, and 5 are deficient in most fine units.

A few fine deposits, up to 1/2 m in size, are observed sporadically within 30 m of the crater rim on both crests and troughs. Where observed, these deposits are usually draped across previously deposited welded blocks suggesting a pliable (wet?) condition when deposited. Since they are not covered by other deposits, including much fallout, they are interpreted as late-time impacts. If similar

deposits exist farther out, they are covered by mix and/or fallout units.

c. Mix Units

Mix units, consisting of undifferentiated mixed fines from the "p" unit and above, cover most surfaces out to the continuous ejecta boundary; but are strongly concentrated within rays, particularly R-1, 4, 7, and 9. In this sense the distribution of mix units closely follows the distribution of the smooth morphologic areas (Fig. 34). During geologic mapping it was not possible, with only surface exposure, to differentiate between the various types of mix units as in the trench.

d. Fallout Unit

The fallout unit, covering the entire ejecta blanket, was not mapped and only briefly examined in the field. It is a very fine-grain mixed unit deposited last from the base surge and cloud. It consists of approximately 10% small welded tuff shards, 70% weakly welded and nonwelded tuff fines, and 20% shocked tuff fragments.

Initially, these deposits were up to 1/2 m thick near the crater rim, over 1 cm at 1000 m, and extended to at least 1500 m to the southwest (upwind) and 9 km to the northeast (downwind). Present thickness ranges from 10 cm near the crater rim to less than 1/2 cm at distances exceeding 600 m.

Welded fragments, typically 1 to 2 cm in length, are present from all in situ units. No stratigraphic order is observed; but "R", "U", and caliche fragments dominate, being particularly concentrated

near the crater rim. Caliche comprises 5-10% of all fragments on ray surfaces increasing to 10-30% at the crater rim. Fines are probably derived from all units above the ZP (108 m); but there has been so much mixing prior to deposition that individual units are unidentifiable. Size grades from coarse sand to silt with the finer fractions preferentially deposited on the surface. Most of the finest fractions have been winnowed since the event.

A full range of shock lithified material is present. Fragments average several centimeters long with some reaching 1/3 m. Most appear to have originated from below the "p" unit, with at least four different types present based on color and texture. One sample from near the crater rim on Ray 1 was identified by Moore (1977) as probable Grouse Canyon (below 103 m). At a few locations near the crater rim, meter-size fragments are observed draped over welded blocks and appear to have been in a pliable (semi-molten?) condition at deposition. Shocked fragments typically cover 10-20% of the surface; but in the northeast quadrant coverage increases sharply.

4. Crater

All outcrops observed within the crater are fine units and probably represent portions of the mound that collapsed into the crater cavity after venting. Block fields of a single mapping unit are not observed except those obviously derived from post-crater slumping. It appears that many, if not most, of the welded blocks making up the present talus surface were derived from late-time and post-crater rim failure. Mix units observed in the ejecta blanket are not recognized

in the crater. The crater floor to a depth of a least 8 m and more probably 13 m consists solely of fine units, whose homogeneous light tan to white color suggests derivation primarily from the "w" unit.

Fine outcrops, most 5 to 10 m across, are exposed over less than 20% of the fallback surface. They are contained within the five geomorphic smooth areas mapped in Figure 34. Outcrop locations tend to be aligned beneath crests devoid of fine ejecta units. The largest outcrop area on the east side of the crater lies below Crest 4 and 5 which contain few fine units. The second largest outcrop area on the southwest is beneath Crest 10 which also contains few fine units.

Units identified in the outcrops are "g" through "p". They are distributed in normal stratigraphic order with the higher in situ units lying above the lower units. The "yml" units are not recognized; but should be present just above the "g" unit in which case they are probably covered by blocky talus. Locally, units exhibit a cyclic ordering; i.e. "w-p-w-p", apparently due to downward sliding after initial emplacement.

CHAPTER VII

DISTRIBUTION OF EJECTA BLOCKS AND SECONDARY CRATERS

A. Overview

Distributions of ejecta blocks and secondary craters within the ejecta field were briefly investigated. While emphasis was placed on the discontinuous ejecta field, sufficient data were collected within the continuous ejecta field for correlation. First, a count of blocks and secondary craters out to 1219 m from SGZ was made from aerial photographs to determine general distributional characteristics and to compare these with the Ray-Valley structure of the apparent lip. Second, field measurements of blocks and secondary craters were made along and between Ray 1 and Valley 11 radials out to 1524 m to follow stratigraphic relationships observed in the continuous ejecta field and to define and compare specific distributional characteristics for this Ray-Valley set. Figures 55 and 56 present selected photographs of the discontinuous ejecta field.

In general, blocks and secondary craters are distributed in a regular manner outward from the crater. Blocks decrease both in frequency and size rapidly to 100 m past the continuous ejecta boundary (4.7 R_a). Beyond that distance, block frequency decreases at a slower rate while block size remains relatively constant, particularly from 1200 m (9.3 R_a) to the maximum ejecta range (16.5 R_a). Azimuthal variations of block frequency and size also

Figure 55

a. Large "L" block encased in fused glass at 1200 m from SGZ and 150° azimuth. No secondary crater found. Clipboard is 35 cm long. Photo date: 7/69.

b. Shallow secondary crater 1 1/2 m in diameter formed in moderate depth soil at 1400 m. "L" block 1.2 x 1.0 m exhibiting large joint face with traces of fused glass. Block did not break up on impact, bounced out of crater. Photo date: 6/73.

c. Shallow secondary crater 3 m in diameter formed in very shallow soil at 1000 m. The "U" block brecciated in place. Stake with flag is 1 m long. Photo date: 2/70.

d. Deep secondary crater 2 m in diameter formed in deep soil at 1300 m. Impacting block bounced out. Photo date: 7/69.

e. Secondary crater 3 m in diameter at 500 m on Ray 10. Formed by an "R" block that broke in place. Largest blocks are 2/3 m across. Photo date: 2/73.

f. Nearly circular secondary crater 10 m from crater rim, Crest 10. Impacting "L" block almost totally buried in crater. Stake is 1 m long. Photo date: 11/74.

a.

b.

c.

d.

e.

f.

Figure 55. **Selected Photographs of the Discontinuous Ejecta Field**

Figure 56

a. Looking at Trough 11 from Valley 11, 250 m from SGZ. Crest 1 is to the right. Crest 11 is to the left. Photo date: 8/74.

b. Looking at Trough 11 from Valley 11, 457 m from SGZ. Crest 1 is to right, Crest 11 is to the left. White surfaces are secondary deposits on joint surfaces. Photo date: 10/73.

c. Looking at crater from Valley 11, sample station 610 m, 190° (Fig. 57). Ray 1 is off photo to right. Isolated segment of Ray 11 is to left background. Trough 11 is in right background and Crests 10 and 11 in center background. Stake is 1 m. Photo date: 10/73.

d. Looking at crater from 610 m sample station, 170° (Fig. 57). Crest 2 is in center of crater rim. Crests 3 and 4 are to right, Crests 1 and 11 to left. Note low areal density of blocks - compare to Figure 56c. Photo date: 11/74.

e. Block field, mostly "L", 650 m from SGZ, radially out from Ray 5. Note joint controlled blocks, some with white secondary deposits. Man is 1.7 m tall. Photo date: 7/69.

f. Block field 700 m from SGZ, radially out from Ray 5. Note joint controlled blocks. Man is 1.8 m tall. Photo date: 7/69.

a.

b.

c.

d.

e.

f.

Figure 56. Selected Photographs of the Discontinuous Ejecta Field

decrease with distance. At the one distance (610 m) where sufficient azimuthal data are available, they can be related to the Ray-Valley structure of the lip.

Secondary craters increase regularly in frequency to a maximum at 5.4 R_a, approximately 190 m beyond the continuous ejecta boundary, and then decrease steadily, but at a decreasing rate to the maximum ejecta range. Azimuthal variations range up to $\pm$76% about the mean, but unlike block variations, exhibit little correlation with the Ray-Valley structure of the lip.

In detail, distributions of blocks and secondary craters along Ray 1 and Valley 11 radials differ in several important aspects. Blocks not encased in fused glass exhibit an inverted stratigraphic order out to at least 1200 m (9.4 R_a) on V-11 radial and to 850 m (6.6 R_a) on R-1 radial. Inverted stratigraphic order may continue to the maximum ejecta range, but detection is complicated because of the relatively few blocks without fused glass. In addition, volumes of blocks without fused glass decrease less rapidly with distance along V-11 such that volumes are similar for both R-1 and V-11 near their respective continuous block boundaries. Beyond, block volumes along V-11 exceed those along R-1.

Blocks with fused-glass coatings comprise 7% of all blocks counted and increase from 10% at the R_{eb} to near 100% at maximum ejecta range. These blocks are concentrated 2 to 1 along R-1, and unlike blocks without fused glass are both irregularly distributed with distance and lack an inverted stratigraphic order.

Secondary craters are twice as prevalent on R-1 out to 900 m while beyond, distributions are similar for R-1 and V-11 radials. Blocks forming secondary craters, while enhanced with the "R" and "U" units by factors of 3.5 and 1.7 respectively, exhibit little evidence of an inverted stratigraphic order along either R-1 or V-11. Size and particularly shape of secondary craters are strongly influenced by depth of the soil cover.

B. General Distribution

1. Mapping Procedures

The longest observable dimension of ejecta blocks was measured within 76 30.5 x 30.5 m areas located on a polar grid centered on SGZ (Fig. 57). Grid ranges, extending from 152.4 to 1219.2 m in 152.4 m increments, were optimized with respect to the crater and ejecta field while the eight grid azimuths were equally spaced about the crater. Thus, individual sampling locations, while not randomly positioned, were independently positioned with respect to the Ray-Valley structure. Measurements were made from the 1969 B&W aerial photographs (1 cm = 60 m) discussed in Appendix B using a 10-power binocular microscope equipped with an optical comparator. Field checks indicate that under optimum conditions, a 1/3 m block is resolvable with individual measurements accurate to $\pm$1/3 m.

There are several obvious problems associated with achieving these optimum measurement conditions. First, blocks are more difficult to recognize in the discontinuous due to confusion with natural preshot blocks on the ground surface, coverage by base surge

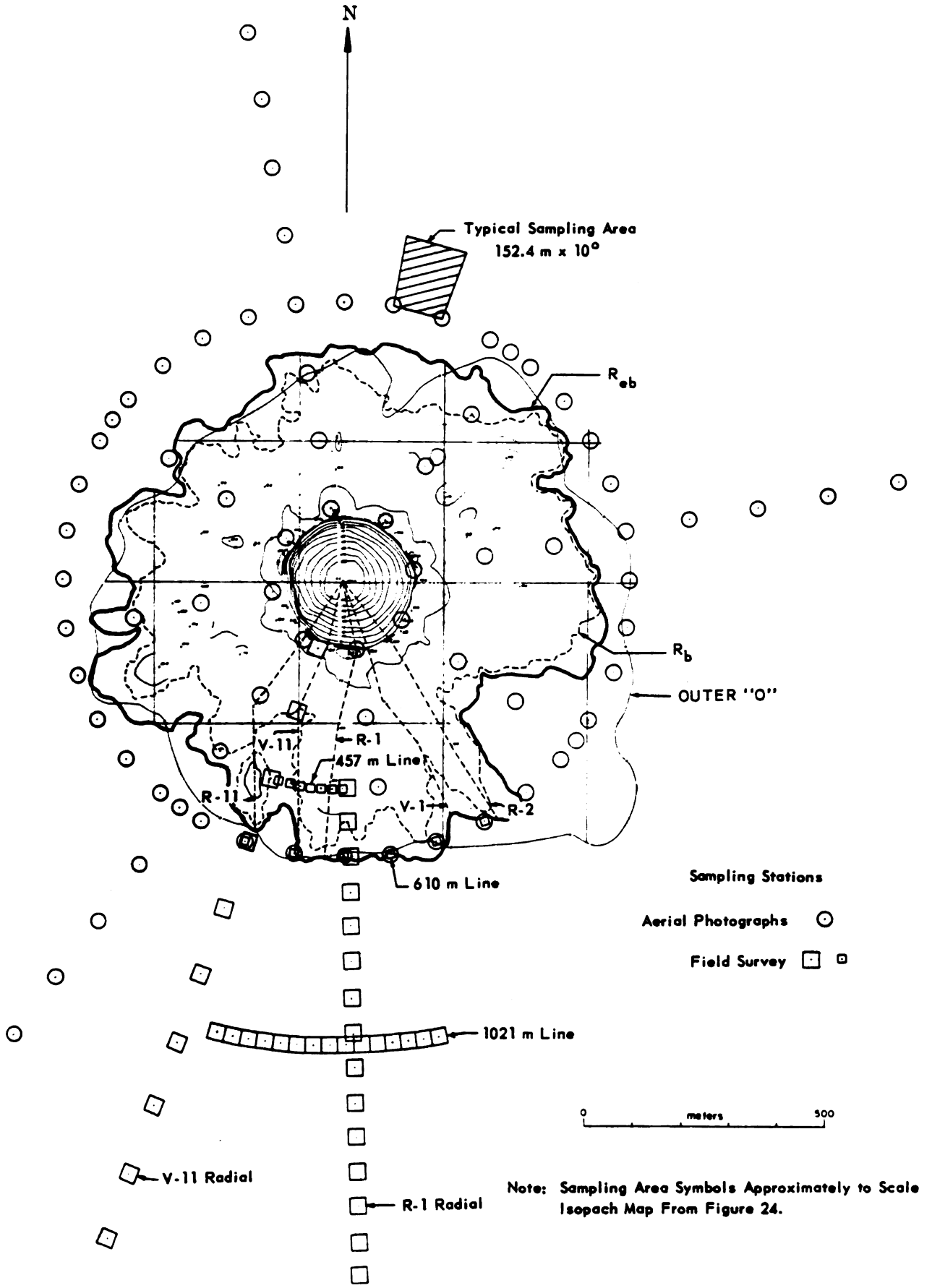

Figure 57. Station Locations for Measurements of Ejecta Blocks and Secondary Craters

deposits, poor color contrast, and partial camouflage by vegatation. Second, shadows from larger blocks in the continuous blanket and from vegetation in the discontinuous ejecta field often partially to totally obscure smaller blocks. Third, field observations indicate that the long dimension of a block is often not exposed to overhead viewing; this is particularly severe in the continuous ejecta field. Fourth, and most important, only surface blocks are observable in the continuous ejecta field.

Secondary craters were also counted in 10^{o} x 152.4 m areas from the crater edge out to 1219.2 m (Fig. 57). Field checks indicate that under optimum conditions, a crater 2/3 m in diameter is resolvable. Observations and measurements of secondary craters suffer from many of the same problems discussed above for blocks. In addition, the typical shallow slope of the crater makes measurement of the diameter particularly difficult. The net result is that many secondary craters less than 1.5 m were probably not counted while dimensions of craters counted are probably accurate to no better than $\pm$ 1 m.

2. Blocks

The maximum, mean, median, and standard deviation of block length for blocks 1/3 m and larger are presented in Figure 58. Solid circles mark the means and bars mark the measured azimuthal ranges, which as exemplified by the 40 stations at 610 m, would probably increase slightly as more azimuthal collection stations were added. Data inside 610 m are low because measurements could only be made

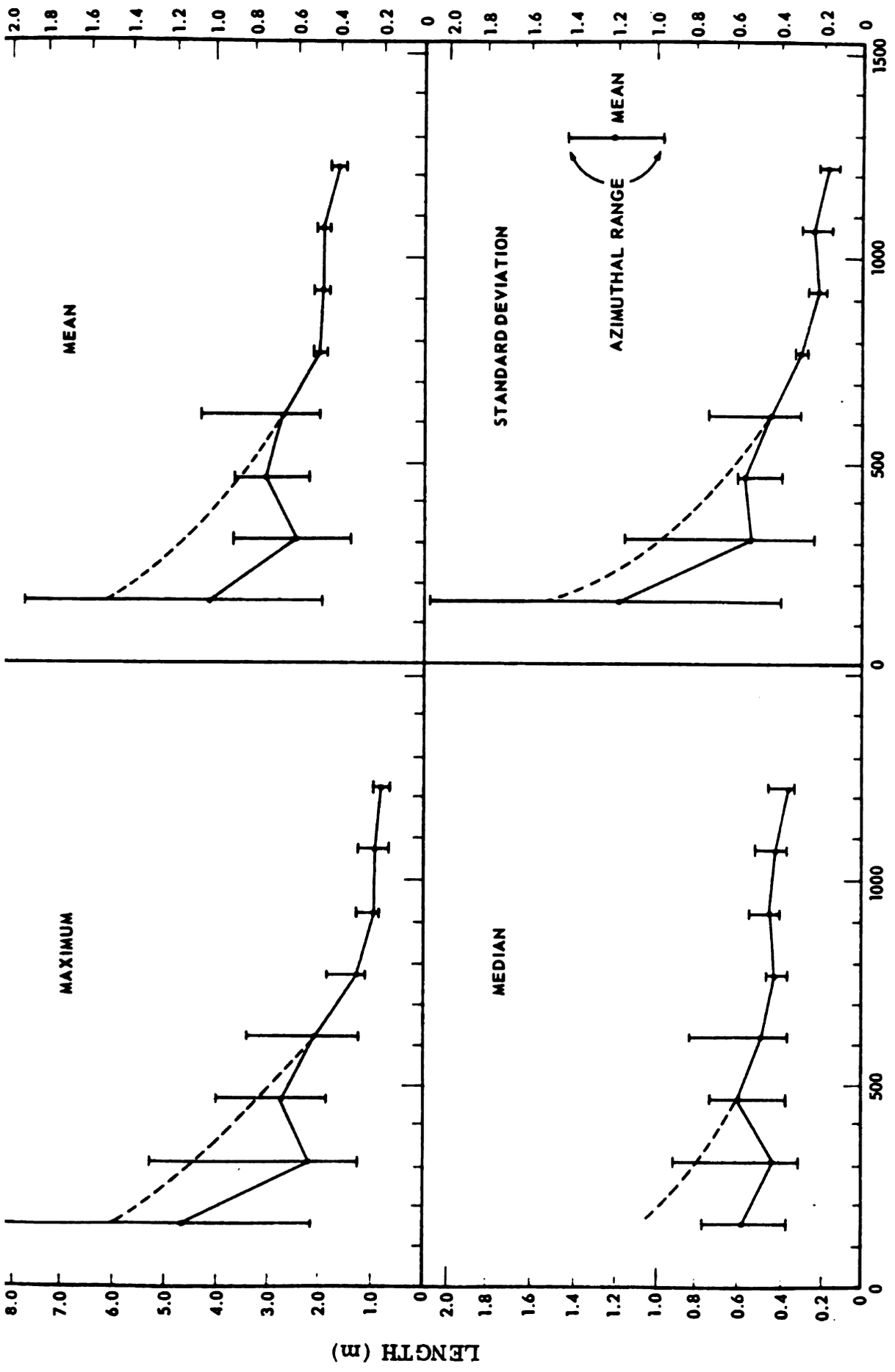

Figure 58. Statistics for Ejecta Block Lengths as a Function of Distance from SGZ with Azimuthal Variations Indicated

along the surface of the continuous ejecta blanket; dashed lines indicate estimated corrective trends based upon field observations.

Both mean and azimuthal variations for each of the four size statistics decrease less and less sharply with distance to 610 m, which is 100 m beyond the average continuous ejecta boundary. Beyond 700 m block length remains relatively constant to 1200 m. Although not measurable from aerial photographs, field observations indicate that block size decreases very little beyond 1200 m to the maximum ejecta range (2150 m). Blocks smaller than 1/2 m are almost always the result of impact breakage.

Figure 59 presents block volume totals for each of the sampling areas at 610 m. Volumes, which fluxuate up to a factor of ± 4 about a mean of 5.6 m^3, were computed from block frequencies and measured block lengths using 3-D shape data obtained from the detailed field observations discussed below. Volume fluxuations display some correlation with the Ray-Valley structure of the lip. Volume highs, and to a lesser extent frequencies and sizes, correlate with rays (e.g. R-1, 4R, 6L, 7, 9, and 11) while volume lows, and to a lesser extent frequencies and sizes, correlate with valleys (e.g. V-3, 4, 6, 7, and 8). That better correlations are not observed is due at least in part to the small number and size of sampling areas relative to ray dimensions and to the fact that rays and valleys are not perfectly linear. In addition, the 610 m stations, while 100 m beyond the average continuous ejecta boundary, are located within a very complex region of the ejecta field. This region not only lies near

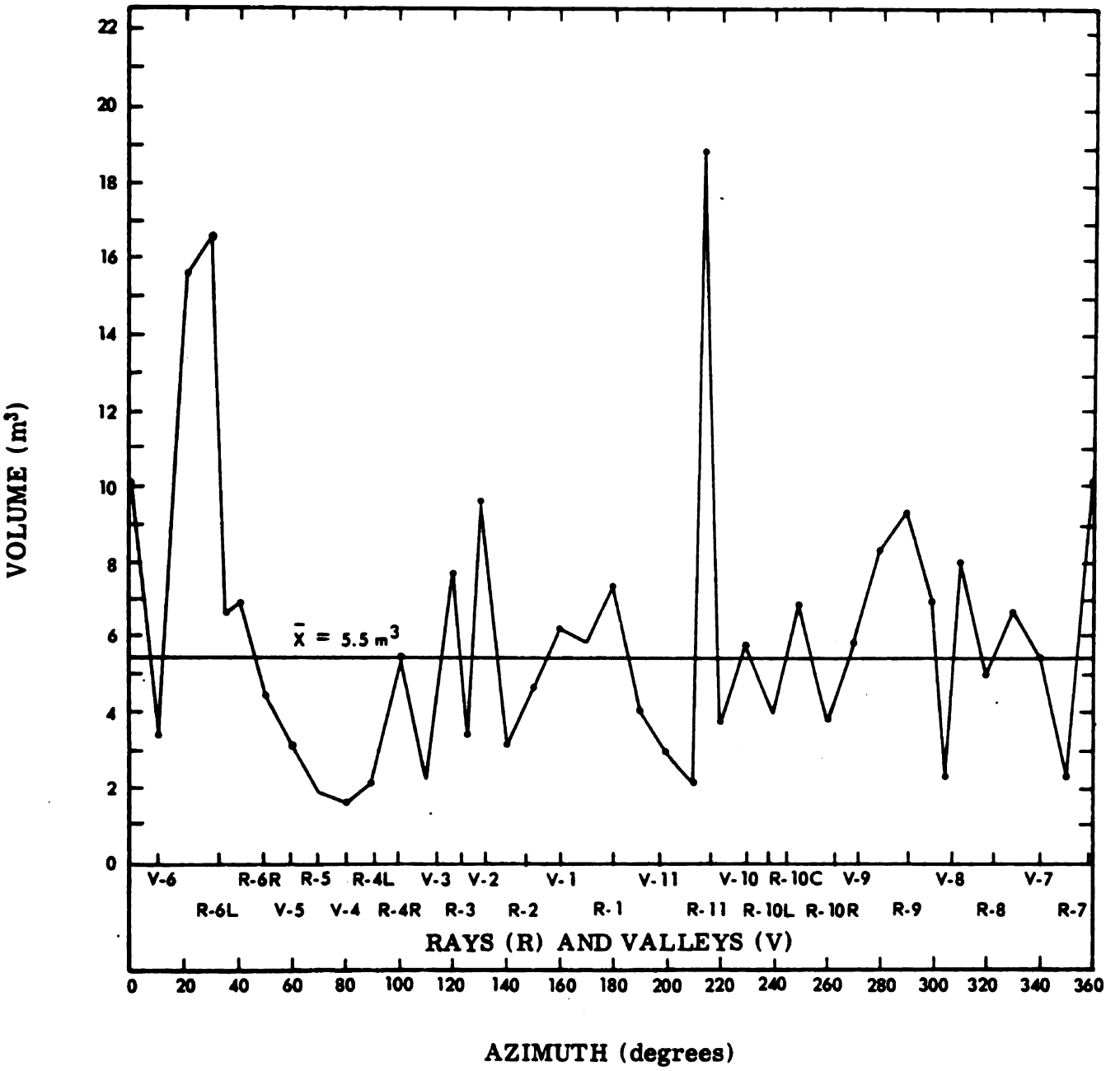

Figure 59. Block Volume as a Function of Azimuth at 610 Meters from SGZ

the maximum concentration of secondary craters, but contains large numbers of blocks that apparently were deposited with, and spread outward from, ray terminal flap segments.

3. Secondary Craters

Frequency and cumulative frequency of secondary craters larger than 1.5 m are presented in Figure 60 as a function of distance from SGZ. Secondary craters are concentrated between 400 and 850 m with the 50th percentile just beyond the continuous ejecta boundary. Secondary crater size, for craters smaller than 6 m, is independent of distance from SGZ.

Area per secondary crater ranges from 1.6×10^3 m^2 at 400 m to 1.8×10^4 m^2 at 1200 m which is a factor of 10 (150 to 750 m) to 100 (250 to 2150 m) higher (fewer secondary craters) than that measured in the field. This is due primarily to the previously mentioned measurement constraints together with the large concentration of secondary craters and attendant overlapping, mutual destruction, and burial near the continuous ejecta boundary. In addition, approximately 5% of all secondary craters are multiple and may have been counted as one. Also, nearly 20% contain significant portions of the impacting block in place and were probably either not observed or counted as a block. The net result is expected to shift the curves of Figure 60 slightly outward (to the right) in addition to broadening them beyond 900 m. Thus, there are at least 15,000 and more probably on the order of 50,000 secondary craters distributed about the Schooner crater.

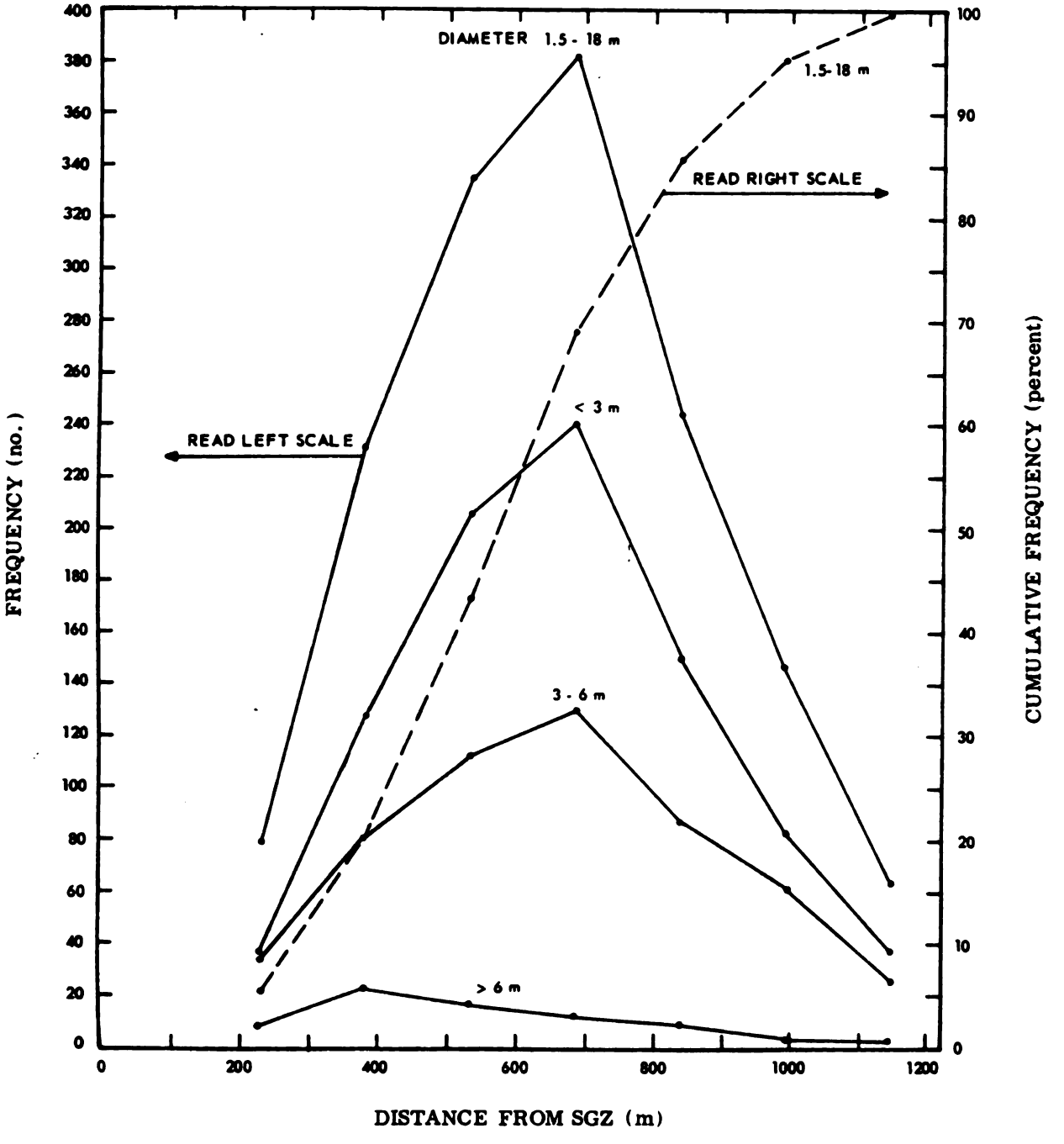

Figure 60. Frequency and Cumulative Frequency of Secondary Craters as a Function of Distance from SGZ

Azimuthal distribution of secondary craters about SGZ varies up to ±76% about a mean of 41.5 impacts per 10° sector (Fig. 61), but neither peaks nor lows appear to correlate with rays or valleys. The high concentration of secondary craters near 140° and 225° are aligned with the downhill and maximum ejecta directions, the latter probably associated with the previously discussed jet (Fig. 10). Reason for the large increase in 1.5 to 3 m craters on the west is unknown, but may be due to the relative sparsity of vegetation in this area, resulting in improved viewing conditions.

C. Detailed Distributions Along Ray 1 and Valley 11 Radials

1. Mapping Procedures

Blocks (and secondary craters beyond 610 m) were counted in the field within 53 sampling areas distributed in a geometric pattern with respect to R-1 and V-11 radials (Fig. 57). All sampling areas were 30.5 x 30.5 m except those along the 457 and 610 m circumferential lines which were reduced to 15.3 m on a side because of the high density of blocks. Stations along the 1021 m line were adjoined; thus, a continuous count was obtained within the 30.5 m band from 167° to 195°.

Blocks were measured along their longest direction and in the two mutually perpendicular directions. Each block was classified according to its mapping unit ("R", "U", or "L") and as to whether it was coated by fused glass. Blocks from the "BOY" units were also observed and measured, but except within previously mapped areas (see Fig. 51) or in localized areas surrounding secondary craters most

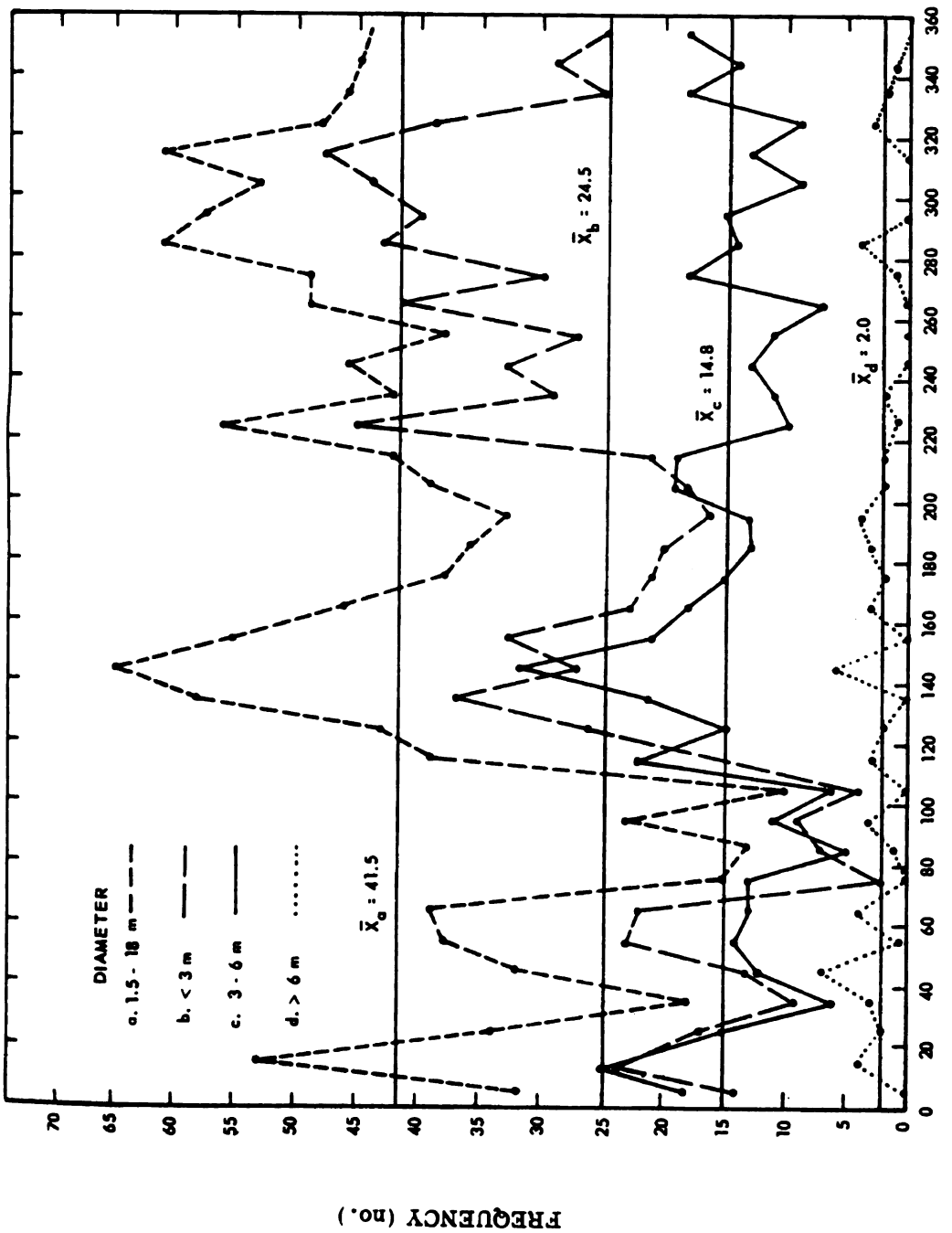

Figure 61. Frequency of Secondary Craters as a Function of Azimuth

such blocks were less than 1/2 m and their total rarely comprised more than 1/2% by volume of the total block population at any sampling location. Interestingly, blocks from the "P" unit were particularly sparce and where observed almost always had brecciated upon impact with largest dimension rarely exceeding 1/6 m. Deposits from below the "Y" unit were not observed.

Secondary craters were measured in three directions with respect to the original ground surface; the longest diameter, the diameter perpendicular to that direction, and the maximum depth. In addition, the mapping unit of the impacting block was recorded. Less than 2% of all secondary craters observed were formed by "B" or "O" blocks and none were formed by "Y" blocks. Therefore, only "R", "U", and "L" blocks and secondary craters are discussed further in this chapter.

Due to rapid decrease in frequency and size of blocks with distance, minimum block size counted was varied from 1 1/2 m at the 152 m stations to 2/3 m out to the 610 m stations, to 1/3 m beyond. While such a scheme is a compromise and admittedly less than ideal for good statistical analysis, it is believed adequate to meet the stated objectives of obtaining relative comparisons along and between the sampling lines.

2. Blocks

a. Fused-Glass Encased Blocks

By volume, 7% of all blocks measured were encased to some degree in fused glass with the percentage increasing significantly with

distance. Along the R-1 radial, the percentage of blocks with fused glass increases from 10% at 450 m to over 90% by 1400 m (Fig. 62). The distribution is not regular due to secondary cratering; e.g. a number of large impacts with fused glass occur at the 914 m station. The percentage of blocks with fused glass along the V-11 radial follows that of R-1 reasonably well out to 900 m, beyond the trend for V-11 is confusing, but totals fall well below those along R-1. Percentage of "L" blocks with fused glass reaches a maximum of 74% near 750 m along radial R-1 in comparison to only 31% along V-11, also at 750 m. Overall, percentage of "L" blocks containing fused glass is greater than for "R" and "U" blocks out to 1050 m and 750 m for R-1 and V-11, respectively; beyond there is little overall difference.

Along the 457 m circumferential stations, blocks containing fused glass are sparce, being found at 182° on Ray 1 (2%) and at 194° in Valley 11 (6%). At both stations percentages of "L" blocks with fused glass approaches 15%. At the 610 m stations, fused-glass covered blocks are concentrated (∿20%) to the counterclockwise side of Ray 1 with percentage of "L" blocks increasing to 50%. There is another small concentration on the clockwise side of R-1. Along the 1021 m arc percent of fused-glass covered blocks averages 42% and ranges from 20 to 40% towards V-1 and V-11 radials and up to 85% along the R-1 radial (Fig. 63).

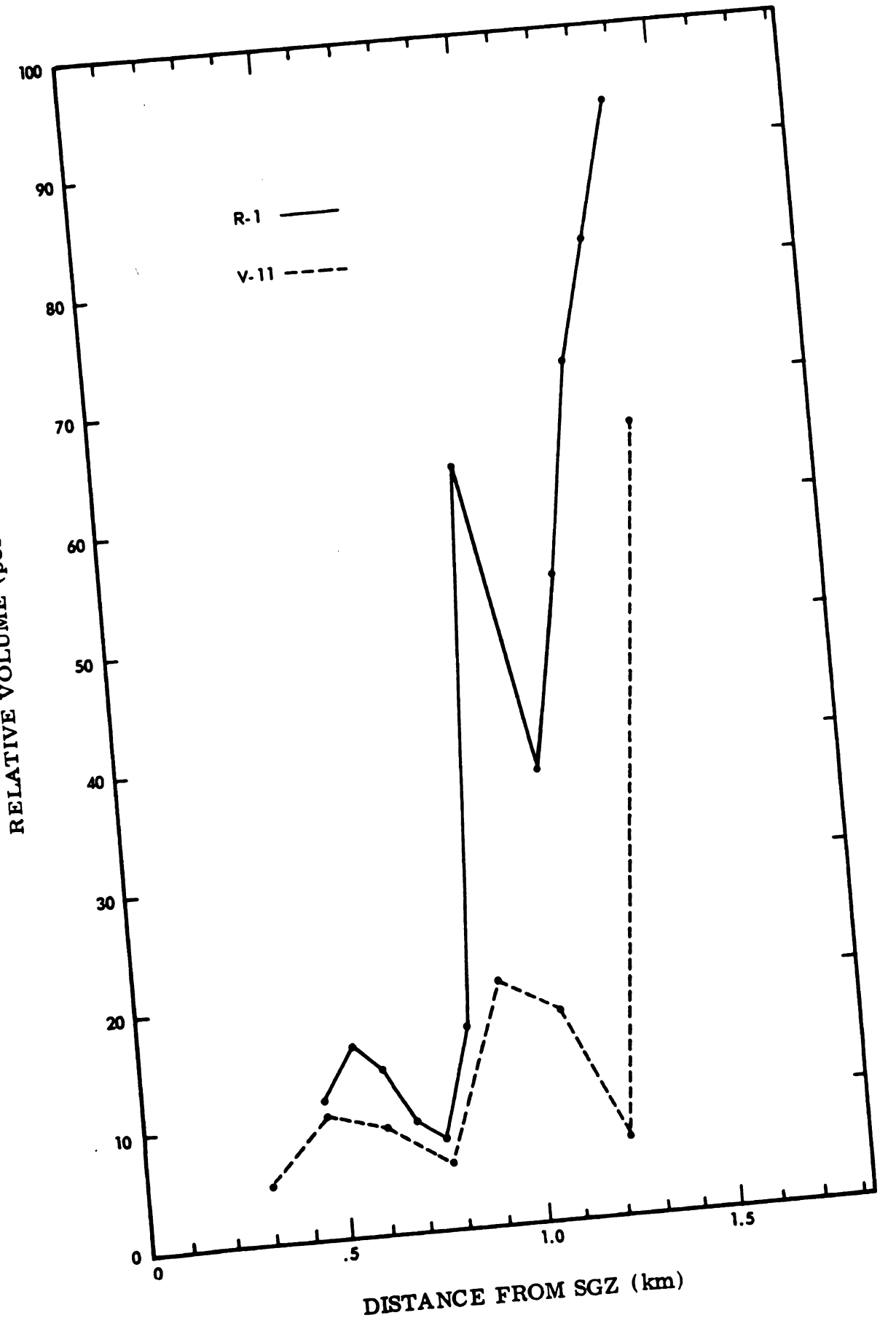

Figure 62. Percent by Volume of Blocks with Fused-Glass Coatings as a Function of Distance along Radials R-1 and V-11

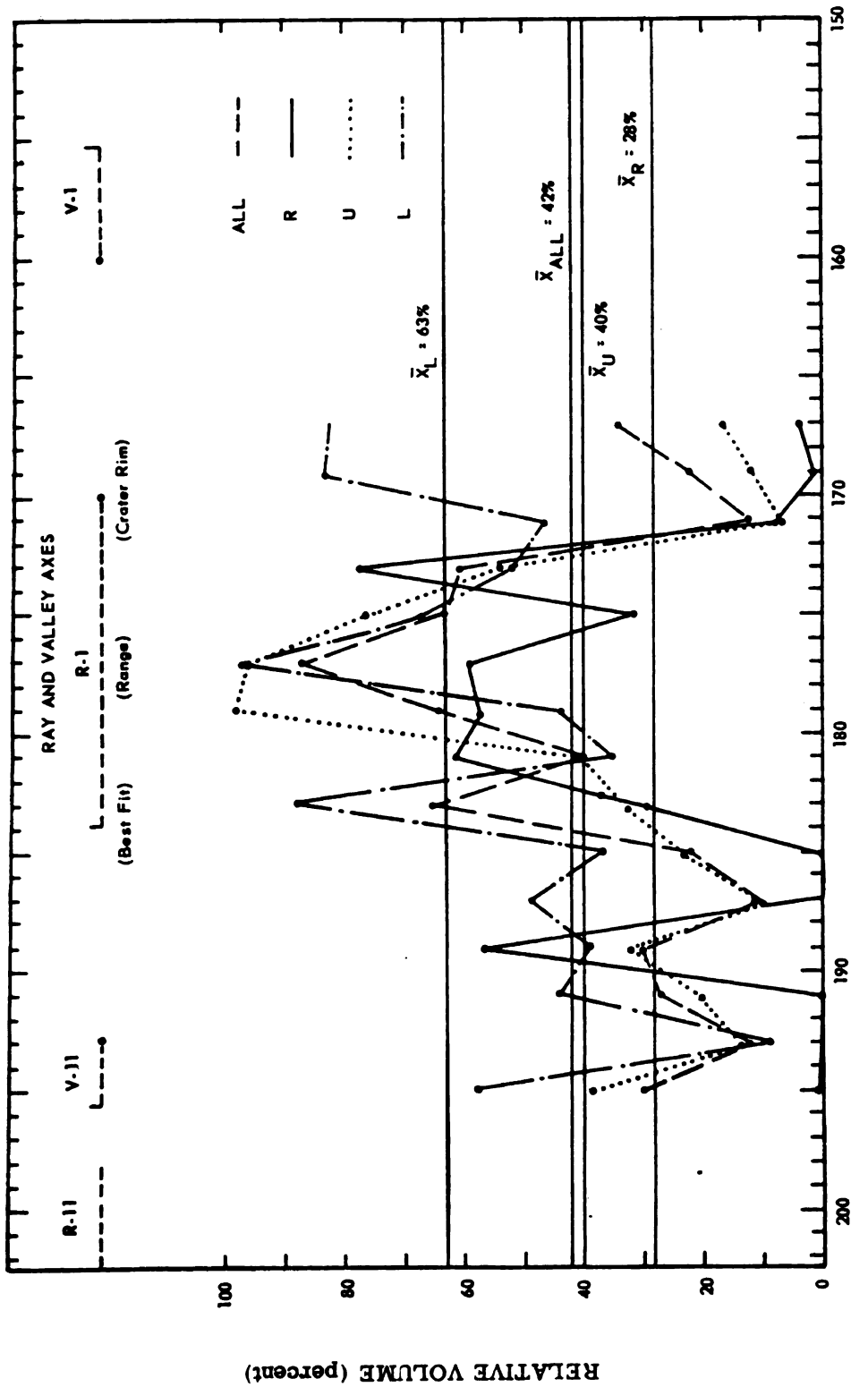

Figure 63. Percent by Volume of Blocks with Fused-Glass Coatings as a Function of Azimuth along the 1021 Meter Circumferential Stations

b. Stratigraphy

Blocks without fused glass exhibit an inverted stratigraphic order on both R-1 and V-1 radials where percentages of "L", "U", and "R" peak successively outward (Fig. 64). The radials differ in two respects; first, the inverted stratigraphic order continues farther out on V-11 (1250 m vs 850 m) and second, the greater frequency of secondary cratering on R-1 results in a less ordered distribution of blocks. For blocks $\geq$ 1 m the inverted stratigraphic order is slightly better defined.

For the fused-glass covered blocks, there is little inverted stratigraphic order with "L" blocks dominating out to near 950 m. Note that for both R-1 and V-11 radials the inverted stratigraphic order deteriorates where fused-glass coated blocks approach 20% of the total block population.

Figure 65 plots percent volumes of "R + U" blocks without fused glass for the circumferential stations. At 457 m percent "R + U" reflects the Ray-Valley structure increasing from 20 to 30% on R-1 to near 100% between R-1 and V-11 (near the R_b of R-1) and then decreasing rapidly as the isolated segment of R-11 is approached. At 610 m percent "R + U", while never below 60%, exhibits a high of 98% near the R-1 radial and a low near the V-11 radial; elsewhere "R + U" percentages are mixed. By 1021 m neither rays nor valleys are reflected with percent "R + U" oscillating between 65 and 95%; the exception is at 181° which contains only small "R + U" blocks and several large "L" blocks from secondary cratering.

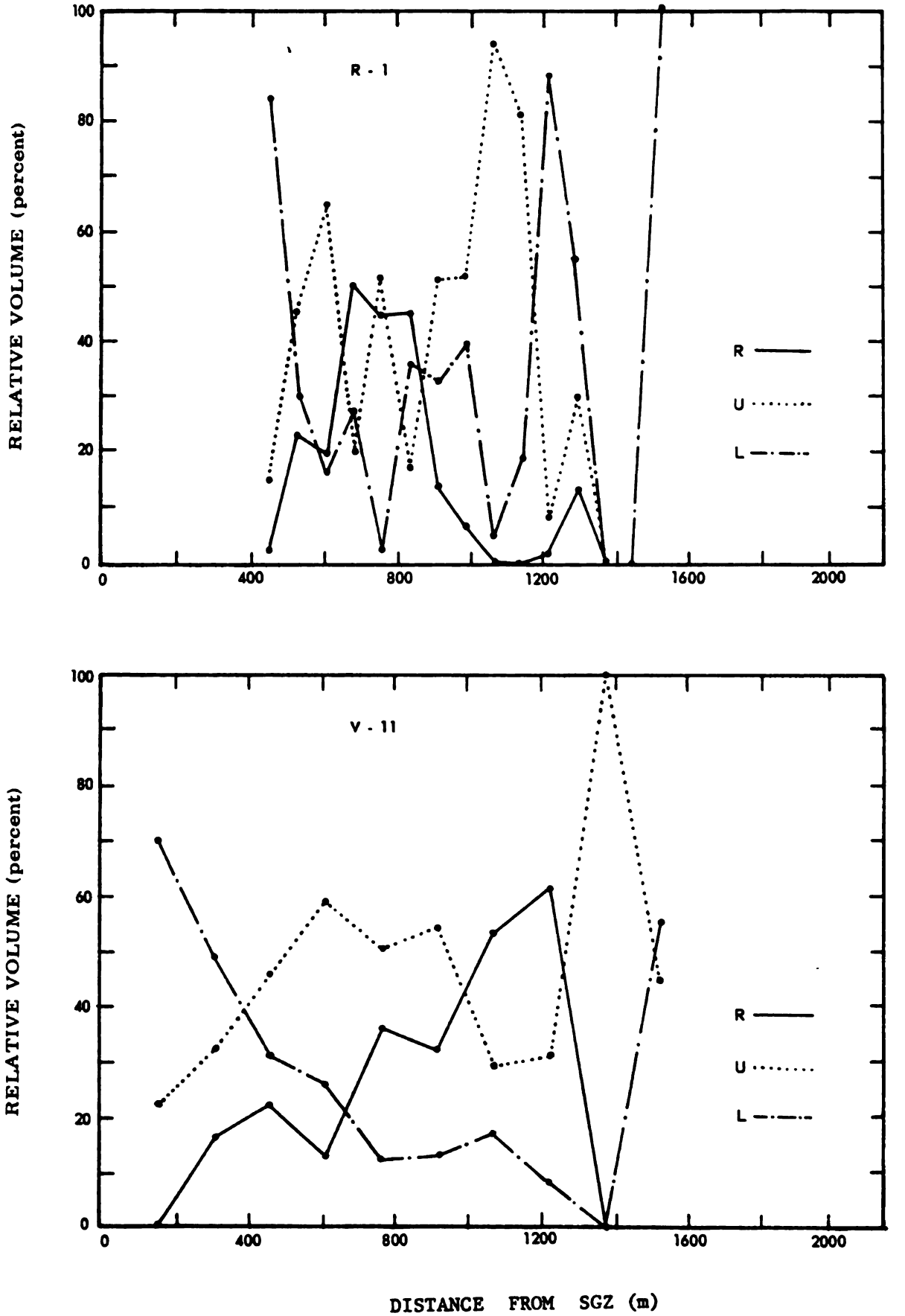

Figure 64. **Percent Composition by Volume of Blocks as a Function of Distance from SGZ along the R-1 and V-11 Radials with Skewed Ray and Valley Axes Indicated**

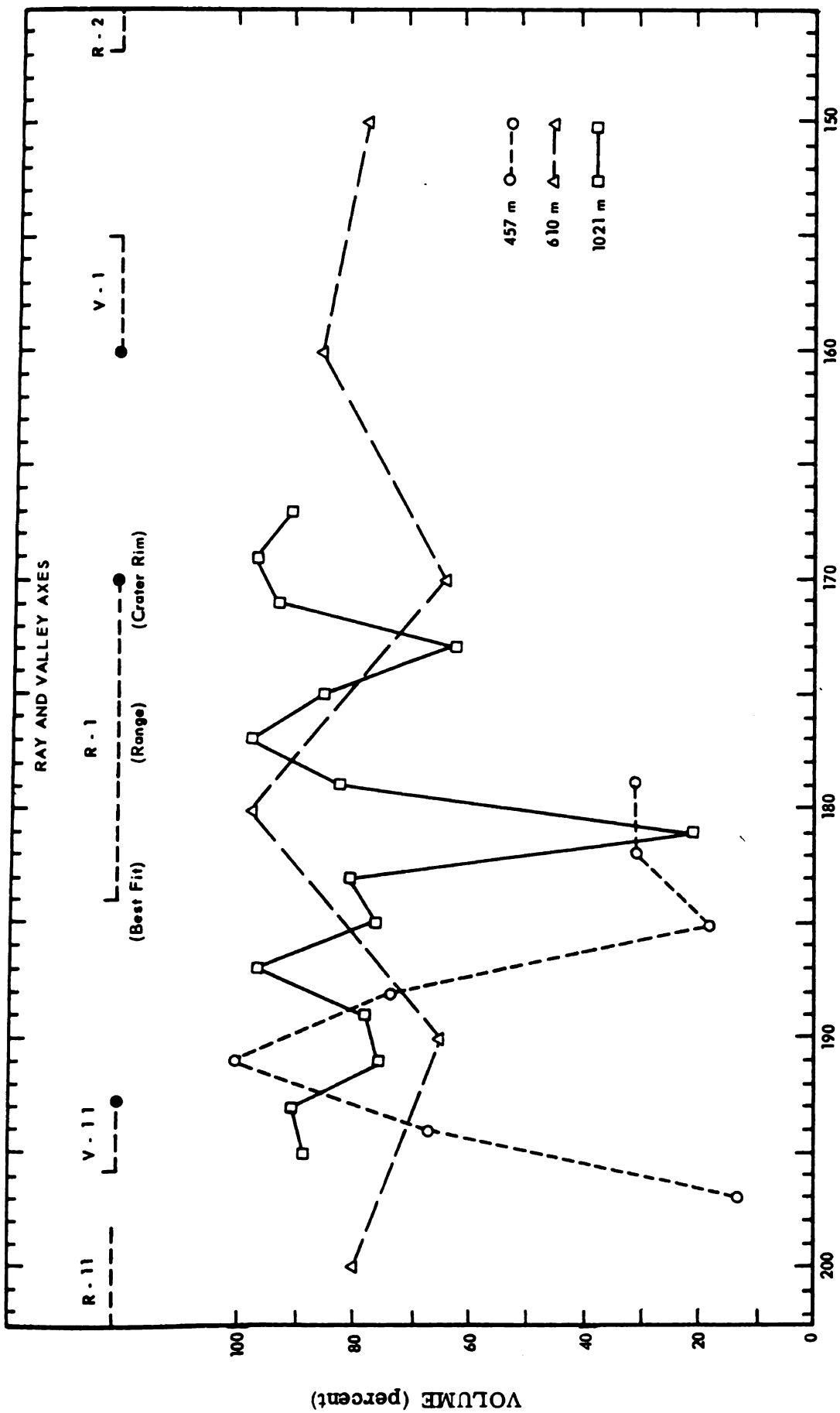

Figure 65. Percent Composition by Volume of "R" + "U" Blocks as a Function of Azimuth at the 457, 610, and 1021 Meter Stations with Skewed Ray and Valley Axes Indicated

c. Size

Along the R-1 radial mean volume of blocks without fused glass decreases rapidly (0.015 m^3 per m) to 700 m, gradually (0.0002 m^3 per m) to 1200 m, and then remains relatively constant to the maximum ejecta range (Fig. 66). Mean block volumes for the V-11 radial are similar to R-1 near their respective continuous block boundaries, but decrease more gradually with distance such that from 700 to 1050 m mean block volumes on the V-11 radial range up to a factor of 2 to 5 larger. Beyond 1050 m mean block volumes are similar along both radials. Blocks from the "L" unit tend to be larger than "R" or "U" blocks out to 600 m, beyond block sizes are similar. Glass-encased blocks are slightly larger on both radials.

Individual block volumes along the circumferential stations are related to the Ray-Valley structure of the lip (Fig. 67). At 457 m, mean block volume is largest near the continuous block boundary of R-1 (less coverage by fines), decreases into V-11, and then increases toward R-11. Within R-1 fines cover blocks and sizes are accordingly reduced. Mean block volume of individual units also vary with the Ray-Valley structure. Near the continuous block boundary of R-1 "L" ≈ 0.57 m^3, "U" = 0.23 m^3, and "R" = 0.08 m^3; while within V-11 "U" = 0.28 m^3, and "R" and "L" = 0.06 m^3. At 610 m, mean block volume increases toward R-1 and R-2 radials and decreases toward V-11. Overall, block volumes range downward from "R" to "U" to "L" with "R" and "U" blocks following the mean volume trend, and "L" blocks exhibiting little trend. At 1021 m, mean volume varies from 0.03 to

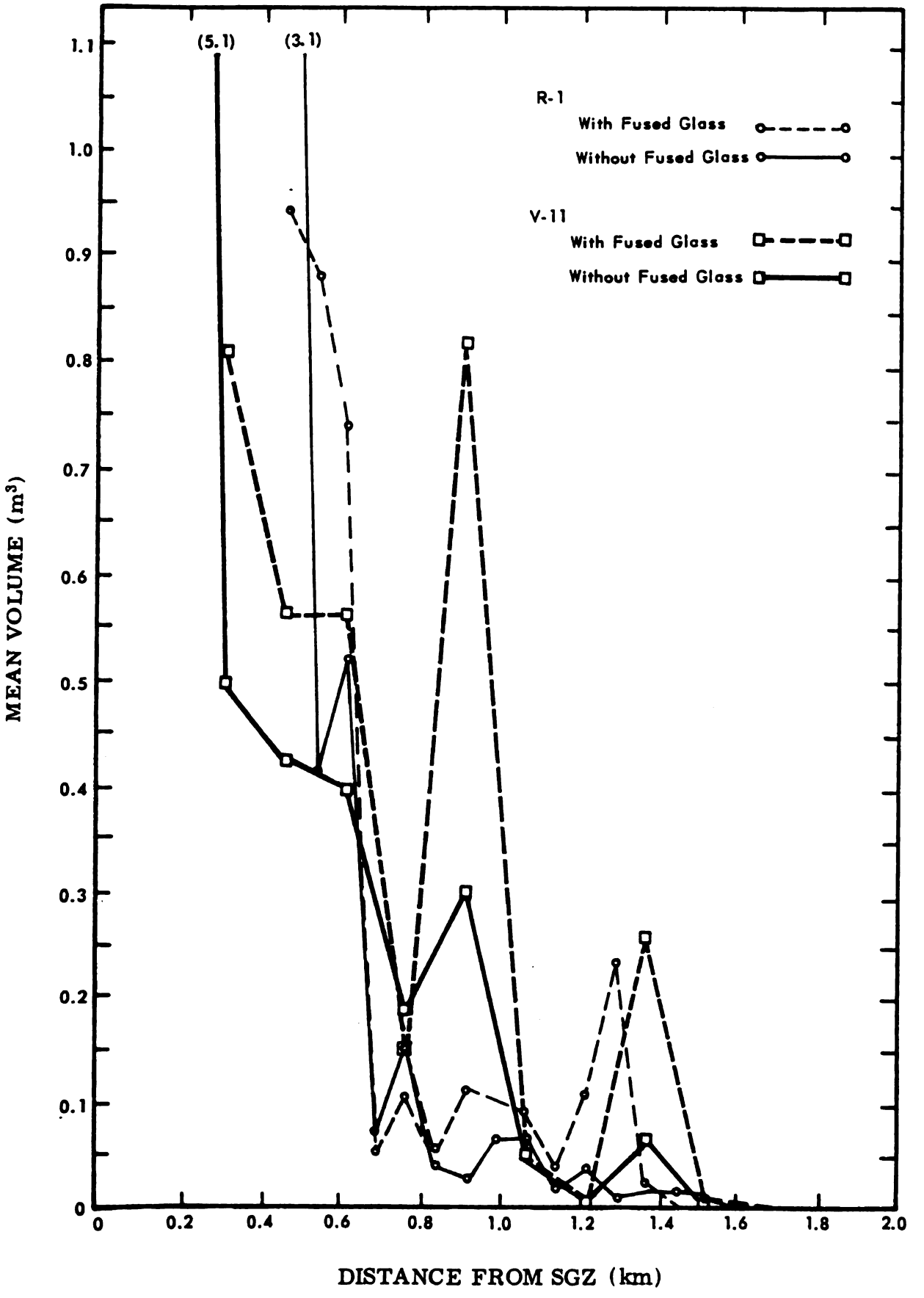

Figure 66. Mean Block Volume as a Function of Distance from SGZ along R-1 and V-11 Radials

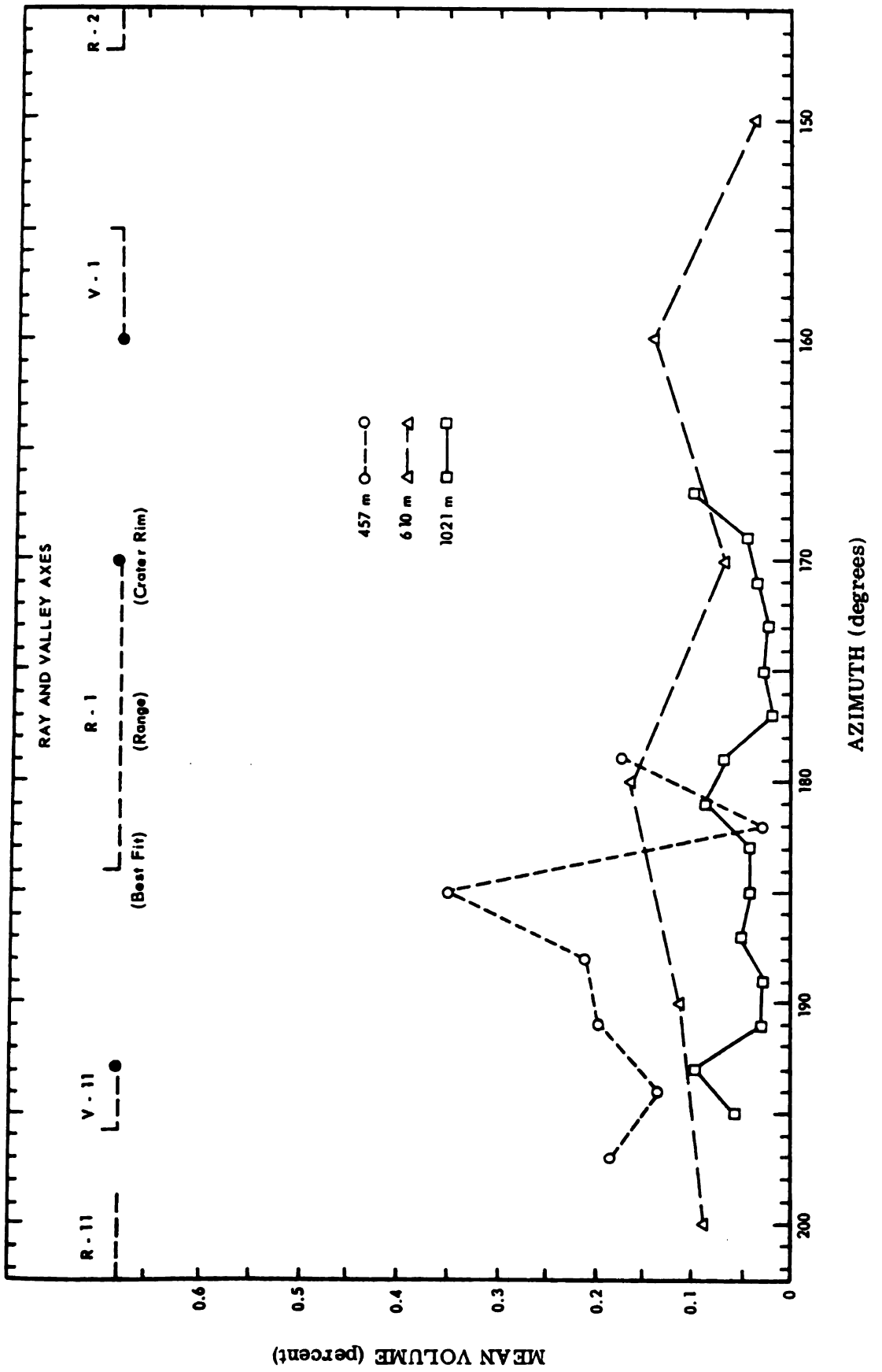

Figure 67. Mean Block Volume as a Function of Azimuth at 457, 610, and 1021 Meter Stations with Skewed Ray and Valley Axes Indicated

0.11 m^3 in an irregular pattern without respect to the Ray-Valley structure. Unlike closer-in stations, there is little difference in mean block volume between the various units. Glass-encased blocks follow a similar pattern, but tend to be 30% larger.

d. Shape

Three-dimensional block shapes were computed using Sneed and Folk's (1958) shape factor [$\psi_p = (S^2/LI)^{1/3}$] where L, I, and S are the mutually perpendicular long, intermediate, and short diameters, respectively. Average block shape increases slowly, but steadily from 0.7 near 300 m to 0.8 near 1200 m with little difference observed between R-1 and V-11 radials. This 13% increase is probably more a reflection of block size than distance; i.e. shape increases slightly with decrease in size which decreases with distance. Near maximum ejecta range most blocks not broken on impact are equi-dimensional, 1/3 to 2/3 m on a side and typically encased in fused glass.

Along the circumferential stations at 610 and 1021 m shapes vary regularly $\pm$5% about their mean, but follow no particular pattern with respect to the Ray-Valley structure. Average shape factor is 10% higher at the 1021 m stations, again probably reflecting a decrease in size. Along the 457 m stations there is a trend to slightly higher shape factors along V-11 (less breakage?) compared to R-1 and R-11. Fused-glass covered blocks tend to have slightly higher ($\sim$10%) shape factors out to at least 900 m.

e. Volume

Total block volume in each of the sampling areas along the R-1 and V-11 radials is presented in Figure 68. Areas over which blocks were counted have been normalized to the largest sampling area; but no factor has been applied to compensate for the changes in minimum block size counted nor for counting only on the surface of the continuous ejecta blanket. Therefore, inside the continuous ejecta boundary, plotted volumes are lower than actual volumes. While R-1 and V-11 radials contain similar total block volumes near their respective continuous block boundaries, beyond 700 m total block volume along V-11 radial becomes significantly higher.

Total volume distributions of fused-glass covered blocks along R-1 and V-11 radials are reasonably similar, particularly beyond the continuous ejecta boundary; but distinctly unlike the distributions of blocks without fused glass.

Thus, whereas Ray 1 clearly contains the larger volume of blocks out to the continuous ejecta boundary, Valley 11 contains the larger volume of blocks beyond, by a factor of 2 to 8. This correlates with the larger number of impacts for valleys versus rays observed from event aerial photography (Fig. 15) and provides one line of support for extending the relationships observed between R-1 and V-11 radials to the entire ejecta field.

3. Secondary Craters

a. Frequency and Volume

Frequency of secondary craters per sample area along the R-1 radial decreases rapidly and regularly with distance (Fig. 69). The

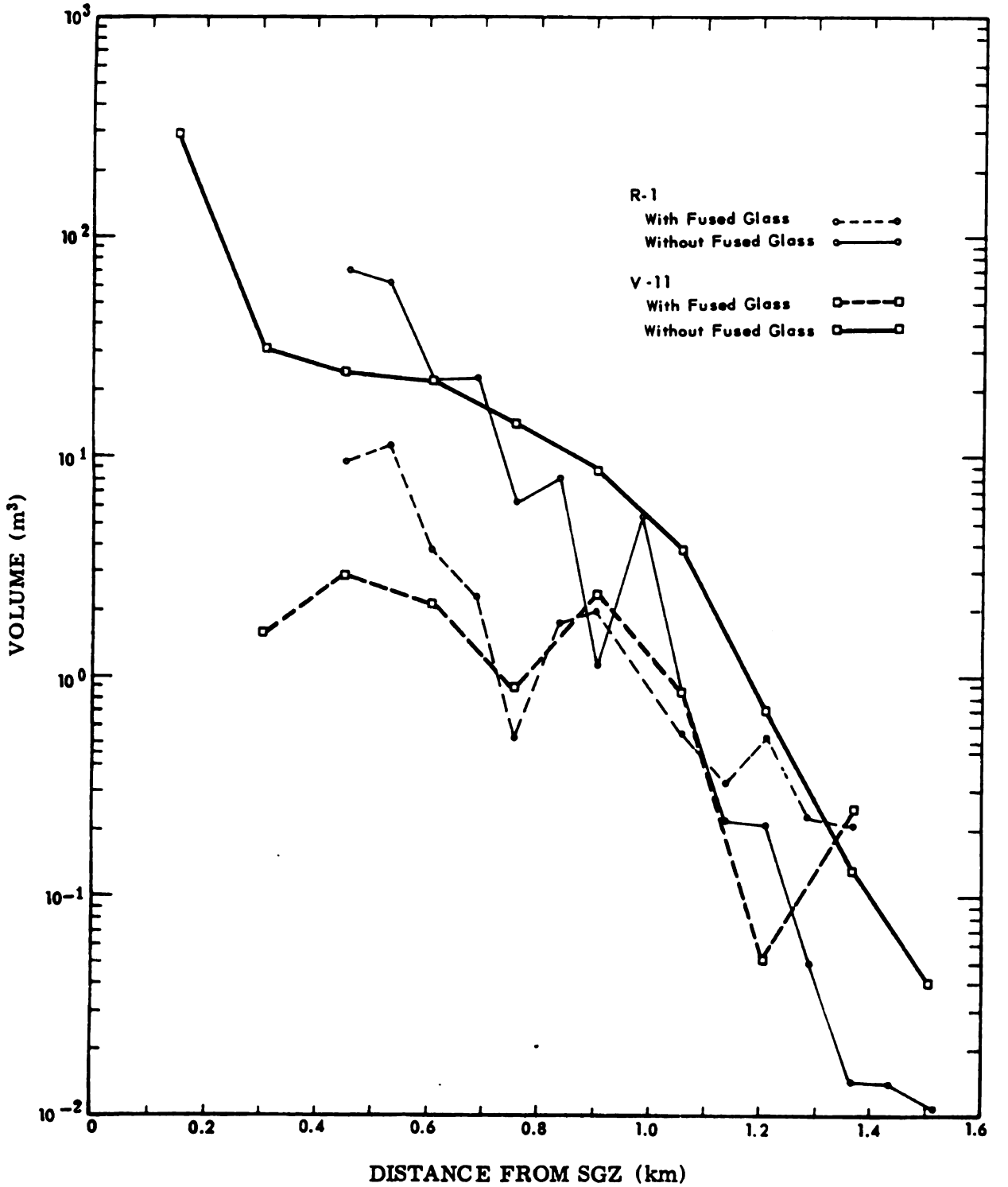

Figure 68. Block Volume as a Function of Distance from SGZ along R-1 and V-11 Radials

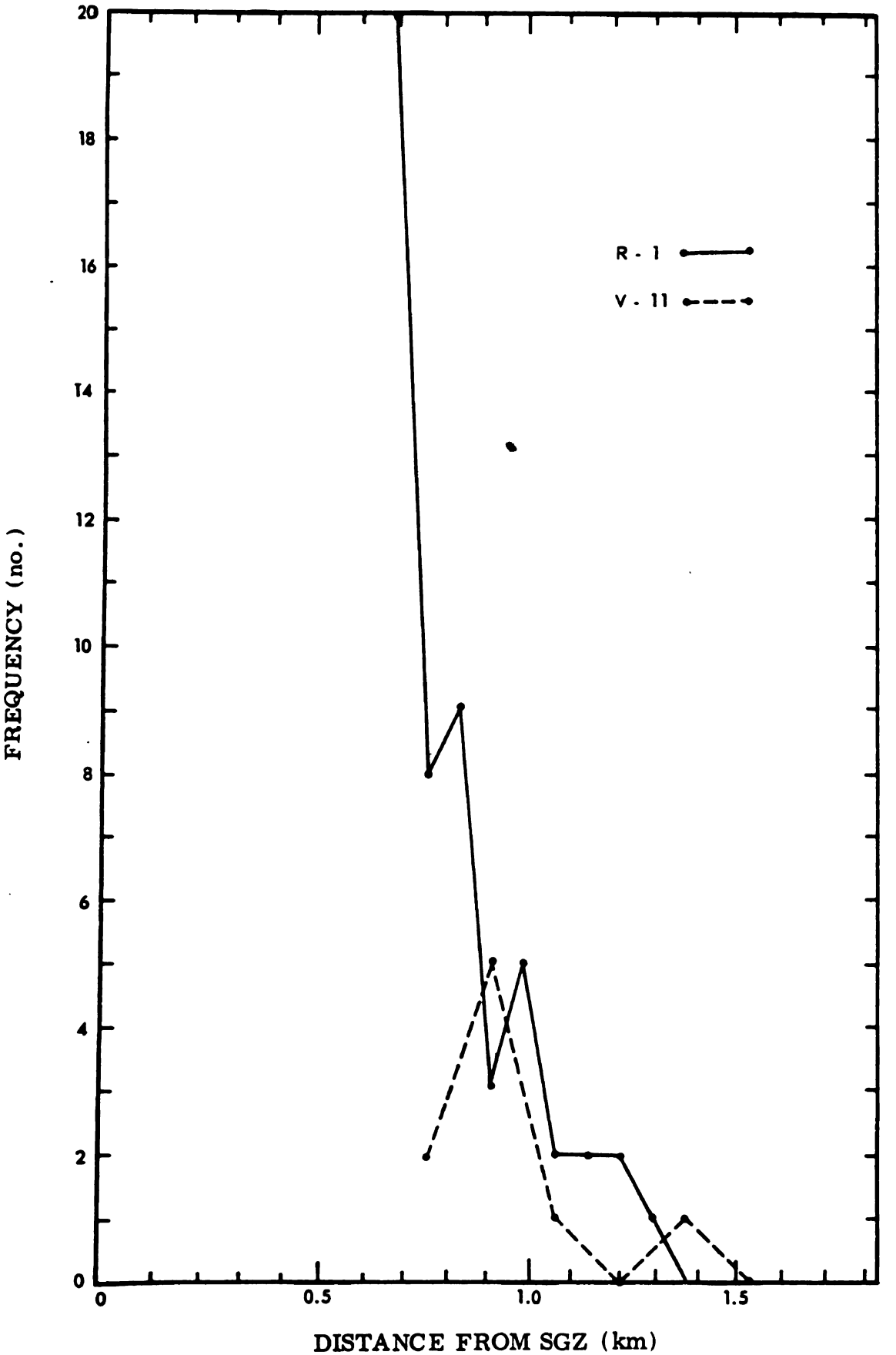

Figure 69. **Frequency of Secondary Craters as a Function of Distance from SGZ along R-1 and V-11 Radials with Skewed Ray and Valley Axes Indicated**

R-1 radial contains significantly more secondary craters than V-11 out to 850 m, beyond the distributions are similar. Total volume of secondary craters per sample area, which is proportional to the volume of impacting blocks, reaches a high of 22 m^3 per sampling area on R-1 near the continuous ejecta boundary, but only 5 m^3 on V-11 at 900 m. Along the 1021 m arc, secondary craters per sampling area average 5.7 and range from 1 to 11. There is a general decrease from east to west independent of the Ray-Valley structure of the lip (Fig. 70). Total volume of secondary craters follows the frequency distribution except that there are concentrations aligned with the east (10 m^3) and west (9 m^3) borders of Ray 1 compared to an average volume for all stations of only 2.4 m^3 sampling area.

b. Size

Size of secondary craters along the R-1 and V-11 radials range from less than 0.03 m^3 to a maximum of 9.6 m^3 about a mean of 1.1 m^3. While there is a general decrease with distance, secondary crater size is controlled to a large extent by local ground conditions with little difference between the two radials. Along the 1021 m arc, size of secondary craters averages 0.5 m^3 and, similar to block size, exhibits no trend with respect to the Ray-Valley structure of the lip. There is also little difference in size between secondary craters formed by either the "R", "U", or "L" units.

c. Shape

Aspect ratios (R_a/D_a) of secondary craters along both R-1 and and V-11 radials range from 1.5 to 6.5 about an average of 3. Shape,

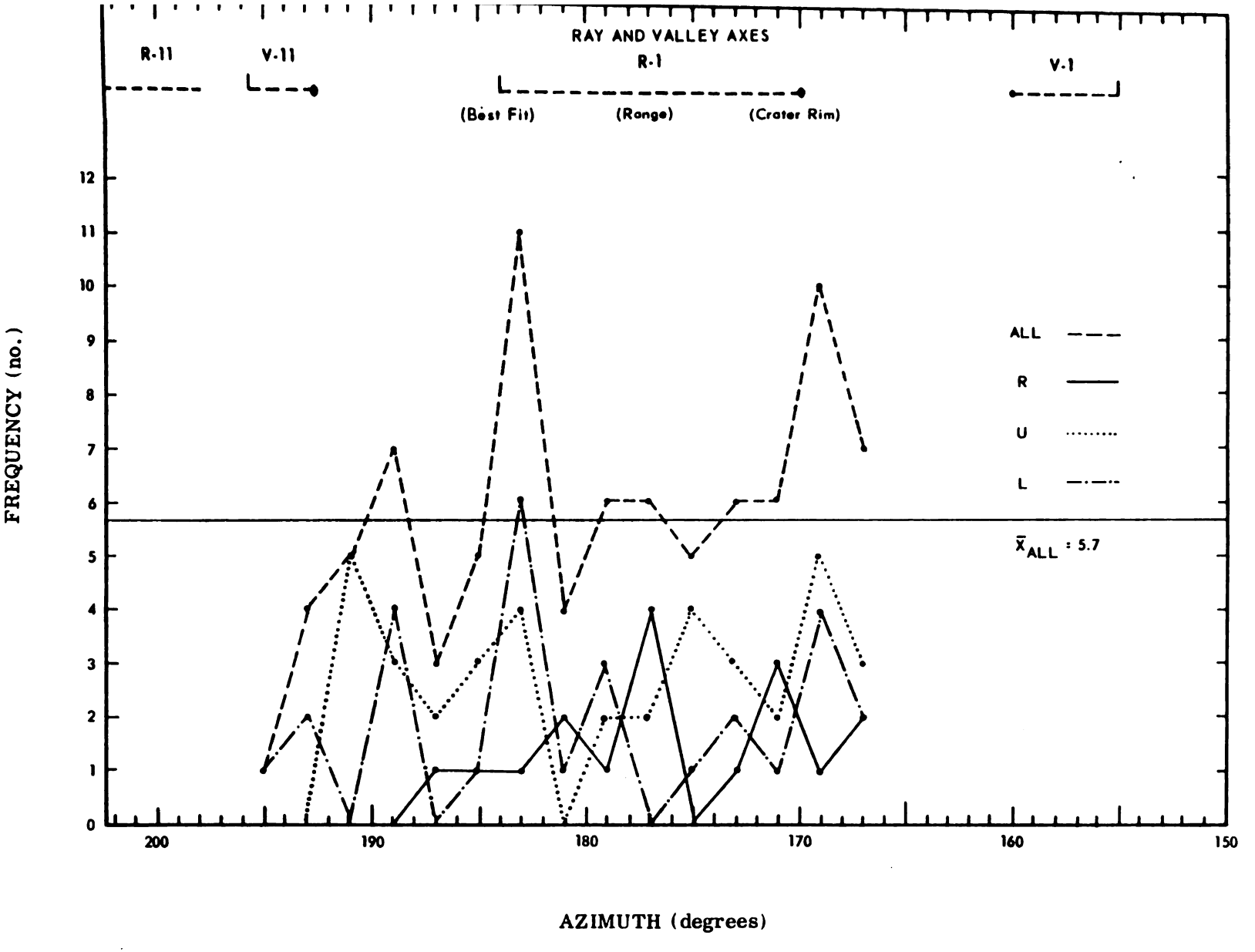

Figure 70. Frequency of Secondary Craters as a Function of Azimuth along the 1021 Meter Stations

like size, appears to be related primarily to ground surface conditions; i.e. the deeper the soil the greater the depth and smaller the aspect ratio. Aspect ratios of secondary craters along the 1021 m arc vary from 1 to 4 about an average of 3 and like size exhibit no trend relative to the Ray-Valley structure.

d. Stratigraphy

For all secondary craters measured, the relative percentages of the impacting blocks were: "L"(35%), "U"(44%), and "R"(21%). While both the "R" and "U" percentages are increased with respect to in situ, 3.5 and 1.7 respectively, there is only a slight indication of inverted stratigraphic order with distance. Along the V-11 radial, secondary craters formed by "R" blocks dominate between 700 and 900 m reaching 60% by number and 90% by volume of the total population. Along the R-1 radial "R" unit secondary craters are concentrated between 700 and 850 m, but do not exceed 40% by number or 20% by volume of the total population. Beyond 900 m "R" secondary craters make up only a few percent of the population on the R-1 radial while on the V-11 radial "R" secondary craters are present in near equal volumes to secondary craters from the "U" and "L" units. Along the 1021 m stations "R" and "U" secondary craters exhibit average volume increases over that in the core of 5.5 and 1.5, respectively, while "L" secondary craters are decreased by a factor of 3.

CHAPTER VIII

RELATIONSHIPS BETWEEN THE GEOLOGIC SETTING AND THE CRATER AND EJECTA FIELD

The Schooner crater and ejecta field and the processes involved in their formation are the result of a set of complex interactions between parameters of the source and the geologic setting. A major hypothesis of this study is that certain geologic parameters of the Schooner site played a dominant role in the formation of the crater and ejecta field. Although few of the processes or resultant effects could be observed in their entirety, many important portions were, and have been documented in the preceding chapters. This chapter first briefly compares Schooner to three other buried nuclear events and then assesses the effect of key geologic parameters on the observed crater and ejecta field.

A. Schooner Compared

The Schooner site was specially selected to combine strong and weak layering with a water table, a geological setting not previously tested.

1. Crater Shape

The shape of Schooner's crater differs from other buried explosive craters in two important respects, its steep wall and its shallow flat floor. Figure 71 compares the average crater profile of Schooner with average profiles of Sedan, 104 KT in desert alluvium; Danny Boy, 0.42 KT in basalt; and Cabriolet 2.3 KT in

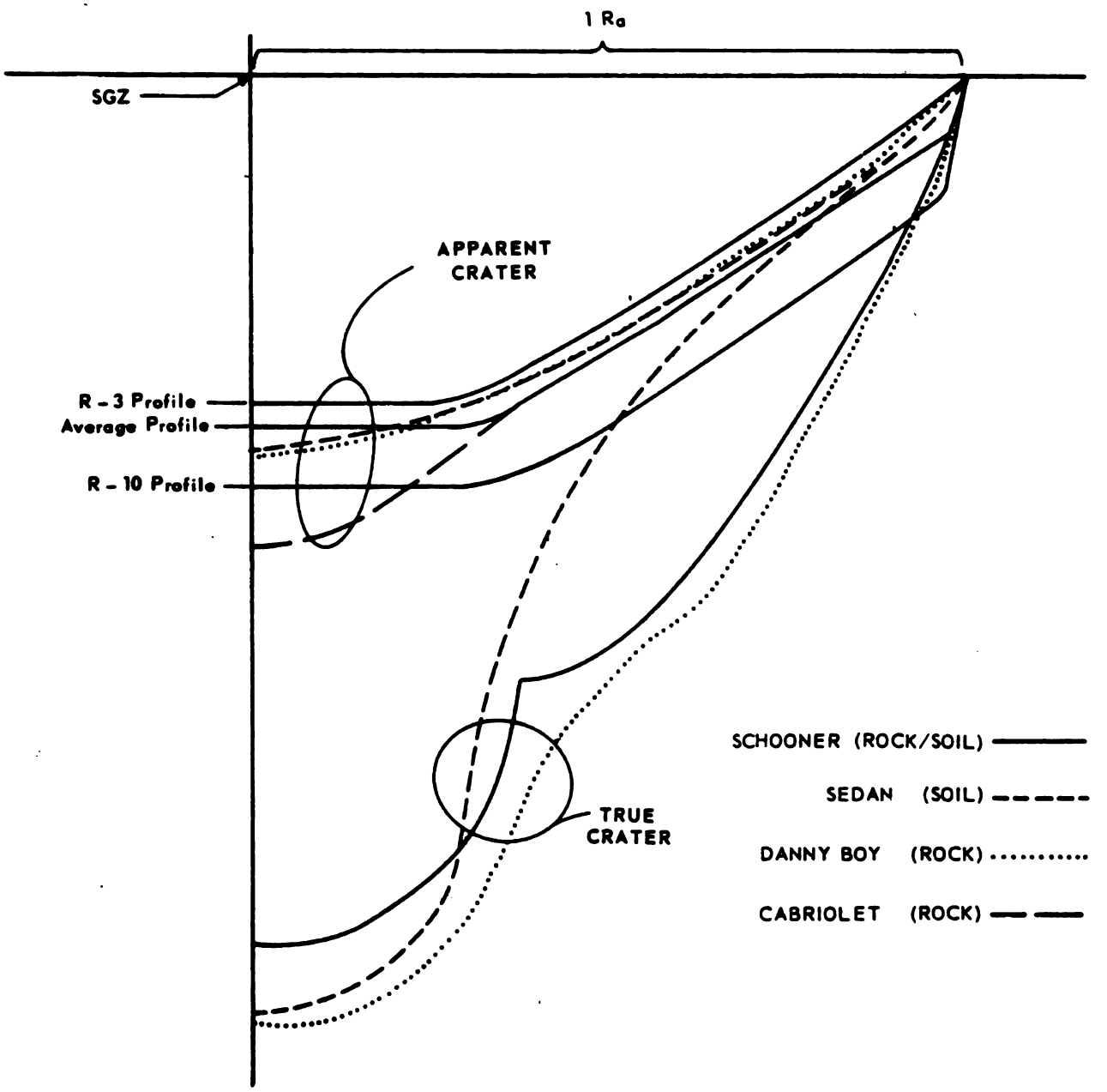

Figure 71. Comparison of Apparent and True Crater Shapes from Buried Nuclear Detonations in Rock and Soil

rhyolite. Two additional Schooner profiles from Figure 29 are also plotted, the R-10 profile from the west or uphill side of the crater and the R-3 profile from the southeast or downhill side of the crater. Profiles were normalized by superimposing SGZ's and setting the apparent crater radii equal.

As anticipated, the apparent crater profiles traversing the fallback portions of all the craters are similar with slopes typical of natural talus slopes. Also as expected, the upper portions of the true crater profiles for rock craters (Schooner and Danny Boy) are significantly steeper than the soil crater (Sedan). The major difference in profiles is that the true crater is exposed on over 75% of Schooner's surface while fallback covers the other true craters; i.e. relatively more of the material from Schooner was ejected.

Figure 71 also indicates Schooner's floor is anomalously flat and that its average profile is shallow with respect to the other average profiles. Schooner's average aspect ratio (R_a/D_a) is 2.04 compared to values ranging from 1.55 to 1.89 for the other three craters. Applying the average aspect ratio from the other craters, Schooner's "corrected" apparent crater depth (D_a') would be 76 m or 20% larger than the present apparent crater depth. The volume of material between D_a and D_a' is 1.91×10^4 m^3 or 1% of the apparent crater volume.

2. Scaled Crater Dimensions

Given the geologic setting and with proper stemming of the device, the yield (W) and the depth of burst (DOB) of the device determine the size of the crater and distribution of the ejecta field. Both were accurately measured (W = 31 $\pm$ 4 KT and DOB = 108.2 m), while the vent history discussed in Chapter III demonstrates that the stemming was adequate.

Figure 72 compares, on a scaled basis, Schooner's apparent crater radius and depth, to current prediction curves for buried nuclear events in dry hard rock (data base primarily basalt and rhyolite) and dry soil (data base primarily desert alluvium) (Fisher, 1968). As observed, Schooner's scaled radius is only slightly smaller than that of a soil crater. The present scaled depth is slightly smaller than a rock crater; but the corrected scaled depth (D_a') is very close to a soil crater.

While there are no curves for layered media, Schooner would be expected to lie between the soil and rock curves and most probably closer to the rock curves. Thus, clearly the Schooner crater is significantly larger than one would predict using current empirical techniques. Code calculations by Terhune (in Lessler, 1968) based on first principles and using the measured properties of the site, likewise predicted a significantly smaller crater: R_a = 20% low, D_a = 7% high, D_a' = 11% low, and V_a = 40% low (where $V_a = F\pi R_a^2 D_a$ and F = 0.46, an average shape factor for Schooner).

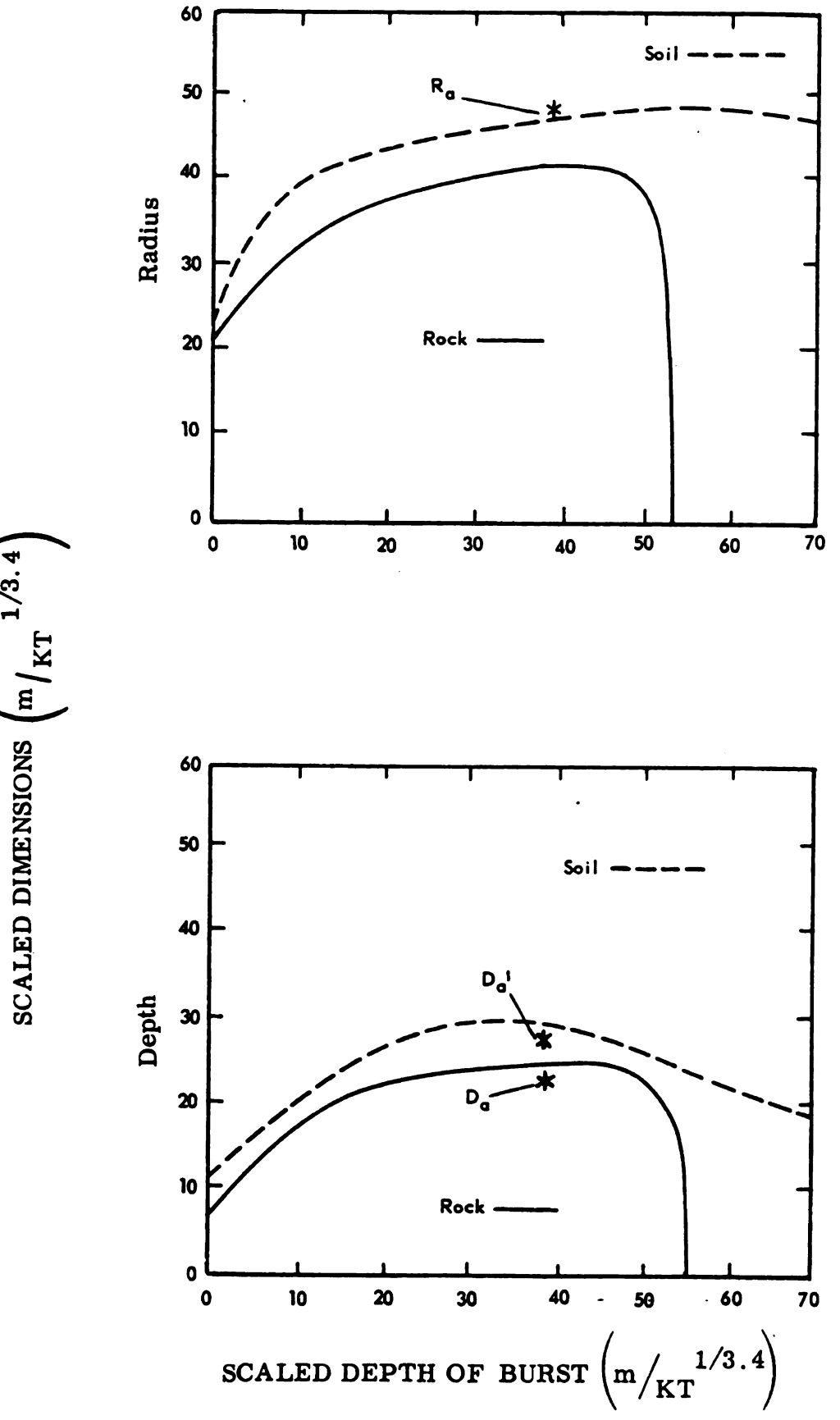

Figure 72. Scaled Crater Dimensions for Buried Nuclear Detonations in Rock and Soil

3. Mass Balance

For cratering events, the mass of material affected should be nearly conserved. Thus, analysis of mass partitioning using mass balance ratios provides a means of quantifying the cratering processes. Mass balance ratios, described and calculated in Appendix D, are presented in Table 4 and compared with similar ratios for Sedan. The apparent differences in cratering processes between Schooner and Sedan are significant in two respects. First, on Schooner ejection was a dominant process with over twice the relative material ejected as on Sedan. Second, net compaction on Schooner was a minor process being less than one-third as great as that of Sedan.

4. Distribution of Ejecta Mass

Figure 73 compares ejecta distributions in terms of incremental mass as a function of crater radii for Schooner, Sedan, and Danny Boy. Although over 80% of Schooner's ejecta mass is composed of welded tuff blocks it is distributed significantly farther out on a relative basis than the basalt blocks of Danny Boy. In fact, out to 3 R_a Schooner and Sedan ejecta distribution are nearly identical. Beyond 3 R_a the remaining 20% of Schooner's ejecta mass is distributed relatively closer to the crater than Sedan; but still extends over four times farther than Danny Boy.

B. Relationships

There are a number of important relationships between the crater and ejecta field and the geologic setting. These range from

TABLE 4

MASS BALANCE RATIOS FOR SCHOONER AND SEDAN

Ratio	Schooner	Sedan
M_e/M_t	0.43	0.20
M_f/M_t	0.47	0.43
M_k/M_t	0.01	0.01
M_Δ/M_t	0.09	0.36
M_m/M_t	0.53	0.57
M_u/M_t	0.11	0.05
M_e/M_m	0.80	0.36
M_e/M_a	0.88	0.42
M_d/M_e	0.09	-

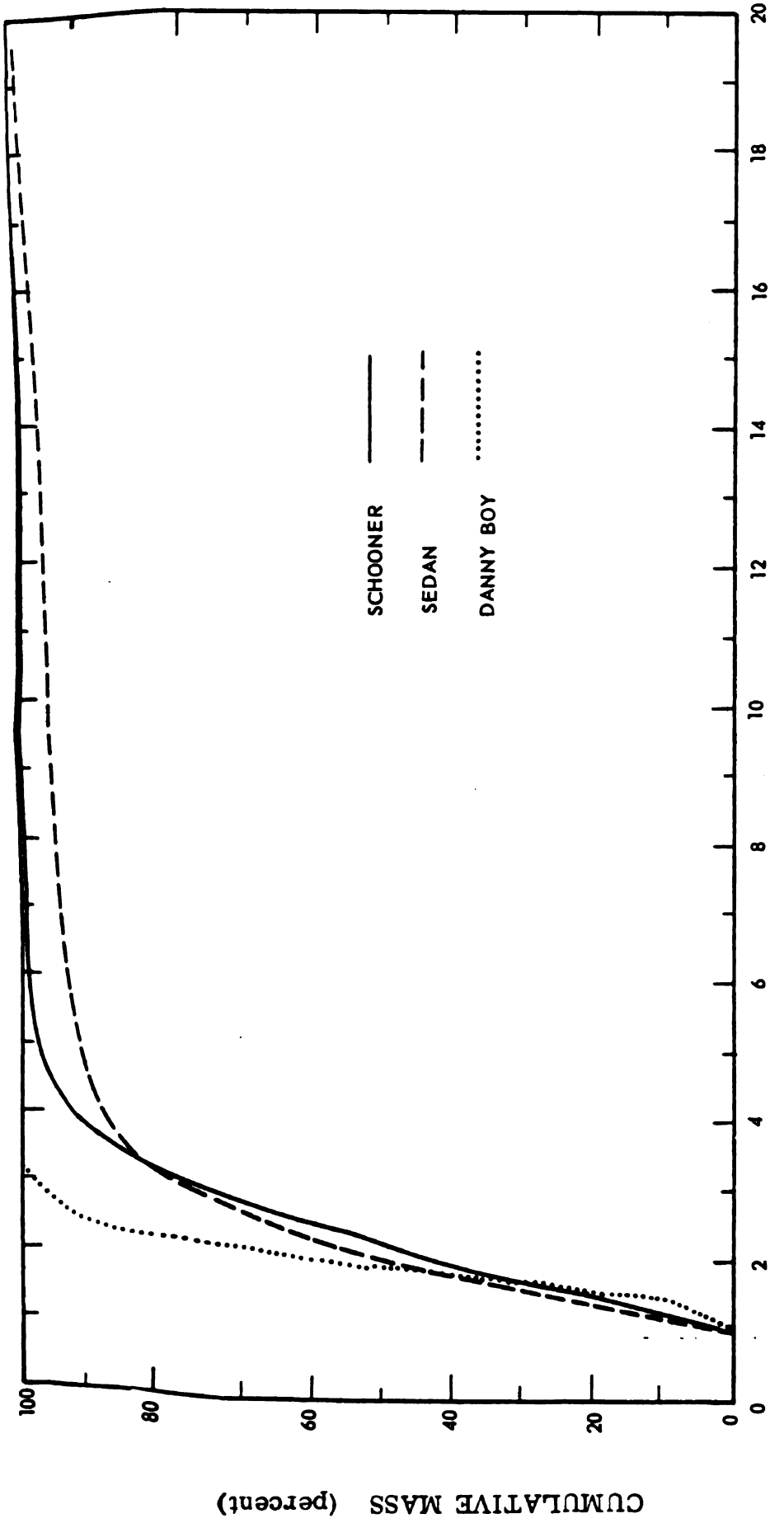

Figure 73. Incremental Distribution of Ejecta as a Function of Distance from SGZ for Schooner, Sedan, and Danny Boy

reasonably well delineated relationships to simple conjecture based on only limited observations. The more important relationships are outlined below and discussed with others in the remaining portion of this chapter.

	Geologic Parameters	Crater and Ejecta Parameters
(1)	Joint Orientations	. Formation and orientation of the Ray-Valley structure of the apparent lip.
		. Distribution of ejecta blocks in the discontinuous ejecta field.
(2)	Bulk Lithologic Characteristics	. Bimodal ejecta size--blocks and fines.
		. Preferential brecciation of blocks on impact.
		. Structure and surface morphology of the crater and ejecta field.
		. Movement of ejecta along the ground surface after initial emplacement.
		. Formation and emplacement of the mix unit.
(3)	High Water Content	. Strong gas acceleration phase excavating a thick stratigraphic section, producing the large apparent crater and distributing ejecta to great distances.
		. Movement of ejecta along the ground surface after initial emplacement.
		. Formation and emplacement of the mix unit.
		. Small permanent upthrust and compaction beyond true crater.

		. Formation of present flat crater floor.
(4)	Joint Plane Spacing and Foliation Characteristics	. Sizes and shapes of ejecta blocks.
		. Preferential brecciation of ejecta blocks on impact.
(5)	Surface Gradient	. Asymmetries in mound growth, venting patterns, the crater, and discontinuous ejecta field.

1. Weather

a. During the Event

Wind conditions during the event played a minor, but visibly conspicuous part in the final distribution of the ejecta field. Surface winds were from the south through southwest at 1 to 5 m/sec while winds above 700 m were from the southwest through the west-southwest at 7 to 18 m/sec. The effect was to push ejecta masses down-wind, north through east-northeast. It is doubtful if more than 5% of the total ejecta mass was significantly affected. This ejecta was primarily fines from the cloud, base surge, mound disassembly, streamer contrails, secondary crater clouds, and individual fragments less than a few centimeters in diameter.

The effect of the wind on the overturning flap segments with their large upward and outward momentum was nil; however, fines generated during mound disassembly were pushed down wind which probably accounts for their extended distribution in the northeast quadrant (Fig. 34). Where studied in previous events, individual ejecta masses moving down wind travel faster and impact later, farther away, and at a shallower angle. Upwind the opposite effects are

observed. While not measured, the expected net effect of the wind on ejecta blocks would have been a function of their direction and time-of-flight. Since 50% of observed impacting ejecta masses were deposited within 25 sec, the maximum change in their impact distance (directly upwind or downwind) probably did not exceed 125 m. The last missiles to impact (71 sec) may have been changed a maximum of 355 m. While a comprehensive survey was not conducted, field observations indicate that maximum quantity as well as distance of ejecta impacts was essentially upwind to the southeast and southwest (Figs. 15 and 17). Thus, major effects of the wind were obviously overwhelmed by other factors.

Wind had little initial effect on the base surge which formed from the flap segments impacting the ground. The base surge expanded outward at an average velocity of 12 to 18 m/sec until 63 sec after which it slowed to zero by 71 sec (Fig. 13). Southerly winds undoubtedly aided in this slowing down and resulted in a sharp delineation of the base surge deposits on the ground along the north. Between 71 sec and vertical stabilization at 4 min southerly winds held up the base surge probably producing the thicker base surge deposits on the south. This may explain the difference between the stereogrammetrically determined outer "0" contour and the field determined continuous ejecta boundary (Fig. 24). The base surge cauliflower pattern on the south has been diffused on the north with large distances existing between the 71 sec and final patterns, indicating that the wind pushed the base surge to the north and

northeast.

As in the case of the base surge, wind played little part during the initial formation of the cloud which was generated by the venting of the hot cavity gasses rising upward and drawing fines from the disassembled mound. During the first 4 minutes of growth, the cloud gradually moved to the northeast as reflected by the heavy deposition of shocked pumice fragments on that side of the ejecta blanket. After stabilization (4 min) the cloud was pushed downwind, northeast to east-northeast, at the prevailing wind velocity.

b. After the Event

Since the detonation, weather conditions (wind velocity typically 1 to 5 m/sec and annual precipitation of 15 cm) have modified the overall crater and ejecta field very little, with only minor changes noted between 1968 and 1973. Most noticeable has been the consolidation and winnowing of the fallout. It is estimated that up to 50% of the fallout has been removed by wind, while that remaining has been compacted by up to a factor of two.

There has been some erosion of ejecta deposits along preshot stream beds, partial infilling of some secondary craters, and minor sheet wash and gullying of fines from along the crater rim into the crater and from the fine deposits within the crater onto the crater floor. Most important has been the "cleaning" by wind and rain of all surfaces, particularly along the trench and crater lip, which has greatly enhanced their mapping and analysis during this study.

2. Surface Terrain

a. Area Gradient

The preshot ground surface sloped 1.5° smoothly downhill across the cratered region with the gradient (line perpendicular to topographic contours) curving slightly clockwise through SGZ from azimuth 295° to 135°. While such a shallow slope would seem to be insignificant, a sufficient number of transient processes and final crater and ejecta field features are aligned either with or against this gradient that cause and affect relationships are suggested.

Mound growth and early venting patterns were elongated perpendicularly to the gradient (Fig. 12). The plasma blanket and the lobe to the southwest that developed into a large jet were aligned as above while a second lobe was directed downhill. The only observed radial vent, through which a large mass of plasma exited for a relatively long period of time, was directed downhill. Distribution of impacting ejecta masses was noticeably different downhill with approximately 4 times as many impacts as uphill (Fig. 15). Downhill impacts went farther (1500 vs 1200 m) and began and finished almost 10 sec earlier. Also, the average ground speed of the outward progressing curtain of impacts was almost twice as fast downhill (88 vs 43 m/sec).

The apparent (and true) crater is elongated downhill (~12%) and shortened uphill (~12%) while the crater sides are significantly steeper on the uphill side. Note that these crater features are not 180° apart, but aligned with the curving gradient. There is in

addition more fallback (and possibly late-time slump) on the downhill side which accounts in part for the shallow crater slope.

Figure 74 quantifies the relationship between the apparent crater and the preshot topography. Plotted, for each 10 degrees of azimuth (ϕ), is the difference between the actual and average apparent crater radius ($\bar{R}_a - R_a$) versus an expression for the topography [$-1.5 \cos(\phi+\Delta)$]. This expression simplifies the preshot topography to a plane, tilted in the direction of the gradient (Δ). The highest correlation coefficient ($r = 0.94$) occurs with Δ set at 160°. Since the actual gradient is curved rather than the constrained straight line in the above formulation, the actual correlation should be somewhat better than that shown in Figure 74.

The volume of ejecta in Ray 3, which is directed downhill, is the smallest of all the rays, 50% below the mean. In addition, there are few ejecta deposits from below 39 m along the southeast quadrant, but there is a large deposit of these units in the crater below.

Vesic, et al. (1967), using gram-size charges in river sand, studied the effect of surface terrain on cratering. They observed that upward cavity growth follows the path of least resistance or overburden weight. Thus, in a sloping terrain where the immediate SGZ area is leveled and a vertical emplacement hole is drilled, the true crater could be shifted downhill by as much as the tangent of the gradient multiplied by the DOB. For Schooner this would amount to a 3 m increase in crater radius downhill and corresponding decrease uphill. Admittedly, this 2% change is a small value, but

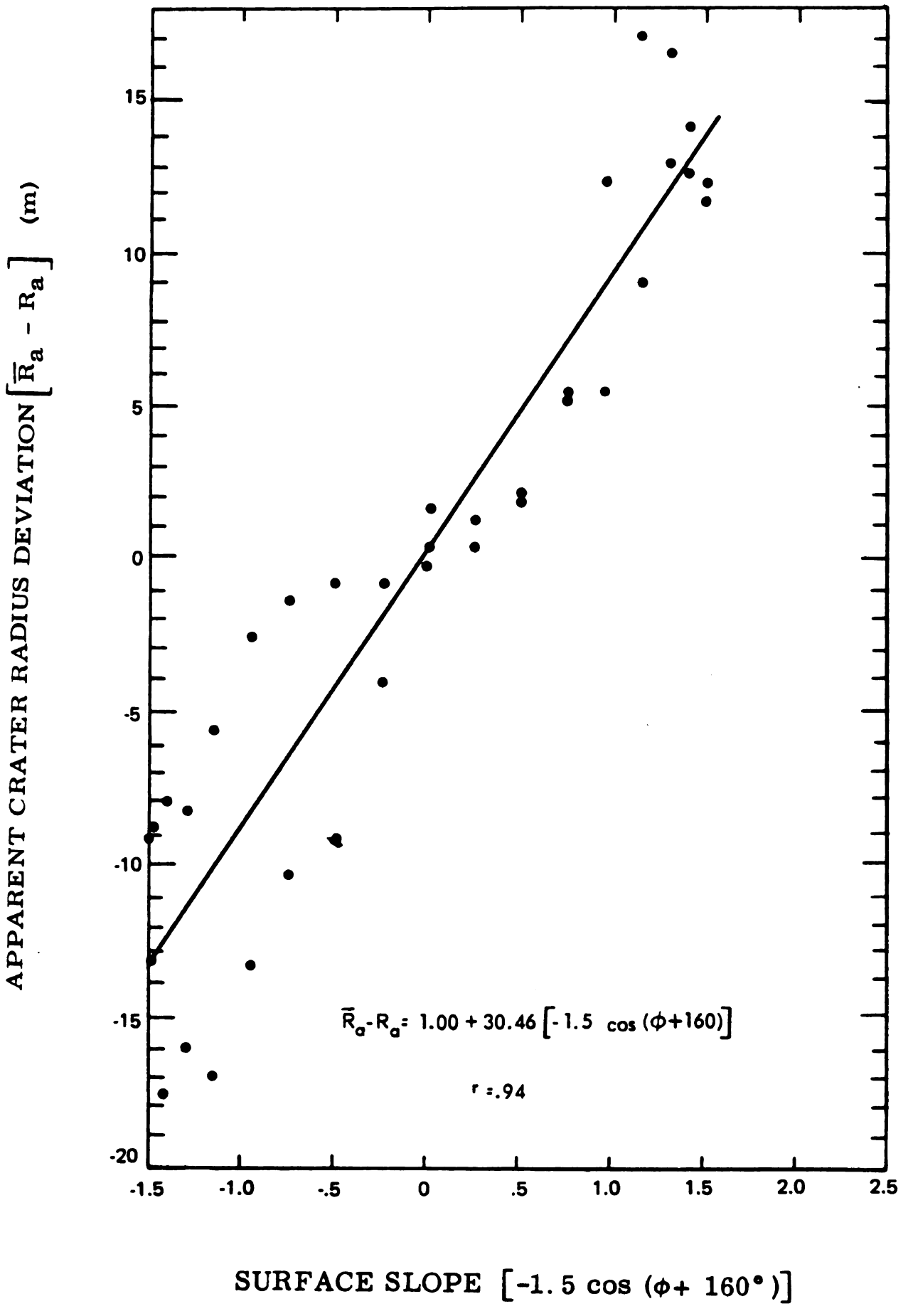

Figure 74. Correlation between Apparent Crater Radius and Preshot Topographic Gradient

nonetheless in the right direction.

Possibly more important, the unequal cavity growth might be expected to produce an earlier and perhaps more sustained vent on the downhill side which could explain many of the above observations. The large radial vent is aligned and might be responsible for the gap in the crater rim, large slump failure, and shallow profile of the crater between 115° and 135°. A similar feature on the Sedan crater was associated with such an early vent (Strohm, et al., 1964). Continuing this argument, if the vent were large enough, it may have broken up and dispersed the mound section of Ray-3 resulting in poor ray development. This could account for the larger than usual amount of fine fallback and the more widely distributed block field.

Vesic, et al. (1967) also observed that while ejected material had approximately the same velocities, exit angles were steeper on the uphill side. This could explain the relatively fewer observed ejecta impacts on the uphill side since they would impact closer to the crater and thus be more easily and sooner obscured by the base surge and mound disassembly. Additional evidence supporting this is that 2 to 3 times as many secondary craters were observed on the uphill side than elsewhere in the continuous ejecta field.

It seems plausible then that the above observations are related, in the main, to some preferential channeling of energy toward the downhill side of SGZ through a combination of processes involved in asymmetric cavity growth, mounding, and finally venting. Since, according to Sargent and Jenkins (1968) the present surface gradient

likely follows the original depositional surface, perhaps some buried structural element paralleling and related to the surface gradient is responsible. Such a feature might be a linear or planar set of open flow fractures such as suggested by the caliper and density logs of the four holes drilled in the cratered region (Fig. 8). Possibly such fractures might contain a higher degree of saturation.

b. Local Topography

The surface topography also affects the local distribution of ejecta. Two stream cuts, 400 m to the east and southeast of SGZ, selectively concentrated blocks over fines and large blocks over small blocks, apparently due to preferential downward tumbling.

Along the southeastern quadrant ejecta contours, including the R_b and R_{eb} contours closely follow portions of the preshot topographic contours (Figs. 24 and B1). Most significant, on the downhill side of the crater (southeast quadrant) the surface is strewn for over 200 m with ejecta blocks beyond the R_{eb} that have obviously tumbled from uphill towards the crater. This is in contrast to the uphill side of the crater where few blocks tumbled much beyond the R_b.

c. Soil Cover

The depth of soil varies widely about the crater from close to zero on the west and northwest to 1 to 2 m along the southwest and southeast quadrants. This lack of soil on the west and northwest may, in part, explain the sparsity of observed impacts from overhead. That is the less the soil depth the smaller the secondary crater and

thus the smaller the resultant ejecta cloud.

3. Lithologic Characteristics

a. Bulk Properties

In Chapter II the geologic column of Schooner was subdivided into four physical property units: upper densely welded tuff (0 to 38.7 m), weakly welded tuff (38.7 to 61.9 m), nonwelded tuff (61.9 to 103.3 m), and a lower densely welded tuff (103.3 to 148.1 m) (Fig. 6 and Table A2). Each of these units possesses a distinct set of properties which in bulk were very important in the formation of the crater and ejecta field.

The densely welded tuffs are hard rocks; they are strong, dense, brittle, low in porosity and permeability, and contain little water. Thus they retain a well developed and relatively open joint system while being susceptible to blast- and impact-induced fracturing. In contrast the weakly welded and nonwelded tuffs range from soft rock to unconsolidated; they are weak, low in density, very porous, and permeable. They are thus compressible and susceptible to stretching, thinning, and flow. In addition several horizons contain significant amounts of water which further decreases their strength while decreasing their permanent compactability as well.

The net effect of these bulk properties is displayed by the structure and morphology of the crater and ejecta field which reflects the cratering processes involved.

Within the crater the dominant feature is the upthrusted and blast-fractured true crater wall of welded tuff which, because of its

inherent strength, maintains a slope averaging 65° (Fig. 71). With the vertical joint planes of the in situ welded tuff units, the wall should be more nearly vertical as observed along the mesa cliffs that surround the Schooner site. The difference lies in the amount of net upthrust at the wall surface, with the steeper, uphill portions of the wall perhaps reflecting less net upthrusting; i.e. less initial upthrusting or more late-time relaxation.

The weakly welded and nonwelded tuff deposits along the lower one-half of the crater are primarily fallback (and probably some flowback). Overall, these deposits exhibit a definite bulging outward (toward the ZP axis) indicating movement during and/or immediately after emplacement, probably as a result of their initially high water content (deposits are now dry). This initial water content would also explain their present light cementation, which is sufficient to maintain locally vertical slopes.

The crater floor was emplaced prior to first visual inspection, 5 hours after the detonation, and more likely within minutes after detonation; but after fallback was emplaced. Its near perfect flatness suggests that portions of one or more of the high water content horizons within the nonwelded tuff became liquified during release of cavity pressure and flowed into the bottom of the crater. Note that the present floor is nearly at the preshot level of the top of the "w" unit and several meters below its expected upthrusted position.

It is suggested that at least the floor and perhaps portions of the nonwelded deposits were derived by such a flowback mechanism. As an added conjecture the steeper wall on the west might reflect more flowback of material than on the east. The floor is shifted in that direction. An alternate, and perhaps preferred, explanation for most of the weakly welded and nonwelded deposits in the fallback (not including the floor) is that they resulted from collapse of portions of the cavity roof upon venting and that these masses fell/slid down the crater cavity to their present observed positions. Supporting this contention is the observation that in general, weakly welded and nonwelded units are located in the crater beneath crests deficient in these units. The bulging outward of these deposits may still be due to some flowback "pressure" from beyond the crater cavity.

The fallback also contains blocks and mixtures of blocks and fines derived in part from mound collapse, but primarily from late-time and post-crater failure along the crater rim (the overturned hinge). These deposits are typical of natural talus slopes.

The overturned flap above the wall maintains a slope depending upon the properties of the ejecta units. The welded tuff units become increasingly dislocated and bulked (decrease in bulk density due to breakage and rearrangement) with distance above the upthrusted preshot ground surface. Correspondingly, their slopes become increasingly shallower with distance upwards. The fine deposits exhibit shallow slopes and are slowly eroding into the crater.

In the ejecta field the most obvious consequence of the bulk physical properties of the media is in the bimodal size distribution of the ejecta. The welded tuff units produced boulder-size blocks and the weakly welded and nonwelded tuff units produced sand-size tuff fragments. Block sizes, together with total volumes, are important in the size and structure of the flap segments and in their post-depositional movement.

Weakly welded and nonwelded tuff blocks are not observed; but some small masses of one or more of these units are present on rays partially buried by the top mix unit. These masses apparently had sufficient strength due to their water content and/or shock compaction to maintain their integrity during ejection, transport, and impact.

During mounding, units were obviously subjected to tensional stresses, with the welded tuff units separating along joint and foliation planes. Upon impact units were further bulked. Crest flap segments, observed in the trench and along the crater lip, appear to have been gently "set down" since they retain to a large degree their in situ structure with only a minimum of bulking. With distance outward and upward distortion and bulking increases. Bulked flap segments of welded tuff form the major topographic relief of the ejecta blanket. Movement of these masses after impact consisted primarily of en masse, outward spreading which increased with distance from SGZ due to increasing impact velocity. Frictional forces between the ground surface and the flap segments retarded the

movement, as evidenced by the generally sharp drop off at the continuous block boundary, the deflated areas near ray termini, and the "stair-step" structures just behind leading edges of rays. Along segment boundaries individual blocks tumbled downhill.

The weakly welded and nonwelded tuff units contained within the overturning flaps were stretched as evidenced by their thickened, thinned, and often interrupted exposures in vertical cuts along the crater lip and trench. Where present in a flap segment they are observed to locally fill in underlying topographic irregularities indicating some local movement. With distance outward nonwelded units exhibit increased movement after emplacement evidenced by increased mixing with distance.

The mix unit overlying both welded and nonwelded deposits exhibits strong flow characteristics. Viewed from the surface this unit smoothed out all topographic irregularities within ray interiors by filling in lows and flowing around highs. In cross section this unit is observed to have eroded previous deposits picking up 1/3 m blocks and transporting them outward for up to 30 m. The special flowing capability of this mix unit may be due to movement on a trapped cushion of air similar to that proposed for some major landslides (Shreve, 1968). More likely it is due to a combination of a strong horizontal velocity component from the strong gas acceleration and the fineness of the material involved, possibly further mixed with air.

b. Specific Properties

Terhune and Stubbs (1970) list in order of importance water content, shear strength, porosity (compactability), and compressibility as the key material properties in cratering. Compressibility and porosity are the dominant factors in determining peak pressures while shear stress and its duration primarily determine the shock or spall velocity. Water content is most important since it decreases porosity, compressibility, and shear strength of the media while its vaporization increases spall velocity by up to 10% and most significantly provides "fuel" for a stronger and longer lasting gas acceleration phase.

The initial shock and more importantly the rarefraction wave breaks up the media; i.e. forms the true crater. Spalling and more importantly the gas acceleration ejects the material; i.e. forms the apparent crater and lip. The Schooner site was selected for its high water content in several horizons which, as observed in the event photographs (Fig. 10), produced a substantial gas acceleration phase. Comparison of mound rise data from a number of events indicates that without the large gas acceleration phase the Schooner crater would have been significantly smaller. Layering considerations, discussed in the next subsection, would tend to further reduce crater size. According to Terhune (1976) without this strong gas acceleration phase the Schooner crater would have been significantly smaller due to infill by ejecta deposited proportionally closer towards SGZ.

In the preshot code calculation of Schooner discussed above, water in the nonwelded horizons above the shot point was allowed to vaporize only within the zone of tuff vaporization (∿8 m from the ZP). This resulted in a calculated peak mound velocity 30% lower than measured and consequently the calculated crater was considerably smaller than the actual crater. Butkovich (1971) modified the model allowing free water to vaporize out to its own partial pressure limit (∿25 m from the ZP) and demonstrated that such a model would predict a peak mound velocity within 5% of that measured. Presumably the apparent crater dimensions would also have been proportionately larger and closer to actual values, but that calculation was not carried out.

The higher water content of Schooner and the resulting strong gas acceleration phase probably account for its significantly larger crater (Fig. 72) and ejecta mass (Table 4) than would be predicted considering the geologic setting without the saturated horizons. The much smaller net compaction at Schooner versus Sedan can be explained by the higher water content at Schooner, especially the concept of liquification of saturated fine units. The substantial difference in the stratigraphic section ejected at Schooner (77 m) vs Sedan (10 m) is further evidence of the effect of Schooner's high water content. Finally, the strong gas acceleration phase at Schooner probably accounts for the distribution of ejecta significantly farther out from the crater relative to the dry rock crater Danny Boy (Fig. 73) and as mentioned above probably contributes to

the mixing and movement of fines after initial emplacement.

4. Layering

The effect of the strong-weak-strong layering sequence on the cratering processes and resultant crater and ejecta field, other than the lithologic properties, is complex. The layering sequence is expected to have modified the distribution of energy during the shock and spall phases resulting in the ejection of material relatively closer to the crater thus producing a smaller apparent crater. Whatever the actual effect, it was obviously overwhelmed by other geologic parameters, primarily the high water content previously discussed.

Terhune (1976), who calculated the Schooner event, noted that particle paths were nearly all vertical which he attributed to the layered geometry since these results were not observed in his previous calculations of the non-layered events, Sedan and Danny Boy. Terhune concludes that without the large gas acceleration phase of Schooner to turn these paths outward, the ejecta would have been deposited significantly closer to the crater and the apparent crater would have consequently been significantly smaller. Observations of the event (Fig. 10) clearly indicate that during early times, material was ejected nearly vertical, but later a strong horizontal component developed.

There is speculation that the two hard layers may have effectively squeezed the middle weak layer. Such a "tooth-paste-tube" effect might have pushed portions of the weak layer back into

the formation, some of which would then be available for flowback into the crater region after venting and reduction of the cavity pressure. Both the outward bulged, fine outcrops in the crater and particularly the flat crater floor could be explained in part by such a flowback mechanism which conceivably would be enhanced by this "tooth-paste-tube" effect.

Vesic, et al. (1972) have observed a similar effect in small laboratory explosive experiments. When a charge was detonated in a weak layer underlying a strong layer (roughly the configuration of Schooner) the cavity formed in the weak layer was larger than for either of the individual layers alone. They attributed this to the top layer reflecting energy back into the weaker layer.

5. Joint Trends

Major joint trends in the upper densely welded tuff units had a dominant effect on the distribution of ejecta. The Ray-Valley structure of the apparent lip, the ejecta impacts observed from overhead event photography, and the distribution of welded ejecta blocks in the discontinuous ejecta field all correlate with the joint system at the Schooner site.

a. Ray-Valley -- Structure of the Apparent Lip

Sixty-four percent of the axes connecting SGZ with troughs (1, 3, 4, 6, 7, 9, and 11) are aligned with joint trends that exceed the average trend (Fig. 75). Trough axes 2 and 8 are aligned with joint trends that while slightly less than the average are more prominent than neighboring trends. The two major rays (1 and 7), in

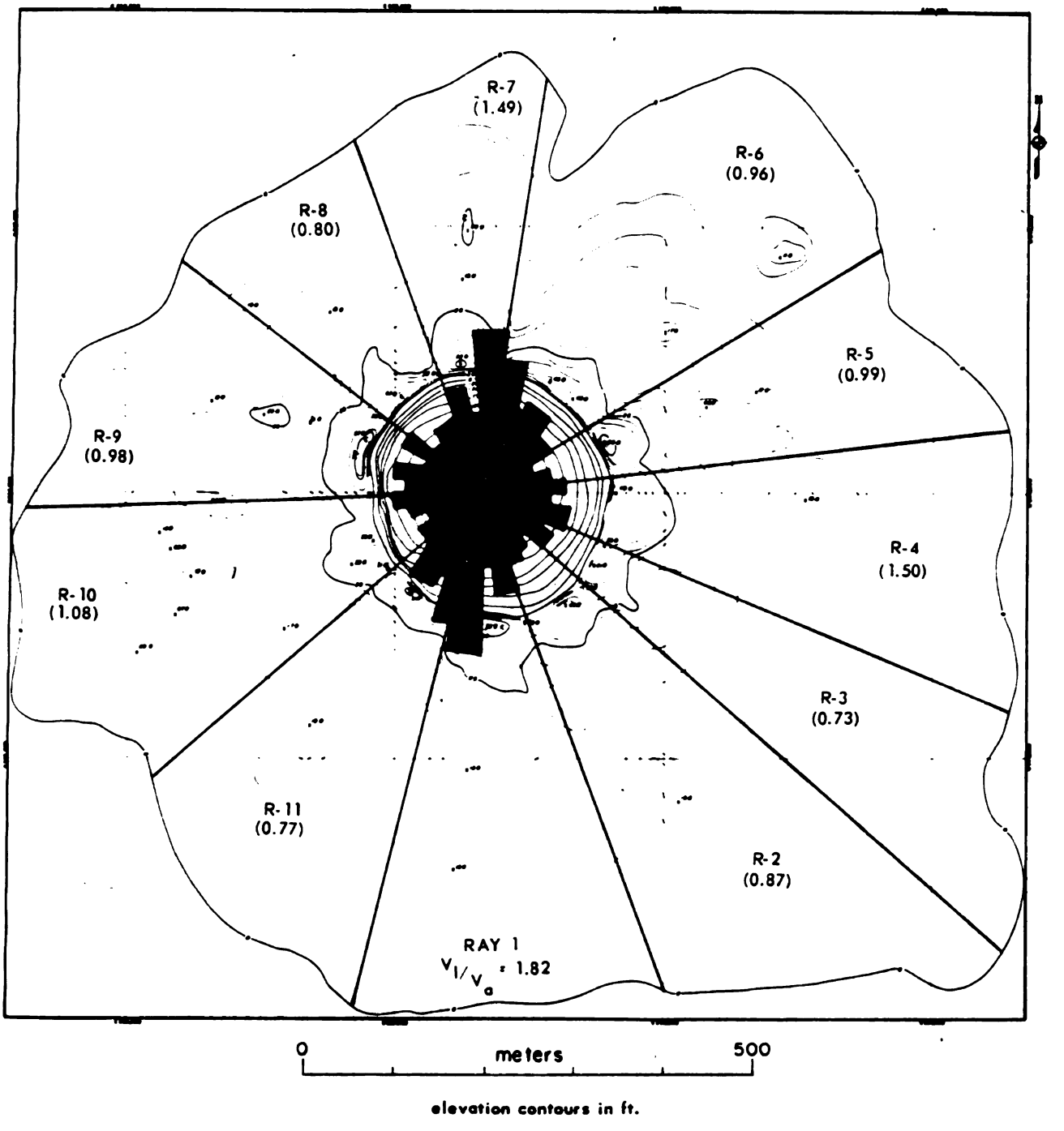

Figure 75. Correlation between Joint Trends and the Ray-Valley Structure of the Continuous Ejecta Field

terms of total accumulated ejecta (Fig. 28), thickness of the inverted stratigraphic section (Figs. 37, 49, and 51), and linear alignment of flap segments (Fig. 34) are bound by the major north-south joint trends common to all upper densely welded tuff units. The intermediate rays (4 and 9), judged in the same manner are bound by intermediate joint trends. Finally the minor rays, in terms of one or more of the above criteria, are aligned with minor joint trends.

Previous experience has shown for buried events in unconsolidated soil that a number of poorly to moderately developed, but randomly orientated rays are typically formed. For example, the Sedan event produced 4 moderately developed and 2 poorly developed rays, none of which extended beyond 2.5 R_a and all were randomly orientated (Strohm, et al., 1964). In a series of high-explosive experiments in playa at varying depths-of-burst 4 to 10 well-developed rays were formed extending outward to between 3 and 5 R_a (Carlson and Jones, 1964). The best developed set occurred at a scaled depth-of-burst only slightly shallower than Schooner. There was no azimuthal consistency between events nor symmetry with respect to SGZ.

Rays also have been observed from buried events in rock (Johnson, 1962) differing from events in soil in that often one or more of the better developed rays can usually be associated with joint trends. Where the joint system is not well developed rays are poorly developed and randomly orientated similar to the case of unconsolidated soils. For example, both Cabriolet (Fransden, 1970) and Danny Boy (Nugent and Banks, 1966) with poorly developed joint systems,

exhibit no rays.

It is postulated for Schooner, that as the mound expanded and hoop stresses increased, the vertical joint planes served as planes of weakness along which the mound preferentially ruptured. These breaks were possibly in addition to the two early vents to the southwest and southeast which may have been due to other causes; i.e. a buried geologic structure paralleling the surface gradient.

It is suggested that the joint system of Schooner was superimposed on a random mound rupture pattern that would have occurred if the media were not jointed. Therefore, the mound would break up into a number of radially orientated sections (like opening petals on a flower) such that the first breaks would form the largest and best developed rays and the last breaks, the smallest and least developed rays. Thus, it seems reasonable that the major north-south joint trend common to the "R", "U", and "L" units would open first and provide the best developed rays (1 and 7) in terms of the previously mentioned criteria. Areas where no dominant joint trends existed would break up last and provide the least developed rays. Perhaps many of the observed variations in the crater and ejecta field, particularly the relative skewing of the various segments and units within segments, are reflections of slight differences in the joint system with depth.

b. Ejecta Impacts

Maximum accumulations of ejecta impacts are aligned with trough axes and minimum accumulations are aligned with crest axes. Figure 76

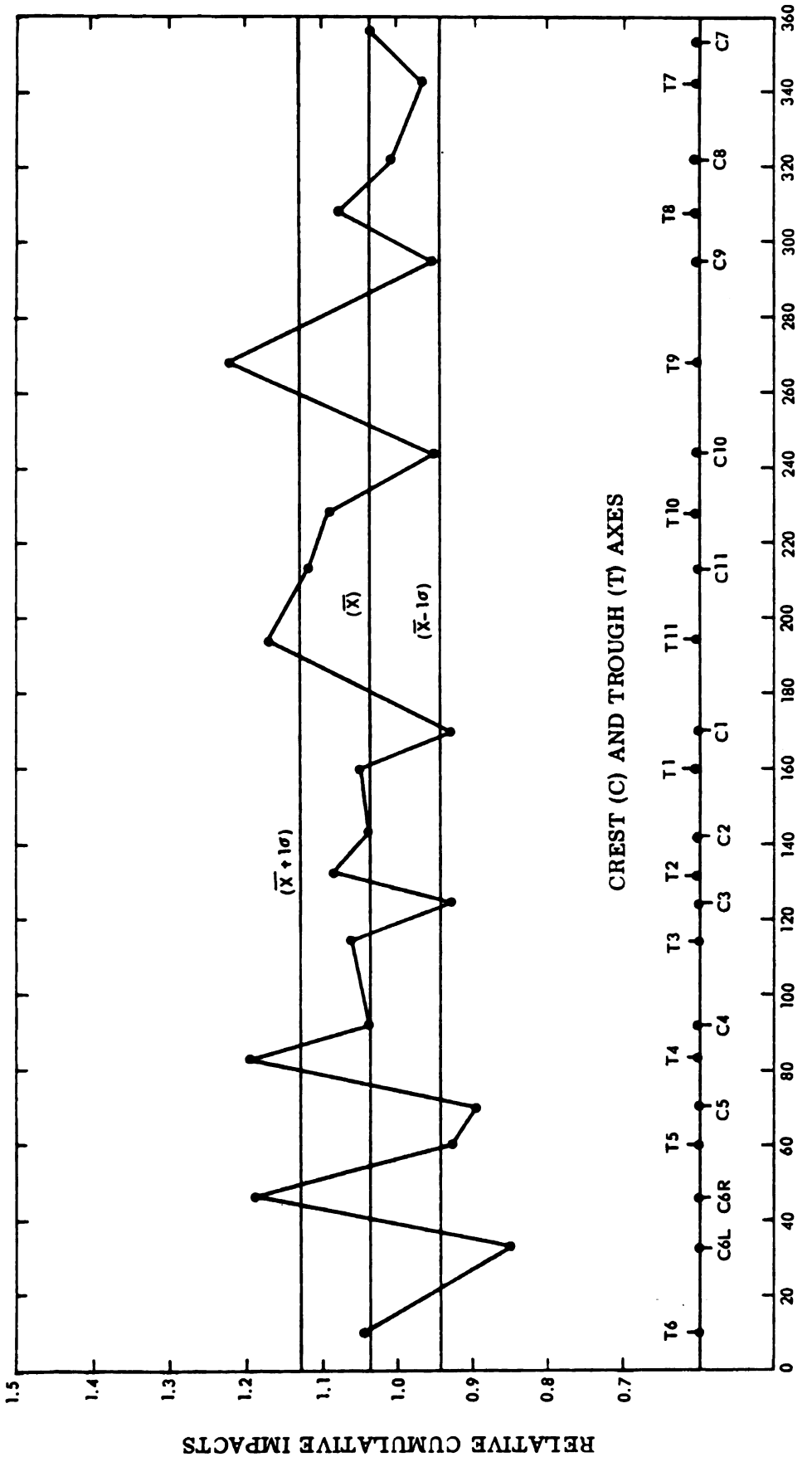

Figure 76. Correlation between Ejecta Impacts and Crest and Trough Axes

quantifies the relationship between the Ray-Valley structure of the ejecta field (Fig. 24) and the ejecta impacts observed from overhead during the event (Fig. 15). Plotted is a count of residual impacts averaged over a constant 6^{o} azimuthal band centered on each crest and trough axis. Residual values were obtained for each of the original 10^{o} sectors of Figure 15 by dividing by the averaged count of the two neighboring 10^{o} sectors. This in effect eliminates trends due to topography, early venting, etc. The mean number of impacts for all crest and trough axes ($\bar{X}$) is drawn together with the $\pm$ one standard deviations boundaries. As shown, 82% of the trough axes contain more impacts than the mean ($\bar{X}$) and 36% contain more than $\bar{X}+1\sigma$. Also, 66% of the crest axes contain fewer impacts than the mean ($\bar{X}$) and 33% contain fewer than $\bar{X}-1\sigma$.

It is suggested that as the mound ruptured along joint trends, welded blocks were preferentially channeled through the openings. With a vent opening beginning at the top of the mound (as observed in Figs. 10 and 11) and propogating downward towards the ground surface, exit angles would initially have been high and subsequently decrease with time. Furthermore, early-time ejecta would have exited at high velocities under high cavity pressures and rapid streaming of plasma through constricted vent openings. As cavity pressure rapidly decreased and vent openings opened exit velocities would decrease. Such processes would account for the time history of impacts observed (Fig. 18); i.e. steadily outward progression of impacts followed by

an oscillation of impacts.

c. Blocks in the Discontinuous Ejecta Field

Comparison of the distribution of blocks in the discontinuous ejecta field along R-1 and V-11 radials indicates that beyond the R_{eb} there are significantly more blocks (by volume) without fused glass along the valley radial (Fig. 68). Such a pattern also suggests that the vent openings provided effective channels through which individual blocks were preferentially ejected. The fact that these blocks retained their inverted stratigraphic order out to the maximum ejecta range (Fig. 64) indicates that the processes involved were orderly. Why there are as many blocks with fused glass along the R-1 radial as along the V-11 radial is not known. Perhaps blocks with fused glass exited at early times from the top of the mound and thus were not controlled by vent openings, but rather randomly distributed. Their lack of an inverted stratigraphic order also suggests such a process.

6. Joint Spacing and Foliation Characteristics

The final size and shape of discrete masses that make up the ejecta field is a function of their in situ characteristics modified by the cratering processes including shock, spall, mounding, ejection, deposition (impact), post-depositioned movement, and post-depositional impact. The in situ size and shape of welded blocks is primarily a function of unit thickness, the vertical joint spacing and orientation, and the development and intensity of flow foliation. Weakly welded and nonwelded blocks are not observed in the ejecta field. Blocks

from all of the upper densely welded tuff units are observed, each exhibiting their own set of characteristic sizes and shapes based on in situ sizes and shapes modified by their inherent strength, particularly susceptibility to brecciation upon impact.

The "R" blocks are limited by unit thickness (1 to 2 m) which is controlled primarily by intensity of weathering. While weathering is gradational downward, there are local zones of weakness along horizontal foliation planes that result in horizontal separations. Most separations are not pronounced; but provide a preferential plane of weakness, particularly on impact. Some are opened sufficiently to have been thinly veneered with secondary deposits. The vertical joint pattern is rectangular (90^{o}) with spacing typically 2 to 3 m. Thus, "R" blocks are rectangular, 1 to 2 m thick by 1 to 3 m long (lengths are parallel to the unit's upper surface). The upper surface is typically irregular and desert varnished; many vertical surfaces are slightly curved and heavily coated with caliche.

Blocks from the "U" unit are similarly jointed, but are not thickness limited (the "U" unit is 8 m thick); thus, they tend to be larger and more nearly equidimensional (1 to 3 m on a side) while still trending toward rectangular shapes. The long dimension is parallel to the unit's upper surface because of horizontal flow separations; vertical surfaces are predominantly joint planes veneered with secondary deposits.

Blocks from the "M" unit, like the "R" unit, are thickness limited (2/3 to 1 1/3 m). The "M" unit is fine grained and

homogeneous without foliation planes. Contacts between "U" and "L" units are sharp; but due to its lower degree of welding, separations usually occur a few centimeters into the "M" unit. Jointing is rare and vertical block faces are smooth, but uneven. Thus, typical block shapes range from equidimensional to rectangular with long dimensions 1 to 3 1/2 m and parallel to the unit's upper surface.

The "L" unit exhibits a moderate to well-developed hexagonal structure with columns 3 to 10 m across and up to 20 m in length. With its well foliated nature, the effective in situ block thickness is on the order of 2 to 3 m and blocks are thus rectangular in cross section and hexagonal to subhexagonal in plan view.

Blocks from the "P" unit are similar to "L" unit blocks except they are intensely foliated with incipient partings spaced every few centimeters or less. In addition, "P" blocks are more brittle. Close to the crater they are only slightly smaller than "L" blocks; but with distance they become smaller than "Y" blocks due to their high susceptibility to brecciation.

Blocks from the "B" unit are subhexagonal, but lack the foliation of the "L" and "P" units. They are thus rectangular to equidimensional with long dimensions typically perpendicular to the unit's upper surface. Sizes range from 1 to 2 2/3 m across and 1 1/2 to 3 m thick. Blocks from the "O" unit are similar to "B" blocks; they are thickness limited, 1 to 2 m across to 1 to 1 1/2 m thick. Both "B" and "O" blocks are vitrophyres and quite brittle. "Y" blocks are thickness limited and, unlike the "B" and "O" blocks,

exhibit neither hexagonal jointing nor foliation planes. Blocks are almost always equidimensional, 1/3 to 1 m on a side. Upper and lower surfaces are typically flat; vertical surfaces are fresh and without secondary deposits.

As observed in the ejecta field the large majority of welded blocks retain to a substantial degree their in situ characteristics. Apparently little breakage of welded tuff blocks occurred during the mounding or ejection processes. Peak stresses during the shock phase are estimated to have been between 10 to 100 MPa within the upper densely welded tuff unit, sufficiently low for stress release to have occurred along joint and foliation planes. During spall and mound growth, tensile stresses would result in blocks further spreading along joint and foliation planes.

There was some breakage of blocks along the crater wall which tended to parallel existing vertical joint planes and horizontal foliation planes (Fig. 42). There was also some breakage along the hinge line of the overturned flap as observed on the talus slopes beneath. In the ejecta unit lying immediately above the in situ unit the lowermost portions are gently overturned and their in situ structure is essentially intact. With distance upwards, breakage of blocks does not necessarily increase; but amount of displacement and dislocation of blocks (bulking) does. Thus, except for along the crater wall and in the hinge zone, breakage of welded blocks appears to be primarily the result of depositional processes.

Breakage of blocks in the ejecta field is observed in and surrounding secondary craters, in lenses within flap segments, and most significantly within the large rubble tracts comprising the termini of most rays. Flap segments are apparently emplaced at low velocities since all such deposits even terminal ones, contain large surrounding areas of unbroken blocks (Fig. 34). The conditions necessary to cause brecciation observed in the rubble zones, are not well known; but appear to be a function of impact mass, impact velocity, impacted surface, and ability of the impacting mass to withstand brecciation. That is, for a given impact surface the smaller the mass the larger the impact velocity required for brecciation. This would explain the observed increase in brecciation in flap segments with distance, while also explaining why individual blocks that fringe the flap segments are not brecciated. Thus, the observed retarcs (local mounds of broken and brecciated material) represent an impacting mass-velocity condition intermediate to secondary craters and small flap segments.

CHAPTER IX

TIME HISTORY OF CRATER AND EJECTA PROCESSES

A. General Sequence

Terhune and Stubbs (1970) identify four sequential phases involved in the formation of a crater from a buried nuclear detonation.

Shock. Shock wave is generated by the deposition of energy into the ground and travels outward.

Spall. Shock wave reaches the ground surface, a rarefaction wave is reflected back towards the source region developing tensile stresses which separate material by spalling it upward to form a mound.

Gas Acceleration. Pressures in the media above the cavity are relieved and mound expands upward at a faster rate, driven by gas generated from the earlier vaporized media surrounding the device.

Ballistic Trajectory. Venting reduces cavity pressure, mound disassembles and ejected material begins free fall affected only by gravitational and frictional forces.

This chapter provides a detailed sequential history of processes involved in the Schooner event based primarily on the data presented and relationships developed in the preceding text. While individual sequences are in general order, there is considerable overlap. Where possible, real times are provided. Emphasis is placed on the

ejection, deposition, and movement of ejecta after deposition which essentially continues Terhune and Stubb's (1970) "ballistic trajectory" phase. Since obviously neither all nor generally even substantial portions of the various processes are observed in their entirety considerable reliance is placed on inferences drawn from the final observed dimensions, morphology, stratigraphy, and structure of the crater and ejecta field.

B. Detailed Sequence

1. Mounding Phase (0 to 1.75 sec)

The mounding phase essentially incorporates Terhune and Stubb's (1970) shock, spall, and gas acceleration phases.

(a) Energy from the Schooner device, a 31 KT source equivalent to 1.3×10^{21} ergs, was deposited in the media surrounding the shot point within a few microseconds.

(b) A very high pressure (100-200 GPa) shock wave was generated which propagated spherically outward at superseismic velocity.

(c) Device and surrounding media were vaporized, forming a spherical cavity which according to formulas of Butkovich and Lewis (1973) had a radius of $\sim$8 m.

(d) Velocity attenuated quickly to the wave speed of the media as peak pressures decreased outward due to geometric dispersion and to the work done on the material through which it passed.

(e) Beyond the vaporized region, materials were successively melted, compressed, crushed, displaced, and finally plastically and then elastically deformed.

(f) Extent of each zone was dependent upon specific material properties. According to Butkovich (1971) water was partially vaporized out to 5 GPa (~25 m from the ZP).

(g) Ground surface began to rise at 0.08 sec when the outward traveling compression wave intersected the surface (a free surface) generating a rarefaction or tensile wave which traveled back towards the cavity. Media above the cavity was spalled upward layer by layer with a velocity representative of the energy trapped. Cavity at this time was nearly spherical (it had not "felt" the returning tensile wave) with a calculated radius of 16 m (Terhune, in Lessler, 1968). Shear zones formed close to the final true crater boundary.

(h) Cavity growth below the ZP was retarded, but not stopped by the returning rarefaction wave. According to Closmann's formula (1969) final radius for the lower hemisphere of the cavity reached 47 m.

(i) Mound grew upward with spall velocity increasing to 50 m/sec by 0.2 sec; velocity then remained relatively constant until 0.6 sec.

(j) Mound growth was asymmetrical, elongated to the northeast-southwest and shortened to the southeast-northwest with maximum radius reaching twice the minimum radius.

(k) Upper cavity continued to grow driven by the high pressures of the vaporized materials (primarily water). By 0.6 sec the gas acceleration phase become dominant increasing the mound velocity to 58 m/sec immediately prior to venting.

(l) Highest measured peak vertical mound velocity, 24 m to the southwest of SGZ, was 65 m/sec or 12% higher than that above SGZ.

(m) During mound growth, hoop stresses developed by the expanding mound failed material in tension with welded blocks continuing to separate along joint and foliation planes.

(n) Nonwelded units continued to be stretched and thinned.

(o) According to empirical formulas of Butkovich and Lewis (1973) peak stresses in the upper densely welded tuff units ranged from 10 to 100 MPa, low enough for joint and foliation planes to provide adequate stress release paths. The net result was little crushing of blocks except near the true crater boundary. There breakage was limited primarily to separations parallel to existing planes of weakness; i.e. joint and foliation planes.

(p) Due to the strong-weak-strong layered structure of the site, portions of the weak nonwelded tuff layer were "squeezed" between the upper and lower hard layers with some of the weak layer pushed back into the formation.

(q) As the mound grew, large circumferential cracks formed in the soil overburden due to gravitational sliding.

(r) Immediately prior to venting the upper densely welded tuff still retained its in situ section intact; but due to spalling and the geometrical expansion of the mound was separated into individual blocks bound by vertical joint planes and horizontal foliation planes. The weakly welded and nonwelded tuffs, on the other hand, were significantly thinned due to compaction and flow.

(s) First venting occurred directly above SGZ at 1.75 sec when the surface of the mound was 88 m high.

2. Ejection Phase (1.75 to ∿71 sec)

The ejection phase extended from first ejection of material to last impact of material.

(a) First venting was followed at 1.88 sec by three new vent centers equally spaced along a southwest to west arc approximately 60 m from SGZ.

(b) First vent expanded parallel to the elongation of the mound (northeast-southwest) and by 2.0 sec had coalessed with the other three vent centers.

(c) Plasma, consisting of gases and melted tuff, began streaming out mound vents with highest temperature measured at 2590°C. By 2.1 sec a broad triangular-shaped blanket of plasma covered the mound area. This blanket, centered some 60 m to the southwest of SGZ, had its three vertices (lobes) directed to the southeast (135°), southwest (225°), and north (355°).

(d) Hot gases together with entrapped fines from mound disassembly were convected upward forming the cloud.

(e) The plasma blanket continued expanding until 5.4 sec with the lobe on the southwest (225°) developing into a luminous jet approximately 60 m above the ground surface and extending horizontally out to 600 m by 7.9 sec. Several other jets also formed, but none extended outward as far, nor persisted as long.

(f) Plasma blanket cooled rapidly, changing color from an original yellow-white to an orange-red by 5.4 sec and to a dark red by 8.5 sec. By this time the entire region had become obscured by debris from the disassembled mound which had reached a height of approximately 500 m.

(g) Beginning shortly after first vent, radial cracks developed in the mound first along major joint trends, second along minor joint trends, and third in remaining areas without joint trends. Cracks propagated rapidly outward and downward from the top of the mound. One of the first cracks, perhaps due to a buried geologic structure, developed between 115° and 125° with a large and persistent plasma plume marking its location.

(h) Eleven mound sections, formed by the radial cracks, separated as they continued to move upward and outward. Each remained hinged to the original upthrusted ground surface near the crater rim.

(i) Beginning at 3 sec, several thousand luminous ejecta masses encased in molten glass (partially solidified plasma) and up to 3 m across exited the top center of the mound. Initial exit angles were near vertical. Boosted by plasma initially rushing through constricted vents, masses reached velocities between 300 and 400 m/sec. With time, exit angles decreased to between 40° and 60° commensurate with downward development of the radial cracks. Exit velocities decreased rapidly to between 60 and 130 m/sec with subsequent drop of cavity pressure.

(j) Beginning at 5 sec compressed and perhaps partially saturated nonwelded tuff masses exited the mound in ballistic trajectories leaving contrails of fines marking their trajectories.

(k) With venting of high pressure gases upthrusting ceased and relaxation of the ground surface and cavity walls began. Nonwelded units originally compressed and stretched along the cavity wall began to slump back into the cavity while similar units on the underside of the mound shell, not carried with the mound sections, fell down the cavity walls.

(l) Portions of the nonwelded units, originally "squeezed" between the two hard layers and forced back into the formation, liquified upon release of cavity pressure and began to flow into the cavity causing further relaxation of the upthrusted ground surface.

(m) Mound sections (flaps) continued to overturn and stretch outward causing each to break up into several segments including a "hinged" or crest segment, a terminal segment, and one or more intermediate segments.

(n) The "elbow" of the hinge segment failed in shear and began to fall/slide into the crater cavity.

(o) Flap segments followed general ballistic trajectories. Welded units continued to separate and nonwelded units continued to stretch and in some cases became discontinuous. Degree of dispersion between and within segments increased with time and distance.

(p) During the overturning, stretching, and breakup of flaps, discrete masses of ejecta were separated to form a dispersed fringe

zone surrounding the flap segments. Masses within this fringe zone followed ballistic trajectories of the flap segments from which they were derived.

(q) Throughout their trajectory flap segments retained stratigraphic order and individual units retained their integrity with little or no mixing between units. With overturning the stratigraphic order was inverted.

(r) During transit, ejecta masses were affected by drag with smaller masses (less than 1/3 m) preferentially winnowed out with distance such that very few reached 1200 m.

3. Deposition Phase (4 to ~81 sec)

The deposition phase began with first impact of ejecta and terminated with last movement of ejecta on the ground.

(a) Flap segments were emplaced in an orderly manner and in an ordered sequence beginning with the crest segments (4 to 6 sec) and progressing outward to the terminal segments (8 to 12 sec). Movement of ejecta continued for at least 10 sec after initial emplacement.

(b) With the inverted stratigraphic order of the flap segments, welded tuff units impacted first and with their large volume, further enhanced by bulking, produced the major topographic relief of the continuous ejecta field.

(c) Weakly welded and nonwelded tuff units were deposited with and on top of the welded units, filling in and smoothing out local surface irregularities. Except near the crater rim, where volumes

were relatively large, these units did little to modify the basic topographic expressions of the welded units.

(d) Emplacement of flap segments became increasingly disruptive with distance outward, corresponding primarily to increased velocity of impact and thus post-emplacement movement, but also due to increasing in-flight dispersion between units.

(e) Crest segments were gently folded over and little disrupted with the now underlying welded block units retaining most of their in situ features. At the base of the crest segment, blocks were little broken and retained their jointed structure. With distance upward this structure became increasingly disrupted. In terminal flap segments, no in situ structures were preserved.

(f) Brecciation of blocks within flap segments increased with distance as impact velocity increased. The processes of brecciation were orderly with little mixing between units indicating that segments were emplaced en masse at which time brecciation occurred.

(g) Movement of, and within, flap segments after emplacement increased with distance due primarily to increased impact velocity together with increased separation of flap segments in-flight. Movement was an orderly process with little disturbance of the inverted stratigraphic order.

(h) For crest segments, movement was confined to minor outward sliding or "squishing" en masse and to individual blocks tumbling downhill.

(i) Movement of terminal segments after emplacement consisted of a general outward spreading of ejecta leaving a slightly depressed region, followed by a bunching up of ejecta in a "stair-step" structure at the ray termini. Along leading ray edges small lobate masses of ejecta moved outward. Similar lobes were formed along lateral edges, but skewed radially outward from SGZ. Individual blocks from the fringe zones surrounding terminal segments, for the most part unbroken on impact, tumbled farther outward.

(j) Movement of intermediate segments after emplacement was intermediate to crest and terminal segments.

(k) Movement of weakly welded and nonwelded tuff units within flap segments also increased outward grading first into slightly mixed and farther out moderately mixed units.

(l) Following the emplacement of flap segments a well mixed fine unit was formed from the weakly welded and nonwelded units. Concentrated within rays, this unit covered all previous ejecta deposits, reaching maximum thickness near ray centers. This unit flowed outward, perhaps with the aid of entrapped air, sufficiently to smooth out most topographic irregularities. Portions of this unit flowed through topographic breaks in the underlying welded units "drowning" portions of several valleys. Little of this mix unit flowed across ray perimeters.

(m) Individual weakly welded and nonwelded masses (streamers) were deposited along rays from 8 to 15 sec. Impacts occurred after the segments were deposited, but during the formation of the mix

unit. During this same time period small masses of these units were deposited along the crater rim.

(n) Individual ejecta blocks, which exited preferentially through the mound vents, impacted regularly outward in a moving curtain traveling at an average ground speed of 55 m/sec until 25 sec. Impacts were concentrated out from valleys with up to 30% of these blocks encased in fused glass. After 25 sec, impacts oscillated back and forth partially filling in the intervening areas. Most impacts created a secondary crater, secondary ejecta field, and cloud. There were, however, a number of 1 to 2 m conspicuous blocks impacted out to 1200 m which exhibit no secondary craters. Maximum distance of a recorded impact was 2134 m at 34 sec and last recorded impact was at 71 sec and 1067 m.

(o) Emplacement of flap segments generated a base surge that expanded outward at an average ground speed of 20 m/sec. Outward movement continued to 1370 m by 71 sec. Vertical stabilization occurred at approximately 4 minutes after which the remaining mass was pushed downwind (northeast) at 1 to 5 m/sec.

(p) Cloud development began after first vent and continued until vertical stabilization at approximately 4 min. Cloud then traveled with the wind to the east-northeast at 12 to 18 m/sec. Fall-out from the base surge and cloud, within the boundaries of the ejecta field, effectively ceased by 12 min.

CHAPTER X

SUMMARY, CONCLUSIONS, AND APPLICATIONS

The study of Schooner provides for the first time detailed considerations on the dimensional, morphological, stratigraphical, and structural aspects of a relatively large explosively-produced crater and ejecta field. Relationships between the observed features and key parameters of the geologic setting are derived and then used to infer crater and ejecta processes. Two major conclusions emerge: (1) the Schooner crater and ejecta field were produced by a set of orderly processes (as detailed in Chapter IX) and (2) these processes were strongly affected by the geologic setting (as detailed in Chapter VIII).

The application of these results to cratering is twofold. First, as an analog to aid in the interpretation of existing craters through direct comparison of similar features. Second, as a basis from which to hypothesize crater and ejecta processes for other geologic and source conditions. In any application of Schooner, appropriate care must be exercised because Schooner is one event with a singular set of source and site parameters.

A. Orderly Processes

Processes involved in the formation of the Schooner crater and ejecta field are believed to have been orderly because nearly all observed features of the crater and ejecta field are logically

superpositioned and stratigraphically ordered to the finest detail. The few unordered features can be explained by movement of ejecta after initial emplacement or by postshot slumping and erosion. Where direct observations were possible, mounding, early ejection of material, and impacting of individual ejecta masses proceeded in an orderly manner.

The detonation of the Schooner device produced an apparent crater with a radius of 130 m, a depth of 63 m, and a volume of 1.7×10^6 m^3. Over 90% of the ejecta was distributed continuously to an average of 510 m. Maximum ejecta range was at least 2150 m. Ejecta sizes are strongly bimodal with boulder-size blocks from the welded tuff units and sand-size fines from the weakly welded and nonwelded tuff units.

The dominant feature of the continuous ejecta field is the Ray-Valley structure beginning with 11 crests (topographic highs) and intervening troughs (topographic lows) spaced unevenly around the crater rim. Some crests and most troughs form sets which are aligned through surface ground zero (SGZ). With upthrust nearly constant around the crater perimeter, differences between crest and trough heights are a direct function of the volume of ejecta contained. Crests and troughs continue outward as rays (concentrations of ejecta) and valleys (little to no ejecta), respectively. The distributional pattern of rays is similar to spokes radiating from a wheel hub (the crater). The components of the Ray-Valley structure; i.e. crests, troughs, rays, and valleys are closely and logically related

dimensionally, morphologically, stratigraphically, and structurally.

The continuous ejecta field is in near perfect inverted stratigraphic order. Overall, it can be viewed as an upside-down layer cake. In detail, the layering follows the Ray-Valley structure such that in traversing outward, either radially, or perpendicularly, to a ray axis, higher and higher in situ units are encountered. In greater detail, the truncated layers are discontinuous, with each ray consisting of several segments of a mound section arranged sequentially outward in a slightly skewed pattern.

Ray segments moved along the ground surface to varying degrees after initial emplacement resulting in morphological and structural, but few stratigraphical, modifications. Distortion and dispersion of segments prior to deposition, brecciation and dislocation during deposition, and movement on the ground after deposition increased with distance outward. Thus, segments spread out and coalesce with distance, producing a general broadening and diverging of rays. Even so, stratigraphic units comprising segments retain their identity with only minor mixing even within the most distant segments. Segments are in turn overlain by a continuous layer of mixed ejecta fines which exhibits strong flow characteristics. This mix unit smoothed out topographic irregularities by filling in lows and encircling highs. It also eroded portions of the underlying ejecta deposits, transporting them outward for up to 30 m.

The major portion of the discontinuous ejecta field is also related to the Ray-Valley structure; but with distance, ejecta

becomes aligned with troughs rather than rays. Inverted stratigraphic order is preserved to maximum ejecta ranges, but becomes increasingly difficult to trace beyond the continuous ejecta boundary. This is because there are two populations of blocks comprising the discontinuous ejecta field. Approximately 7% of all blocks are encased in fused glass and were not deposited in an inverted stratigraphic order. The majority of blocks are not encased in fused glass and were deposited in an inverted stratigraphic order. The ratio of fused- to nonfused-glass covered blocks increases from less than 3% at the continuous ejecta boundary to nearly 100% at maximum ejecta range.

It is concluded that the crater and ejecta field were formed by the orderly break up of the mound into 11 major triangularly-shaped sections which were ejected, overturned, and deposited en masse. The fact that rays and their component segments are ordered to the finest detail indicates that processes involved in their formation were likewise ordered. During breakup of the mound blocks of ejecta were preferentially ejected through mound vents (between mound sections) and followed ballistic trajectories to impact. The fact that the majority of the discontinuous ejecta field exhibits an inverted stratigraphic order indicates that the responsible processes were also ordered.

B. Important Geologic Parameters

Features of the crater and ejecta field can be related to one or more parameters of the geologic setting. Water content was clearly the most important controlling geologic parameter. The high water

content of some horizons within the weakly welded and nonwelded tuff units provided "fuel" for the strong gas acceleration phase. This was primarily responsible for the significantly larger crater and the more widely dispersed ejecta field than had been predicted, considering the geologic setting without water. The large gas acceleration boost probably also contributed to movement of ejecta along the ground and the resulting formation of the mix unit overlying the stratified ejecta deposits. The high water content of one or more nonwelded units above the present crater floor was probably responsible for the late-stage formation of the flat crater floor. Finally, the large quantity of fused glass produced by Schooner was probably due to the high water content.

Overall strength of the various units was responsible for the strong bimodal size distribution of ejecta. Ejecta sizes together with unit volumes played a major role in the distribution and movement of ejecta after initial emplacement and the resultant structure and morphology of the crater and ejecta field.

Major joint trends were important in controlling the formation and orientation of the Ray-Valley structure of the ejecta field by causing the mound to break preferentially along major joint trends producing the dominant rays. The more dominant the joint trend the more dominant the ray. As the mound disassembled, ejecta blocks were channeled preferentially through vent openings between mound sections.

Joint spacing and foliation characteristics controlled the sizes and shapes of the ejected welded tuff blocks. The high degree

of jointing and foliation in the welded units apparently provided sufficient stress release paths, resulting in little breakage of blocks during early stages of cratering. Large volume breakage of blocks on impact was localized within flap segments. Therefore, sizes and shapes of ejecta blocks reflect to a high degree in situ conditions.

The surface gradient of 1.5^{o} across SGZ, while seemingly insignificant, correlates with a number of crater and ejecta features; e.g. mounding and venting patterns, crater shape, and ejecta impact patterns, such that cause and effect relationships appear probable. Either the gradient was directly responsible, or indirectly responsible due to some buried structural feature reflecting the present surface; e.g. a set of flow or fracture planes.

C. Applications

The observations and analysis of the Schooner crater and ejecta field are potentially useful in generalizing to other explosive events within constraints imposed by Schooner's source and site characteristics. As an analog, the observed features of Schooner can be compared to similar features of other events to aid in the interpretation of geologic settings and crater and ejecta processes. In this sense surface morphology and geologic characteristics of the ejecta field are indicators of the subsurface stratigraphy and structure. In addition, the now well established details of the Schooner crater and ejecta field provide a basis for

the design of mapping, sampling, geophysical studies, etc., for other craters and ejecta fields. Schooner also can be used as a basis from which to generalize to other cratering situations; i.e. variations in the geologic setting, yield, depth of burst, mode of energy release, (chemical, nuclear, or impacting meteorite), and planetary parameters (gravity and atmospheric pressure).

In support of the above, the Schooner crater and ejecta field provides a ready means for testing hypotheses and for searching out and examining in greater detail features observed on, or hypothesized for, other events. Thus the importance of Schooner lies not only in its immediate application, but in its future use as an interactive analog.

In the application of Schooner's results to other cratering events care must be exercised because Schooner is one event with a singular set of source and site parameters. On Schooner, there is ample evidence that the effect of the various geologic parameters on crater and ejecta processes were superimposed. For certain conditions, one parameter may even completely negate the effects of another; e.g. on Schooner the high water content probably negated effects from the strong over weak layered geometry.

In general, where first order features of the crater and ejecta field of another event compare favorably to Schooner, then at least some of the higher order features, studied in detail on Schooner, are to be expected. Major differences between events should then be primarily a consequence of differences in the geologic

settings. Differences between source and planetary parameters are also important, but probably to a lesser degree. Overall, as an event's source and site parameters increasingly diverge from those of Schooner's, then increasingly greater care must be applied to extra polation.

Within these guidelines it is safe to expect reasonably direct application of Schooner results to other buried explosive events and to the large class of bowl-shaped meteorite craters. The latter, which includes Meteor Crater, Arizona, range up to 10 km in diameter on the Earth and possibly as large as 20 km on the Moon.

General application of Schooner to cratering is discussed below. Neither specific events nor specific geologic settings are included, since the range of possibilities is great and the necessary details are either hypothetical, insufficiently defined, or simply not available. Nor is any attempt made to include effects due to source or planetary parameters since these have been considered by others. Specifically, Nordyke (1961) has discussed explosive source parameters, Chabai (1965) has assessed gravity parameters, and Oberbeck (1971) has contrasted impact and explosion sources.

Investigation of the Schooner event has demonstrated that the best approach in examining a cratering event and interpreting the processes involved in its formation is to begin at the crater edge and work outward. Since cratering processes and resultant features are ordered, observed stratigraphic and structural features at the

crater edge provide the key to what lies outward. Along the crater edge the most complete and undistorted inverted stratigraphic sections of ejecta are preserved. Beyond the crest, good stratigraphic sections can be obtained at topographic highs (flap segments), particularly along the dominant rays. While inverted stratigraphic order is to be expected in the discontinuous ejecta field, sampling can lead to erroneous results without careful attention to the continuous ejecta field, particularly where there is no well defined Ray-Valley structure.

Since nearly all ejecta is distributed radially outward from the crater in a symmetrical and orderly manner, departures from such symmetry and order indicate either nonsymmetrical cratering processes or more likely discontinuities in the geologic setting. Regular departures from crater circularity may be due to regional surface gradients as small as 1 1/2°. Local and abrupt departures from circularity are more likely caused by local venting or postshot slumping, both probably related to geologic factors. Whatever the cause, the ejecta distribution radially outward should be accordingly perturbed. Departures from cross sectional symmetry of the crater are due to either excavation or fallback. Both of which are primarily geology dependent and should be traceable in either the ejecta field or the fallback.

It appears that in general, explosively produced events are capable of generating radial concentrations of ejecta (rays) although other geologic factors (small gas acceleration phase due to

low water content, certain layering sequences such as a thick soil layer over rock, etc.) may inhibit their development or conceal their presence. Thus, the presence or absence of rays is neither necessary nor sufficient to indicate the presence or absence of joint trends. However, dominant joint trends are indicated where dominant rays exist (in terms of size, volume, linearity, etc.) and particularly where ray sets are symmetric through SGZ.

On Schooner, primarily as a consequence of the water saturated layers, the Ray-Valley structure is particularly well developed, extending continuously out to an average of 510 m (3.9 R_a) and discontinuously out to the maximum ejecta range of 2150 m (16.5 R_a). In addition, large blocks 1/3 to 1 m^3 in volume were ejected to maximum ejecta ranges. Thus on events where such features extend to similarly scaled ranges and with due consideration for gravity, the presence of water saturated layers in the geologic setting should be considered. Ejecta block sizes and shapes are a good reflection of in situ conditions for well-jointed sites. Where a lack of joint-faced blocks prevail in the ejecta field, excluding obvious brecciated zones, it can be reasonably concluded that in situ jointing is lacking. As in situ jointing and foliation decrease, then percent breakage should increase and block sizes and shapes should tend to reflect rock strength more than in situ structure.

Aside from secondary craters, block breakage is concentrated within flap segments. Thus, the best place to observe blocks for interpretation of in situ structural characteristics is away from

flap segments; i.e. near and beyond the continuous ejecta boundary or along the crater wall or lip. Alternatively, the best place to observe blocks for interpretation of in situ strength characteristics is within flap segments.

Since blocks can only become smaller during cratering, observed block sizes in the ejecta field represent minimum in situ sizes. Ejecta fines, on the other hand, can aggregate due to shock compression, presence of moisture, or cohesive constituents. Upon impact these aggregates are partially or totally destroyed, but in the process create secondary craters. Thus, ejecta fines are representative of the clast fraction of the in situ media, while aggregates (and the secondary craters they formed) can be useful in inferring physical properties of the media.

A strong bimodal (or trimodal) ejecta size distribution, especially one symmetrical about SGZ, is indicative of a layered geologic setting. Where a strong over weak layered condition exists (as in Schooner) an inverted stratigraphic order is probable. As the thickness of the weak layer increases at the expense of the strong layer the block distribution will become increasingly covered by fines. A Ray-Valley structure, if formed at all, may be concealed and its inverted stratigraphic order destroyed.

For the reverse of Schooner; i.e. a weak over strong layered setting, the inverted stratigraphic order would tend to be destroyed with distance due to relatively higher air drag on the fines. Even dominant joint trends existing in the underlying strong layer may not

lead to preferred venting in the overlying soft layer. Or, if a ray pattern is developed it may be skewed with respect to any ray pattern developed within the overlying weak layer. Obviously there should be little drowning of blocks by fines.

Interpretation of event processes based solely on photogeologic mapping, particularly when the geologic setting is unknown, must be approached cautiously since similar surface features can be formed in different ways. Schooner has demonstrated that ejecta can move significantly after initial emplacement. Where deposited as large masses (flap segments), ejecta spreads out en masse. Individual blocks tumble and fines flow under dry (possibly enhanced with entrapped gases) and presumably, wet conditions. Where unconsolidated or weakly cemented layers underlie rock layers the fines generated will be deposited last and their movement can cover and smooth out an otherwise blocky ejecta surface. Thus, smooth or level surfaces and surfaces exhibiting "flow-like" features can be the result of fine, as well as the more typically considered volcanic, flows.

Schooner has also demonstrated that smooth features within the crater, particularly level surfaces, can result from the liquification and flow of fines from saturated zones. Thus, craters that do not contain a flat or level floor may not have contained a saturated zone of unconsolidated material above the present crater floor. If such a layer did exist, it may have been of insufficient volume to produce a level surface. In this case partial filling of the floor or flow structures along the crater sides may be expected.

For Schooner little secondary cratering of the ground surface occurred during emplacement of the continuous ejecta blanket; i.e. beneath flap segments. While there was extensive secondary cratering of the ground surface during deposition of the discontinuous field, the volume of material affected was relatively minor.

Finally, two miscellaneous observations. First, care must be exercised in using secondary crater sizes and shapes to interpret terminal parameters (size, mass, velocity, angle, etc.) of the impacting mass because ground conditions (soil/rock, soil depth, etc.) are usually the controlling factor in these characteristics. Second, in the interpretation of cratering events, it should be remembered that coverage and/or partial camouflage of the ejecta field, particularly within the continuous blanket, by base surge and cloud deposits can, until eroded, significantly alter the surface morphology.

APPENDIX A

APPENDIX A

STRATIGRAPHIC AND PHYSICAL PROPERTY DATA FOR THE SCHOONER SITE

Table A1 presents field descriptions of the 28 mapping units listed in Figure 6 and used in the geologic mapping of the crater and ejecta field. Descriptions are based on megascopic examination of the U20u-2 continuous core followed by correlation with ejecta deposits.

Lawrence Livermore Laboratory measured physical properties of the Schooner media using both in situ and laboratory techniques. Results of their downhole seismic survey for the Ue20u-3 are presented in Figure A1. Their three-layer fit matches the superimposed physical property units of Figure 6 except for the velocity break at 42.7 m, which as shown by the dashed line can also be interpreted at 38.7 m. The slightly higher velocities of the upper densely welded tuff, compared to the lower densely welded tuff, are explainable by the previously mentioned higher degree of fracturing within the latter. The low and high velocity zones (∿1100 and 1800 m/sec) between 72 and 79 m correspond to mapping units "p" and "1".

Bulk density profiles for Ue20u-3 and U20u, using data from a lock-in density tool and laboratory tests, are compared to physical property units in Figure A2. Mapping unit "c" (57.6 to 60.7 m), a moderately welded tuff, and "p" (72.2 to 77.1 m), a consolidated reworked tuff, are clearly defined. The lower density values for the

TABLE A1

DESCRIPTION OF MAPPING UNITS BASED
ON FIELD EXAMINATION OF U20u-2 CORE AND EJECTA DEPOSITS

UNIT	DEPTH (m)	
s	(Var)*	Soil zone, variable thickness 0-2 m, average 1 m. Fine grained, tan, contains fragments (2-6 cm) of caliche and desert-varnished tuff ("R").
R	(0-1.8)	Ash-flow tuff, moderately to densely welded. Weathered portion of underlying unit; amount of oxidation and porosity decreases with depth. Grades downward from red to maroon, dark and dull when wet.
U	(1.8-8.5)	Ash-flow tuff, moderately to densely welded, devitrified, with vapor-phase crystallization. Contains 20-30% phenocrysts (1-4 mm) of feldspar and 5-10% fragments (2-15 mm) of rhyolite and pumice. Grades downward from maroon to purple gray, dark and slightly dull when wet. Light color feldspars have rectangular habit producing a "salt and pepper" texture.

*Variable thickness, not included in depths of other units.

TABLE A1 (cont'd)

UNIT	DEPTH (m)	
M	(8.5-9.8)	Ash-flow tuff, moderately welded. Fine grained with distinctive black pumice fragments (15-35 mm), many with rectangular outlines, no feldspar phenocrysts. Medium gray. Soft, more porous than "R" and "U", very dark and dull when wet.
L	(9.8-29.9)	Ash-flow tuff, densely welded, devitrified. Contains 10-20% feldspar phenocrysts (1-5 mm) and 5-10% fragments of rhyolite and pumice. Pumice fragments (15-75 mm) are flattened and aligned horizontally producing an eutaxitic texture. Porosity less than "R" and "U", shiny when wet. Grades up to medium gray from purplish gray at base.
P	(29.9-33.2)	Ash-flow tuff, moderately to densely welded, devitrified. Contains 20-25% phenocrysts (1-4 mm) of feldspar and 5-10% fragments of rhyolite up to 10 mm. Horizontal vugs of devitrified pumice up to 75 mm with extensive flow foliation and partings 2-10 mm wide and 10-75 mm apart, results in a sheeted texture which grades up from "B". Porosity between "U" and "M". Medium purple grading downward to purple black at base.

TABLE A1 (cont'd)

UNIT	DEPTH (m)	
B	(33.2-35.7)	Ash-flow tuff, densely welded, devitrified vitrophyre with no glass present. Contains 15-20% phenocrysts (1-4 mm) of feldspar, 15% fragments (4-25 mm) of rhyolite and pumice. A few horizontal vugs near top as well as horizontal flow foliation. Porosity less than "L" from 35.7-34.1, slightly more porous below. Black.
O	(35.7-36.7)	Ash-flow tuff, densely welded, devitrified vitrophyre with some glass present in black pumice fragments. Contains 15-20% phenocrysts of feldspar, 2% fragments of rhyolite and pumice. Numerous elongated vugs 1-5 mm wide and up to 25 mm long. Orange, grading to black at top. Contact with "Y" at base is sharp with rounded weathered fragments of rhyolite.
Y	(36.7-38.7)	Ash-flow tuff, moderately welded, devitrified vitrophyre with some glass present. Chemically altered. Yellow green to yellow brown. Becomes very porous toward base.

TABLE A1 (cont'd)

UNIT	DEPTH (m)	
y	(38.7-39.3)	Reworked ash-flow tuff, nonwelded, pumice rich, friable. Light yellow to yellow brown. Tan pumice fragments up to 20 mm containing small shards of black glass.
m	(39.3-41.1)	Reworked ash-flow tuff, nonwelded, pumice rich, friable. Orange yellow to reddish brown with depth, oxidized. Tan pumice fragments up to 20 mm containing small shards of black glass, some rhyolite fragments.
l	(41.1-43.3)	Ash-fall tuff, nonwelded, pumice rich, friable, very fine grained. Grades upward from dark purple gray at base to lavender near top. Contains a tan (soil?) horizon several cm thick at top with limonitic staining.
g	(43.3-49.1)	Ash-flow tuff, weakly welded, friable, fine grained. Contains 5% phenocrysts of feldspar and 10-20% equidimensional fragments of pumice some up to 10 cm. Contains zones of semi-welded, vitric, gray tuff.
t	(49.1-53.0)	Ash-flow tuff, nonwelded to weakly welded. Transitional between "g" and "v". Medium gray.

TABLE A1 (cont'd)

UNIT	DEPTH (m)	
v	(53.0-57.6)	Ash-flow tuff, weakly welded, vapor-phase altered? Contains 5-10% phenocrysts of feldspar. Zones of moderately welded tuff with horizontally orientated vugs filled with feldspar and quartz crystals up to 25 mm. Medium to purple gray.
c	(57.6-60.7)	Ash-flow tuff, moderately welded, vapor-phase altered? Contains 5-10% phenocrysts of feldspar. Zones with horizontally orientated vugs filled with clear quartz and feldspar up to 25 mm. Chocolate to reddish brown, oxidized.
i	(60.7-61.9)	Reworked ash-flow tuff, friable, very fine grained, argillaceous, chemically altered, oxidized. Contains black pumice flakes up to 5 mm. Reddish brown to orange.
w	(61.9-72.2)	Ash-flow tuff, nonwelded, uniformly very fine grained. Small inclusions of orange pumice up to 5 mm. Very few phenocrysts of feldspar. Light purple gray to white.
p	(72.2-77.1)	Ash-flow tuff, very fine grain, nonwelded, reworked, argillaceous, oxidized. Some lithic (rhyolite) fragments up to 50 mm. Yellowish orange to pale orange.

TABLE A1 (cont'd)

UNIT	DEPTH (m)	
1	(77.1-78.6)	Ash-flow tuff, lithic rich (rhyolite and pumice fragments up to 50 mm), friable to consolidated. Purple gray to yellowish brown to light tan. Reworked.
2	(78.6-83.8)	Ash-fall (or flow) tuff, reworked, bedded, friable. Vitric pumice fragments up to 20 mm with feldspar phenocrysts. Some rhyolite fragments. Light gray to greenish white to bluish white.
3	(83.8-90.5)	Ash-fall (or flow) tuff, friable to consolidated. Contains 20-25% fragments (1-8 mm) of pumice. Buff to brownish gray.
4	(90.5-93.3)	Ash-fall (or flow) tuff, friable to consolidated, fine grain, pumiceous, no fragments. Light gray to tannish white.
5	(93.3-95.7)	Ash-fall (or flow) tuff, reworked, bedded, pumiceous, friable. Contains 20-25% fragments (1-8 mm) of pumice. Brownish gray to buff.
6	(95.7-100.0)	Ash-flow tuff, reworked, bedded, partially welded with a few phenocrysts of feldspar and fragments of pumice up to 12 mm. Tan to medium brown.

TABLE A1 (cont'd)

UNIT	DEPTH (m)	
7	(100.0-102.7)	Ash-fall tuff, reworked, bedded, friable. Contains mostly pumice fragments. Similar to previous unit. Light gray to tan.
8	(102.7-103.3)	Ash-flow tuff, reworked, argillaceous, partially welded. Few feldspar phenocrysts or rhyolite fragments. Brown to pale orange to yellow brown.
G	(103.3-112.2)	Ash-flow tuff, moderately to densely welded, devitrified. Abundant dark gray to black horizontally aligned collapsed pumice fragments up to 75 mm with vugs containing vapor-phase crystals of feldspar and quartz. Fragments of rhyolite up to 25 mm. Feldspar phenocrysts 5-10%. Light greenish gray to olive gray, local iridescent luster.
	T.D. = 112.2 m	

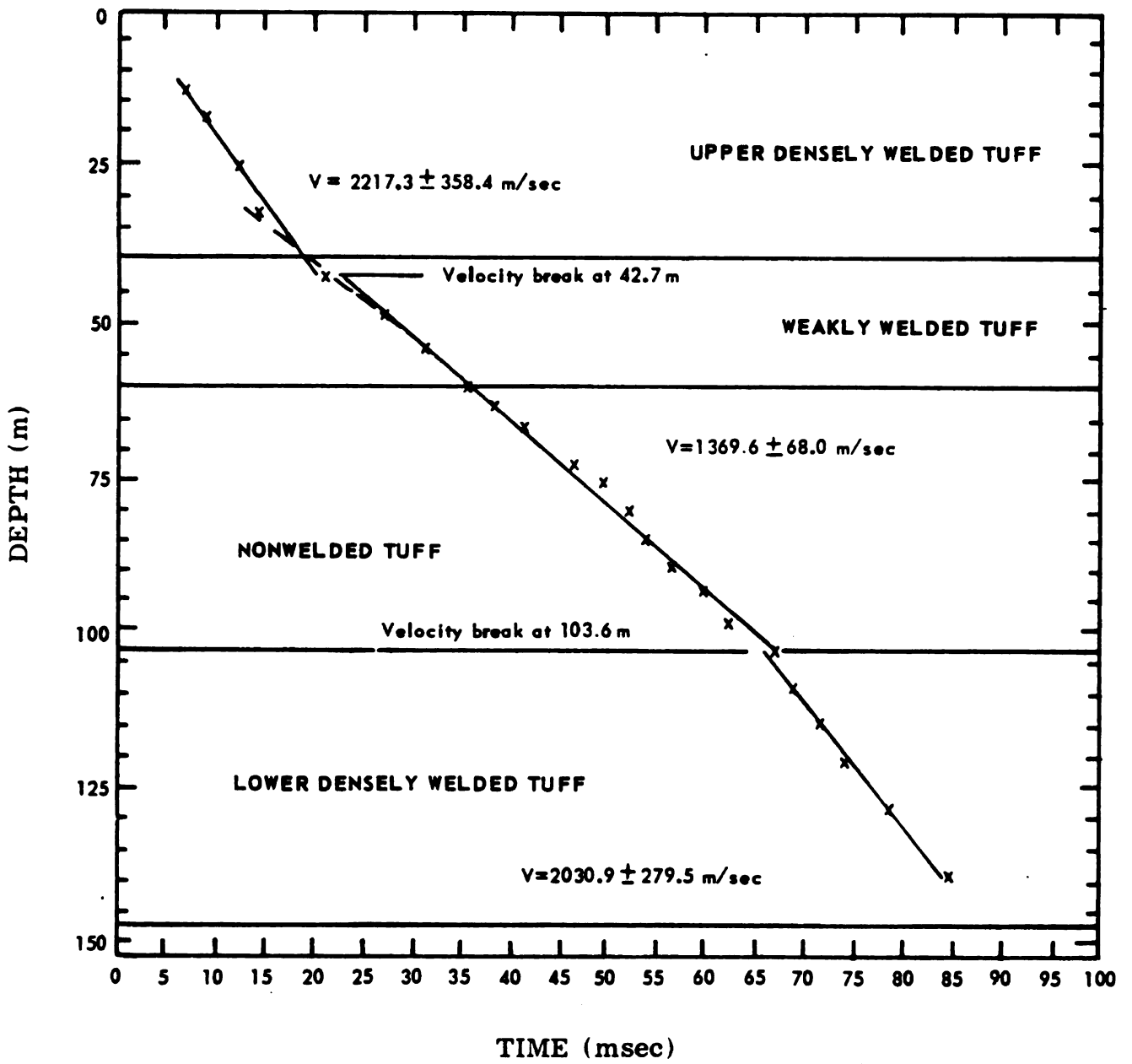

Figure A1. Downhole Velocity Profile for Ue20u-3 (From Tewes, 1970)

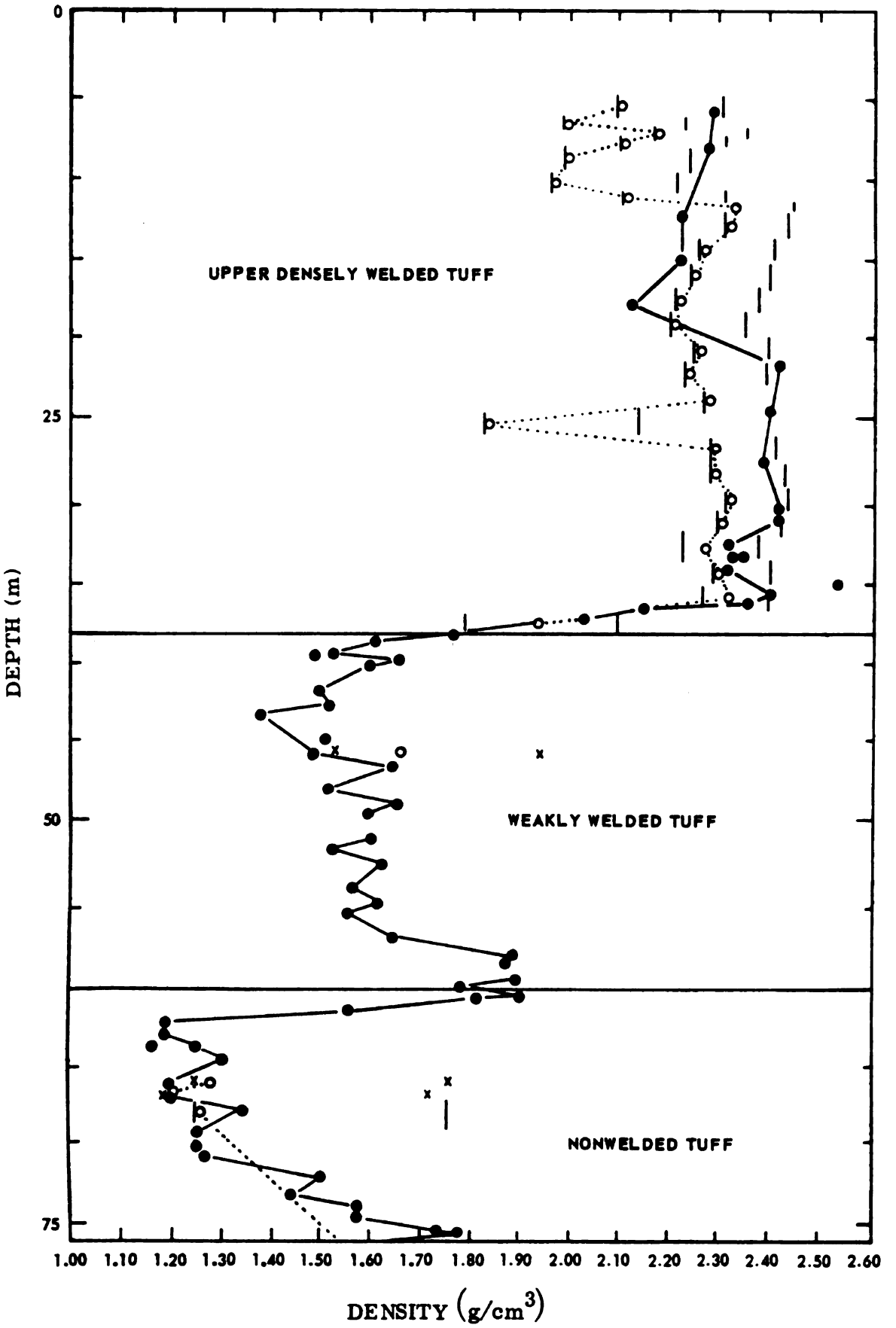

Figure A2. Bulk Density Profiles from In Situ and Laboratory Measurements for Ue20u-3 and U20u (From Tewes, 1970)

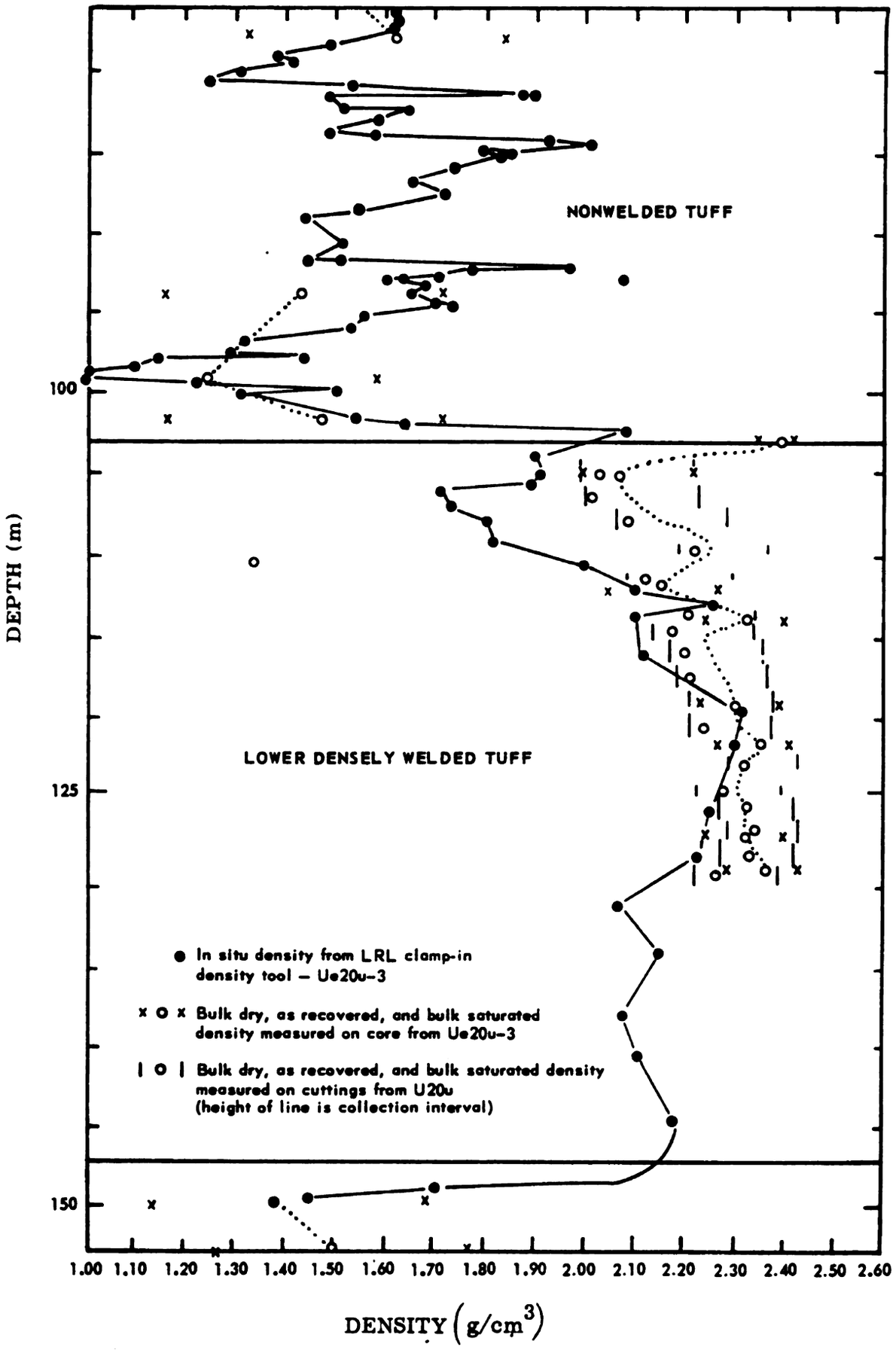

Figure A2. (cont'd)

top 15 m of the lower densely welded tuff, compared to the upper densely welded tuff, are again due to the higher degree of fracturing in the former. The previously mentioned high variability of the nonwelded tuff, particularly below 77 m, is apparent. With grain densities for all Schooner media ranging between 2.5 and 2.7 g/cc, variations in observed bulk densities are primarily a function of porosity and water content.

Since porosity and water content so strongly affect the response of geologic materials to explosions (Butkovich, 1971), U20u and Ue20u-3 were vacuum drilled and samples tested on site, immediately upon retrieval. Porosities generally follow the degree of welding with values of 50 to 60% in the nonwelded tuff, 20 to 40% in the weakly welded tuff, and 10 to 20% in the densely welded tuff (Fig. A3). Fracturing in the upper portions of the densely welded tuffs result in slightly higher porosities. Mapping units "y", "m", and "l" (38.7 to 43.3 m), a nonwelded zone within the weakly welded tuff, are well defined.

There are several zones with high, but unsaturated water contents within the weakly welded and nonwelded tuffs (Fig. A4). The top of the weakly welded tuff (mapping units "y", "m", and "l") and the middle and lower portions of the nonwelded tuff (mapping units "p" and "4" through "8") are highest in percent saturation (40 to 70%). These zones are associated with contacts of the major ash-flows and are probably due to argillaceous soil zones underlying flows, to baking at the contacts, or both (Ramspott, 1968).

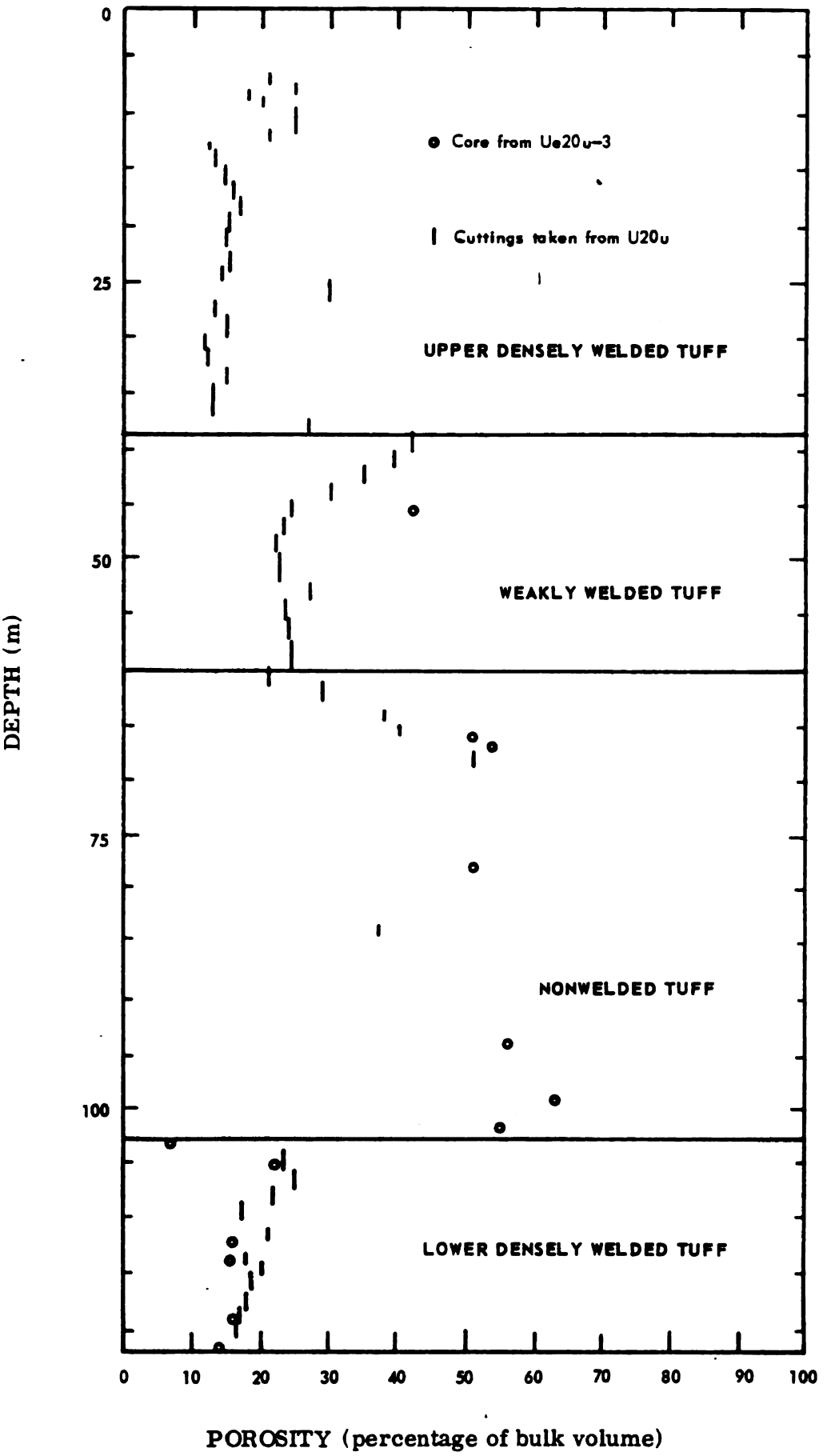

Figure A3. Porosity Profiles from Laboratory Measurements for Ue20u-3 and U20u (From Tewes, 1970)

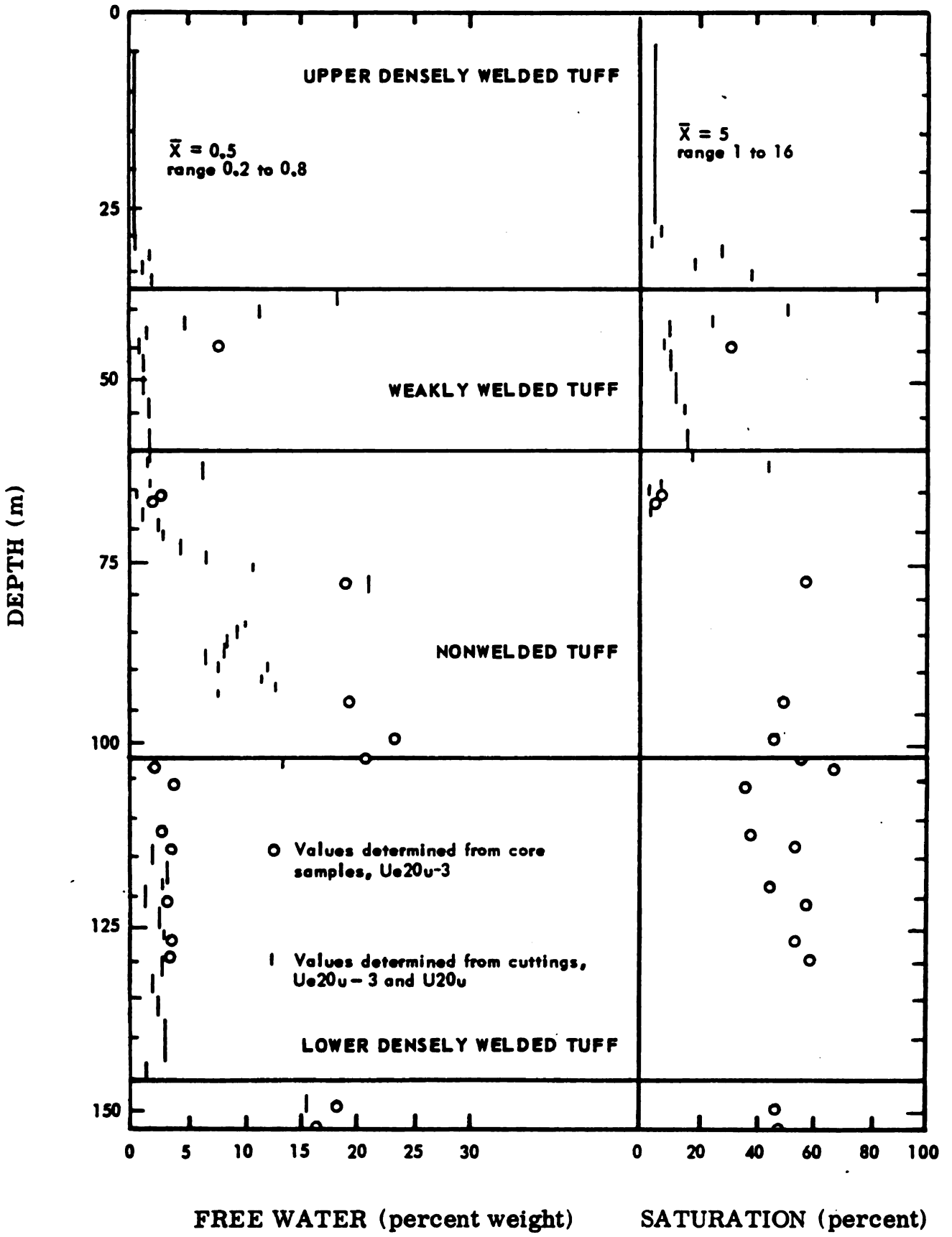

Figure A4. Free Water and Saturation Profiles from Laboratory Measurements for Ue20u-3 and U20u (From Tewes, 1970)

Representative core samples from each of the four physical property units were selected for high pressure testing by Stephens and Lilley (1970). Tests provided equation of state data for mathematical models used in the calculation of the Schooner event (Cherry and Petersen, 1970 and Terhune and Stubbs, 1970). Figure A5 presents loading and unloading pressure-volume relationships and Table A2 lists typical physical property data.

The two densely welded tuffs are similar, both exhibiting about the same amount of compressibility at 2.8 GP_a (∿14%) with little permanent compaction (∿3%) on unloading. Both the weakly welded and the nonwelded tuff exhibit twice the compressibility (30 and 36%) and 4 to 9 times the permanent compaction (13 and 27%) because of their higher porosities. The lower permanent compaction of the nonwelded tuff is due to its higher water content.

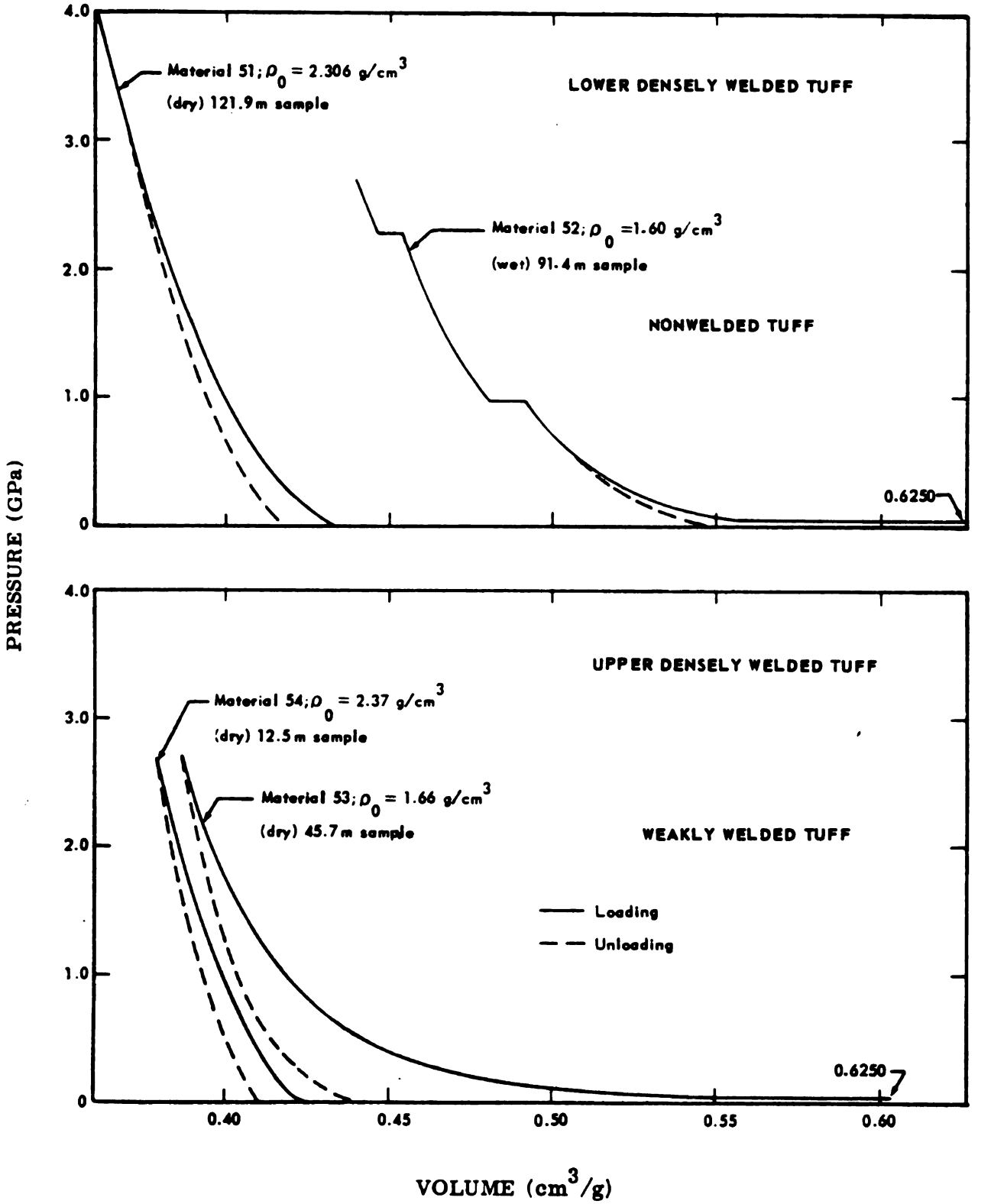

Figure A5. Loading and Unloading Pressure-Volume Curves for Four Representative Samples from Ue20u-3 (From Lessler, 1968)

TABLE A2

PHYSICAL PROPERTIES OF SCHOONER MEDIA

Physical Property Unit	Depth (m)	Logged Density Range (g/cc)	Logged Density Mean (g/cc)	Logged V_p (m/sec)	Water Content (%)	Minimum Gas-Filled Porosity (%)	Experimental Bulk Modulus (GP_a)	Poisson Ratio (Est.)
Upper Densely Welded Tuff	0-38.7	2.22-2.39	2.30	2200	0.3	3.4	6.3	0.25
Weakly Welded Tuff	38.7-60.7	1.40-1.90	1.60	1170	8.5	25.0	2.8	0.11
Nonwelded Tuff	60.7-103.3	1.15-1.90	1.50	1340	12.0	12.0	1.5	0.11
Lower Densely Welded Tuff	103.3-148.1	1.70-2.30	2.20	2030	5.3	5.3	7.9	0.25

APPENDIX B

APPENDIX B

STEREOPHOTOGRAMMETRIC MAPPING, PROFILING, AND VOLUMETRIC COMPUTATIONS

1. Stereophotogrammetric Mapping

The dimensional characterization of the Schooner crater and ejecta field was accomplished by aerial stereophotography and photogrammetric analysis. The procedures, as they are commonly applied to cratering, have been previously discussed by Love and Vortman (1968) and Harron (1969). Briefly, after appropriate surveyed ground control is established, aerial stereophotography is performed both pre- and postshot. Pre- and postshot stereo models are optically constructed from rectified photo images and contoured in a stereoplotter to produce a pre- and postshot topographic map. By "subtracting" the preshot map from the postshot map, an isopach or difference map is produced expressing the net topographic change as a result of the event. Basic crater and ejecta field measurements are computed from the isopach map by planimetering and cross-sectioning. Figures B1, B2, and B3 present preshot, postshot, and isopach maps of the Schooner crater and continuous ejecta field.

For Schooner, the aerial mapping was accomplished by American Aerial Surveys, West Covina, California (preshot December 68, postshot December 68 and January 69) at a range of photo scales from 1 in. = 280 ft* (1 cm = 33.6 m) to 1 in. = 1200 ft (1 cm = 144.0 m). The photo

*Photomapping and analysis performed in engineering units.

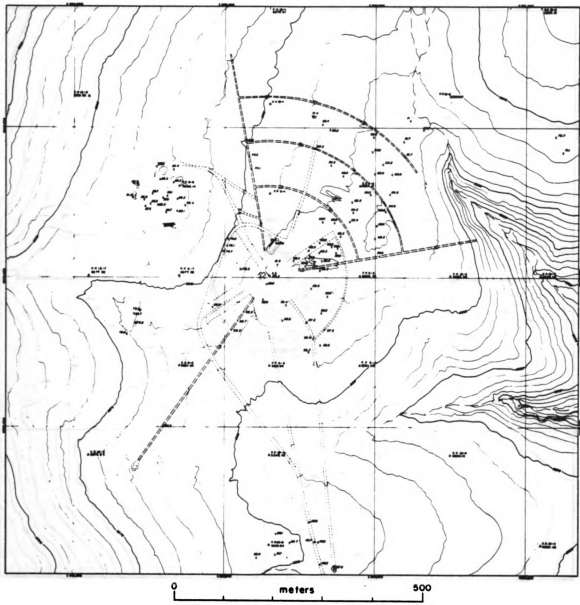

Figure B1. Preshot Topographic Map of Schooner SGZ Area

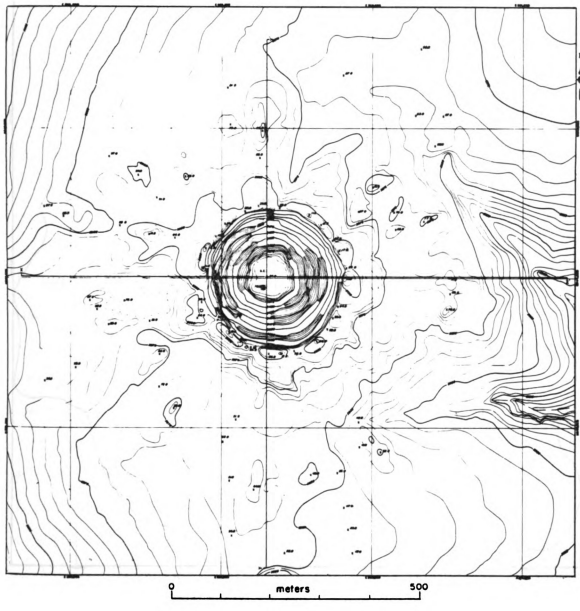

Figure B2. Postshot Topographic Map of Schooner Crater and Ejecta Blanket

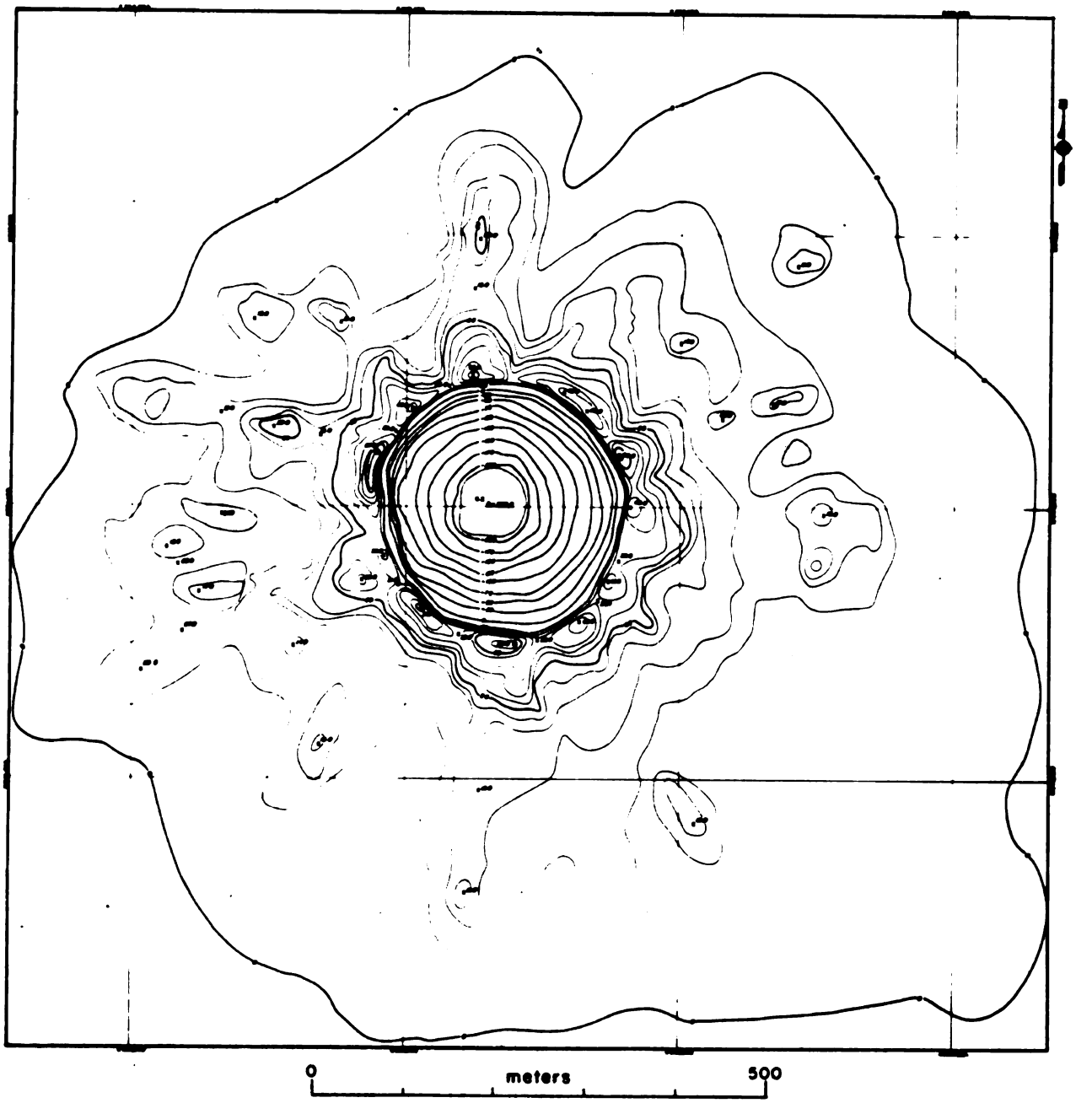

Figure B3. Isopach Map of Schooner Crater and Ejecta Blanket

scale used in preparation of the topographic maps was 1 in. = 1000 ft (1 cm = 120.0 m) allowing a stereoplotter manuscript scale of 1 in. = 100 ft (1 cm = 12.0 m) for contouring.

The contour interval is 5 ft (1.5 m) for the lip and 25 ft (7.6 m) for the crater. Standards followed by the aerial mapping industry provide for a vertical positional accuracy of the contours such that 90% of the points are within $\pm$ 1/2 a contour interval of their true position while the remaining 10% are within $\pm$ 1 contour interval. While there is no explicit horizontal positional accuracy, it is implied in the vertical positional accuracy. A general rule-of-thumb states that the planimetric position of any feature is within a distance equal to 1/40th of an inch (1/16th of a centimeter) of the stereoplotter manuscript scale. For Schooner this is 2.5 ft (0.75 m).

The practical problems involved in delineating a zero thickness (outer "0" contour), especially when a 5 ft (1.5 m) contour interval is used, are substantial, hence portions of the outer "0" contour could be inaccurately positioned. With these limitations, the computed volumes are estimated to be conservatively within 5% of their true values and, if the outer "0" contour is accurately position (as the R_{eb} contour is in the modified isopach map of Figure 24), within 2% (Harron, 1975).

2. Isopach Modifications

During detailed field mapping of Schooner, the following modifications were made to the original isopach map and are incorporated in the modified isopach map (Fig. 24):

(1) The 10 ft (3.0 m) contour was redrawn over portions of Rays 5 and 6,

(2) A 5 ft (1.5 m) contour reflecting the isolated ejecta mass of Ray 11 was added,

(3) The continuous ejecta boundary was mapped in the field and is labeled the R_{eb} contour. The R_{eb} contour replaces the outer "0" contour, previously determined by stereophotogrammetric methods, for dimensional computations,

(4) The continuous extent of ejecta blocks was mapped in the field and is labeled the R_b contour which is approximately a 1 ft (0.3 m) contour,

(5) A nonlinear thickness profile was constructed between the 5 ft (1.5 m) and the R_{eb} contours.

The first two modifications are self-explanatory; the last three are discussed below.

By definition, the R_{eb} contour bounds the continuous coverage of the ground surface by ejecta; it was mapped directly in the field on the new 1973 aerial photography described in Appendix C. Desert-varnished rock fragments on the ground surface provided criteria for the contact. The outward continuous boundary for ejecta blocks (R_b) was also mapped in the field and approximates a 1 ft (0.3 m) contour. Both R_{eb} and R_b contours are plotted on the modified isopach map (Fig. 24).

Except in the southeast quadrant, the R_{eb} contour generally tracks the outer "0" contour while exhibiting a better correlation to the Ray-Valley structure of the ejecta blanket. This general agreement

the outward constriction

rock fragments on the ground surface provided criteria for the contact.

new 1973 aerial photography described in Appendix C. Desert-varnished

the ground surface by ejecta; it was mapped directly in the field on the

Day I and Day II ejecta. Ejecta from the Day II crater was mapped

by definition, the R_{ej} contour bounds the continuous coverage of

discussed below.

The first two modifications are self-explanatory; the last three are

5 ft (1.5 m) and the R_{ob} contours.

(5) A nonlinear thickness profile was constructed between the

(9.3 m) contour.

field and is labeled the R_f contour which is approximately 3 1/2

(3) The continuous extent of ejecta lobe was mapped in the

dimensional computations.

is labeled the R_{ob} contour. The R_{ob} contour replaces the outer "

contour, previously determined by stereophotogrammetric methods, for

(2) A 5 ft (1.5 m) contour replacing the isolated ejecta near

of Day II was added.

(3) The continuous ejecta boundary was mapped in the field and

(1) The 10 ft (3.0 m) contour was retrawn over portions of

legs 5 and 6.

between the outer "0" and R_{eb} contours implies that no major changes have occurred to the ejecta blanket between the January 1969 aerial mapping and the June-October 1974 field mapping. The lack of detailed agreement between the outer "0" contour and the Ray-Valley structure is probably due in part to the impreciseness in determining a zero thickness when photomapping. In addition, base surge deposits which initially covered the ejecta field out to a minimum of 1500 m consisted of silt-size tuff fragments which have been winnowed with time. The large discrepancy in the southeast quadrant between the outer "0" and R_{eb} contours is believed due to heavier than average accumulations of base surge deposits. These resulted from the 6% topographic drop-off combined with the southerly surface winds.

The standard method for computing volumes from an isopach map is to assume a linear fit between contours. During field mapping it was observed that between the 5 ft and R_{eb} contours the decrease in ejecta thickness was not linear because of the bimodal size distribution of ejecta. An approximating profile between the 5 ft and R_{eb} contours was constructed using the following linear segments with the constraint that the R_{eb} contour always terminates a profile:

Contour	Elevation
5 ft to R_b	5 ft to 1 ft
R_b to R_b + 100 ft	1 ft to 0.5 ft
R_b + 100 ft to R_b + 200 ft	0.5 ft to 0.1 ft
R_b + 200 ft to R_{eb}	0.1 ft to 0 ft.

3. Volumetric Computations - Planimeter Method

Volume of each ray was computed from the isopach map (Fig. 24) by determining areas between contours with a compensating polar planimeter and multiplying by the appropriate thickness. Two conditions were computed: (1) with a linear fit between the 5 ft (1.5 m) and outer "0" contours (as in the original photogrammetric computations), and (2) using the above discussed modified fit between the 5 ft (1.5 m) and new R_{eb} contours. Totals for V_a and V_l using condition (1) were 2.2% higher and 2.9% lower than reported photogrammetric values; these factors were applied to adjust all values computed using condition (2). The net effect of using condition (2) rather than (1) is a decrease of almost 10% in V_l; the new apparent lip volume is 1,895,063 m^3. Table B1 presents volumes of the apparent crater and lip for each ray, data are plotted in Figure 28.

4. Volumetric Computations - Profile Method

Volumes of the apparent crater (V_a), true crater (V_t), apparent lip (V_l), and upthrust (V_u) were computed for each ray and valley from profiles constructed along their respective skewed axes (Fig. 24).

True crater and upthrust profiles were constructed using available empirical formulae (Fisher, 1968). Cavity radius (R_c) was determined using Closmann's (1969) equation:

$$R = 21.0\, W^{0.306}\, E^{0.514}\, \bar{\rho}^{-0.244}\, \mu^{-0.576}\, h^{-0.161},$$

TABLE B1

SCHOONER APPARENT CRATER AND LIP VOLUMES FOR EACH RAY

RAY	APPARENT CRATER VOLUME V_a (m^3)	APPARENT LIP VOLUME V_l (m^3)	V_l/V_a
1	155,867	282,926	1.82
2	148,784	129,321	0.87
3	119,191	86,750	0.73
4	157,603	236,118	1.50
5	119,988	118,625	0.99
6	243,131	233,339	0.96
7	143,541	214,334	1.49
8	162,135	129,103	0.80
9	218,411	213,674	0.98
10	122,981	132,970	1.08
11	153,801	117,902	0.77
TOTAL	1,745,433	1,895,063	
MEAN	158,676	172,278	

where

W = yield in KT

E = Young's modulus in megabars

μ = shear modulus in megabars

$\bar{\rho}$ = average overburden density in g/cc

h = DOB in meters.

Using the material property data in Table A2, the resulting R_c values are 46.9 m in the welded tuff below 103.3 m and 49.1 m in the non-welded tuff above. Since the lower hemisphere of the cavity is in the welded tuff, 46.9 m was used. Assuming a constant R_c below the ZP, true crater profiles were constructed by extending a parabola from R_c at 108 m (the ZP depth) to R_t at the preshot ground surface (for Schooner $R_t = R_a$). Individual profiles were adjusted where the crater wall (true crater) was intersected.

Upthrust profiles were constructed by connecting a straight line between the present position of the preshot ground surface observed along the crater (Fig. 26) to a point 1.5 m above the original ground surface at 200 m ($\sim$1.5 R_a). A second straight line connects this point with a point on the original ground surface at 300 m ($\sim$2.5 R_a). This profile is typical of those observed on other buried explosive events (Fisher, 1968).

Volumes were calculated with a computer program designed to accept profile data (range and depth values) and compute volume by the area-moment method (Lockard, 1974). The basic equations used are:

$$\text{Volume} = \int_0^{2\Pi} AM(\phi)d\phi \quad \text{and}$$

$$AM = \int_0^{R_{a\phi}} r\, z(r)dr,$$

where

AM = area moment

r = range

z = depth

$R_{a\phi}$ = radius of crater on a given radial.

Volumes of annuli are summed using a straight-line fit between data points along a profile. Volumes presented in Table B2 and plotted in Figure 30 are for 360° and are, by design, maximized for each ray and minimized for each valley. Therefore, while relative volume comparisons are valid, absolute values require adjustment as in Table 2.

TABLE B2

SCHOONER CRATER AND LIP VOLUME COMPONENTS FOR EACH RAY AND VALLEY

RAY-VALLEY	V_t (m^3)	V_a (m^3)	V_f (m^3)	V_l (m^3)	V_u (m^3)	V_e (m^3)
R-1	4,139,042	1,658,078	2,480,964	4,117,931	425,284	3,692,647
V-1	4,467,161	1,737,812	2,729,349	1,864,355	365,112	1,499,243
R-2	4,771,452	1,918,429	2,853,023	2,756,468	378,130	2,378,338
V-2	4,595,181	1,930,804	2,664,377	1,071,499	375,005	696,494
R-3	4,554,702	1,981,682	2,573,020	1,538,752	379,309	1,159,443
V-3	4,399,982	2,000,767	2,399,215	1,462,983	386,646	1,076,337
R-4R	4,400,800	1,999,819	2,400,981	3,048,060	311,130	2,736,930
R-4L	4,400,800	1,993,173	2,407,627	2,911,906	309,352	2,602,554
V-4	4,403,890	2,016,983	2,386,907	1,202,004	374,496	827,508
R-5	4,243,051	1,978,035	2,265,016	2,858,532	303,204	2,555,328
V-5	4,085,396	1,906,524	2,107,362	1,158,253	332,056	826,197
R-6R	4,001,471	1,801,453	2,200,018	2,682,426	315,874	2,366,552
R-6L	3,897,004	1,780,448	2,116,556	2,188,592	370,102	1,818,490

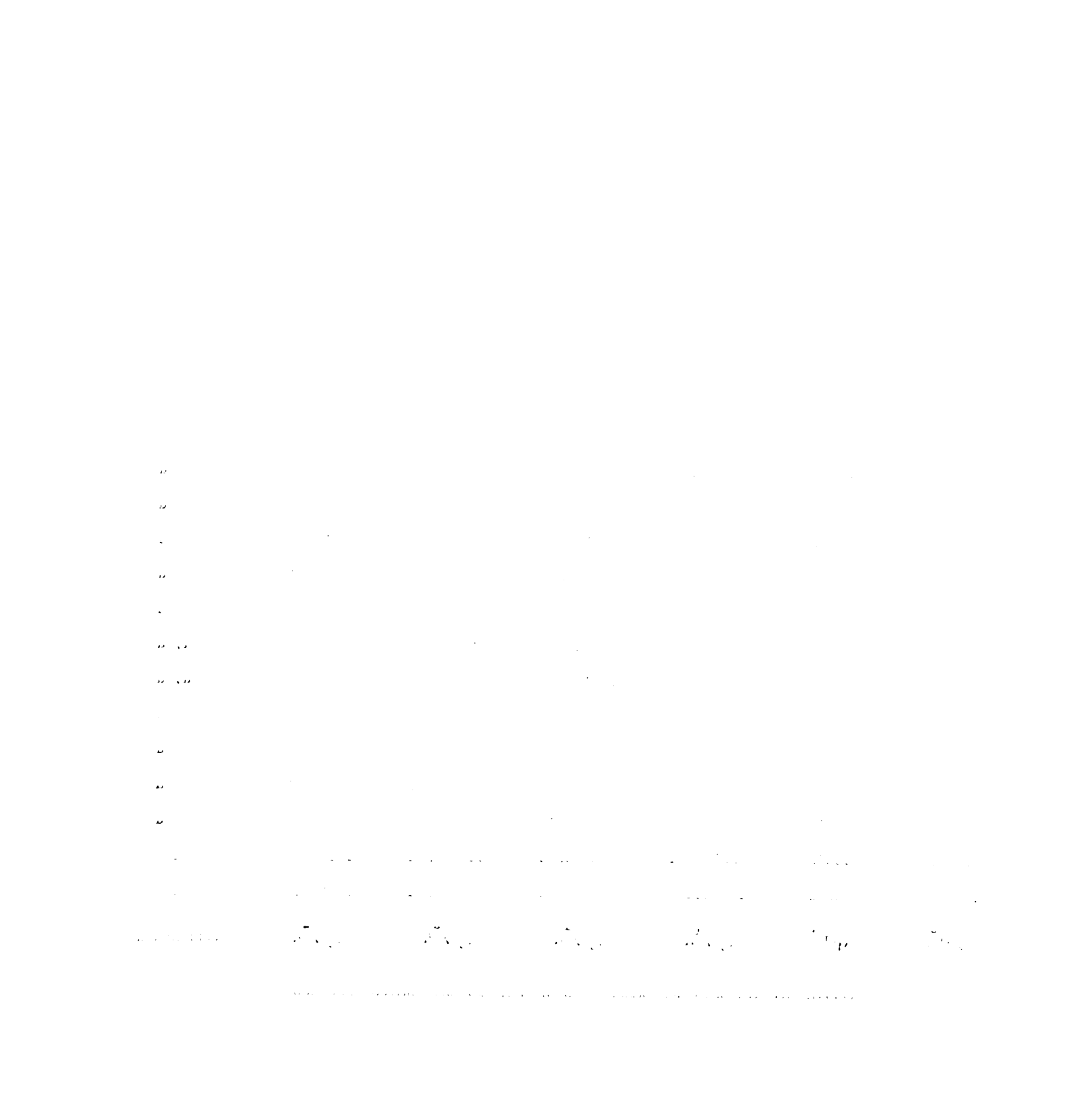

TABLE B2 (cont'd.)

RAY-VALLEY	V_t (m^3)	V_a (m^3)	V_f (m^3)	V_l (m^3)	V_u (m^3)	V_e (m^3)
V-6	3,568,471	1,800,383	1,768,088	879,334	277,716	601,608
R-7	3,548,775	1,781,791	1,766,984	3,477,965	453,768	3,095,168
V-7	3,504,022	1,745,287	1,758,735	738,653	382,798	355,855
R-8	3,385,232	1,667,846	1,717,386	2,533,795	398,482	2,135,313
V-8	3,327,595	1,692,560	1,635,035	1,024,417	450,796	573,621
R-9	3,362,478	1,654,942	1,707,536	3,461,213	453,325	3,007,888
V-9	3,070,100	1,469,334	1,600,766	1,085,124	384,447	700,677
R-10R	3,023,918	1,533,852	1,490,066	2,156,598	417,166	1,215,212
R-10C	3,133,336	1,544,962	1,588,374	3,386,780	416,491	2,970,289
R-10L	2,984,404	1,536,150	1,446,254	1,874,904	416,635	1,458,269
V-10	3,370,860	1,610,156	1,760,704	1,032,186	459,691	572,495
R-11	3,495,656	1,479,044	2,016,612	2,438,043	428,078	2,009,965
V-11	3,779,817	1,543,543	2,236,274	728,456	406,902	321,554

$$\frac{\lambda^{(m)}_{\Sigma}}{\lambda^{(m)}_{\Sigma}}$$

$$\frac{\lambda^{(m)}_{\Sigma}}{\lambda^{(m)}_{\Sigma}}$$

$$\frac{\lambda^{(m)}_{\Sigma}}{\lambda^{(m)}_{\Sigma}}$$

$$\lambda^{(m)}_{\Pi}$$

$$\lambda^{(m)}_{\Sigma}$$

APPENDIX C

APPENDIX C

GEOMORPHIC REGIMES, MAPPING PROCEDURES, AND DATA TABULATION

1. Morphologic Regimes

The initial distribution of blocks and fines followed by post-impact movement gives rise to a large variation of surface morphologies which have been grouped into seven distinct regimes applicable to ejecta, fallback, or both. These are described below.

Blocky Areas (Ejecta and Fallback)

Blocky areas contain a mappable set of blocks; i.e. sufficient number, size, and density of blocks such that the area can be delineated from surrounding areas.

Rubble Areas (Ejecta)

Rubble areas contain moderately to highly brecciated blocks with mean size usually less than 1/6 m and few, if any, in situ surfaces preserved. Many contain a high concentration of multiple secondary craters in varying degrees of obliteration and burial.

Smooth Areas (Ejecta and Fallback)

Smooth areas contain a sufficient quantity of fines to totally cover blocks or rubble. Smooth areas are subdivided into level areas (termed flats) and nonlevel areas (crests, fallback outcrops, topographic highs, etc.).

Drowned Areas (Ejecta)

Drowned areas contain insufficient fines to completely cover underlying blocks or rubble. Degree of drowning varies depending upon size and number of blocks, topographic relief, and quantity of fines. While fines cover, to some extent, all surfaces out to the continuous ejecta boundary, drowned areas are designated only where fines significantly alter the surface morphology.

Hummocky Areas (Ejecta)

Hummocky areas exist where fines lightly cover portions of a rubble area producing a pockmarked or dimpled surface.

Mixed Areas (Fallback)

Mixed areas consist of mixtures of blocks and fines with no stratification.

Transitional Areas (Ejecta)

Transitional areas contain a discontinuous distribution of blocks covered by up to 15 cm of fines. Stratification is generally preserved.

2. Mapping Procedures

General features of the Schooner crater and ejecta field have been discussed in Chapter IV. To provide a more detailed study of the surface morphology, high-resolution aerial photography was flown in 1973 by the U. S. Geological Survey and Williamson Aircraft Co. of

Santa Barbara, California. Both black and white and color photography were obtained over a range of scales from 1 cm = 36.0 m to 1 cm = 6.0 m.

Geomorphic mapping utilized the 1 cm = 18.0 m color photography. The continuous ejecta blanket was subdivided into specific areas, each delineating a singularly distinguishable surface feature in terms of morphology (blocky, rubble, smooth, drowned, hummocky, mixed, and transitional) and physiography (crest, valley, local topographic high, flat, etc.). Each area was assigned an average block size and a relative block areal density. These values are averages over each morphologic area and were determined by visual examination of aerial photographs with limited field verification. The degree of drowning of a particular area is reflected, in part, by the size and areal density values ascribed. Secondary craters and their ejecta fields, shocked pumice fragments, fused-glass fragments, and fallout deposits were not mapped.

Areas were mapped on individual photographs and then compiled using a survey control net established for this purpose. The survey net, accurate to $\pm$ 0.15 m, consisted of stations located every 10^{o} at 610 m, every 20^{o} at 366 m, and 40 stations spaced along the crater rim (see Chapter VI.A). In addition, stations were established every 152.4 m along a radial at 180^{o} azimuth to 1524 m and approximately every 3 m along an excavated trench radially outward from the crater (see Chapter VI. B). Secondary control consisted of the established ground control for the earlier (1968-9) stereophotography, special topographic features, cultural features (roads, drill holes, bunkers,

etc.), and ancillary aerial and ground photographs.

Crater mapping utilized the same photos, survey control, and mapping procedures. In addition, because of the large elevation difference from crater rim to floor (~80 m) other photography were used. These included overheads, aerial obliques, and 35 mm slides taken from the rim and from within the crater.

Over 550 separate areas were required to map the crater and ejecta blanket. These areas are numbered on the maps and listed in Table C1, which also contains an example of the coding used. Data accumulated are presented in three geomorphic maps: (1) a surface feature map; (2) a block size map; and (3) a block areal density map. Maps 1, 2, and 3 are provided in the map pocket and reduced to page size in Figures 34, 35, and 36.

TABLE C1

GEOMORPHIC REGIMES

1.	Se6e*	18.	m-Bb4c	38.	Bb2a
2.	Se6e	19.	m-Bb3b	39.	m-Bb3c
2a.	Se6e	20.	m-Bb2b	39a.	Sa6e
3.	Se6e	21.	m-Bb4b	39b.	Sa6e
4.	Se6e	22.	m-Bb3b	40.	Bw
5.	Se6e	23.	Sb5d	40a.	Bw
6.	Se6e	24.	m-Bb4c	41.	Bb2a
7.	Se6e	25.	m-Bb4c	42.	Sz6e
8.	Be3a	26.	m-Bb3b	43.	Bb2a
9.	So6e	27.	S16e	44.	Sz6e
9a.	So6e	28.	Bb2a	45.	Bb2a
10.	So6e	29.	m-Bb4c	46.	Sz6e
11.	So6e	30.	Bb3a	47.	Sb5d
12.	So6e	31.	Bb2a	48.	Sz6e
13.	So6e	32.	Bb2a	49.	Sz6e
13a.	So6e	33.	Bb3a	50.	Sz6e
14.	So6e	34.	Bb5b	50a.	Sz6e
15.	Bb2a	35.	Bb3a	51.	Sa6c
16.	Sa5c	36.	Sa6e	52.	Bb2a
17.	m-Bb2a	37.	Bb3a	53.	m-Bb1b

*See Geomorphic Regime Code at end of Table C1

TABLE C1 (cont'd)

54.	m-Bb2b	78.	Bb2a	102.	Bb3a
55.	Bb3a	79.	m-Bb2b	103.	Bb2a
56.	Bb3a	80.	Sb5d	104.	m-Bb1c
57.	Bb1a	81.	Sz6e	105.	Bb1a
58.	Bb5c	82.	m-Bb1b	106.	m-Bb3c
59.	Sa6e	83.	m-Bb2b	107.	Bb1a
60.	Bw	84.	Sb5d	108.	m-Bb1b
61.	Bb3a	85.	Bb2a	109.	Sb5d
62.	Sa6e	86.	Sz6e	110.	Bb1a
63.	Bb1a	87.	Bw	111.	Sz6e
64.	Sa6e	88.	Sa6e	112.	Bb1a
65.	Bb4a	89.	Bb5a	113.	Bb1a
66.	m-Bb3c	90.	Bb4a	114.	Sa6e
67.	Sb5d	91.	Sz6e	115.	Bb5a
68.	m-Bb2b	92.	Bb3b	116.	Sa6e
69.	m-Bb2b	93.	Bb1a	117.	Sa6e
70.	Bb1a	94.	Sz6e	118.	Bb5a
71.	Sz6e	95.	Sz6e	119.	Sa6e
72.	Bb2a	96.	Sz6e	120.	Sa6e
73.	Bb3a	97.	Sz6e	120a.	Sa6e
74.	Sa4a	98.	Sz6e	121.	Sa6d
75.	Sa6e	99.	m-Bb1a	122.	Bb3a
76.	Bb3c	100.	m-Bb3c	123.	Bb1a
77.	m-Bb5d	101.	Bb5a	124.	Bb2a

TABLE C1 (cont'd)

125.	Sb5d	149.	_____	173.	d-Rr3a
126.	Bb1a	150.	Sc6e	174.	d-Rr5c
127.	Sz6e	151.	Bc2a	175.	Rh5b
128.	Bb1a	152.	Sp6e	176.	C4d
129.	Sz6e	153.	d-Bcp4b	177.	C5d
130.	Sz6e	154.	Bp2b	178.	d-Br2c
131.	Sz6e	155.	Bp2b	179.	Bg4b
132.	Bb1a	156.	d-Bv3c	180.	d-Rr5d
133.	Sz6e	157.	Ss6e	181.	d-Rr6b
134.	Bb1a	158.	Sp6e	182.	H6e
135.	Bb1a	159.	Sh6e	183.	C5c
136.	_____	160.	d-Rh5d	184.	d-Rr5c
137.	_____	161.	Ss6e	185.	d-Rr3b
138.	_____	162.	Sf6e	186.	d-Rr2a
139.	_____	163.	H6e	187.	d-R4c
140.	_____	164.	d-Rr5c	188.	d-Rr6d
141.	_____	165.	d-Rr5c	189.	d-Rr4b
142.	_____	166.	d-Bg3c	190.	d-Rr5c
143.	_____	167.	Rm4a	191.	d-Br5b
144.	_____	168.	C4c	192.	d-Br4e
145.	_____	169.	d-Ri4c	193.	d-Br3d
146.	_____	170.	d-Bg4b	194.	d-Br4d
147.	_____	171.	Ri4c	195.	d-Br3c
148.	_____	172.	d-Rr4a	196.	d-Br2b

TABLE C1 (cont'd)

197.	d-Bg4b	221.	d-Br5c	244.	Bc3d
198.	d-C3c	222.	Ss6e	245.	Sv6e
199.	C4c	223.	d-Bv3b	246.	Bc2a
200.	d-Br3b	224.	Bg4b	247.	Bv1a
201.	d-Bps4b	225.	Rr3a	248.	d-Bp2b
202.	d-Bp3a	226.	C4b	249.	d-Bp3c
203.	d-Bp13c	227.	C5c	250.	d-Bp3d
204.	Sps6e	228.	C4c	251.	d-Bp2b
205.	Sc6e	228a.	C5c	252.	S16e
206.	d-B3d	229.	Rr5a	253.	d-Bh5d
207.	d-Bv2d	230.	d-Rr5b	254.	Sf6e
208.	Sps6e	231.	H6e	255.	S16e
209.	Sp6e	232.	d-Rh6c	256.	d-Bh2d
210.	St6e	233.	d-Rh4b	257.	Sh6e
211.	Sc6e	234.	d-Rh5b	258.	d-Bh4d
212.	d-Bp3c	235.	Sh6e	259.	d-Rh5c
213.	Sp6e	236.	d-Rr5c	260.	d-Bh4c
214.	d-Bp5d	237.	Rr4a	261.	d-Bk5d
215.	d-Bp2c	238.	d-Rg5c	262.	d-Bk3b
216.	d-Bp4c	239.	Sh6e	263.	C4c
217.	d-Bv3c	240.	d-Br5d	264.	C5c
218.	d-Bp4c	241.	d-Bh5d	265.	d-Br4c
219.	d-Bv5c	242.	Rx5a	266.	C4c
220.	d-Bp3b	243.	Sf6e	267.	d-Br5d

TABLE C1 (cont'd)

268.	H6e	292.	Sv6e	316.	d-Rr4c
269.	d-Ri5c	293.	d-Bv4d	317.	d-Rr3b
270.	d-Ri5c	294.	d-Br4d	318.	d-Rr4c
271.	d-Ri5c	295.	d-Bv2b	319.	-
272.	d-Rr5c	296.	d-Bv3d	320.	Bg4b
273.	d-Rr3b	297.	d-Bp4c	321.	Rx5a
274.	d-Bg4d	298.	d-Bh3d	322.	Rx5a
275.	d-Bg3d	299.	Sf6e	323.	Ri4a
276.	d-Bg4b	300.	d-Bp2b	324.	d-Bg4c
277.	Sh6e	301.	d-Bh5d	325.	d-Rr6c
278.	d-Bh5c	302.	d-Bh5d	326.	d-Rr6d
279.	d-Bh4d	303.	d-Bh5d	327.	d-Rh6c
280.	d-Bh4d	304.	d-Br3c	328.	Sh6e
281.	Sv6e	305.	d-Bg4c	329.	d-Rm5b
282.	Sh6e	306.	d-C3c	330.	d-Rh6d
283.	d-Bh3b	307.	C5d	331.	d-Rh6d
284.	Si6e	308.	C5c	332.	d-Bh5c
285.	3-Bp3c	309.	C4d	333.	Rr3a
286.	Sp6e	310.	Ri3b	334.	-
287.	Sc6e	311.	C4c	335.	d-Bg4c
288.	d-Bp5c	312.	C5c	336.	d-Rr4c
289.	Sp6e	313.	Br4b	337.	d-Rr5d
290.	d-Bt3b	314.	C3c	338.	d-Bp2c
291.	d-Bt5c	315.	Rr3a	339.	Ss6e

TABLE C1 (cont'd)

340.	Sp6e	364.	Rr5a	387.	Sv6e
341.	Sc6e	365.	d-Rr3c	388.	d-Bp1a
342.	Bt1b	366.	d-Rr5d	389.	Sc6e
343.	Bt1a	367.	Rr3a	390.	Bt3a
344.	d-Bv3c	368.	d-Rg4c	391.	Sps6e
345.	d-Bp2d	369.	Bg4b	392.	Sp6e
346.	Ssv6e	370.	C5c	393.	Sc6e
347.	d-Bv4c	371.	C4c	394.	Sf63
348.	d-Bv5c	372.	C4b	395.	Bp1a
349.	d-Bv2c	373.	d-Rr4b	396.	Sp6e
350.	d-Bv3d	374.	d-Bg4c	397.	d-Bv3d
351.	d-Bg4c	375.	Bg4c	398.	d-Bt2c
352.	d-Br3a	376.	d-Rr3b	399.	d-Bv4d
353.	d-Br5c	377.	d-Bg4c	400.	d-Bv3b
354.	d-Br3b	378.	d-C5d	401.	Sv6e
355.	d-Br3d	379.	d-Rr5c	402.	Bp2a
356.	d-Br3d	380.	Rr3a	403.	Sh6e
357.	Rr5a	380a.	d-Rr4b	404.	d-Rh5c
358.	d-Rr5d	381.	d-Rr4b	405.	d-Rh5c
359.	Bg4b	382.	d-Rr5d	406.	d-Rh5c
360.	Rr3b	383.	Ss6e	407.	d-Rr5c
361.	d-Rr5d	384.	d-Bs2a	408.	H6e
362.	d-Rr6b	385.	d-Bs3d	409.	d-Rr5b
363.	d-Rr6d	386.	Sp6e	410.	Rr3a

TABLE C1 (cont'd)

411.	C4c	435.	d-Bc3b	459.	d-Rh4b
412.	Bg4b	436.	Bc4a	460.	d-Rh5d
413.	Bg4b	437.	B1a	460a.	d-Rh4b
414.	C4b	438.	d-Bp4c	461.	Bg4a
415.	d-Bg4b	439.	Bp2b	462.	d-Bg4b
416.	C5d	440.	d-Bp4c	463.	d-Ri3a
417.	d-C3c	441.	Bt2a	464.	Rr3a
418.	Bg4c	442.	Sp2c	465.	Br3a
419.	d-Rr6d	443.	d-Bvp4c	466.	C3b
420.	Bg4b	444.	Sc6e	467.	C4c
421.	C4c	445.	d-Bp5c	468.	d-Bg4c
422.	d-Ri5c	446.	d-Bpv3b	469.	d-Rr4a
423.	C5c	447.	d-Bp4c	470.	d-Rr4b
424.	Rr3a	448.	d-Bv3e	471.	d-Bg5c
425.	d-Rr4b	449.	Sp6e	472.	Sf6e
426.	d-Rr5d	450.	d-Bv3d	473.	Rr4b
427.	H6e	451.	Sf6e	474.	Bg4b
428.	d-Rix5a	452.	d-Bh3c	475.	d-Rr5c
429.	d-Bh3c	453.	d-Bp4c	476.	H6e
430.	B1a	454.	Sh6e	477.	d-Rr4c
431.	B1a	455.	d-Rh5d	478.	d-Rr5c
432.	Sh6e	456.	d-Bh4c	479.	Rr4a
433.	Sp6e	457.	d-Rr6d	480.	d-Rr6d
434.	Sc6e	458.	d-Rh5c	481.	d-Rr4c

TABLE C1 (cont'd)

482.	C4c	506.	Bt1a	530.	Bg4b
483.	C4b	507.	Bv2a	531.	Rr3b
484.	C4b	508.	d-Bv2a	532.	d-Rr4a
485.	C5c	509.	d-Bv3b	533.	d-Rh5c
486.	Bg3b	510.	d-Bv4d	534.	B3b
487.	C4c	511.	d-Bv3a	535.	C3c
488.	C3c	512.	d-Bv3c	536.	d-Bg4c
489.	C4b	513.	d-Bg4c	537.	d-Rr4a
490.	Rr3a	514.	d-Bv4d	538.	_____
491.	d-Rr5b	515.	C4b	539.	H6e
492.	H6e	516.	C5c	540.	d-Rh5b
493.	d-Rg4c	517.	C4b	541.	d-Rh5c
494.	d-Rh5c	518.	Bg4b	542.	Bh4c
495.	Shs6e	519.	d-Rr5d	543.	d-Br3b
496.	d-C5d	520.	C5d	544.	Bh4c
497.	d-Rr4b	521.	H6e	545.	d-Br3d
498.	d-Rh5c	522.	d-Rr5c	546.	d-Bg3b
499.	d-Bp3c	523.	Rr4a	547.	d-Bh3c
500.	d-Bp4d	524.	C5c	548.	H6e
501.	d-Bp2c	525.	C5d	549.	d-Rh6c
502.	Sp6e	526.	C4c	550.	d-Rh6d
503.	Sp6e	527.	d-Rr5b	551.	_____
504.	B1a	528.	d-Rg3b	552.	d-Bi5c
505.	d-Bv2d	529.	d-C5c	553.	Ss6e

TABLE C1 (cont'd)

554. d-Bv3e

555. d-Bv2b

556. d-Bv2b

557. d-Bp4b

558. Sp6e

559. Sc6e

TABLE C1 (cont'd)

GEOMORPHIC REGIME CODE

Example:

(1)	(2)	(3)	(4)	(5)
459 :	d-R	h	4	b

(1) 459 : Map Area Code

(2) d-R : Morphology = Drowned, Rubble

(3) h : Physiography = Local Topographic High

(4) 4 : Average Block Size = 1/2 m

(5) b : Relative Block Areal Density = High

MORPHOLOGY

B	Blocky Area
R	Rubble Area
S	Smooth Area
H	Hummocky Area
C	Transitional Area
d-	Drowned Area
m-	Mixed Area

TABLE C1 (cont'd)

PHYSIOGRAPHY

Crater	
a	Ejecta Detritus
b	Talus
e	Ejecta
l	Floor
o	Soil Horizon (in situ + ejecta)
w	Wall
z	Outcrop
Ejecta	
c	Crest
f	Flat
g	Ground Surface
h	Local Topographic High
i	Isolated Unit
k	Stream Cut
l	Circumferential Valley
m	Retarc
p	Plateau
r	Ray Terminus
s	Slope
t	Trough
v	Valley
x	Secondary Crater

TABLE C1 (cont'd)

BLOCK SIZE

Number Code	Average Block Length (m)
1	$\geq$ 2
2	1 1/2
3	1
4	1/2
5	$\leq$ 1/6
6	Fines

BLOCK AREAL DENSITY

Letter Code	Relative Areal Density
a	Very High
b	High
c	Intermediate
d	Low
e	Fines

APPENDIX D

APPENDIX D

MASS BALANCE COMPUTATIONS

Mass balance relationships were calculated using procedures and formulations slightly modified from those developed by Carlson and Jones (1965). Figure D1 presents a sketch of an idealized crater and ejecta field showing the various quantities involved and Table D1 lists densities, volumes, and computed masses. The basic equations are:

$$M_t = M_m + M_f$$

$$M_m = M_e + M_k + M_\Delta$$

$$M_\Delta = f\ (M_\beta \text{ and } M_u).$$

M_Δ is the mass that cannot be accounted for after fallback mass (M_f), ejecta mass (M_e), and cloud mass (M_k) have been subtracted from the true crater mass (M_t). M_Δ is a function of compaction outside and below the true crater and upthrust above. The net mass lost to vaporization of material surrounding the device was significantly less than 1% of the true crater mass and is ignored in further discussions here.

The various masses were computed in the following manner:

(1) True Crater Mass (M_t)

$$M_t = \rho_t V_t$$

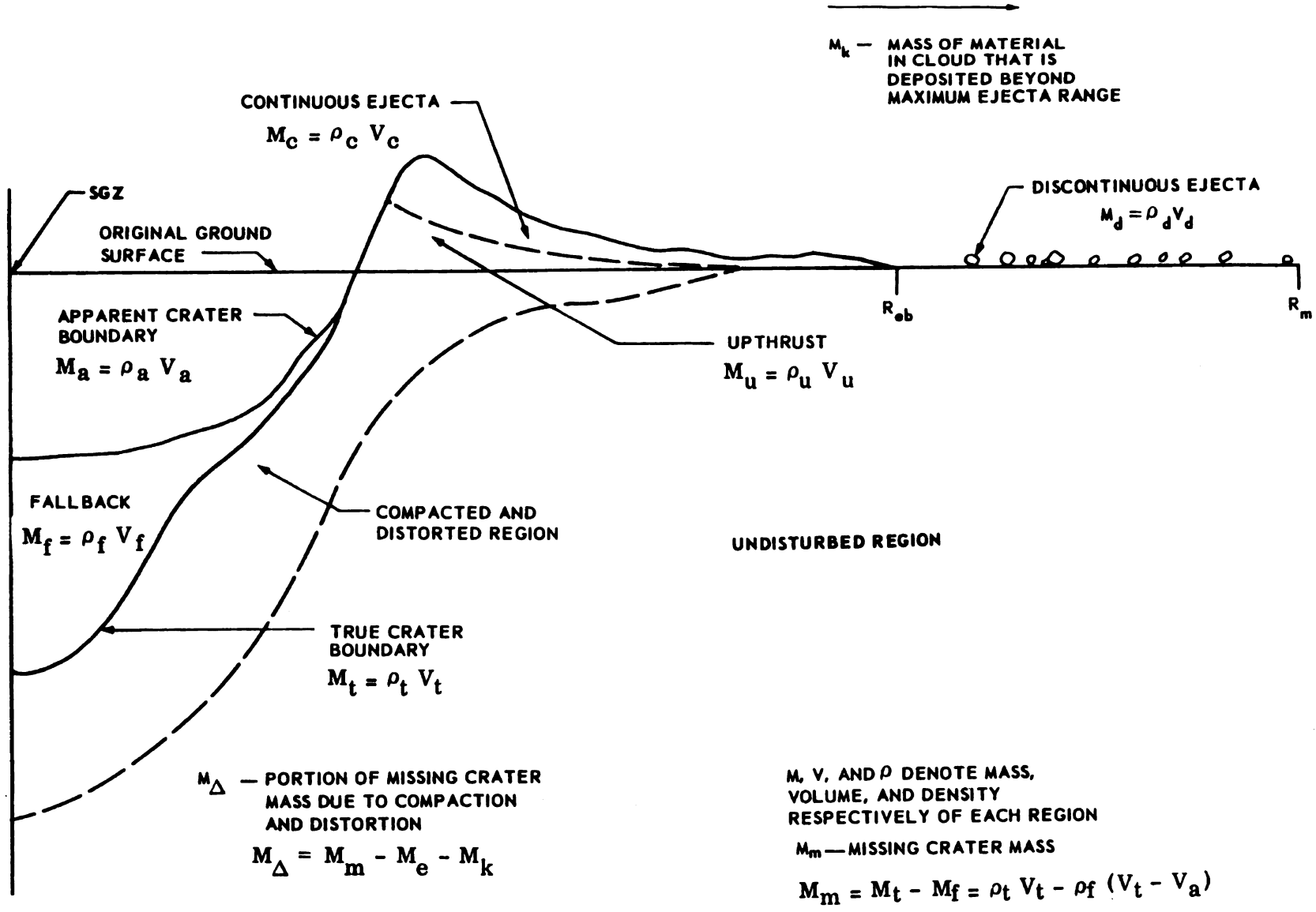

Figure D1. Sketch Illustrating Mass Balance Relationships

TABLE D1

SCHOONER VOLUME, DENSITY, AND MASS DATA

	Density (g/cc)	Volume (m^3)	Mass (kg)
True Crater		3,840,130	7,495,999,100
Upper Densely Welded Tuff	2.30	1,838,942	4,229,566,600
Weakly Welded Tuff	1.60	822,347	1,315,755,200
Nonwelded Tuff	1.50	911,035	1,366,552,500
Lower Densely Welded Tuff	2.20	260,594	573,306,800
Lower Nonwelded Tuff	1.50	7,212	10,818,000
Missing Crater			3,976,908,140
Fallback	1.68	2,094,697	3,519,090,960
Upthrust	2.19	383,538	839,948,220
Ejecta			
Continuous	1.97		2,953,761,129
Discontinuous	2.30		247,219,822
Total			3,200,980,951
Cloud			74,959,991
Unaccounted			700,967,198

True crater volumes were calculated, using procedures developed in Appendix B, incrementally for each of the 5 major units intersected by the true crater (Fig. 7). Density values are from Table A2.

(2) Fallback Mass (M_f)

$$M_f = \rho_f (V_t - V_a)$$

True and apparent crater volumes are from Table 2. Fallback density was computed based on the relative proportions of the various units present and their assumed bulking characteristics.

(3) Upthrust Mass (M_u)

$$M_u = \rho_u V_u$$

Upthrust volume was calculated using procedures of Appendix B while density was estimated to be 95% of the average density of the upper densely welded tuff.

(4) Cloud Mass (M_k)

$$M_k = 0.01 (M_t)$$

The mass of the Schooner cloud deposited beyond the continuous ejecta field was estimated to be 1% of the true crater mass based on analyses by Gudiksen (1970).

(5) Ejecta Mass (M_e)

$$M_e = M_c + M_d$$

The ejecta mass is the sum of the continuous ejecta mass (M_c) and the discontinuous ejecta mass (M_d). The continuous ejecta mass was calculated by integrating an average areal density profile from the average crater edge out to the average continuous ejecta boundary and revolving this 360°. The equation is of the form

$$M_c = 2\pi \int_{1R_a}^{R_{eb}} \delta(D)\, DdD \quad .$$

Similarly for the discontinuous ejecta, from the average continuous ejecta boundary to the maximum recorded ejecta range, the equation is of the form

$$M_d = 2\pi \int_{R_{eb}}^{R_m} \delta(D)\, DdD \quad .$$

Schooner areal density data are presented with best fit straight lines in Figure D2. Data for the continuous ejecta field were derived from the ejecta portion of the average apparent lip profile (Fig. 23) using a density of 1.97 g/cc. This density was estimated from

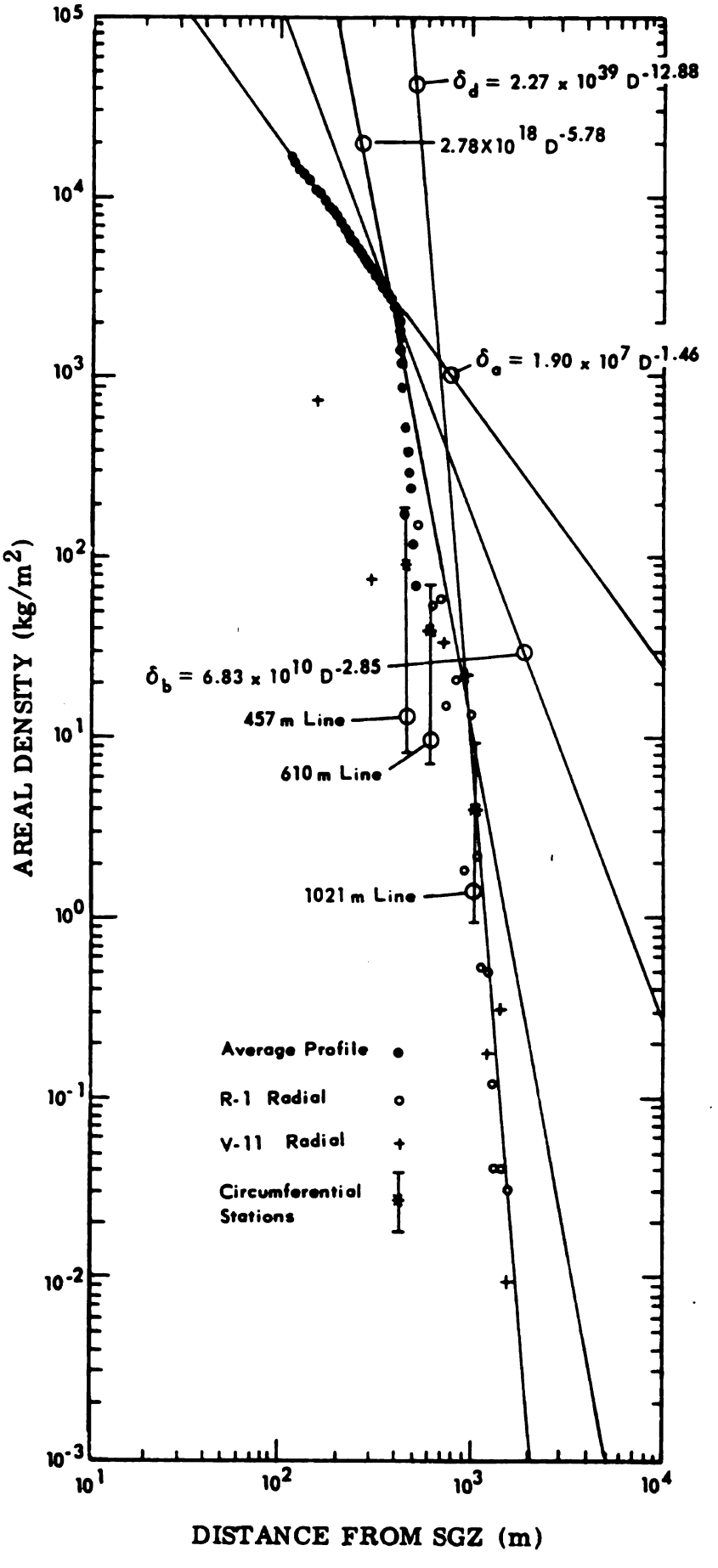

Figure D2. Ejecta Areal Density as a Function of Distance from SGZ

observed ratios of blocks and fines in the trench and their corresponding bulk densities. Areal density data in the discontinuous ejecta field are from volume measurements along R-1 and V-11 radials (Fig. 66) using the welded tuff block density of 2.30 g/cc. The previous two equations together with their boundary conditions give:

$$M_c = 2\pi \left[\int_{130\ m}^{360\ m} \delta_a(D)\ DdD + \int_{360\ m}^{420\ m} \delta_b(D)\ DdD + \int_{420\ m}^{510\ m} \delta_c(D)\ DdD \right]$$

and

$$M_d = 2\pi \left[\int_{510\ m}^{900\ m} \delta_c(D)\ DdD + \int_{900\ m}^{2134\ m} \delta_d(D)\ DdD \right]$$

where $\delta(D)$ terms are given in Figure D2.

Computed masses are presented in Table D1 and mass balance ratios in Table 4.

REFERENCES

REFERENCES

Ahlers, E. B., 1962, "Throwout Study of an Underground Nuclear Detonation-Project Danny Boy", Illinois Institute of Technology, Defense Nuclear Agency Report, POR-1814.

Andrews, R. J., 1975, "Origin and Distribution of Ejecta From Near-Surface Laboratory-Scale Cratering Experiments", University of Dayton Research Institute, Air Force Weapons Laboratory Report, AFWL-TR-74-314.

Baldwin, R. B., 1963, "The Measure of the Moon", University of Chicago Press.

Butkovich, T. R., 1971, "Influences of Water in Rocks on Effects of Underground Nuclear Explosions", Journal of Geophysical Research, Vol. 76, No. 8.

Butkovich, T. R. and Lewis, A. E., 1973, "Aids for Estimating Effects of Underground Nuclear Explosions", Journal of Geophysical Research, Vol. 76, No. 8.

Butkovich, T. R. and Lewis, A. E., 1973, "Aids for Estimating Effects of Underground Nuclear Explosions", Lawrence Livermore Laboratory, UCRL-50929 (Rev. 1).

Carlson, R. H. and Jones, G. D., 1964, "Project Air Vent - Ejecta Distribution Studies", The Boeing Company, Report-D2-90575.

Carlson, R. H. and Jones, G. D., 1965, "Distribution of Ejecta from Cratering Explosions in Soils", Journal of Geophysical Research, Vol. 70, No. 8.

Carlson, R. H. and Newell, R. T., 1970, "Ejecta from Single-Charge Cratering Explosions", The Boeing Company, Sandia Laboratories Report SC-RR-69-1.

Chabai, A. J., 1962, "Radioactive Tagging of Crater Ejecta", Chapter 5, Project Stagecoach, Sandia Laboratories Report, SC-4595(RR).

Chabai, A. J., 1965, "On Scaling Dimensions of Craters Produced by Buried Explosives", Journal of Geophysical Research, Vol. 70, No. 20.

Cherry, J. T., 1967, "Computer Calculations of Explosion - Produced Craters", International Journal of Rock Mechanics and Mining Science, Vol. 4.

Cherry, J. T. and Petersen, F. L., 1970, "Numerical Simulation of Stress Wave Propagation from Underground Nuclear Explosions", Proceedings-Symposium on Engineering with Nuclear Explosives, The American Nuclear Society, CONF-700101.

Christiansen, R. L. and Noble, D. C., 1968, "Geologic Map of the Trial Ridge Quadrangle, Nye County, Nevada", Geologic Quadrangle Map GQ-774.

Circeo, L. J., 1969, "Nuclear Excavation: Review and Analysis", Engineering Geology, Vol. 3.

Closmann, P. J., 1969, "On the Prediction of Cavity Radius Produced by an Underground Nuclear Explosion", Journal of Geophysical Research, V. 74, No. 15.

Danielson, G. E., 1975, "Our Present View of Mercury and Venus", Proceedings of the Sixteenth General Assembly International Union of Geodesy and Geophysics, U.S. National Report for 1971-1974.

Day, W. C., 1972, "Craters as Engineering Structures", U.S. Army Engineer Waterways Experiment Station, Miscellaneous Paper E-72-2.

Diehl, C. H. and Jones, G. H., 1964, "A Tracer Technique for Cratering Studies", Journal of Geophysical Research, Vol. 70, No. 2.

Fisher, P. R., 1968, "Engineering Properties of Craters", U.S. Army Engineer Nuclear Cratering Group, PNE-5012.

Fransden, A. D., 1970, "Engineering Properties Investigations of the Cabriolet Crater", U.S. Army Engineer Nuclear Cratering Group, PNE-957.

Freeberg, J. H., 1966, "Terrestrial Impact Structures - A Bibliography", U.S. Geological Survey Bulletin 1220.

Gault, D. E., Quaide, W. L., and Oberbeck, V. R., 1968, "Impact Cratering Mechanics and Structures", in Shock Metamorphism of Natural Materials, Mono Book Corporation, Baltimore.

Gudiksen, P. H., 1970, "Mass Concentrations and Particle Size Distributions as a Function of Time Within a Nuclear Cratering Cloud", University of California Lawrence Radiation Laboratory, UCRL-50844.

Hansen, S. M., et al., 1964, "Recommended Crater Nomenclature", Geophysics, Vol. 29, No. 5.

Harron, W. J., 1969, "Large Scale Photogrammetry in an Explosive Testing Program", Proceedings of the Convention of the American Society of Photogrammetry and American Congress on Surveying and Mapping.

Harron, W. J., 1975, "Personal Communication", Limbaugh Aerial Mapping Division of Bovay Engineers, Albuquerque, N.M.

Hasler, J. W., 1965, "Preliminary Report on the Lithology of Drill Hole Ue20j, Pahute Mesa, Nevada Test Site", U.S. Geological Survey Technical Letter: Special Studies I-35.

Hasler, J. W. and Byers, F. M., 1965, "Preliminary Report on the Lithology of Pahute Mesa Drill Hole No. 2, Pahute Mesa, Nevada Test Site", U.S. Geological Survey Technical Letter: Special Studies I-39.

Henny, R. W. and Carlson, R. H., 1968, "Distribution of Natural Missiles Resulting from Cratering Explosions in Hard Rock", Annals of the New York Academy of Sciences, Vol. 152, Art. 1.

Henny, R. W., 1970, "Schooner Ejecta Studies", Proceedings-Symposium on Engineering with Nuclear Explosives, The American Nuclear Society, CONF-700101.

Hess, W. N. and Nordyke, M. D., 1961, "Throwout Calculations for Explosion Craters", Journal of Geophysical Research, Vol. 66, No. 10.

Jenkins, E. C., 1969, "Summary Geologic Report on the Ue20p Exploratory Hole, Area 20, Pahute Mesa, Nevada Test Site", U.S. Geological Survey Technical Letter: Special Studies-75.

Jenkins, E. C., 1969, "Summary Geologic Report on the U20p Emplacement Hole, Pahute Mesa, Nevada Test Site", U.S. Geological Survey Technical Letter: Special Studies-75 (Supplement 1).

Johnson, R. B., 1962, "Effect of Geologic Factors on Cratering Experiments in Basalt--Buckboard Mesa Test Site, Nevada", U.S. Geological Survey Technical Letter: Area 18-1.

Johnson, S. W., Galbraith, B. G., Bessert, G. C., Henny, R. W., and Swift, H. F., 1971, "Motion of Ejecta from Small Cratering Events", Abstract--52nd Annual Meeting of the American Geophysical Union, EOS Transaction, Vol. 52, No. 4.

Lessler, R. M., 1968, "Schooner Preshot Analysis", Lawrence Radiation Laboratory, UCRL-50530 (Rev. 1).

Lockard, D. M., 1974, "The LAUNI 2 Code: A Program for Calculating Crater Volume", Air Force Weapons Laboratory, AFWL-TR-73-265.

Love, G. C. and Vortman, L. J., 1968, "Photogrammetric Techniques Associated with Model Studies of Earth-Moving Explosions", Preprint, American Society of Civil Engineers National Meeting on Transportation Engineering.

Lutton, R. J. and Girucky, F. E., 1966, "Project Sulky Geologic and Engineering Properties Investigations", U.S. Army Engineer Waterways Experimental Station, PNE-720.

Moore, H. J., 1976, "Missile Impact Craters (White Sands Missile Range, New Mexico) and Application to Lunar Research", Geological Survey Professional Paper 812-B.

Moore, H. J., 1977, "Nevada Test Site Craters Used for Astronaut Training", U.S. Geological Survey Professional Paper, In Print.

Mutch, T. A. and Head, J. W., 1975, "The Geology of Mars: A Brief Review of Some Recent Results", Proceedings of the Sixteenth General Assembly International Union of Geodesy and Geophysics, U.S. National Report for 1971-1974.

Nordyke, M. D., 1961, "Nuclear Craters and Preliminary Theory of Mechanics of Explosive Crater Formation", Journal of Geophysical Research, Vol. 66, No. 10.

Nugent, R. C. and Banks, D. C., 1966, "Project Danny Boy--Engineering Geologic Investigations", U.S. Army Engineer Waterways Experiment Station, PNE-5005.

Oberbeck, V. R., 1971, "Laboratory Simulation of Impact Cratering with High Explosives", Journal of Geophysical Research, Vol. 76, No. 23.

Orkild, P. P., 1969, "Summary Geologic Report on the U20m Emplacement Hole, Pahute Mesa, Nevada Test Site", U.S. Geological Survey Technical Letter: Special Studies I-35 (Supplement 1).

Orkild, P. P., Sargent, K. A., and Snyder, R. P., 1969, "Geologic Map of Pahute Mesa, Nevada Test Site and Vicinity, Nye County, Nevada", U.S. Geological Survey Miscellaneous Geologic Investigation Map I-567.

Piekutowski, A. J., 1974, "Laboratory-Scale High-Explosive Cratering and Ejecta Phenonenology Studies", University of Dayton Research Institute, Air Force Weapons Laboratory Report, AFWL-TR-72-155.

Post, R. L., 1974, "Ejecta Distributions from Near-Surface Nuclear and HE Bursts", Air Force Weapons Laboratory, AFWL-TR-74-51.

Purtymun, W. D., Harrill, J., and Rush, F. E., 1969, "Geologic Data for U20u Satellite Holes 1, 2, 3, and 4, and Studies of the Orientation of Joints in the Thirsty Canyon Tuff, Area 20, Pahute Mesa, Nevada Test Site", U.S. Geological Survey Open File Report.

Ramspott, L. D., 1968, Internal Memorandum, University of California Lawrence Livermore Laboratory, Livermore, CA.

Richards, W. D., 1964, "Geologic Study of the Sedan Nuclear Crater", Lawrence Radiation Laboratory, PNE-240.

Roddy, D. J., 1968, "The Flynn Creek Crater, Tennessee", in Shock Metamorphism of Natural Materials, Mono Book Corporation, Baltimore.

Roddy, D. J., 1970, "Geologic Studies", Operation Prairie Flat Symposium, DASA-2377, Vol. I.

Roddy, D. J., 1973, "Geologic Studies of the Middle Gust and Mixed Company Craters", Proceedings of the Mixed Company and Middle Gust Results Meeting, Defense Nuclear Agency, DNA-3151.

Roddy, D. J., Boyce, J. M., Colton, G. W., and Dial, A. L., 1975, "Meteor Crater, Arizona, Rim Drilling with Thickness, Structural Uplift, Diameter, Depth, Volume, and Mass Balance Calculations", Proceedings--Sixth Lunar Science Conference.

Rohrer, R. F., 1972, "Schooner Surface Motion and Vented-Gas Temperature Measurements", University of California Lawrence Livermore Laboratory, UCRL-51181.

Sakharov, V. N., Kolesnikov-Svinarev, V. I., Nazarenko, V. A., and Zabidarov, E. I., 1959, "Local Distribution of Earth Thrown Up by Underground Explosions", Doklady Akad. Nauk., Vol. 125, No. 2.

Sargent, K. A. and Jenkins, E. C., 1968, "Summary Geologic Report on the U320u-1 and Ue20u-3 Drill Holes, Area 20, Pahute Mesa, Nevada Test Site", U.S. Geological Survey Technical Letter: Special Studies-68.

Shackelford, T. J., 1971, "Crater Stability Under the Influence of Large Seismic Motions", U.S. Army Engineer Nuclear Cratering Group, PNE-5013.

Sherwood, A. E., 1967, "Effect of Drag on Particles Ejected During Explosive Cratering", Journal of Geophysical Research, Vol. 72, No. 6.

Shoemaker, E. M., 1963, "Impact Mechanics at Meteor Crater, Arizona", in The Solar System, Vol. IV, The Moon, Meteorites, and Comets, University of Chicago Press.

Short, N. M., 1964, "Project Danny Boy; the Definition of True Crater Dimensions by Postshot Drilling", Lawrence Radiation Laboratory, WT-1834.

Short, N. M. and Bunch, T. E., 1968, "A Worldwide Inventory of Features Characteristic of Rocks Associated with Presumed Meteorite Impact Craters", in Shock Metamorphism of Natural Materials, Mono Book Corporation, Baltimore.

Shreve, R. L., 1968, "The Blackhawk Landslide", Geological Society of America, Special Paper 108.

Sneed, E. D. and Folk, R. L., 1958, "Pebbles in the Lower Colorado River, Texas-a Study in Particle Morphogenesis", Journal of Geology, Vol. 66.

Stephens, D. R. and Lilley, E. M., 1970, "Loading-Unloading Pressure Volume Curves for Rocks", Proceedings--Symposium on Engineering with Nuclear Explosives, The American Nuclear Society, CONF-700101.

Stoffler, D., Gault, D. E., Wedekind, J., and Polkowski, G., 1975, "Experimental Hypervelocity Impact into Quartz Sand: Distribution and Shock Metamorphism of Ejecta", Journal of Geophysical Research, Vol. 80, No. 29.

Strohm, W. E., Ferguson, J. S., and Krinitzsky, E. L., 1964, "Project Sedan--Stability of Crater Slopes", U.S. Army Engineer Waterways Experiment Station, PNE-234F.

Terhune, R. W. and Stubbs, T. F., 1970, "Nuclear Cratering on a Digital Computer", Proceedings--Symposium on Engineering with Nuclear Explosives, The American Nuclear Society, CONF-700101.

Terhune, R. W., 1976, "Personal Communication", Lawrence Livermore Laboratory, Livermore, CA.

Tewes, H. A., 1970, "Results of the Schooner Excavation Experiment", Proceedings--Symposium on Engineering with Nuclear Explosives, The American Nuclear Society, CONF-700101.

Vaile, R. B., 1961, "Pacific Craters and Scaling Laws", Journal of Geophysical Research, Vol. 66, No. 10.

Vesic, A. S., Boutwell, G. P., and Tai, T. L., 1967, "Theoretical Studies of Cratering Mechanisms Affecting the Stability of Cratered Slopes", Duke University School of Engineering, Soil Mechanics Series No. 11.

Vesic, A. S., Ismael, N. M., and Bhushan, K., 1972, "Cratering in Layered Media", Duke University School of Engineering, U.S. Army Engineer Waterways Experiment Station Report, E-72-31.

Vortman, L. J., 1969, "Ten Years of High Explosive Cratering Research at Sandia Laboratory", Nuclear Applications and Technology, Vol. 7.

Vortman, L. J., 1970, "Nuclear Excavation", in Education for Peaceful Uses of Nuclear Explosives, University of Arizona Press.

Pocket has:
7 Maps